50 Copies

NATIONAL AERONAUTICS AND SPACE ADMINISTRATION

Technical Report 32-1285

The Surveyor I and Surveyor II Flight Paths and Their Determination From Tracking Data

T. H. Thornton, Jr., R. G. Labrum, W. R. Wollenhaupt, and S. K. Wong
Jet Propulsion Laboratory

C. M. Meredith, L. H. Davids, J. F. Gans, R. W. Gillett, and J. J. Ribarich
Hughes Aircraft Company

JET PROPULSION LABORATORY
CALIFORNIA INSTITUTE OF TECHNOLOGY
PASADENA, CALIFORNIA

August 1, 1968

NATIONAL AERONAUTICS AND SPACE ADMINISTRATION

Technical Report 32-1285

The Surveyor I and Surveyor II Flight Paths and Their Determination From Tracking Data

T. H. Thornton, Jr., R. G. Labrum, W. R. Wollenhaupt, and S. K. Wong
Jet Propulsion Laboratory

C. M. Meredith, L. H. Davids, J. F. Gans, R. W. Gillett, and J. J. Ribarich
Hughes Aircraft Company

Approved by:

for: E. Cutting, Manager
Systems Analysis Section

JET PROPULSION LABORATORY
CALIFORNIA INSTITUTE OF TECHNOLOGY
PASADENA, CALIFORNIA

August 1, 1968

TECHNICAL REPORT 32-1285

Prepared Under Contract No. NAS 7-100
National Aeronautics & Space Administration

Foreword

The *Surveyor I* and *II* flight path analyses — both inflight and postflight — were accomplished in joint efforts of personnel from the California Institute of Technology's Jet Propulsion Laboratory and the Hughes Aircraft Company. C. M. Meredith, team Director of the flight path analysis and command (FPAC) group, coordinated the Hughes analysis, and T. H. Thornton coordinated the JPL analysis. For the most part, the Hughes personnel were concerned with the maneuver analysis and trajectory design and the JPL staff with orbit determination.

In this report, C. M. Meredith summarizes the function and organization of the FPAC group and co-authored the introductory material and the *Surveyor II* mission summary. Four other Hughes staff members contributed to this document: L. H. Davids and J. F. Gans, members of the FPAC maneuver analysis group, together with J. J. Ribarich, head of that group, prepared the section on midcourse and terminal maneuver analysis for *Surveyor I*; R. W. Gillett, head of the FPAC trajectory analysis group, presented the trajectory analysis for the first *Surveyor*.

T. H. Thornton, who served as Systems Analysis Project Engineer and as a member of the mission advisors, was Meredith's co-author for the Introduction and Section VIII. Other JPL staff members contributed sections of the report: All three — R. G. Labrum and S. K. Wong, members of the FPAC orbit determination group *Surveyor II* mission, and W. R. Wollenhaupt, head of the group — collaborated on the postflight analysis of the DSS transponder tracking data for *Surveyor II*. Wong and Wollenhaupt prepared corresponding material for *Surveyor I*. In addition, Wollenhaupt supplied the inflight orbit determination analysis for *Surveyor I*; and Wong contributed the analysis of the Air Force Eastern Test Range tracking data for the first *Surveyor* flight.

Contents

Contents (contd)

Contents (contd)

Tables

Contents (contd)

Tables (contd)

Figures

Contents (contd)

Figures (contd)

Contents (contd)

Figures (contd)

Contents (contd)

Figures (contd)

Abstract

This report describes the current best estimate of the *Surveyor I* and *Surveyor II* flight paths and the way in which they were determined. The function and organization of the flight path analysis and command (FPAC) group – within which the flight path and the midcourse and terminal-descent maneuvers were determined in real time – are described. Detailed accounts are given for each phase of the flights. Data summaries and analyses include: the orbit determination process and the best estimates of the pre-midcourse correction orbit and the post-midcourse correction orbit; the postflight analysis of the transponder tracking data to give the final best estimates of the pre- and postmaneuver orbits, as well as the estimated values for station locations and certain physical constants; the philosophy used for determining the midcourse correction and the terminal maneuver; pertinent trajectory characteristics; and the inflight and postflight analysis of the Air Force Eastern Test Range tracking data.

The *Surveyor I* and *Surveyor II* Flight Paths and Their Determination from Tracking Data

I. Introduction and *Surveyor I* Mission Summary

This report, which describes the current best estimate of the *Surveyor I* and the *Surveyor II* flight paths and their determination, concentrates on *Surveyor I*, since failure of a vernier engine to fire during midcourse maneuver caused the *Surveyor II* mission to be incomplete.

The prelaunch landing site selected for *Surveyor I* was −3.25 deg lat, 316.17 deg lon. Four major objectives influenced the site selection; they were:[1] (1) to land in the *Apollo* zone of interest, (2) to land with an unbraked impact angle near zone, (3) to land in as smooth a terrain as possible, and (4) to allow for a landing dispersion as large as 50 km.

Surveyor I was launched into a near nominal lunar trajectory from launch pad 36A of the Air Force Eastern Test Range (AFETR) by the *Atlas/Centaur 10* at 14:41 GMT on May 30, 1966. After a 63-h, 36-min flight, at 06:17 GMT on June 2, 1966, the spacecraft soft-landed on the surface within 15 km of the desired landing site. Shortly after landing, the first television picture was transmitted from the surface of the moon and was received on earth. During the following days pictures in excess of 10,000 were transmitted to the earth.

The transit phase of the mission proceeded in almost *textbook* fashion. The direct-ascent boost phase was nominal and resulted in an uncorrected trajectory that would arrive at the moon within 400 km of the premission *targeted* aim point. Subsequent to injection, and prior to separation, the *Centaur* issued preprogrammed commands to extend the landing gear and the omnidirectional antennas, and to turn the spacecraft transmitter to high power. Telemetry data indicated successful execution of these commands except that the omnidirectional antenna A did not extend. This proved to be the only significant anomaly in the entire mission.

First visibility at Johannesburg Deep Space Station (DSS 51) occurred at approximately launch (L) + 24 min. Acquisition procedures were initiated; angle and doppler predictions were computed in real time and transmitted to the station. The predictions were based on an estimate of the launch time made at L − 5 min. Predicts based on AFETR tracking data and computations at that facility could not be used because of lack of sufficient pre-*Centaur* retromaneuver tracking data.

[1]From JPL internal document on *Surveyor* landing site selection by A. L. Filice, T. H. Thornton, Jr., and D. E. Willingham.

With the exception of a bias in the Goldstone tracking data, all pre-midcourse tracking, orbit computations, and maneuver studies proceeded normally. It was soon obvious that the required midcourse correction was well within the capability of the spacecraft. To take advantage of the reduced estimated uncertainties in executing the maneuver, a result of the small correction requirement, the aim point was biased to the north approximately 0.92 deg from the original landing site. By changing the aiming point, the probability of landing in a smooth area was maximized.

All midcourse operations were performed normally. When the spacecraft was in view of Goldstone, the maneuver sequence was initiated by the Pioneer Deep Space Station (DSS 11). The first maneuver (minus roll of 86.5 deg) was started at L + 15 h, 49 min. The second maneuver (minus yaw of 57.9 deg) was executed at L + 15 h, 54 min; vernier engine ignition occurred at L + 16 h, 03 min (06:45 GMT on May 31, 1966). The engines were commanded to burn for 20.8 s at a constant acceleration of 0.1 g to impart a total correction of 20.35 m/s.

Post-midcourse tracking and orbit determination of *Surveyor I* indicated that the actual landing site would be well within the 3σ dispersions predicted prior to the maneuver.

As was the midcourse phase, the terminal descent sequence was nominal. Three attitude maneuvers were performed. The first two aligned the retroengine in the proper direction and the third ensured optimum telecommunications during the retrophase and vernier descent. The final descent sequence was initiated by the altitude marking radar (AMR). At approximately L + 63 h, 33 min, the automatic sequence of events, vernier ignition, retroengine ignition, retroengine burnout, and separation, the 1000-ft mark, the 10-ft/s mark, and the final 13-ft mark occurred as predicted. Confirmation of touchdown was received at 06:17:37 GMT with the Deep Space Instrumentation Facility (DSIF) receiver retaining its *lock-on* configuration. Strain gage telemetry data indicated that the touchdown velocity was approximately 10 ft/s.

The following Sections II–VII detail the flight path analysis activities relating to *Surveyor I*; Sections VIII–XI summarize the pertinent data for *Surveyor II*.

II. Flight Path Analysis and Command Group

A. Function

Within the organization of the *Surveyor* Mission Operations System (described in Ref. 1), there are three analysis-and-command groups: (1) the flight path analysis and command (FPAC), (2) the spacecraft performance analysis and command (SPAC), and (3) the space science analysis and command (SSAC). In general, it is the responsibility of FPAC, first – using the DSIF tracking and pertinent spacecraft telemetry data – to obtain the best estimate of the actual trajectory of the spacecraft and, second – supported by the DSIF – to interpret the tracking data supplied by the tracking stations. It is also the responsibility of FPAC to generate the required spacecraft commands affecting the flight path, using the support of SPAC and SSAC to the degree required.

B. Organization

To perform the above tasks, FPAC is organized into five operating groups under the supervision of the FPAC Director. The organizational chart, as applicable to the *Surveyor I* space flight, is shown in Fig. 1.

The computer support group (CS) acts in a service capacity to the other four FPAC groups by providing an efficient interface between FPAC engineers and the data processing equipment. The group is responsible for the complete checkout of all FPAC computer programs and for the efficient use of the computing complex. The CS group keeps the FPAC Director apprised of the current computer system and user program status.

The tracking data analysis group (TDA) evaluates DSIF tracking data to assist the station in maintaining tracking data qualities and provides information necessary for orbit determination. The TDA group also collects other specific information from various sources required for orbit determination and, in addition, analyzes and checks the quality of predicts and determines which set of predicts the stations should be notified to use. In addition, TDA provides direction liaison between such data users as the orbit determination group (OD), and the Deep Space Station. During the midcourse and terminal maneuvers, the doppler shift in the tracking data is compared with the expected shift.

The OD group formats the raw tracking data by using two computer programs: the tracking data processor

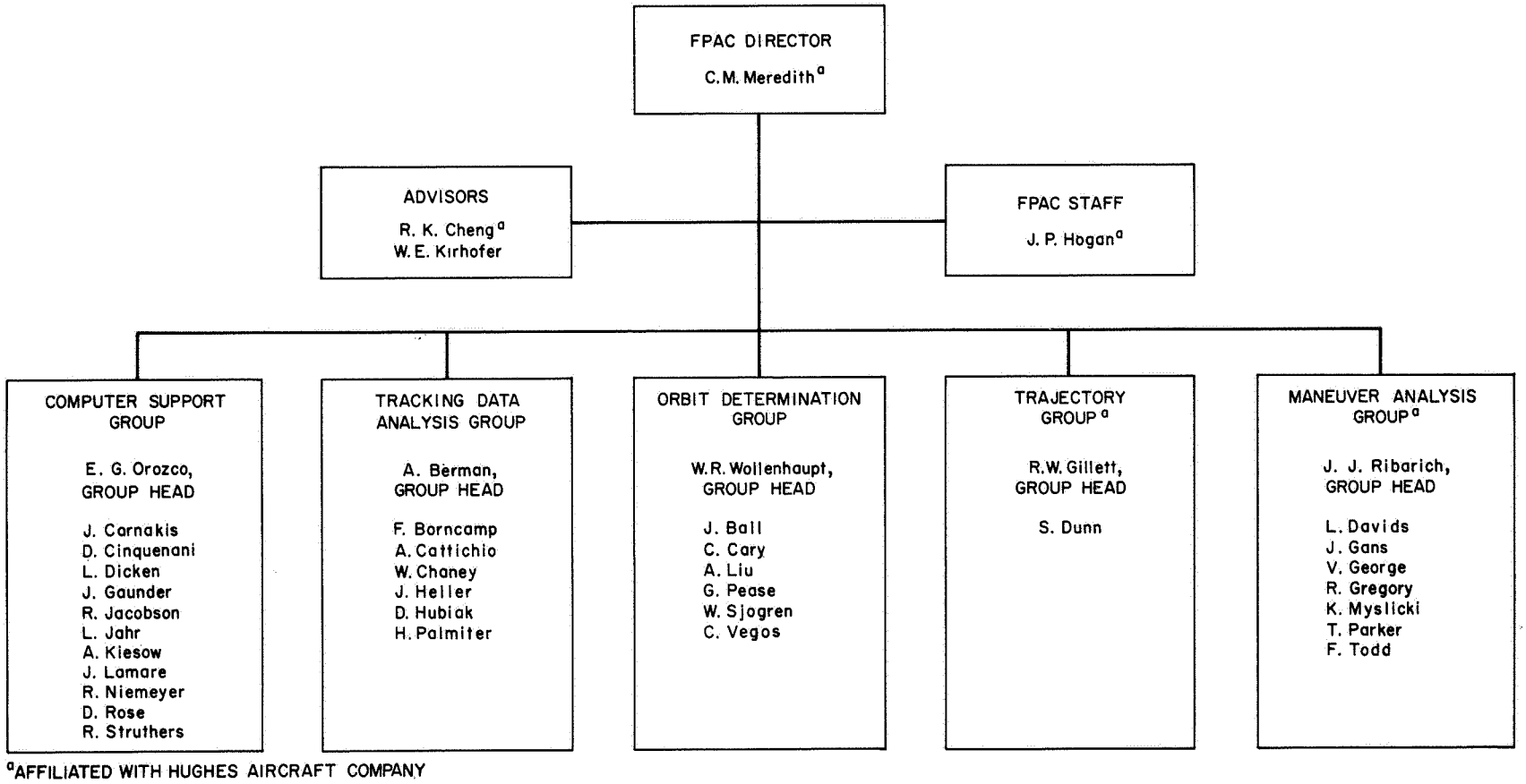

[a]AFFILIATED WITH HUGHES AIRCRAFT COMPANY

Fig. 1. FPAC organization, *Surveyor I*

(TDP), and the orbit data generator (ODG). The group then calculates the best estimate of the spacecraft orbit and the associated statistics by using the single precision orbit determination program (SPODP).

The trajectory group (TG) calculates the nominal injection conditions based on a given launch time and a nominal launch-vehicle performance. These nominal injection conditions are available to be used as predicts for the Deep Space Stations. During the mission, this group calculates the spacecraft's trajectory to the moon for given injection conditions obtained from the OD group. The trajectory group uses three major computer programs: (1) direct-ascent powered flight simulator (DPFS), (2) JPL trajectory program (TRJX), and (3) Hughes post processor (HPPS).

The maneuver analysis group (MA) is responsible for computing the guidance and maneuver information required at the midcourse and terminal phases of the mission. Computations are performed by use of the midcourse and terminal guidance program (MTGS).

III. *Surveyor I* Inflight Orbit Determination Analysis

The results of the *Surveyor I* inflight orbit computations, together with the philosophy used in making these computations and a summary of the data available for the inflight computations, are presented in this section.

A. Data and Programs Used

Since data taken during free flight, only, was used for the realtime orbital solutions, there was a discontinuity at the midcourse maneuver epoch and a logical division of the tracking data into two blocks: (1) data taken prior to midcourse maneuver execution and (2) data taken after midcourse maneuver execution. Results of the inflight orbit solutions, based on these two blocks of data, are used primarily by the MA group to compute the midcourse and terminal maneuvers and to provide the best estimate of the time at which a ground command should be sent to initiate the terminal retroignition sequence, in the event the onboard altitude marking radar (AMR) does not function. The solutions are also used by the trajectory group to obtain spacecraft trajectory information and view-period summaries, and by the TDA group to generate acquisition predictions for the Deep Space Stations performing the tracking.

The Jet Propulsion Laboratory's SPODP (Ref. 2) is the principal analysis tool. This program utilizes an iterative, modified least-squares technique to find that set of initial conditions at a given epoch that causes the weighted sum of squares of the tracking data residuals (defined as observed values minus computed values) to be minimized. Here the term *modified* is used to indicate that the weighting of individual data types is accomplished in a manner different from the usual least-squares method. The single-precision Cowell trajectory program (SPACE) (Ref. 3) and the double-precision JPL ephemeris tape (EPHEM-1) are used in conjunction with the SPODP.

B. Deep Space Stations Supporting *Surveyor I* Mission

The prime stations for providing tracking data during the *Surveyor I* mission were: Johannesburg Deep Space Station (DSS 51) in South Africa, Tidbinbilla Deep Space Station (DSS 42) in Australia, and Pioneer Deep Space Station (DSS 11) at Goldstone, California. Robledo Deep Space Station (DSS 61) near Madrid, Spain, and Ascension Island Deep Space Station (DSS 72) also participated in the mission on a training basis — i.e., they were not committed to provide real-time tracking data. These latter two stations tracked the spacecraft in the receive mode only; at no time was the transmitter from either station used to interrogate the spacecraft transponder. The nominal locations of the tracking station, as used during the *Surveyor I* mission, are given in Table 1.

Table 1. Nominal locations of Deep Space Stations, *Surveyor I*

Station	Geocentric radius, km	Geocentric latitude	Geocentric longitude
DSS 11	6372.0135	35.20807°N	243.15092°E
DSS 42	6371.7108	35.219630°S	148.98138°E
DSS 51	6375.5133	25.739204°S	27.685513°E
DSS 61	6369.9353	40.238000°N	355.75110°E
DSS 72	6378.2386	7.8999140°S	345.67361°E

Figure 2 summarizes the tracking station view periods and their data coverage for the period from launch to lunar touchdown. Figures 3, 4, and 5, which are tracking station stereographic projections for the prime tracking stations, show the trace of the spacecraft trajectory for the view periods in Fig. 2.

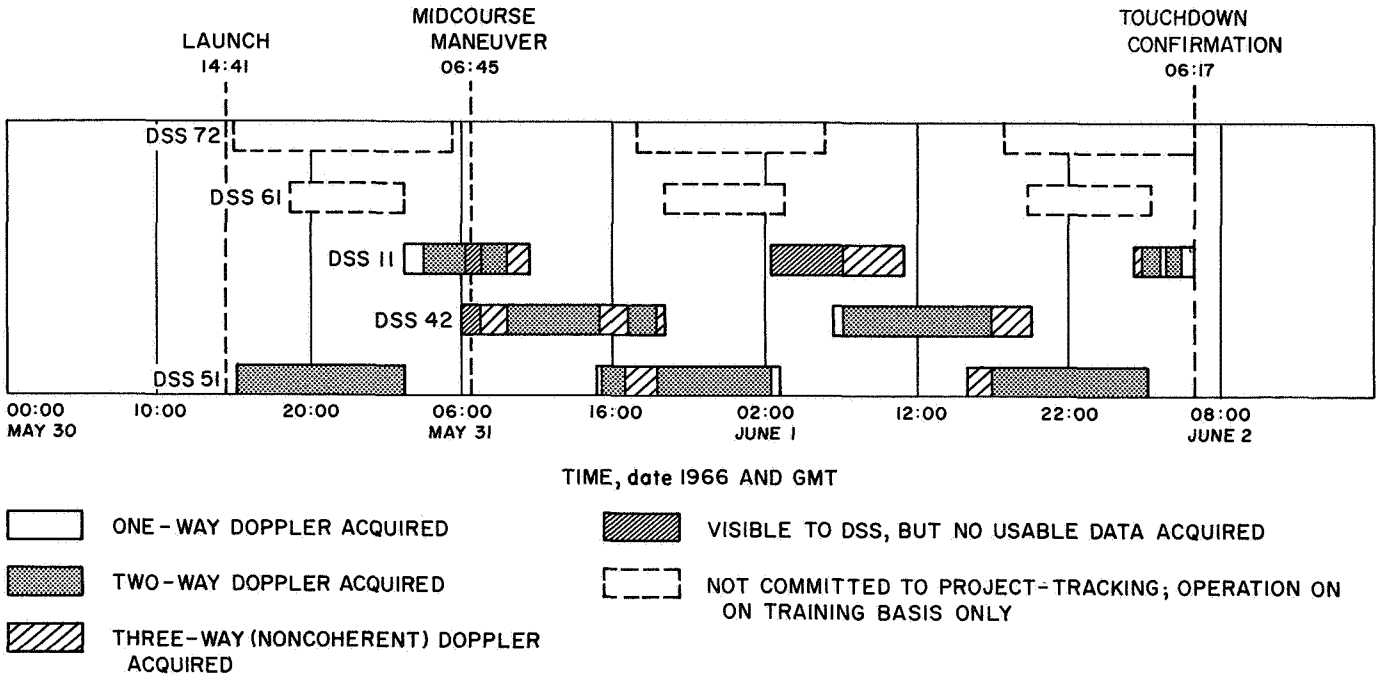

Fig. 2. Deep Space Station view period summary

C. Philosophy Used for Inflight Orbit Computations

The weighted least-squares technique used for the parameter estimates has the refinement that *a priori* information on the parameters, together with their statistics, influences the estimate. The basic equations are:

$$\Delta \mathbf{q}_i = [\mathbf{A}^T\mathbf{W}\mathbf{A} + \tilde{\mathbf{\Gamma}}^{-1}]^{-1} \quad [\mathbf{A}^T\mathbf{W}(\mathbf{O} - \mathbf{C}) + \tilde{\mathbf{\Gamma}}^{-1}\,\Delta\tilde{\mathbf{q}}_i]$$

and

$$\mathbf{q}_{i+1} = \mathbf{q}_i + \Delta \mathbf{q}_i$$

where

$\mathbf{q}_i$ = the estimate of the solution parameter vector ($m \times 1$) on the ith iteration

$\mathbf{A}$ = the matrix of first order partial derivatives on each observable with respect to each solution parameter ($m \times n$)

$\mathbf{W}$ = the diagonal weighting matrix formed by taking the reciprocal of the *a priori* estimated effective variance on each observable ($n \times n$)

$\tilde{\mathbf{\Gamma}}$ = the *a priori* covariance matrix on the solution parameters ($m \times m$)

$\mathbf{O} - \mathbf{C}$ = the vector of differences between the observed data and the calculated data ($n \times 1$)

$\Delta\tilde{\mathbf{q}}_i$ = the difference between the *a priori* solution estimate and the ith iteration estimate ($m \times 1$)

The statistics associated with the parameter estimates are given in the covariance matrix $[\mathbf{A}^T\mathbf{W}\mathbf{A} + \tilde{\mathbf{\Gamma}}^{-1}]^{-1}$. From this expression, it can be seen that the statistics are a direct reflection of the data weights.

1. Data weighting. The philosophy used for weighting data in the SPODP is to calculate a weight value based on the effective (or expected) variance of a given data type. The effective variance for a given data type is determined by summing the variances caused by all known error sources. For two-way doppler data,[2] the error sources were divided into two general classes: (1) hardware, or station equipment, errors, and (2) software, or computing and model, errors. For the first class of errors, such items as transmitter reference-oscillator stability, doppler-counter roundoff error or quantization, and doppler-counter error due to dropped or added cycles in the presence of a low signal-to-noise ratio were considered. Of these, the major contributor is counter

[2]See Appendix A for a definition of tracking data types.

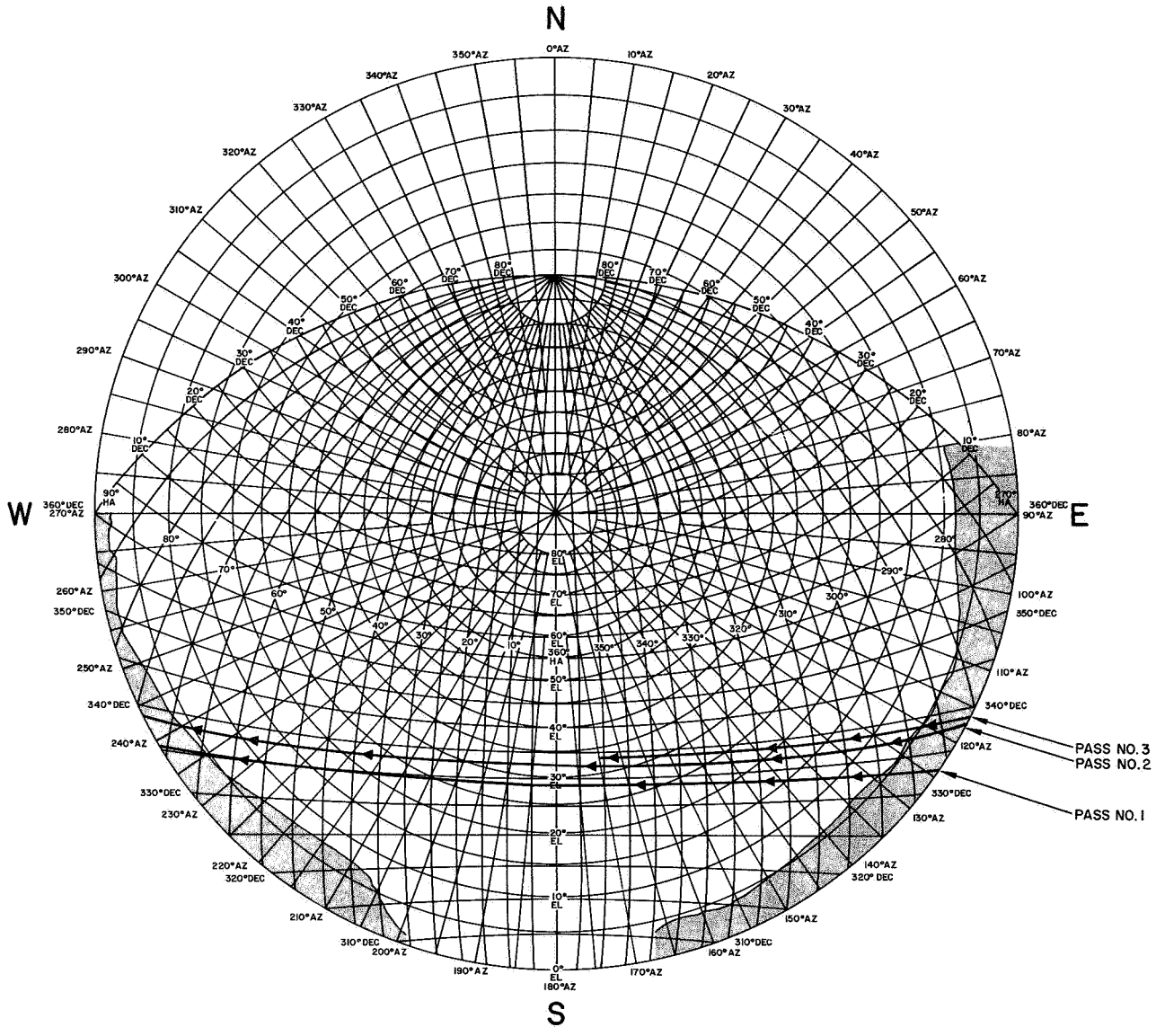

Fig. 3. Stereographic projection, DSS 11, Pioneer Deep Space Station, *Surveyor I*

quantization error which is estimated to be 0.0011 m/s for a data sample rate of 60 s. For the second class of errors, it is known that certain model errors exist that are not adequately accounted for in the SPODP and are not sufficiently known to be reflected in the effective variance. Among these are planetary and earth–moon ephemerides errors. The planetary ephemerides errors are negligible, at least for a lunar trajectory, but earth–moon ephemerides errors will affect such quantities as predicted unbraked impact time — i.e., unbraked time of arrival. This is evidenced by the fact that the predicted time tends to vary as more near-moon tracking data is included in the orbit solution. For this mission, it was estimated that the position of the moon on the JPL ephemeris tape was in error by approximately 100 m in lunar longitude and 300 m in earth–moon distance.[3] The error in the refraction correction model used to correct low-elevation data contributes a negligible amount (approximately 0.107×10^{-4} m/s for a 60-s sample rate) to the total effective variance. Computing errors incurred within the programs are the major contributors to the two-way doppler data weight. These errors result from the fact that most of the computations are done in single precision which results in interpolation errors and the buildup of roundoff errors. The effective variance of

[3]These values, which are based on a letter from Dr. W. J. Eckert dated March 7, 1966, are applicable at lunar encounter.

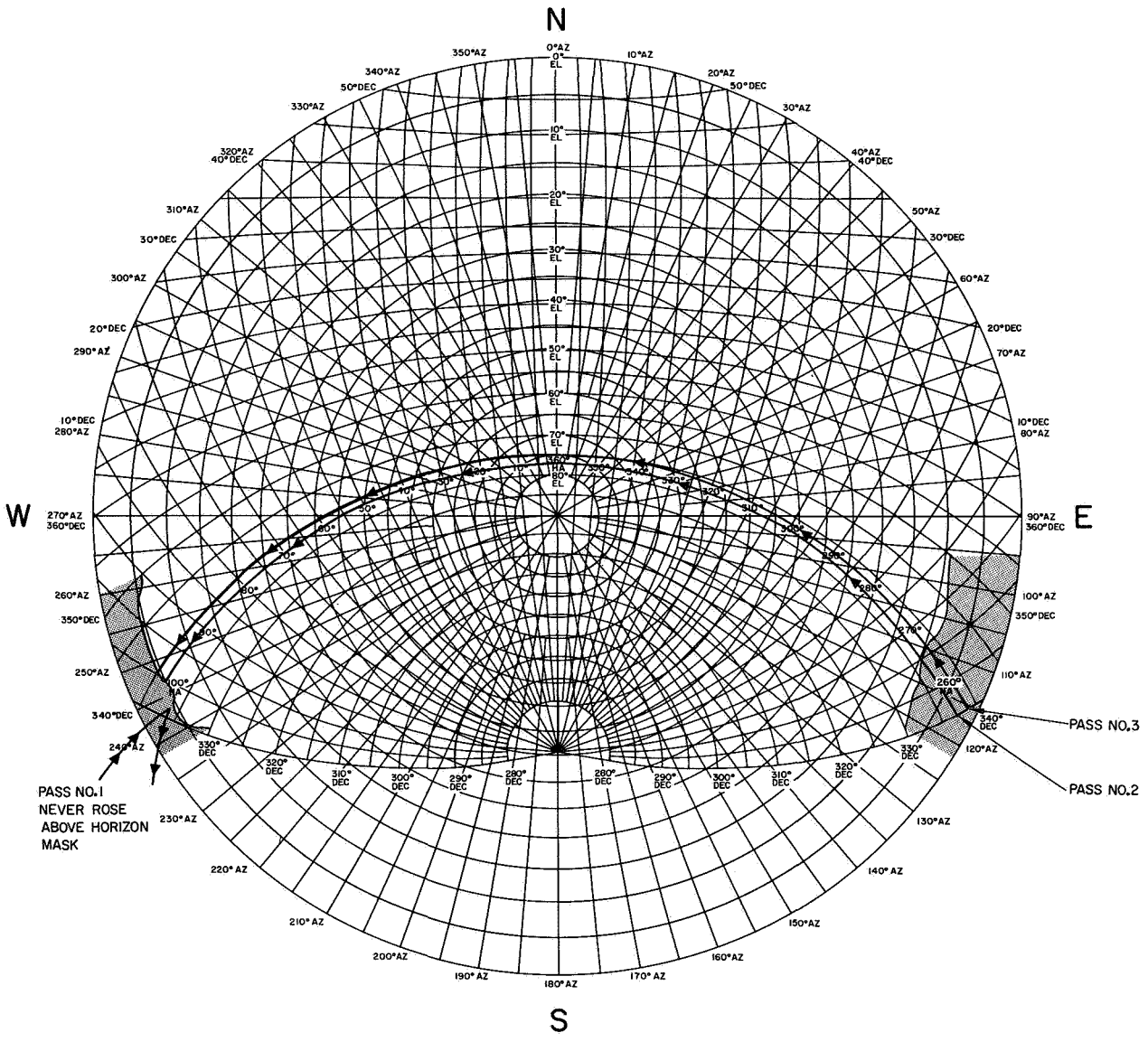

Fig. 4. Stereographic projection, DSS 42, Tidbinbilla Deep Space Station, *Surveyor I*

these errors is 0.012 m/s for a 60-s sample rate. Based on the above error sources, the effective two-way doppler data weight is 0.013 m/s, which corresponds to 0.2 Hz for S-band stations (DSS 11 and DSS 42) and 0.08 Hz for L- to S-band stations (DSS 51).

The error sources associated with angular data — hour angle (HA) and declination angle (dec) are:

(1) Angle jitter or variation about the aiming point caused by antenna drive servomechanisms.

(2) Angle correction errors caused by differences between the empirical correction model, which is based on the antenna optical axis, and the RF pointing axis.

(3) Angular encoder readout errors caused by inaccuracies in the compensation cams. Resolution of the encoder is plus or minus one count, which corresponds to 0.002 deg.

(4) Refraction correction errors caused by the difference between the atmospheric model used in the SPODP and the actual atmosphere at a given time.

Of these, the dominant error sources are angle correction errors which contribute an estimated effective variance of 0.033 deg^2 for a sample rate of 60 s. Based on this, an effective data weight of 0.18 deg was used for both HA and dec data. In past missions, it was noted that a bias remained after applying the corrections to the angular

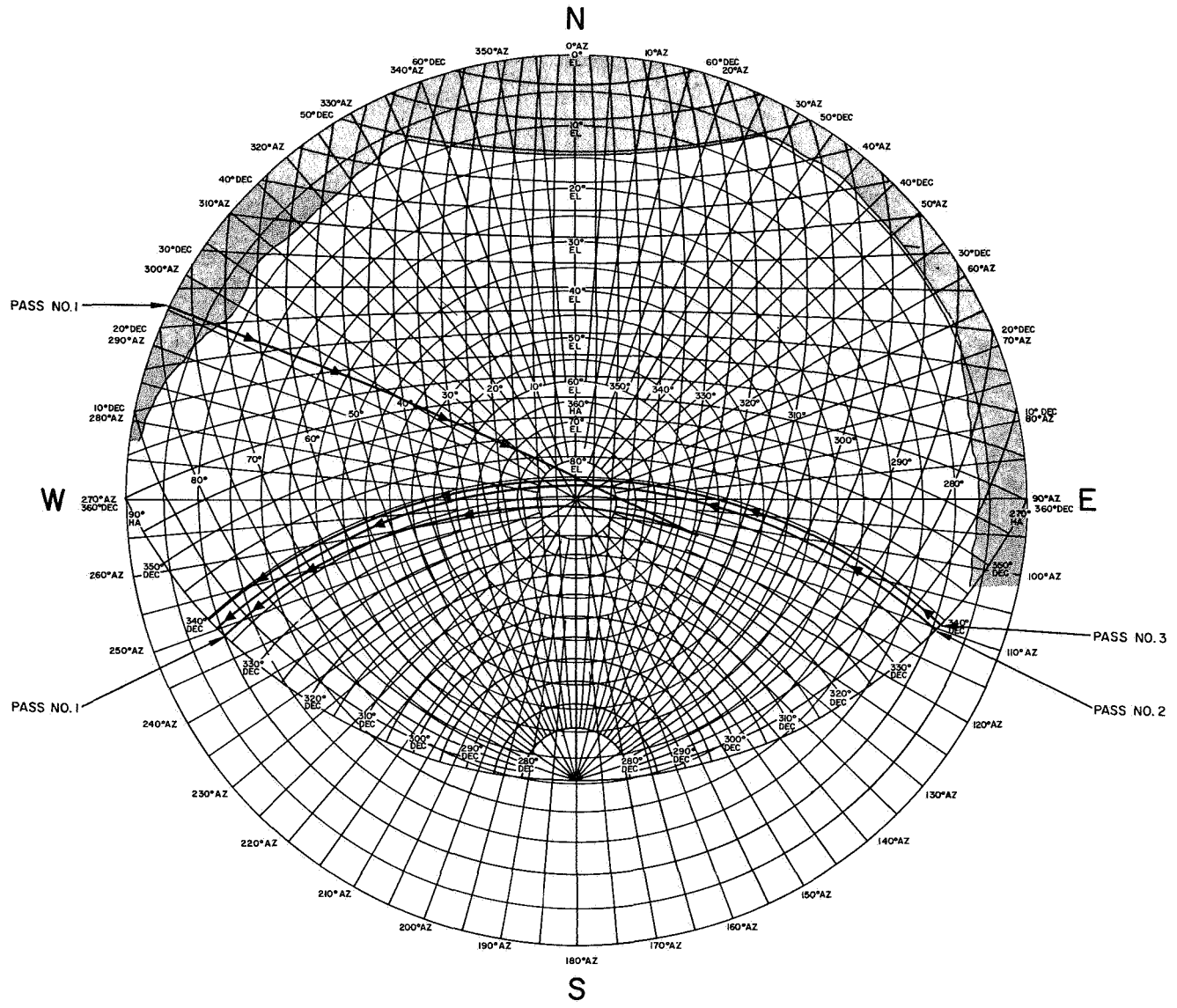

Fig. 5. Stereographic projection, DSS 51, Johannesburg Deep Space Station, *Surveyor I*

data; therefore, these data are usually omitted from the orbit solution as soon as enough two-way doppler data is available to obtain a good solution.

2. Inflight orbit computation types. During the flight, the orbit solution is periodically updated as new tracking data become available. The nominal schedule on which these computations are made and the purpose of the computation is given in Table 2. Since a number of different engineering programs must be run at various time intervals and the computers are heavily loaded throughout most of the mission, the type of orbit solution should be held to a minimum. The number of parameters estimated in a solution should be restricted to the minimum set that will still allow the orbit determination accuracy requirements to be met. Based on *Ranger* Block III inflight and postflight analysis, it was determined that, for most phases of the mission, these requirements could be met by estimating only the position and velocity of the spacecraft at a given epoch. This type orbit solution is commonly referred to as a 6×6, or *standard 6*. The need for only a 6×6 is largely due to the improved physical constants and station location parameter solutions obtained from the *Ranger* Block III and *Mariner II* and *IV* tracking data. Numerical values of these, plus other critical constants, are given in Table 3. (See Refs. 4 and 5.)

Table 2. Nominal inflight orbit computation schedule and purpose

Orbit ID	Time of computation, h, min from launch		Solution type	*A priori* to be used	Purpose of computation
	Start	End			
ETR	18 min	57 min	6 × 6	Loose diagonal[a]	Back up AFETR orbit computation, using AFETR C-band *Centaur* tracking data.
PROR	1 h, 10 min	1 h, 40 min	6 × 6	Loose diagonal	Estimate initial spacecraft orbit, based on DSS data-orbital elements used to generate acquisition predictions for DSS stations.
ICEV	2 h, 10 min	2 h, 56 min	6 × 6	Loose diagonal	Evaluate initial injection conditions.
PREL	3 h, 20 min	4 h, 10 min	6 × 6	Loose diagonal	Provide (1) orbital and target information for preliminary midcourse study and (2) elements for updating acquisition predictions.
DACO	5 h, 45 min	8 h, 40 min	6 × 6	Loose diagonal	Make data consistency check of computations–i.e., validate consistency of all available data.
LAPM	12 h, 30 min (MC − 3 h, 30 min)	13 h, 30 min (MC − 2 h, 30 min)	6 × 6	Loose diagonal	Compute final pre-midcourse orbit to be used for determining midcourse maneuver corrections.
Pre-midcourse cleanup	17 h, 40 min (MC + 2 h)	18 h, 40 min (MC + 3 h)	6 × 6	Loose diagonal	Clean up orbit for purpose of generating a *priori* covariance matrix for post-midcourse orbit computations.
1 POM	22 h, 40 min (MC + 7 h)	25 h, 30 min (MC + 9 h, 50 min)	6 × 6	Pre-midcourse data[b]	Make preliminary evaluation of midcourse maneuver execution; provide orbital elements to generate acquisition predictions for DSS stations.
2 POM	29 h	32 h	6 × 6	Loose diagonal	Update post-midcourse orbit solution based on post-midcourse data only.
3 POM	38 h, 10 min	41 h	6 × 6	Loose diagonal	Update post-midcourse orbit solution.
4 POM	49 h, 5 min	52 h, 5 min	6 × 6	Loose diagonal	Update post-midcourse orbit solution.
5 POM(1)	57 h, 30 min (Retro — 5h, 30 min)	60 h, 20 min	6 × 6	Loose diagonal	Reach final post-midcourse orbit solution for determining terminal spacecraft altitude maneuvers.
5 POM(2)	57 h, 30 min	60 h, 20 min (Retro − 2 h, 40 min)	10 × 10	Post-midcourse data to E − 5 h, 40 min[c]	Obtain best estimate of unbraked impact time.
FINAL OD	61 h (Retro − 2 h)	62 h, 20 min (Retro − 40 min)	10 × 10	Post-midcourse data to E − 5 h, 40 min	Obtain best estimate of unbraked impact for AMR backup.

[a] Loose diagonal used consisted of a one standard deviation of 1×10^4 km on position components and 1×10^1 km/s on velocity components.
[b] *A priori* information from pre-midcourse data is in the form of covariance matrix (based on all pre-midcourse data) at MC epoch in which the diagonal elements of the velocity elements were relaxed to 100 m/s.
[c] *A priori* information from data between MC and *E* − 5 h, 40 min is in form of a covariance matrix at *E* − 5 h, 40 min, in which position diagonal elements have been degraded by 0.5 km and velocity diagonal elements by 0.01 m/s.

Table 3. Nominal physical constants used for *Surveyor I* mission

Constant	Value	SPODP symbolic designation	Space symbolic designation	Basic source
Earth's gravitational coefficient, km^3/s^2	398601.28	KE	GME	*Ranger VII* tracking data (Ref. 4)
Moon's gravitational coefficient, km^3/s^2	4902.5801	KM	GMM	*Ranger VII* tracking data (Ref. 4)
Earth's radius to convert lunar ephemeris to km, km	6378.3144[a]	RE	REM	*Ranger VII* tracking data (Ref. 4)
Earth's radius to be used in the earth's oblate potential, km	6378.1650		RE	Internal publication
Ephemeris–universal time reduction $\Delta T = ET - UT$, s	37.0	DUT	DUT	Internal publication
Earth–moon mass ratio	81.304389			*Ranger VII* tracking data
Moments of inertia of moon for lunar oblate potential, kg-km^2	$0.88778216 \times 10^{29}$		A	Derived from *Ranger VII* value for KM
	$0.88796612 \times 10^{29}$		B	Derived from *Ranger VII* value for KM
	$0.88833394 \times 10^{29}$		C	Derived from *Ranger VII* value for KM
Coefficient of second harmonic in earth's oblateness	0.00162345	J	J	Internal publication
Coefficient of third harmonic in earth's oblateness	0.00000575	H	H	Internal publication
Coefficient of fourth harmonic in earth's oblateness	0.000007875	D	D	Internal publication
Speed of light, km/s	299792.5			Internal publication
Mean lunar radius, km	1738.09[b]			Internal publication

[a]During the AMR backup computations, this value was changed to 6378.3100 to account for the estimated error (Dr. W. J. Eckert) of 300 m in earth-moon radial distance.

[b]During the post-midcourse orbit computations, this value was changed to 1735.6 km.

In the pre-midcourse maneuver phase, all orbit solutions were obtained by estimating only the standard 6 parameters. After midcourse maneuver execution, all pre-midcourse tracking data, from initial DSS acquisition until start of maneuver roll turn, were used to obtain a best estimate pre-midcourse 6×6 orbit solution. The state vector at injection epoch was integrated forward to the end of midcourse (MC) motor burn (also referred to as midcourse epoch) and incremented by the commanded midcourse velocity change. The resulting vector was then used as the initial estimate of the spacecraft post-midcourse orbit. The covariance matrix containing the statistics associated with the state vector at injection epoch was also mapped to the end of burn epoch. Prior to using this covariance matrix as *a priori* information for the post-midcourse orbit, the diagonal elements of the velocity components were relaxed to a 100 m/s standard deviation, which essentially disregards the *a priori* information on the midcourse velocity change.

In the post-midcourse maneuver phase from end of midcourse motor burn until approximately lunar encounter minus 5 h ($E - 5$ h), the orbit solutions were based on estimating only the standard 6 parameters. *A priori* information from premaneuver tracking data was used only until sufficient postmaneuver data was available to obtain an independent solution (i.e., post data only). This approach is used to avoid propagating errors, if any, from the premaneuver orbit into the postmaneuver solution. The spacecraft terminal attitude maneuvers

were computed from a 6 × 6 orbit solution, which included data from end of motor burn to approximately 6 h before lunar encounter. The rationale here was the same as that used for the premaneuver 6 × 6 solutions. In other words, even though model and ephemerides errors existed, and errors might occur because of differences between the assumed values for the physical constants and station location parameters and the *true* values, the aiming of the spacecraft within the required uncertainty could be accomplished by estimating only the standard 6 orbital parameters.

To provide an effective backup for the AMR, the philosophy had to be changed. The backup consists of transmitting a retroignition sequence turn-on command (from a ground station) at a time such that if a turn-on pulse has not been generated by the AMR by the time the backup command reaches the spacecraft, it will initiate the sequence. Operationally, the transmission time is intentionally biased late so that the AMR has ample opportunity to function, yet in time to have a high probability of saving the mission in the event the AMR does not function. This requires that the SPODP be capable of predicting the unbraked impact time to within a 1σ uncertainty of approximately 0.5 s. The uncertainty must include all error sources. Error sources, exclusive of tracking data errors, that significantly affect the predicted unbraked impact time are: (1) assumed value of lunar elevation at the impact point, (2) errors in earth–moon ephemerides, and (3) timing errors. For the first error source, it was noted that the elevation based on the appropriate Air Force Aeronautical Chart and Information Center (ACIC) lunar chart was approximately 2.5 km higher than that obtained from the *Ranger VI, VII,* and *VIII* tracking data. For *Ranger IX,* the ACIC value was approximately 1.9 km higher rather than 2.5 km. This may result from the fact that *Ranger IX* impacted in a crater (Alphonsus); whereas *Rangers VI, VII,* and *VIII* impacted in relatively flat regions. An error of 2.5 km corresponds roughly to a 1-s error in predicted unbraked impact time. For the AMR backup computations, 2.4 km was subtracted from the lunar elevation indicated on the appropriate ACIC chart (LAC 75), which resulted in a lunar elevation of 1735.6 km at the predicted unbraked impact point. An *a priori* 1σ uncertainty of ± 1 km (roughly equivalent to ± 0.4 s) was assigned to the corrected elevation. A study that used *Ranger* Block III tracking data indicated that the remaining two error sources could be accounted for by relying heavily on the near-moon tracking data and processing the data in the following described three steps.

First, process all available two-way doppler from MC epoch to approximately $E - 5$ h, 40 min, and map the resulting solution, plus covariance matrix, to the time of the last data point. There is nothing significant about the $E - 5$ h, 40 min epoch, other than the fact that it is consistent with nominal sequence of events items. There were two principal reasons for selecting an epoch in this region: (1) It was far enough away from encounter so that sufficient data could be accumulated to reestablish the orbit; and (2) it was near enough to encounter to minimize the effect of SPODP model errors. After the two-way doppler data processing, degrade the diagonal elements of the mapped to covariance matrix by 0.5 km on position components and 0.01 m/s on velocity components.

Second, expand the estimate list to include geocentric radius (corresponds to distance of tracking station off earth spin axis) and longitude of the two observing stations. That is, the type of solution has been expanded to a 10 × 10. *A priori* uncertainties of 12 m in spin-axis distance, 40 m in station longitude, and 25 m in longitude difference between the two stations were added to the mapped to covariance matrix.

Third, reduce the effective data weight to 0.003 m/s to obtain realistic statistics on predicted unbraked impact time. This reduction is valid since computational errors are no longer a major error source; i.e., the trajectory is only being integrated over a 6-h period. Also, the model errors have been taken into account by degrading the covariance matrix and by adding the station parameters to estimate list.

D. Summary of Data Used In Orbit Determination

Table 4 summarizes the tracking data used for both the inflight and the postflight orbital calculations and analyses. This table provides a general picture of the performance of the data recording and handling systems. The JPL tracking data processor and orbit data generator programs were used to edit all incoming tracking data and to prepare a data file for input to the SPODP. The *points received* column shows the total number of data points received in near real time. These points are first read into the TDP, which checks each data sample for acceptable format — i.e., it checks to determine (1) if it is one of 30 acceptable message formats, (2) if each item in the sample is in the proper field, and (3) if any item contains a missing or illegal character. The data

Table 4. *Surveyor I* tracking data summary

Station and pass	Data type	Points recd	Points used in real time		Bad format		Bad data condition code		Blunder points		Rejection limits on blunder points	Points used in postflight analysis, obtained from station tapes[a]
			Number	% of recd	Number	% of recd	Number	% of recd	Number	% of recd		
Pre-midcourse correction												
DSS 11, pass 1	CC3[b]	377	109	28.91	20	5.31	11	2.92	140	37.14	0.06	206
DSS 42[c]		0										
DSS 51, pass 1	CC3	956[d]	687	71.86	40	4.18	33	3.45	16	1.67	0.30	642
	HA	993	561	56.50	40	4.02	46	4.63	13	1.31	0.20	0
	Dec	993	559	56.29	40	4.02	46	4.63	15	1.51	0.20	0
Post-midcourse[e] correction												
DSS 11, pass 1	CC3	221[f]	94	42.53	8	3.62	9	4.07	0	0.0	0.03	89
DSS 11, pass 2	CC3	144	0	0.0	1	0.69	77	53.47	66	45.83	0.03	0
DSS 11, pass 3	CC3	147	122	82.99	4	2.72	21	14.29	0	0.0	0.03	122
DSS 42, pass 1	CC3	437	410	93.82	4	1.07	8	2.14	15	3.43	0.03	405
DSS 42, pass 2	CC3	588	552	93.88	19	3.23	4	0.68	23	3.91	0.03	572
DSS 51, pass 2	CC3	466	456	97.85	54	11.59	8	1.72	12	2.58	0.05	456
DSS 51, pass 3	CC3	579	479	82.73	65	11.23	10	5.79	10	5.79	0.05	474

[a]Data points are obtained from station tapes to avoid transmission errors.

[b]CC3 refers to two-way doppler.

[c]Station acquired spacecraft during launch pass but local elevation did not exceed 5 deg; therefore, data were not considered.

[d]Includes 180 points of 10-s data taken during Canopus roll search which were not used in the orbit computations.

[e]Angular data were not used in post-midcourse orbit computations and, therefore, were not considered.

[f]Includes data taken during midcourse thrust and Canopus reacquisition.

points that failed this test are shown under the column *bad format/% recd.* It should be noted that, during flight operations, no attempt is made to reconstruct data points that were rejected for bad format. The next item the TDP checks is the data condition code. A data point is given a bad data condition code when automatic detectors, at the station, sense that the data would be unusable. These detectors have manual overrides that are used whenever an equipment malfunction is suspected and, also, during periods when the transmitter is being returned prior to transferring transmitter assignment to another station. The number of data points that had a bad data condition code are shown under the column so designated. A coarse in-range value check is made to determine if each data type is within an acceptable limit – i.e., within 360 deg for angles and 10^4 cycles for doppler. All data that have passed these checks or are not rejected on a user option are time-sorted and written on both disk and magnetic tape for access by the ODG. The ODG reads the data file and, if it includes angular data, the values are corrected to remove systematic antenna-pointing errors (mechanical deflection as the antenna tracks from horizon to horizon). Next, the doppler data are checked for monotonicity, valid tracking mode, valid sample rate, and are converted from cycles to cycles/second by differencing adjacent samples and dividing by the sample time. Pertinent transmitter and receiver frequencies are entered on the file with each doppler sample (these frequencies are read in by the user or, in some cases, are included in the data sample). The data are then written on both disk and magnetic tape for access by the SPODP.

The blunder points shown in Table 4 are the data points rejected by the TDP and ODG during the validity checks and by application of the rejection limits (from the *rejection limits on blunder points* column) during the orbit computation. These limits are based on experience gained in previous missions and on the philosophy that it is better to reject questionable points immediately, which could create difficulties in converging to an orbit, than to attempt to salvage every point. This is particularly true when very few data are available during the early phase of the mission.

E. Premaneuver Orbit Estimates Based On DSS Tracking Data

The realtime computing facility at Cape Kennedy obtained the initial estimate of the postinjection orbital elements. This estimate was based on AFETR C-band *Centaur* tracking data taken during the period between *Centaur* main-engine cutoff and *Centaur*–spacecraft separation. This solution indicated an out of tolerance injection. However, the confidence level associated with this solution was reported to be relatively poor because of what appeared to be extremely noisy data. Since all spacecraft *mark* events occurred within a 3σ tolerance and since DSS 51 had acquired the spacecraft by using the $L - 5$ min predictions, a decision was made to use the preflight nominal injection conditions (generated at $L - 4$ min) as starter values for the initial orbit computation.

The first estimate of the spacecraft lunar transfer orbit based on DSS data only was completed at $L + 1$ h, 40 min. Approximately 37 min of DSS 51 angular and two-way doppler data were available for this computation. When this solution was mapped forward to the target, it was apparent that lunar encounter would be achieved without a midcourse correction. Further, it indicated that the correction required to achieve a landing at the prelaunch aiming point was well within the midcourse correction capability. This was verified by the second (ICEV) and third (PREL) orbit computations completed at $L + 2$ h, 23 min, and $L + 3$ h, 40 min, respectively.

At the beginning of the data-consistency-orbit (DACO) time block, usable tracking data were available from one prime tracking station, only – the Johannesburg Deep Space Station. The Tidbinbilla Deep Space Station did acquire the spacecraft in a three-way mode on the launch pass because the local elevation angle never exceeded 5 deg. Hence, these data were not used. In addition, angular and three-way doppler data were available from two of the uncommitted tracking stations, the Robledo Deep Space Station and the Ascension Island Deep Space Station. Since there are only a limited number of data consistency computations that can be made with data from only one station, a decision was made to use the DSS 61 data in an attempt to validate the DSS 51 data. The DSS 72 data were not used in these computations because this was a relatively new tracking station for which data accuracy characteristics had not been completely determined. During the DACO period, five orbital computations were made using different combinations of DSS 51 angular and two-way doppler data and DSS 61 angular and three-way doppler data. A comparison between DACO XA which used all DSS 51 data (angles and two-way doppler), and DACO YB which used all DSS 51 data plus all DSS 61 data (angles and

three-way doppler) showed very good agreement. Also, good agreement was noted between DACO XB which used all DSS 51 two-way doppler data, DACO XC which used all DSS 51 two-way doppler data except the early 10-s data, and DACO YA which used both the DSS 51 doppler and the DSS 61 three-way doppler data. However, a comparison between the doppler-plus-angle solutions, and the doppler-only solutions shows a difference in **B**-plane[4] target parameters of approximately 25 km in $\mathbf{B}\cdot\mathbf{T}T$ and approximately 15 km in $\mathbf{B}\cdot\mathbf{R}T$. These differences, even though they are within the calculated uncertainties, clearly demonstrate how the orbit solution is corrupted by using the biased angle data. Based on the results of the data consistency orbit solutions, it appeared that the DSS 51 and DSS 61 data were consistent. The DSS 61 data were not used after the DACO computations since the station was not officially committed to provide tracking data.

Prior to starting the last pre-midcourse (LAPM) orbit, the tracking data analysis group discovered that the Pioneer Deep Space Station doppler data were excessively noisy and notified the station. During the first LAPM computation, the DSS 11 not only indicated a much higher noise standard deviation, but it appeared biased with respect to the DSS 51 data. The malfunction was traced to a faulty electronic component in the doppler counter circuit, which was immediately replaced. Inflight, the exact time that the repair was completed was not well defined. As a result, some of the biased data were used in the orbit computations.

The OD situation, at the end of the LAPM time block, was that the DSS 51 and DSS 11 data did not appear to be consistent. Further, there was not time in the sequence (if a maneuver were to be executed during the first DSS 11 view period) to wait for an additional 2 to 3 h of tracking data and recompute the orbit. The considerations were that either: (1) the DSS 51 data were biased in which case the predicted unbraked impact point could be in error in excess of 100 km, or (2) the DSS 11 data were biased in which case the error in predicted impact point would be considerably less than 100 km (primarily due to the fact that there was considerably less DSS 11 data in the solution). However, during the data consistency computations in which various combinations of DSS 51 and DSS 61 data were used, it was noted that the data from these two stations appeared to be consistent. This increased the confidence in the DSS 51 data; therefore, if a bias existed it was concluded that it must be in the DSS 11 data. Judging from the predicted unbraked impact points obtained from previous solutions (particularly the DACO 1.5 orbit), it was estimated that a possible error of 10 to 15 km on the lunar surface could be incurred if the midcourse maneuver was based on the LAPM XB orbit solution. Immediately following the final midcourse maneuver computation, two special orbits (LAPM XC and LAPM XD) were run to determine the effects of the biased DSS 11 data. A number of computer failures delayed the results of the LAPM XD run until after the actual maneuver sequence had started. The results of the special computations were inconclusive. As the suspected error was small and because it was too late to do anything except cancel the maneuver, the decision was made to continue. This experience should certainly indicate the advantage of having at least two tracking stations support the launch pass if a midcourse maneuver is to be executed during the first DSS 11 view period.

An item of particular interest during the premaneuver phase was the two-way doppler residuals observed during Canopus acquisition. A plot of these residuals, Fig. 6, shows that the roll period was approximately 12 min, and that the duration of the roll was approximately 20 min, which corresponds to 1⅔ turns. The roll rate was approximately 0.5 deg/s, which corresponds to 0.00873 rad/s. Since the omnidirectional antenna is approximately 2.5 m from the spacecraft center of gravity, the predicted maximum amplitude of the doppler residuals can be calculated, as follows:

Let $\dot{S} = l\,\dot{\theta}$

where $\dot{S}$ = change in range rate

l = distance of omnidirectional antenna from spacecraft $cg \cong 2.5$ m

$\dot{\theta}$ = angular rate of change $\cong 0.00873$ rad/s

then $\dot{S} \cong 0.021825$ m/s

To convert this to cycles/s at an L- to S-band station where 1 cycle $\cong \frac{1}{4.8}$ m yields

$\dot{S} \cong 0.1$ Hz = maximum amplitude of doppler residual

[4]See Appendix B for definition of B-plane.

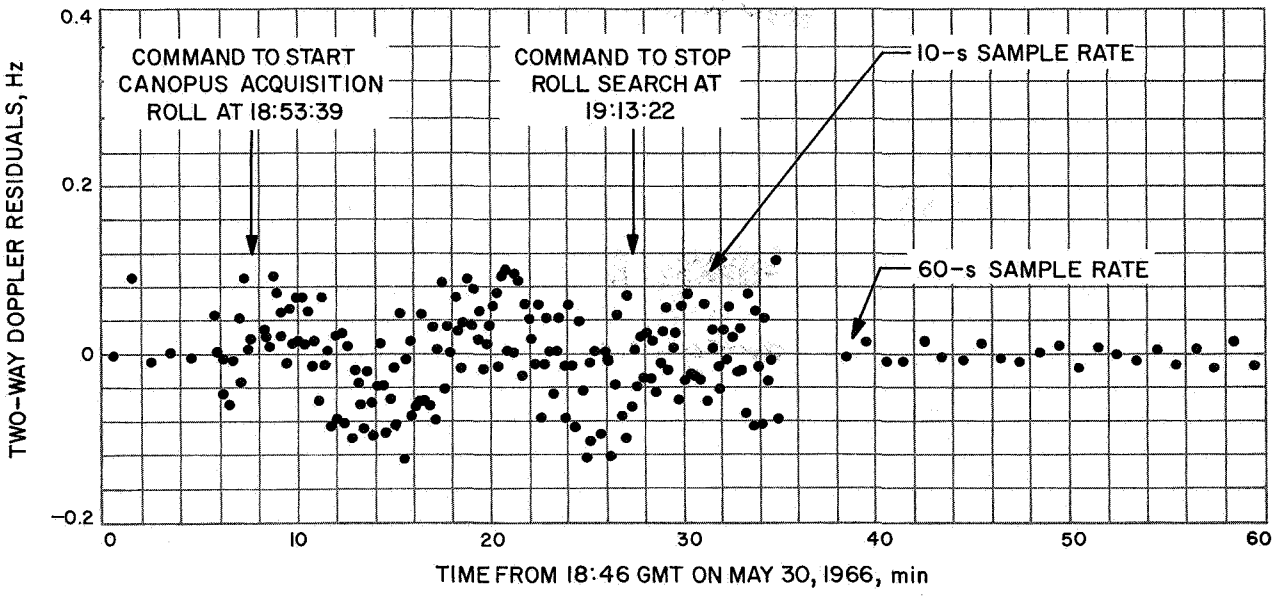

Fig. 6. DSS 51 two-way doppler residuals during Canopus roll search

The amplitude of the actual residuals seen in Fig. 6 is approximately 0.1 Hz. Since this is also the magnitude of the predicted maximum amplitude, it is concluded that the plane of omnidirectional antenna motion is coincident to the line of sight of the tracking station.

The numerical results of the premaneuver orbit computations are presented in Tables 5 and 6. Figure 7 is a plot showing the premaneuver predicted unbraked impact points in the **B**-plane referenced to the lunar equator. Amounts and types of tracking data used in the various orbit computations, together with the associated noise statistics, are given in Table 7.

F. Postmaneuver Orbit Estimates

The first post-midcourse orbit computation was completed approximately 8 h, 30 min, after the midcourse maneuver. For this computation, approximately 2 h of DSS 11 and 5 h of DSS 42 two-way doppler data were available. In addition, *a priori* information from the premaneuver tracking data was used. This information was in the form of a covariance matrix (at midcourse epoch) obtained from the pre-midcourse data evaluation orbit (PRCL XA) computed at approximately MC + 3 h. The diagonal elements of the velocity vector (in the covariance matrix) were relaxed to 100 m/s, and the position elements were left unchanged since the magnitude of the position change due to the maneuver was much less than the 1σ uncertainty indicated in the covariance. When this orbit solution was mapped to the moon, it indicated that unbraked impact would occur approximately 18.25 km to the east and approximately 0.9 km north of the aiming point. At this time, the best estimate of the lunar elevation for the predicted landing point was determined by subtracting 2.4 km from the elevation indicated at this point on the appropriate ACIC lunar chart (LAC 75). The resulting value, 1735.6 km, was used for all post-midcourse computations. Subsequent inflight post-midcourse orbit computations, based only on postmaneuver tracking data, refined the estimated unbraked impact point to 15.70 km east and 3.96 km south of the aiming point.

During the postmaneuver phase, there were two items of particular significance. The first item was that the two-way doppler data taken at DSS 11 during its second view period was unusable because of station equipment malfunction. This resulted in the loss of approximately 5 h of tracking data; but since a second maneuver was not required, the loss of this data did not significantly affect the orbital computations. The second item was the anomaly seen in the DSS 42 two-way doppler residuals during its second view period (Fig. 8). A check with the SPAC area revealed that this anomaly coincided with a gyro drift check started at 07:34:15 GMT on June 1. At this time, the spacecraft was allowed to drift in all three axes. The drift was allowed to continue until 09:52:16 GMT, at which time the spacecraft was returned to Canopus lock. Figure 8 shows an abrupt shift in the doppler residuals at this latter time.

Table 5. Estimated premaneuver position and velocity at injection epoch[a]

Orbit ID	Geocentric space-fixed position			Geocentric space-fixed velocity			Uncertainties, 1σ					
							Position			Velocity		
	x_r, km	y_r, km	z_r, km	Dx_r, km/s	Dy_r, km/s	Dz_r, km/s	σ_{x_r}, km	σ_{y_r}, km	σ_{z_r}, km	σ_{Dx_r}, m/s	σ_{Dy_r}, m/s	σ_{Dz_r}, m/s
PROR YA	2810.9619	5576.3927	1981.7886	−8.3686349	5.5278756	−4.4521800	1.4245	1.1183	2.3510	0.6300	1.7584	1.0209
ICEV XA	2813.4267	5574.2190	1979.8673	−8.3680177	5.5318564	−4.4513452	0.7271	0.7308	1.5332	0.5861	1.0356	0.9618
PREL XA	2813.9671	5573.9882	1979.2326	−8.3671033	5.5325060	−4.4525833	0.6054	0.7110	1.3551	1.3016	0.9845	2.1801
DACO XA	2814.0743	5574.1332	1978.9573	−8.3667956	5.5323738	−4.4531520	0.2803	0.1845	0.4028	1.1119	0.4461	1.7301
DACO XB	2813.6738	5574.0391	1979.6555	−8.3687618	5.5320198	−4.4499853	0.9046	0.2306	1.2936	3.7156	1.2099	5.7639
DACO XC	2813.6043	5574.1043	1979.5980	−8.3686515	5.5319437	−4.4502721	1.8301	0.9858	5.3450	14.6447	2.8691	24.9339
DACO YA	2813.6569	5574.0322	1979.6871	−8.3688392	5.5320106	−4.4498588	0.3750	0.2697	0.4439	1.5291	0.7419	2.2957
DACO YB	2814.1308	5574.0869	1978.9064	−8.3666142	5.5324928	−4.4534066	0.2811	0.2383	0.4190	1.1117	0.5027	1.7312
DACO 1.5	2813.6085	5574.0578	1979.7423	−8.3690235	5.5319232	−4.4495852	0.3404	0.0959	0.5838	1.5332	0.2939	2.4675
LAPM XB[b]	2813.3903	5574.0102	1980.1178	−8.3699527	5.5317561	−4.4480905	0.1563	0.0804	0.2917	0.8491	0.1371	1.3863
LAPM XC	2813.2720	5573.9921	1980.3132	−8.3703360	5.5316818	−4.4474785	0.2295	0.0899	0.4132	1.1341	0.1909	1.8408
LAPM XD	2813.4457	5574.2885	1979.2114	−8.3676717	5.5319001	−4.4522303	0.2873	0.1577	0.5143	1.4297	0.1937	2.3277
LAPM YB	2813.3165	5573.9944	1980.2443	−8.3702613	5.5317004	−4.4475944	0.1473	0.0808	0.2780	0.8230	0.1323	1.3454
PRCL XA	2813.4471	5574.0555	1979.9886	−8.3693630	5.5318311	−4.4490585	0.1791	0.0793	0.3242	0.9008	0.1532	1.4647
PRCL XB	2813.6063	5574.0579	1979.7456	−8.3690332	5.5319205	−4.4495102	0.2824	0.0952	0.4987	1.3107	0.2254	2.1216
Best premaneuver estimate	2813.6136	5574.0461	1979.7524	−8.3688742	5.5320036	−4.4497759	0.3119	0.1453	0.4948	1.4635	0.3174	2.4255

[a]The injection epoch was at 14:53:37.385 GMT on May 30, 1966.
[b]Orbit solution used for midcourse maneuver computations.

Orbit ID	Time computed, GMT		Target				
	Start	Stop	B, km	B•TT, km	B•RT, km	TL, h	S
	Day 150 (May 30, 1966)						
PROR YA	15:51	16:25	787.52	−782.702	86.978	62.75	1
ICEV XA	16:50	17:32	667.89	−663.613	75.435	62.71	
PREL XA	17:55	18:34	637.44	−634.566	60.422	62.70	
DACO XA	22:09	22:52	634.69	−632.873	47.985	62.70	
DACO XB	23:07	23:28	658.10	−655.090	62.894	62.71	
DACO XC	23:31	23:48	659.05	−656.045	62.905	62.71	1
DACO YA	21:29	22:54	659.05	−655.959	63.773	62.71	
DACO YB	23:05	23:24	630.60	−628.755	48.300	62.71	
	Day 151 (May 31, 1966)						
DACO 1.5	01:48	02:09	662.40	−659.302	64.011	62.71	
LAPM XB[b]	03:20	03:34	675.13	−671.102	73.641	62.71	
LAPM XC	05:29	06:00	682.06	−677.360	79.976	62.71	
LAPM XD	06:07	06:38	652.96	−649.873	63.463	62.71	
LAPM YB	04:00	04:17	679.475	−675.101	76.973	62.71	
PRCL XA	10:52	11:46	671.905	−667.849	73.725	62.71	
PRCL XB	11:48	12:15	662.539	−659.434	64.067	62.71	
Best preman-euver estimate	Postflight		660.719	−657.216	67.950	62.71	

[a]B-plane parameters defined in Appendix B. Statistics are defined as follows:

SMAA = semimajor axis of dispersion ellipse.

SMIA = semiminor axis of dispersion ellipse.

THETA = orientation angle of SMAA measured counterclockwise from B•TT axis.

σ_T IMPACT = uncertainty in predicted unbraked impact time.

PHI 99 = 99% lunar approach velocity vector point error.

SVFIX R = uncertainty in magnitude of approach velocity vector at unbraked impact.

[b]Orbit solution used for midcourse maneuver computations.

Table 6. Estimated premaneuver unbraked target parameters and statistics

Parameters and statistics[a]						Selenocentric conditions at unbraked impact			Solution type	Data type and source
AA, n ϑ)	SMIA, km (1σ)	THETA, deg (1σ)	σ_T IMPACT, s (1σ)	PHI 99, deg	SVFIX R, km/s (1σ)	Latitude, deg (Negative S)	Longitude, deg (East)	Time, June 2, 1966, GMT		
23.27	42.73	78.565	91.802	1.9081	0.000633	−11.689	303.132	05:31:52.851	6 × 6	DSS 51, angles and CC3
85.44	17.15	84.136	45.876	1.2706	0.000615	−11.573	305.706	05:29:13.819	6 × 6	DSS 51, angles and CC3
0.78	20.60	84.077	35.085	1.0394	0.000613	−11.295	306.339	05:28:46.064	6 × 6	DSS 51, angles and CC3
18.57	8.96	17.787	12.185	0.1452	0.000610	−11.043	306.388	05:28:39.122	6 × 6	DSS 51, angles and CC3
59.79	9.11	20.307	39.999	0.3089	0.000613	−11.325	305.903	05:28:57.813	6 × 6	DSS 51, CC3 (all data)
34.21	11.23	18.160	137.704	0.7282	0.000681	−11.324	305.882	05:28:57.617	6 × 6	DSS 51, CC3 (no early 10-s data)
26.69	8.87	17.881	15.693	0.1819	0.000610	−11.341	305.883	05:28:58.600	6 × 6	DSS 51, CC3, and DSS 61, C3
18.65	12.87	15.354	12.252	0.1980	0.000610	−11.053	306.475	05:28:36.822	6 × 6	DSS 51 angles and CC3, DSS 61 angles
23.20	2.62	36.447	15.809	0.1746	0.000610	−11.343	305.812	05:29:00.660	6 × 6	DSS 51, CC3 only (update of DACO XB)
0.43	2.23	36.962	7.628	0.0796	0.000609	−11.527	305.551	05:29:10.724	6 × 6	DSS 51, DSS 11, CC3
5.58	2.17	37.357	10.967	0.1154	0.000610	−11.649	305.412	05:29:15.876	6 × 6	DSS 51 and 11, CC3 (1st hour DSS 11 out)
8.36	2.64	37.694	12.994	0.1420	0.000610	−11.343	306.012	05:28:50.961	6 × 6	DSS 51 and 11, CC3 (update of LAPM XC, no early 10-s data from DSS 51)
9.82	2.28	36.525	7.202	0.0744	0.000609	−11.591	305.463	05:29:14.085	6 × 6	DSS 51, DSS 11, CC3
12.28	2.14	37.542	8.376	0.0943	0.000609	−11.533	305.620	05:29:07.139	6 × 6	DSS 51 and 11, CC3 (1st hour DSS 11 out)
19.43	2.27	38.587	13.214	0.1538	0.000610	−11.344	305.809	05:29:00.763	6 × 6	DSS 51, CC3 only
9.725	13.627	57.249	13.240	0.2521	0.000610	−11.425	305.853	05:28:59.537	15 × 15	DSS 51 and 11, CC3

Table 7. Premaneuver tracking data statistics

Orbit ID	Station	Data[a] type	Begin data, time		End data, time		Number of points	Standard deviation	Root mean square	Mean error	Data sample rate, s
			Date 1966	GMT	Date 1966	GMT					
PROR YA	DSS 51	CC3	5/30	15:08:46	5/30	15:44:31	167	0.0649 Hz	0.0653 Hz	−0.0067 Hz	10
		HA	5/30	15:08:21	5/30	15:45:01	172	0.0135 deg	0.0329 deg	−0.0300 deg	10
		Dec	5/30	15:08:21	5/30	15:45:01	173	0.0091 deg	0.0129 deg	−0.0092 deg	10
ICEV XA	DSS 51	CC3	5/30	15:08:46	5/30	16:45:31	213	0.0463 Hz	0.0464 Hz	−0.0032 Hz	10 and 60
		HA	5/30	15:08:21	5/30	16:46:01	222	0.0120 deg	0.0489 deg	−0.0475 deg	10 and 60
		Dec	5/30	15:08:21	5/30	16:46:01	223	0.0099 deg	0.0234 deg	−0.0212 deg	10 and 60
PREL XA	DSS 51	CC3	5/30	15:08:46	5/30	15:39:56	162	0.0506 Hz	0.0506 Hz	0.0004 Hz	10
		HA	5/30	15:08:31	5/30	15:40:01	166	0.0092 deg	0.0590 deg	−0.0583 deg	10
		Dec	5/30	15:08:31	5/30	15:40:01	166	0.0074 deg	0.0093 deg	−0.0057 deg	10
		CC3	5/30	15:42:31	5/30	17:29:31	74	0.0099 Hz	0.0099 Hz	−0.0008 Hz	60
		HA	5/30	15:42:01	5/30	17:30:01	82	0.0094 deg	0.0474 deg	−0.0465 deg	60
		Dec	5/30	15:42:01	5/30	17:30:01	81	0.0182 deg	0.0388 deg	−0.0342 deg	60
DACO XA	DSS 51	CC3	5/30	15:08:46	5/30	15:39:56	162	0.0510 Hz	0.0510 Hz	−0.0004 Hz	10
		HA	5/30	15:08:31	5/30	15:40:01	166	0.0103 deg	0.0610 deg	−0.0601 deg	10
		Dec	5/30	15:08:31	5/30	15:40:01	166	0.0089 deg	0.0089 deg	−0.0003 deg	10
		CC3	5/30	15:42:31	5/30	18:50:31	126	0.0139 Hz	0.0143 Hz	−0.0030 Hz	60
		HA	5/30	15:42:01	5/30	18:51:01	146	0.0092 deg	0.0517 deg	−0.0509 deg	60
		Dec	5/30	15:42:01	5/30	18:51:01	143	0.0142 deg	0.0363 deg	−0.0334 deg	60
		CC3	5/30	18:51:46	5/30	19:21:06	55	0.0446 Hz	0.0447 Hz	0.0031 Hz	10
		HA	5/30	18:51:41	5/30	19:21:11	57	0.0014 deg	0.0607 deg	−0.0607 deg	10
		Dec	5/30	18:51:41	5/30	19:21:11	57	0.0020 deg	0.0389 deg	−0.0388 deg	10
		CC3	5/30	19:24:31	5/30	21:58:31	152	0.0093 Hz	0.0093 Hz	0.0003 Hz	60
		HA	5/30	19:24:01	5/30	21:59:01	154	0.0039 deg	0.0605 deg	−0.0604 deg	60
		Dec	5/30	19:24:01	5/30	21:59:01	154	0.0032 deg	0.0438 deg	−0.0437 deg	60
DACO XB	DSS 51	CC3	5/30	15:08:46	5/30	15:39:36	162	0.0504 Hz	0.0504 Hz	−0.0005 Hz	10
		CC3	5/30	15:42:31	5/30	18:50:31	126	0.0119 Hz	0.0119 Hz	0.0003 Hz	60
		CC3	5/30	18:51:46	5/30	19:21:06	55	0.0446 Hz	0.0446 Hz	−0.0008 Hz	10
		CC3	5/30	19:24:31	5/30	21:58:31	152	0.0092 Hz	0.0092 Hz	−0.0001 Hz	60
DACO XC	DSS 51	CC3	5/30	15:42:31	5/30	18:50:31	126	0.0119 Hz	0.0119 Hz	0.0003 Hz	60
		CC3	5/30	18:51:46	5/30	19:21:06	175	0.0527 Hz	0.0527 Hz	−0.0012 Hz	10
		CC3	5/30	19:24:31	5/30	21:59:31	152	0.0092 Hz	0.0092 Hz	0.0003 Hz	60
DACO YA	DSS 51	CC3	5/30	15:08:46	5/30	15:39:56	162	0.0504 Hz	0.0504 Hz	−0.0006 Hz	10
		CC3	5/30	15:42:31	5/30	18:50:31	126	0.0119 Hz	0.0119 Hz	−0.0002 Hz	60
		CC3	5/30	18:51:46	5/30	21:18:31	266	0.0670 Hz	0.0670 Hz	0.0011 Hz	10 and 60
	DSS 61	C3	5/30	19:23:32	5/30	21:06:32	73	0.0087 Hz	0.0088 Hz	−0.0015 Hz	60
		C3	5/30	21:07:32	5/30	21:18:32	11	0.0071 Hz	0.0078 Hz	0.0032 Hz	60
DACO YB	DSS 51	CC3	5/30	15:08:46	5/30	15:39:56	162	0.0531 Hz	0.0514 Hz	−0.0035 Hz	10
		HA	5/30	15:08:31	5/30	15:40:01	166	0.0108 deg	0.0625 deg	−0.0616 deg	10
		Dec	5/30	15:08:31	5/30	15:40:01	166	0.0093 deg	0.0096 deg	0.0023 deg	10
		CC3	5/30	15:42:31	5/30	18:50:31	126	0.0126 Hz	0.0185 Hz	−0.0135 Hz	60
		HA	5/30	15:42:01	5/30	18:51:01	146	0.0092 deg	0.0523 deg	−0.0515 deg	60
		Dec	5/30	15:42:01	5/30	18:51:01	144	0.0847 deg	0.0885 deg	−0.0256 deg	60
		CC3	5/30	18:51:46	5/30	21:18:31	146	0.0749 Hz	0.0753 Hz	−0.0078 Hz	10 and 60
		HA	5/30	18:51:41	5/30	21:19:01	149	0.0031 deg	0.0610 deg	−0.0609 deg	10 and 60

		HA	5/30	21:07:02	5/30	21:19:02	13	0.0127 deg	0.0231 deg	−0.0193 deg	60
		Dec	5/30	21:07:02	5/30	21:19:02	13	0.0132 deg	0.0892 deg	−0.0882 deg	60
DACO 1.5	DSS 51	CC3	5/30	15:08:46	5/30	15:39:56	162	0.0505 Hz	0.0505 Hz	−0.0011 Hz	10
		CC3	5/30	15:42:31	5/30	18:50:31	124	0.0120 Hz	0.0120 Hz	0.0003 Hz	60
		CC3	5/30	18:51:46	5/30	19:20:56	55	0.0446 Hz	0.0446 Hz	−0.0007 Hz	10
		CC3	5/30	19:24:31	5/31	01:23:31	309	0.0085 Hz	0.0085 Hz	−0.0001 Hz	60
LAPM XB	DSS 11	CC3	5/31	02:24:32	5/31	03:34:47	35	0.0399 Hz	0.0401 Hz	0.0046 Hz	60
	DSS 51	CC3	5/30	15:08:46	5/30	15:39:56	162	0.0504 Hz	0.0504 Hz	−0.0010 Hz	10
		CC3	5/30	15:42:31	5/30	18:50:31	124	0.0125 Hz	0.0128 Hz	−0.0027 Hz	60
		CC3	5/30	18:51:46	5/30	19:20:56	55	0.0446 Hz	0.0449 Hz	−0.0049 Hz	10
		CC3	5/30	19:24:31	5/31	01:39:31	325	0.0089 Hz	0.0089 Hz	−0.0033 Hz	60
		CC3	5/31	01:40:31	5/31	02:16:31	21	0.0105 Hz	0.0131 Hz	−0.0133 Hz	60
LAPM XC	DSS 11	CC3	5/31	03:34:27	5/31	05:00:32	59	0.0126 Hz	0.0388 Hz	0.0366 Hz	60
	DSS 51	CC3	5/30	15:08:46	5/30	15:39:56	162	0.0508 Hz	0.0508 Hz	−0.0007 Hz	10
		CC3	5/30	15:42:31	5/30	18:50:31	124	0.0127 Hz	0.0154 Hz	−0.0088 Hz	60
		CC3	5/30	18:51:46	5/30	19:20:56	55	0.0447 Hz	0.0457 Hz	−0.0097 Hz	10
		CC3	5/30	19:24:31	5/31	01:39:31	325	0.0093 Hz	0.0093 Hz	−0.0011 Hz	60
		CC3	5/31	01:40:31	5/31	02:16:31	21	0.0105 Hz	0.0159 Hz	−0.0119 Hz	60
LAPM XD	DSS 11	CC3	5/31	03:34:27	5/31	06:01:32	109	0.0091 Hz	0.1110 Hz	−0.1110 Hz	60
	DSS 51	CC3	5/30	15:42:31	5/30	18:50:31	124	0.0130 Hz	0.0218 Hz	−0.0175 Hz	60
		CC3	5/30	18:51:46	5/30	19:20:56	55	0.0446 Hz	0.0503 Hz	−0.0232 Hz	10
		CC3	5/30	19:24:31	5/31	01:39:31	325	0.0088 Hz	0.0283 Hz	−0.0269 Hz	60
		CC3	5/31	01:40:31	5/31	02:16:31	21	0.0105 Hz	0.0326 Hz	−0.0308 Hz	60
LAPM YB	DSS 11	CC3	5/31	02:24:32	5/31	03:47:32	83	0.0455 Hz	0.0529 Hz	0.0270 Hz	60
	DSS 51	CC3	5/30	15:08:46	5/30	15:39:56	162	0.0506 Hz	0.0506 Hz	−0.0008 Hz	10
		CC3	5/30	15:42:31	5/30	18:50:31	126	0.0126 Hz	0.0131 Hz	−0.0035 Hz	60
		CC3	5/30	18:51:46	5/30	19:21:06	55	0.0446 Hz	0.0450 Hz	−0.0059 Hz	10
		CC3	5/30	19:24:31	5/31	01:39:31	348	0.0094 Hz	0.0094 Hz	0.0006 Hz	60
		CC3	5/31	01:42:31	5/31	02:16:31	17	0.0114 Hz	0.0151 Hz	−0.0098 Hz	60
PRCL XA	DSS 11	CC3	5/31	03:34:27	5/31	06:18:32	183	0.0171 Hz	0.0658 Hz	−0.0636 Hz	60
		CC3	5/31	06:25:16	5/31	06:29:57	24	0.0183 Hz	0.0437 Hz	−0.0397 Hz	10
	DSS 51	CC3	5/30	15:08:46	5/30	15:39:56	162	0.0556 Hz	0.0556 Hz	−0.0023 Hz	10
		CC3	5/30	15:42:31	5/30	18:50:31	124	0.0127 Hz	0.0356 Hz	−0.0333 Hz	60
		CC3	5/30	18:51:46	5/30	19:20:56	55	0.0446 Hz	0.0517 Hz	−0.0261 Hz	10
		CC3	5/30	19:24:31	5/31	01:39:31	325	0.0089 Hz	0.0192 Hz	−0.0170 Hz	60
		CC3	5/31	01:40:31	5/31	02:16:31	21	0.0105 Hz	0.0255 Hz	−0.0233 Hz	60
PRCL XB	DSS 51	CC3	5/30	15:08:46	5/30	15:39:56	162	0.0505 Hz	0.0505 Hz	−0.0009 Hz	10
		CC3	5/30	15:42:31	5/30	18:50:31	124	0.0120 Hz	0.0120 Hz	0.0003 Hz	60
		CC3	5/30	18:51:46	5/30	19:20:56	55	0.0446 Hz	0.0446 Hz	−0.0007 Hz	10
		CC3	5/30	19:24:31	5/31	01:39:31	325	0.0085 Hz	0.0085 Hz	0.0000 Hz	60
		CC3	5/31	01:40:31	5/31	02:16:31	21	0.0105 Hz	0.0105 Hz	−0.0009 Hz	60
Best prema-neuver estimate	DSS 11	CC3	5/31	03:34:27	5/31	06:18:32	182	0.0109 Hz	0.0110 Hz	0.0001 Hz	60
		CC3	5/31	06:25:16	5/31	06:29:57	24	0.0182 Hz	0.0187 Hz	0.0003 Hz	10
	DSS 51	CC3	5/30	15:12:56	5/30	15:39:56	121	0.0408 Hz	0.0408 Hz	−0.0019 Hz	10
		CC3	5/30	15:42:31	5/30	18:50:31	123	0.0089 Hz	0.0089 Hz	0.0000 Hz	60
		CC3	5/30	18:51:46	5/30	19:20:56	52	0.0400 Hz	0.0400 Hz	0.0009 Hz	10
		CC3	5/30	19:24:31	5/31	01:39:31	325	0.0085 Hz	0.0085 Hz	0.0001 Hz	60
		CC3[b]	5/31	01:40:31	5/31	02:16:31	21	0.0104 Hz	0.0104 Hz	0.0001 Hz	60

[a]CC3 = two-way doppler
HA = *local hour angle*
Dec = local declination angle
C3 = three-way doppler (noncoherent)

[b]Data taken below 17-deg local elevation. All other DSS 51 data before this time plus all DSS 11 data were above 17-deg local elevation.

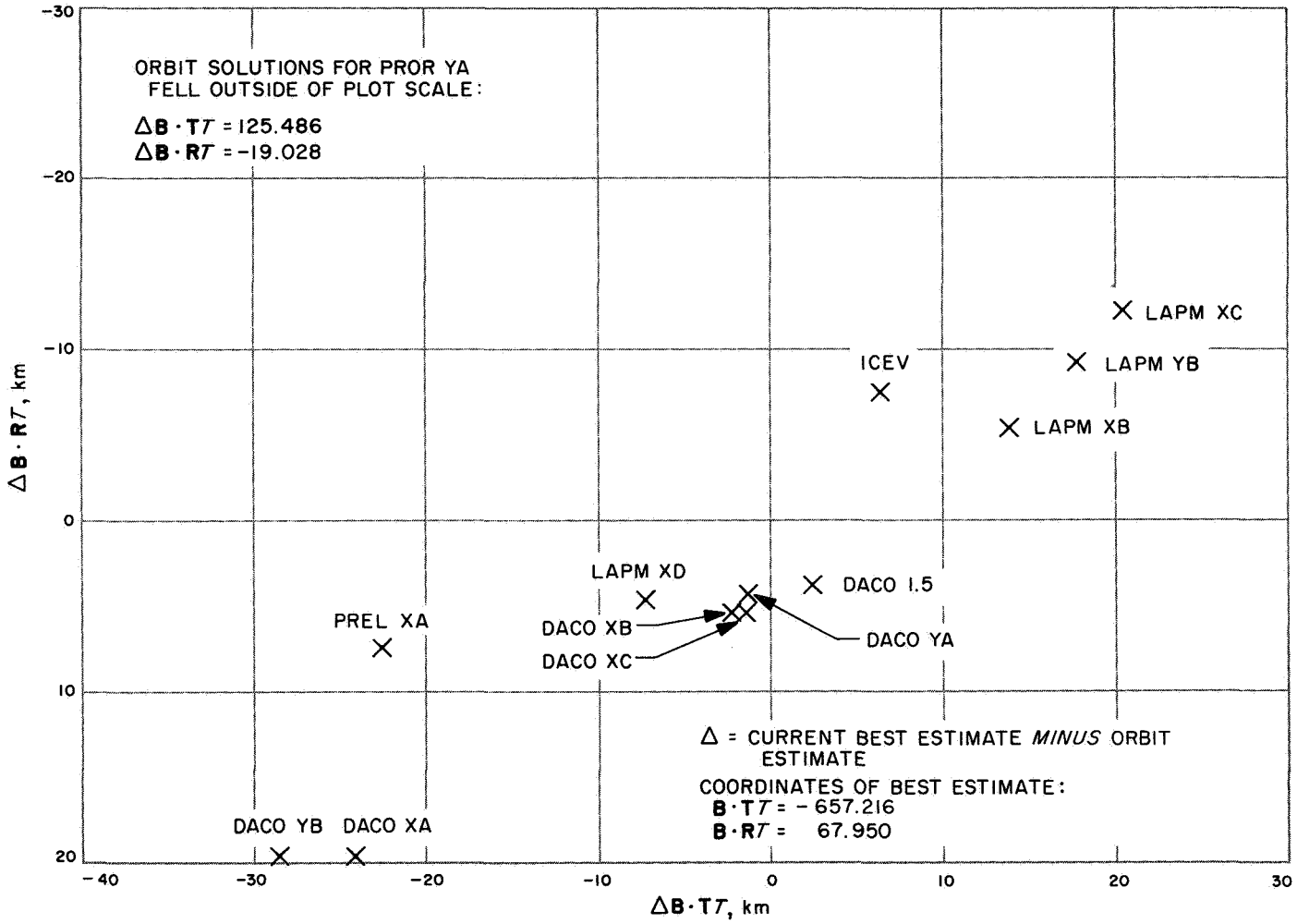

Fig. 7. B-plane differences in predicted unbraked impact point between best premaneuver orbit estimate and inflight solutions

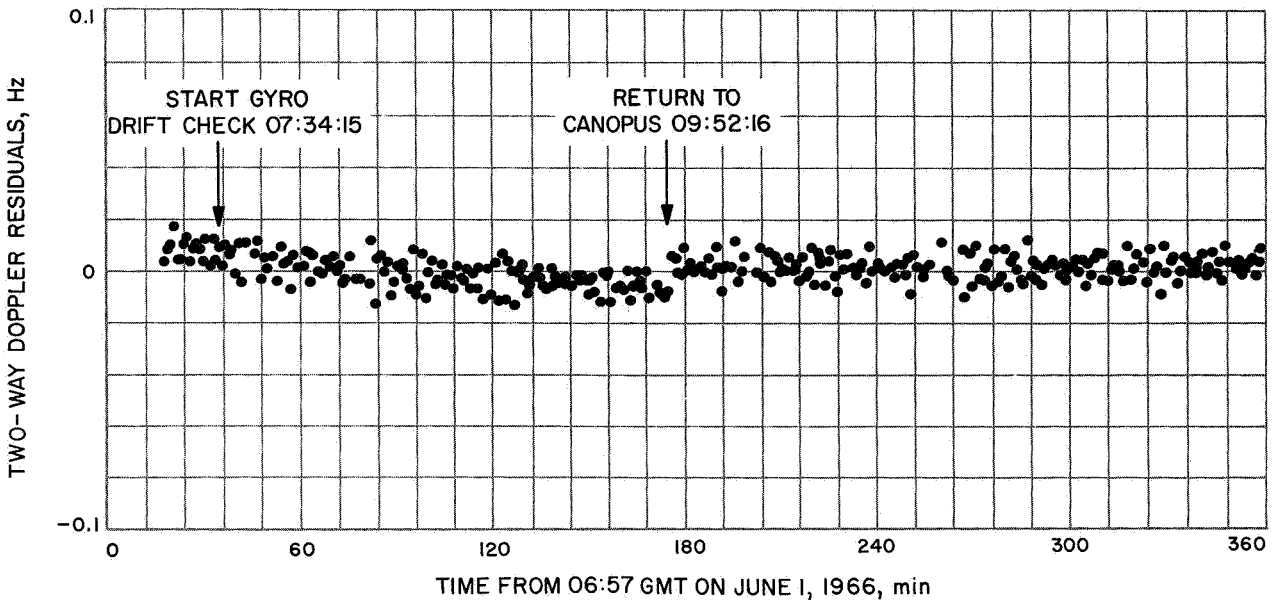

Fig. 8. DSS 42 two-way doppler residuals during gyro drift check

The final spacecraft terminal attitude maneuver computations were based on the fifth post-midcourse orbit solution (5 POM YB) completed approximately 4 h before nominal retroignition. An output of the terminal guidance program is the predicted time at which the onboard AMR will provide a pulse to initiate the terminal retro ignition sequence; i.e., AMR mark time. The predicted AMR time is the time at which the range between the lunar surface and the AMR, along the AMR axis, is approximately 59.63 mi. This time differs from the SPODP predicted unbraked impact time, which is the time the spacecraft would impact the lunar surface if the terminal braking system failed.

After the 5 POM YB computation, primary OD emphasis was placed on obtaining the best estimate of unbraked impact time to be used for sending a ground command to back up the onboard AMR. All subsequent computations used *a priori* information from all post-maneuver tracking data up to the time of the last data point in 5 POM YB. This information was in the form of a covariance matrix mapped to an epoch a few minutes past the time of the last data point in 5 POM YB. The covariance matrix was degraded and expanded as indicated earlier in this section. In addition to being able to account for the SPODP model errors by using this method, a considerable saving in program running time is achieved by working from the updated epoch. This is very important since the basic philosophy is that the near-moon data will yield the best estimate of unbraked impact time. This requires that as much near-moon data as possible be included in the orbit solution and still be able to provide the results at retromaneuver minus 40 min which is the lead time required to implement the backup command transmission. At the time that this number must be available, the best estimate of unbraked impact time was obtained from the final YB orbit computation. For this computation, tracking data up to 1 h, 9 min, from lunar encounter was used. The difference in predicted unbraked impact time between this solution and the 5 POM YB solution was used to update the predicted AMR mark time obtained from the terminal guidance computation (based on 5 POM YB). Based on this new value, a backup command was transmitted from DSS 11 at a time such that it would arrive at the spacecraft 1.2 s after the best estimate of AMR mark time. The problems associated with the AMR backup computations and an evaluation of the effectiveness of the transmitted backup command will be discussed in more detail under part G of this section.

Numerical results of the inflight post-midcourse orbit computations are presented in Tables 8 and 9. Figure 9 is a plot showing the predicted unbraked impact points (referenced to lunar latitude and longitude) obtained from mapping these solutions to the moon. In this figure, the point labelled 1.2 POM appears to be out of line with the other solutions. The explanation for this is that the 1.2 POM was the first post-midcourse orbit computation made without *a priori* information from the pre-midcourse data and, at the time of the computation,

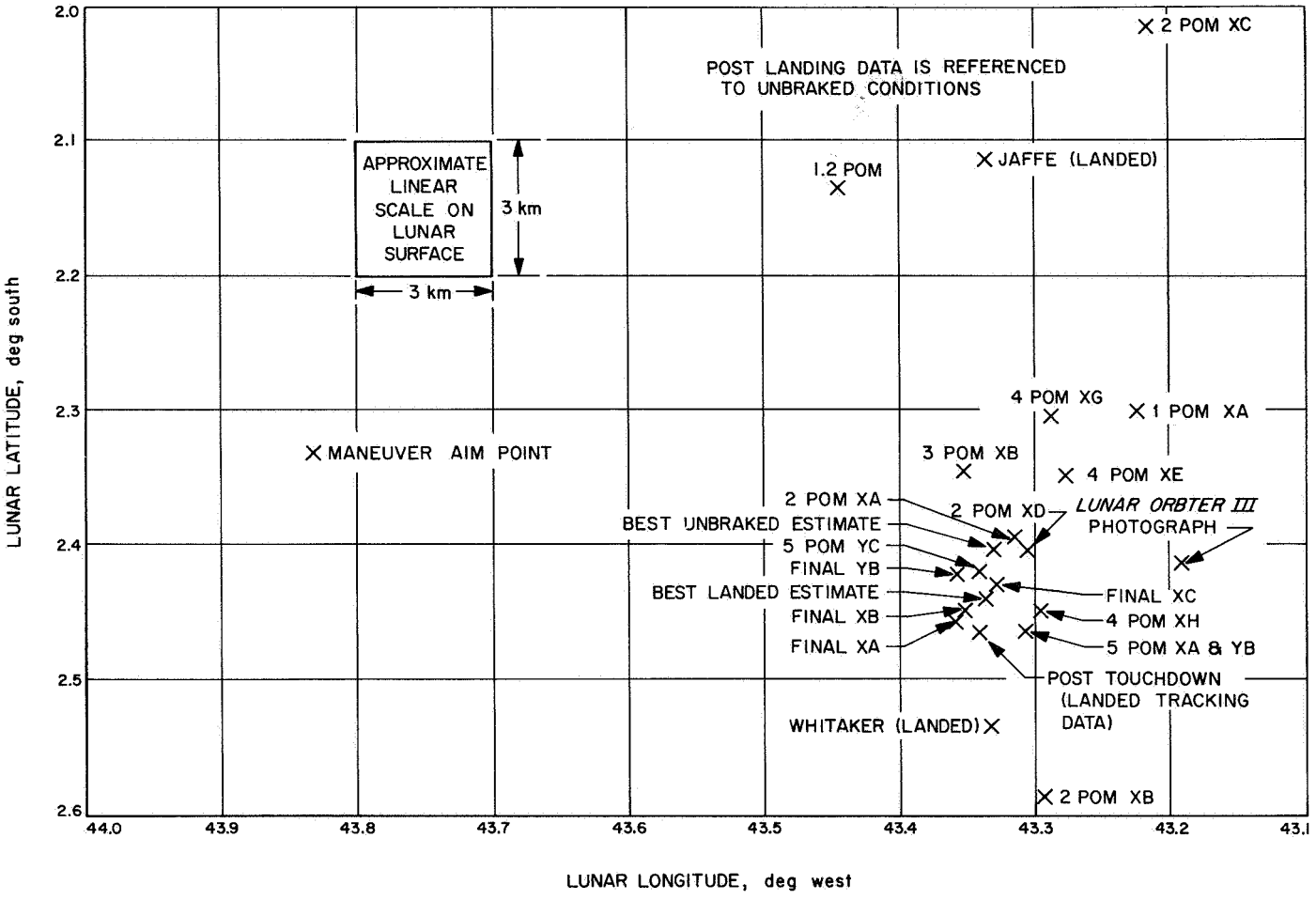

Fig. 9. Postmaneuver estimated unbraked impact locations

there was insufficient post only data to obtain a good orbit estimate. The points labelled 2 POM XB and 2 POM XC also appear out of line. Both of these solutions resulted from data consistency type computations in which data from one of the three tracking stations was deleted from the computation. The amounts of tracking data used in the various orbit computations, together with the associated noise statistics, are given in Table 10.

G. Altitude Marking Radar Backup Computations

Prior to starting the AMR backup computations (listed as final OD computations), it was noted that the postmaneuver tracking data were not fitting as well as expected. This did not appear related to biased or erroneous tracking data, since data-consistency-type orbit computations, made throughout the postmaneuver phase, indicated that all data were consistent. Further, this did not appear to be caused by errors in station locations, since orbit computations in which these parameters were estimated did not improve the fit. Therefore, it was concluded that the poor fit was caused by some trajectory perturbation that was not being taken into account. As a result, the drastic change noted in predicted unbraked impact time during the AMR backup computations (Table 9) was not too surprising. The changes were all in the same direction and were similar to those observed during previous *Ranger* lunar missions. Since all near-encounter data appeared consistent, it was believed that the estimated impact time provided for the AMR backup (FINAL YB) was good to within the stated 0.444-s one-sigma uncertainty. This solution contained tracking data up to 1 h, 9 min, before lunar encounter. The estimated nominal AMR mark time based on this solution was 06:14:37.996 GMT, June 2, 1966. It was used as the basic reference point from which the desired time of backup command transmission from the ground station was calculated.

Table 8. Estimated postmaneuver position and velocity

Orbit ID	Geocentric space-fixed position			Geocentric space-fixed velocity			Uncertainties, 1σ					
							Position			Velocity		
	x, km	y, km	z, km	Dx, km/s	Dy, km/s	Dz, km/s	σ_{x_f} km	σ_{y_f} km	σ_{z_f} km	σ_{Dx_f} m/s	σ_{Dy_f} m/s	σ_{Dz_f} m/s
1 POM XA[a]	−103397.69	−107008.69	−66324.589	−0.88957283	−1.5377885	−0.62095399	1.7115	1.6182	1.1296	0.0886	0.0458	0.0672
1.2 POM	−103399.85	−107006.17	−66321.006	−0.88948756	−1.5378661	−0.62095743	5.3121	10.0302	22.6654	0.3298	0.4612	0.2614
2 POM XA	−103399.17	−107007.47	−66324.379	−0.88953625	−1.5377979	−0.62099513	3.2380	3.9012	4.8776	0.0998	0.0991	0.0351
2 POM XB	−103398.73	−107009.60	−66323.797	−0.88954367	−1.5377599	−0.62104563	3.7399	10.0073	7.1915	0.1117	0.1859	0.2487
2 POM XC	−103399.21	−107005.11	−66321.515	−0.88955852	−1.5378411	−0.62089661	3.4659	13.3069	16.3237	0.1412	0.2729	0.4823
2 POM XD	−103399.11	−107007.60	−66324.545	−0.88953959	−1.5377942	−0.62099587	3.0492	3.3705	4.1985	0.0862	0.0829	0.0336
3 POM XB	−103399.87	−107006.92	−66323.486	−0.88952164	−1.5378142	−0.62098999	2.2380	2.4920	2.8574	0.0595	0.0548	0.0321
4 POM XE	−103399.63	−107007.47	−66325.333	−0.88955358	−1.5377939	−0.62097194	2.5533	3.7533	7.7811	0.0323	0.0479	0.0810
4 POM XG	−103400.19	−107007.68	−66323.862	−0.88954851	−1.5378012	−0.62096535	1.9885	3.0819	5.3249	0.0181	0.0411	0.0626
4 POM XH	−103399.12	−107008.50	−66325.611	−0.88954916	−1.5377801	−0.62099972	1.0948	1.1586	1.1481	0.0109	0.0149	0.0150
5 POM XA	−103399.35	−107008.46	−66325.419	−0.88954449	−1.5377809	−0.62100512	1.0559	1.1524	1.1112	0.0088	0.0146	0.0146
5 POM YB[b]	−103399.36	−107008.47	−66325.410	−0.88954425	−1.5377809	−0.62100543	1.0553	1.1524	1.1112	0.0088	0.0146	0.0146
5 POM YC[c]	−186811.39	−276086.69	−124742.40	−0.43330820	−0.87854835	−0.25172641	0.4831	0.8445	1.7513	0.0132	0.0097	0.0131
FINAL XA	−186811.00	−276086.37	−124744.15	−0.43329115	−0.87856270	−0.25173055	0.9779	2.5652	2.6071	0.0442	0.0497	0.0806
FINAL XB	−186810.87	−276085.97	−124743.91	−0.43329205	−0.87856089	−0.25173296	0.9228	2.4562	1.9305	0.0326	0.0472	0.0802
FINAL XC	−186810.52	−276085.06	−124742.78	−0.43328157	−0.87857218	−0.25172242	0.8161	2.1598	1.5380	0.0312	0.0464	0.0797
FINAL YB[d]	−186810.62	−276086.93	−124742.57	−0.43329332	−0.87855813	−0.25173589	0.3382	0.8165	1.4607	0.0097	0.0080	0.0122
Best[a] postmaneuver estimate	−103397.85	−107007.03	−66324.784	−0.88955294	−1.5377926	−0.62097894	1.2545	2.7590	2.3195	0.0414	0.0410	0.0214

[a]1 POM XA through 5 POM YB, and best postmaneuver estimate are at midcourse epoch, May 31, 1966, 06:45:53.800 GMT.

[b]Orbit solution used for terminal attitude maneuver computations.

[c]5 POM YC through FINAL YB are at unbraked impact minus 5 h, 40 min, on June 2, 1966, 00:35:14.000 GMT.

[d]Orbit solution used for final inflight AMR backup computations.

Orbit ID	Time computed, GMT		B, km	B•TT, km	B•RT, km	TL, h
	Start	Stop				
	Day 151 (May 31, 1966)					
1 POM XA[a]	14:51	15:12	415.306	−107.807	−401.070	47.6
1.2 POM	16:41	16:54	425.617	−118.714	−408.726	47.6
2 POM XA	20:32	20:53	411.662	−112.241	−396.065	47.6
2 POM XB	21:01	21:16	402.132	−111.281	−386.428	47.5
2 POM XC	21:19	21:37	428.395	−107.412	−414.711	47.6
2 POM XD	21:48	22:08	411.080	−111.836	−395.575	47.6
	Day 152 (June 1, 1966)					
3 POM XB	05:54	06:12	414.502	−114.079	−398.495	47.6
4 POM XE	13:27	13:59	413.261	−110.457	−398.226	47.6
4 POM XG	23:02	23:34	415.553	−110.956	−400.466	47.6
4 POM XH	23:40	24:00	408.712	−111.309	−393.263	47.6
	Day 153 (June 2, 1966)					
5 POM XA	01:20	01:43	408.291	−111.887	−392.661	47.6
5 POM YB[b]	01:44	02:11	408.263	−111.917	−392.623	47.6
5 POM YC[c]	03:17	03:32	410.725	−113.530	−394.723	5.7
FINAL XA	04:03	04:26	409.324	−114.514	−392.979	5.7
FINAL XB	04:30	04:58	409.618	−114.128	−393.397	5.7
FINAL XC	05:20	05:56	410.165	−112.960	−394.304	5.7
FINAL YB[d]	05:06	05:20	410.940	−114.443	−394.682	5.7
Best[a] postmaneuver estimate	Postflight		411.415	−113.040	−395.581	47.6

[a]1 POM XA through 5 POM YB and best postmaneuver estimate are based on midcours

[b]Orbit solution used for terminal attitude maneuver computations.

[c]5 POM YC through FINAL YB are based on epoch of June 2, 1966 at 00:35:14.000 GM

[d]Orbit solution used for final inflight AMR backup computations.

Table 9. Estimated postmaneuver unbraked target parameters and statistics

Target parameters and statistics						Selenocentric conditions at unbraked impact			Solution type	Data type and source
SMAA, km (1σ)	SMIA, km (1σ)	THETA, deg (1σ)	σ_T IMPACT, s (1σ)	PHI 99, deg	SVFIX R, km/s (1σ)	Latitude, deg (Negative S)	Longitude, deg (East)	Time, June 2, 1966, GMT		
13.787	5.035	19.859	9.00	0.2212	0.000612	−2.300	316.778	06:15:09.881	6 × 6	DSS 11 and 42 CC3 *a priori* from PRE
96.209	8.074	116.202	35.40	1.01607	0.000624	−2.135	316.556	06:15:19.525	6 × 6	DSS 11, 42, and 51 (no *a priori*)
17.071	5.367	132.915	10.21	0.1626	0.000614	−2.392	316.686	06:15:14.373	6 × 6	DSS 11, 42, and 51 CC3
45.521	13.101	95.191	11.46	0.6225	0.000615	−2.587	316.705	06:15:13.759	6 × 6	DSS 42 and 51 CC3
97.274	17.233	79.804	12.91	1.39103	0.000615	−2.015	316.785	06:15:13.034	6 × 6	DSS 11 and 42 CC3
14.227	5.319	134.344	8.59	0.1396	0.000614	−2.402	316.694	06:15:14.007	6 × 6	DSS 11, 42, and 51 CC3
9.236	5.206	132.555	5.93	0.1012	0.000613	−2.343	316.649	06:15:15.641	6 × 6	DSS 11, 42, and 51 CC3
18.244	4.643	90.907	3.89	0.2719	0.000613	−2.349	316.723	06:15:11.695	15 × 15	DSS 11, 42, and 51 CC3
14.725	1.585	97.493	1.37	0.2036	0.000613	−2.303	316.713	06:15:11.910	15 × 15	DSS 11, 42, and 51 CC3
3.256	1.104	98.690	0.96	0.0421	0.000613	−2.449	316.705	06:15:12.320	6 × 6	DSS 11, 42, and 51 CC3
3.285	0.772	98.698	0.77	0.0418	0.000613	−2.461	316.693	06:15:12.724	6 × 6	DSS 11, 42, and 51 CC3
3.282	0.762	98.803	0.77	0.0418	0.000613	−2.462	316.693	06:15:12.745	6 × 6	DSS 11, 42, and 51 CC3
2.286	0.741	91.607	0.54	0.3062	0.000613	−2.419	316.660	06:15:13.846	10 × 10	DSS 11 and 51 CC3
3.225	2.748	78.841	1.08	0.0467	0.000613	−2.455	316.641	06:15:14.352	10 × 10	DSS 11 and 51 CC3
2.806	2.449	132.231	0.82	0.0430	0.000613	−2.447	316.649	06:15:14.523	10 × 10	DSS 11 and 51 CC3
2.800	1.814	129.600	0.64	0.0401	0.000613	−2.429	316.673	06:15:14.986	10 × 10	DSS 11 and 51 CC3
1.951	0.601	94.180	0.44	0.0262	0.000613	−2.420	316.642	06:15:14.519	10 × 10	DSS 11 and 51 CC3
4.946	2.018	127.429	0.78	0.0682	0.000017	−2.402	316.671	06:15:15.066	9 × 9	DSS 11, 42, and 51 CC3

epoch: May 31, 1966, at 06:45:53.800 GMT.

Table 10. Postmaneuver tracking data statistics

Orbit ID	Station	Data type	Begin data, time		End data, time		Number of points	Standard deviation, Hz	Root mean square, Hz	Mean error, Hz	Data sample rate, s
			Date 1966	GMT	Date 1966	GMT					
1 POM XA	DSS 11	CC3	5/31	06:46:07	5/31	08:58:32	184	0.0415	0.0416	−0.0028	10 and 60
	DSS 42	CC3	5/31	09:04:32	5/31	14:22:32	313	0.0190	0.0190	0.0003	60
1.2 POM	DSS 11	CC3	5/31	07:04:32	5/31	08:58:32	94	0.0049	0.0049	0.0000	60
	DSS 42	CC3	5/31	09:04:32	5/31	15:08:32	317	0.0184	0.0184	0.0000	60
	DSS 51	CC3	5/31	15:15:31	5/31	16:25:31	71	0.0086	0.0086	0.0000	60
2 POM XA	DSS 11	CC3	5/31	07:04:32	5/31	08:58:32	94	0.0055	0.0055	−0.0003	60
	DSS 42	CC3	5/31	09:04:32	5/31	18:49:32	411	0.0051	0.0051	0.0000	60
	DSS 51	CC3	5/31	15:15:31	5/31	20:05:32	145	0.0083	0.0083	0.0001	60
2 POM XB	DSS 42	CC3	5/31	07:04:32	5/31	18:49:32	411	0.0048	0.0048	0.0000	60
	DSS 51	CC3	5/31	15:15:31	5/31	20:05:32	145	0.0083	0.0083	0.0000	60
2 POM XC	DSS 11	CC3	5/31	07:04:32	5/31	08:58:32	94	0.0046	0.0046	0.0000	60
	DSS 42	CC3	5/31	09:04:32	5/31	18:49:32	411	0.0048	0.0048	−0.0001	60
2 POM XD	DSS 11	CC3	5/31	07:04:32	5/31	08:58:32	94	0.0057	0.0057	−0.0001	60
	DSS 42	CC3	5/31	09:04:32	5/31	18:49:32	411	0.0050	0.0050	−0.0001	60
	DSS 51	CC3	5/31	15:15:31	5/31	21:26:32	224	0.0090	0.0090	0.0000	60
3 POM XB	DSS 11	CC3	5/31	07:04:32	5/31	08:58:32	94	0.0051	0.0057	0.0024	60
	DSS 42	CC3	5/31	09:04:32	5/31	18:49:32	411	0.0064	0.0067	−0.0021	60
	DSS 51	CC3	5/31	15:15:31	6/01	02:18:32	458	0.0087	0.0087	0.0007	60
4 POM XE	DSS 11	CC3	5/31	07:04:32	5/31	08:58:32	94	0.0051	0.0051	0.0006	60
	DSS 42	CC3	5/31	09:04:32	5/31	18:49:32	411	0.0051	0.0051	−0.0002	60
		CC3	6/01	07:15:32	6/01	16:20:31	520	0.0053	0.0053	0.0003	60
	DSS 51	CC3	5/31	15:15:31	6/01	02:18:32	458	0.0085	0.0085	0.0000	60
4 POM XG	DSS 11	CC3	5/31	07:04:32	5/31	08:58:32	94	0.0068	0.0068	0.0010	60
		CC3	6/01	02:57:32	6/01	03:08:32	12	0.0068	0.0221	0.0210	60
		CC3	6/01	03:41:32	6/01	04:26:32	35	0.0070	0.0117	−0.0093	60
	DSS 42	CC3	5/31	09:04:32	5/31	18:24:32	390	0.0055	0.0055	−0.0001	60
		CC3	5/31	18:25:32	5/31	18:48:32	20	0.0053	0.0081	−0.0061	60
		CC3	6/01	07:15:32	6/01	07:29:32	15	0.0041	0.0057	0.0039	60
		CC3	6/01	07:30:32	6/01	16:58:32	537	0.0054	0.0054	−0.0002	60
	DSS 51	CC3	5/31	15:15:31	5/31	15:34:31	20	0.0090	0.0090	0.0009	60
		CC3	5/31	15:35:31	6/01	02:18:32	436	0.0086	0.0086	−0.0002	60
		CC3	6/01	02:27:32	6/01	22:02:32	225	0.0093	0.0093	0.0006	60
4 POM XH	DSS 11	CC3	5/31	07:04:32	5/31	08:58:32	94	0.0066	0.0138	0.0122	60
		CC3	6/01	02:57:32	6/01	03:08:32	12	0.0065	0.0075	0.0037	60
		CC3	6/01	03:41:32	6/01	04:26:32	35	0.0056	0.0189	−0.0180	60
	DSS 42	CC3	5/31	09:04:32	5/31	18:24:32	390	0.0087	0.0087	0.0006	60
		CC3	5/31	18:25:32	5/31	18:48:32	20	0.0055	0.0178	−0.0169	60
		CC3	6/01	07:15:32	6/01	07:29:32	15	0.0041	0.0150	0.0145	60
		CC3	6/01	07:30:32	6/01	16:58:32	537	0.0068	0.0099	0.0072	60
	DSS 51	CC3	5/31	15:15:31	5/31	15:34:31	20	0.0089	0.0091	−0.0016	60
		CC3	5/31	15:35:31	6/01	02:18:32	436	0.0090	0.0105	−0.0054	60
		CC3	6/01	02:27:32	6/01	22:02:32	225	0.0092	0.0092	−0.0006	60

	DSS 42	CC3	5/31	09:04:32	5/31	18:24:32	390	0.0089	0.0090	0.0016	60
		CC3	5/31	18:25:32	5/31	18:48:32	20	0.0053	0.0160	−0.0151	60
		CC3	6/01	07:15:32	6/01	07:29:32	15	0.0041	0.0088	0.0077	60
		CC3	6/01	07:30:32	6/01	16:58:32	537	0.0089	0.0109	0.0063	60
	DSS 51	CC3	5/31	15:15:31	5/31	15:34:31	20	0.0089	0.0091	−0.0016	60
		CC3	5/31	15:35:31	6/01	02:18:32	436	0.0091	0.0107	−0.0056	60
		CC3	6/01	02:27:32	6/02	06:29:32	367	0.0097	0.0097	−0.0004	60
5 POM YB	DSS 11	CC3	5/31	07:04:32	5/31	08:58:32	94	0.0064	0.0113	0.0093	60
	DSS 42	CC3	5/31	09:04:32	5/31	18:24:32	390	0.0088	0.0090	0.0017	60
		CC3	5/31	18:25:32	5/31	18:48:32	20	0.0053	0.0160	−0.0151	60
		CC3	6/01	07:15:32	6/01	07:29:32	15	0.0040	0.0083	0.0073	60
		CC3	6/01	07:30:32	6/01	16:58:32	537	0.0091	0.0110	0.0063	60
	DSS 51	CC3	5/31	15:15:32	5/31	15:34:31	20	0.0089	0.0091	−0.0017	60
		CC3	5/31	15:35:31	6/01	02:18:32	436	0.0091	0.0107	−0.0056	60
		CC3	6/01	02:27:32	6/02	00:34:32	372	0.0096	0.0097	−0.0004	60
5 POM YC	DSS 11	CC3	6/02	02:52:32	6/02	03:02:32	11	0.0054	0.0054	−0.0008	60
	DSS 51	CC3	6/02	00:35:32	6/02	02:28:32	107	0.0116	0.0116	0.0002	60
FINAL XA	DSS 11	CC3	6/02	02:52:32	6/02	03:37:32	44	0.0405	0.1920	−0.1880	60
	DSS 51	CC3	6/02	00:35:32	6/02	02:28:32	104	0.0145	0.0204	−0.0143	60
FINAL XB	DSS 11	CC3	6/02	02:52:32	6/02	03:37:32	44	0.0048	0.0048	−0.0004	60
		CC3	6/02	03:38:32	6/02	05:01:32	63	0.0040	0.0040	−0.0002	60
	DSS 51	CC3	6/02	00:35:32	6/02	02:28:32	102	0.0093	0.0094	−0.0005	60
FINAL XC	DSS 11	CC3	6/02	02:52:32	6/02	03:37:32	44	0.0049	0.0050	0.0009	60
		CC3	6/02	03:38:32	6/02	05:28:32	78	0.0041	0.0041	−0.0002	60
	DSS 51	CC3	6/02	00:35:32	6/02	02:28:32	102	0.0093	0.0093	0.0000	60
FINAL YB	DSS 11	CC3	6/02	02:52:32	6/02	03:37:32	46	0.0046	0.0047	0.0006	60
		CC3	6/02	03:38:32	6/02	05:06:32	74	0.0042	0.0042	−0.0005	60
	DSS 51	CC3	6/02	00:35:32	6/02	02:28:32	106	0.0092	0.0092	−0.0003	60
Best postmaneuver estimate	DSS 11	CC3	5/31	07:14:32	5/31	08:58:32[a]	89	0.0047	0.0047	−0.0003	60
		CC3	6/02	02:52:32	6/02	03:37:32	44	0.0059	0.0112	0.0095	60
		CC3	6/02	03:38:32	6/02	05:28:32	78	0.0041	0.0049	−0.0008	60
	DSS 42	CC3	5/31	09:04:32[b]	5/31	18:24:32	390	0.0058	0.0059	0.0009	60
		CC3	5/31	18:25:32[c]	5/31	18:48:32	20	0.0053	0.0082	−0.0062	60
		CC3	6/01	07:15:32	6/01	07:29:32[a]	15	0.0042	0.0099	0.0090	60
		CC3	6/01	07:30:32[b]	6/01	16:58:32	537	0.0053	0.0055	0.0013	60
	DSS 51	CC3	5/31	15:15:31	5/31	15:34:31[a]	20	0.0089	0.0095	0.0032	60
		CC3	5/31	15:35:31[b]	6/01	02:18:32	436	0.0086	0.0086	−0.0008	60
		CC3	6/01	17:03:32[b]	6/02	02:28:32	474	0.0095	0.0095	−0.0009	60

[a]Data before this time was taken below 17-deg local elevation.

[b]Data after this time was taken above 17-deg local elevation.

[c]Data after this time was taken below 17-deg local elevation.

Table 11. Behavior of state vector and predicted unbraked impact time during AMR backup computations

Orbit ID	June 2, 1966 epoch, GMT	x, km	y, km	z, km	Dx, km/s	Dy, km/s	Dz, km/s	Predicted unbraked impact time (June 2, 1966), GMT	Data span
5 POM YB	00:35:14.000	−186813.13	−276085.45	−124743.59	−0.43332421	−0.87854055	−0.25172679	06:15:12.745	Midcourse to $E - 5$ h, 40 min
5 POM YC	00:35:14.000	−186811.39	−276086.69	−124742.40	−0.43330820	−0.87854835	−0.25172641	06:15:13.846	$E - 5$ h, 40 min to $E - 3$ h, 15 min
FINAL XA	00:35:14.000	−186810.86	−276086.73	−124743.29	−0.43330133	−0.87855310	−0.25173526	06:15:14.352	$E - 5$ h, 40 min to $E - 2$ h, 40 min
FINAL YB[a]	00:35:14.000	−186810.62	−276086.93	−124742.57	−0.43329332	−0.87855813	−0.25173589	06:15:14.519	$E - 5$ h, 40 min to $E - 1$ h, 10 min
FINAL XC	00:35:14.000	−186810.52	−276085.06	−124742.78	−0.43328157	−0.87857218	−0.25172242	06:15:14.986	$E - 5$ h, 40 min to $E - 44$ min
Postflight $E - 5$h, 40 min, estimate (similar to 5 POM YB)[b]	00:35:14.000	−186810.15	−276085.32	−124741.39	−0.43330754	−0.87854531	−0.25173736	06:15:14.930	Midcourse to $E - 5$ h, 40 min
Current best postmaneuver estimate[b]	00:35:14.000	−186810.08	−276085.91	−124741.29	−0.43329360	−0.87855480	−0.25173755	06:15:15.066	Midcourse to $E - 44$ min (all postmaneuver data)

[a]Inflight solution used to compute transmission time of AMR backup command.

[b]Nongravitational trajectory perturbations solved for and corrections applied during computation.

Prior to retroengine ignition, an additional orbit solution (FINAL XC) was obtained. For this computation, data up to 45 min before encounter were used. The predicted unbraked impact time from this solution was 0.467 s later than that predicted by the solution used for the AMR backup (FINAL YB). Since this difference was not significantly outside FINAL YB, the 0.444-s uncertainty, the AMR backup sequence was allowed to proceed as planned.

The time obtained from ground station telemetry recordings at which the AMR provided a mark pulse on board the spacecraft was 06:14:38.461, ±0.005 s.[5] This observed time was 0.465 s later than the nominal AMR mark time used for the backup computations. Had the FINAL XC solution been available for the backup computations, the difference between the nominal and observed AMR mark time would have been negligible.

Postflight analysis of the postmaneuver tracking data indicated that the changes in predicted impact time during the last 5 to 6 h of flight were possibly caused by nongravitational trajectory perturbations that were not accounted for in the backup computations before AMR. That is, it appeared that the spacecraft trajectory was being perturbed continuously throughout the entire postmaneuver transit phase by a combination of nongravitational perturbations. The effects of these perturbations were not accounted for in the postmaneuver orbit computations. Hence, at the epoch to be used for the AMR backup computations, the estimated position and velocity of the spacecraft differed from the true position and velocity. As previously stated, the philosophy used for the AMR computations was to fit only near-encounter data, starting from an initial epoch approximately 5 h, 40 min, from encounter. A change in the state vector at this epoch was noted during the inflight computations. This, of course, resulted in a change in predicted impact time. These changes were not observed in the postflight computations in which the trajectory perturbations were corrected. Table 11 shows the behavior of the state vector at the $E - 5$ h, 40 min, epoch and the resulting predicted unbraked impact times. It is significant to note that even with the uncorrected trajectory perturbations in the inflight computations, the difference between the estimated unbraked impact time provided for the AMR backup, and the current best estimate is within the 0.5 s desired OD accuracy.

[5]This time was based on analysis of the ground station telemetry recordings.

H. Observations and Conclusions

The orbit determination inflight results can be evaluated only by comparing them with the results obtained from the postflight computations. The degree to which these results agree is influenced primarily by the success attained in detecting and eliminating bad or questionable tracking data from the inflight computations and in accounting for all trajectory perturbations. Of these, the largest variations are usually caused by bad or questionable data resulting from equipment malfunction, incorrect time information, and incorrect frequency information. Other than gross blunder points, these data are not easily detected unless two-way doppler data are available from more than one station. That is, the least-squares method used to fit data in the SPODP gives no information on constant data biases when data are available from only one station. Therefore, a comparison can be made only when data from more than one source are available.

1. Exploration of bad data points. During premaneuver tracking, there was only one period during which a significant amount of two-way doppler was unusable. This bad data block occurred during the first hour and ten minutes of DSS 11 two-way tracking. The bad data was caused by an equipment malfunction at DSS 11, which was subsequently corrected. However, the exact time that the repair was completed was not known. As a consequence, some of the bad data were included in the orbit solution used for the final midcourse computations. A safety margin would normally be used to ensure that no bad data were included; but in this case, the DSS 11 was very critical, and an attempt was made to obtain as much data as possible. That is, the only data available up to this point (at least from a committed station) was from DSS 51. Therefore, the DSS 11 data were required not only to validate the previous data but, also, to obtain a better estimate of the orbit in terms of the uncorrected impact point, the uncertainties associated with this point, and the direction of these uncertainties. At this point in the mission, there is not enough time to make the computations required to isolate or detect bad data blocks and, then, make a final pre-midcourse orbit computation; if the maneuver is to be executed at the nominal time, there is only one hour allocated for the final pre-midcourse orbit computations. At the beginning of this time period there is usually one hour of DSS 11 data available. Since these data were bad, it was necessary to wait until some good data were accumulated, which thereby reduced the effective final premaneuver orbit computation time. Inflight, the estimated premaneuver orbit error was 10 to 15 km on the lunar surface. This was

based on the assumption that the DSS 51 data were good which, in turn, was based on a data-consistency-orbit computation which indicated that DSS 51 data and data from a noncommitted station (DSS 61) were consistent. Had this assumption been wrong, the premaneuver orbit error could have been in excess of 100 km.

The foregoing discussion should certainly demonstrate the requirement for redundant tracking coverage during the early part of the mission. Provisions should be made in the mission sequence of events to allow switching of transmitter assignments (two-way doppler mode) from one station to another on a periodic basis. Such a tracking coverage pattern would ensure that two-way doppler data were available from more than one station prior to the end of the 3-h time block allocated for the data consistency orbit computations. As a minimum, 3 h of redundant coverage would be required. It would appear that the cost associated with obtaining this additional coverage is small, compared with the advantages gained by not having to execute a second midcourse correction. There is no way of preventing occasional ground station equipment malfunctions. However, the time required to detect such malfunctions can be minimized by utilizing a residual plotting program. This program obtains tracking data residuals by comparing the observed data values with predicted data values, and plots the results in near real time on a plotter in the FPAC area.

During the postmaneuver tracking, no usable two-way doppler data were obtained during the entire DSS 11 second view period. Again, this was due to equipment malfunction which, in this case, affected the station transmitter. Since the orbit solutions based on previous postmaneuver tracking data indicated that a second midcourse correction would not be required, the loss of this data was not critical. The nature of this malfunction, however, should clearly demonstrate one of the benefits to be gained by redundant early tracking coverage, which eliminates the need for a second midcourse correction.

2. *Comparison between inflight and postflight results.* The most meaningful comparison between inflight and postflight orbit determination results can be made by examining the critical target parameters – namely, the unbraked impact time and impact location. These can, in turn, be compared with independent observations by adjusting the unbraked impact point to account for the terminal attitude maneuver and retrograde descent, and by extrapolating the observed AMR mark time to the lunar surface. These results are summarized in Table 12. In the table, it can be seen that the inflight premaneuver impact point was in error by 0.102 deg in latitude and 0.301 deg in longitude. Both, however, were within the uncertainty associated with the inflight estimate. These absolute differences can most likely be reduced by the redundant early tracking coverage scheme proposed above. The inflight postmaneuver impact point associated with the orbit solution (5 POM YB) used for the terminal attitude maneuver computations was in error by 0.060 deg in latitude and 0.022 deg in longitude. It should be noted that these errors are within the stated uncertainties. Postflight analysis indicates that these errors most likely result from nongravitational trajectory perturbations that were not accounted for in the inflight computations. The inflight predicted unbraked impact time associated with the orbit solution (FINAL YB) used to provide the AMR backup was in error by 0.497 s, which was slightly outside the 1σ uncertainty of 0.44 s. This, also, is most likely due to the nongravitational trajectory perturbations that were not accounted for in the inflight computations through 5 POM YB. That is, predicted impact time from AMR backup computations in which only near-moon data were used moved such that the error decreased as additional data were added to the solution. However, the trajectory at the initial epoch (i.e., time of last data point is 5 POM YB solution) was so far off that the true trajectory had not been precisely determined by the time that the AMR backup number was required.

The estimated landing point determined by transit tracking data (the current best postmaneuver orbit), and the landing points determined by independent observations are presented in Table 12. One of the independent observations was obtained by processing tracking data from the landed spacecraft. Two others were obtained via optical methods – correlating *Surveyor I* television photos of surrounding lunar horizon features with earth-based telescope photos of the same lunar region. In the table it can be seen that Jaffe's initial estimate of location (Ref. 6) falls outside of the 3σ dispersion ellipse associated with the transit location. Whitaker's estimate (Ref. 7), which was based on more recent earth telescope photos, was well within the 3σ uncertainty of the transit estimate. The estimated location based on preliminary analysis of the landed spacecraft tracking data (by C. Cary, JPL) also lies within the 3σ dispersion ellipse. The estimate from the *Lunar Orbiter III* photograph is also shown. The *observed* unbraked impact time (obtained by extrapolating the observed AMR mark time to the

Table 12. Comparison between inflight and postflight target parameters

Data source	Estimated impact or landed location		Uncertainty about estimated impact point, 1σ dispersion ellipse[a]			Time of estimated unbraked impact time,[b] GMT	1σ uncertainty in estimated unbraked impact time,[c] s
	South latitude, deg	West longitude, deg	SMAAD, deg	SMIAD, deg	THETA, deg		
Premaneuver uncorrected							
Inflight OD	11.527 ±0.119	54.449 ±0.067	0.130	0.035	36.962	05:29:10.724	7.628
Postflight OD	11.425 ±0.360	54.147 ±0.143	0.360	0.139	57.249	05:28:59.537	13.240
Postmaneuver transit							
Inflight OD	2.462 ±0.061	43.307 ±0.017	0.061	0.015	98.803	06:15:14.519	0.444
Postflight OD	2.402 ±0.084	43.329 ±0.069	0.101	0.040	127.429	06:15:15.066	0.783
Observed unbraked impact time[d]	—	—	—	—	—	06:15:15.016	0.005
Post landing							
Postflight OD (adjusted)[e]	2.439 ±0.084	43.335 ±0.069	0.101	0.040	127.429		
L. D. Jaffe	2.15[f]	43.35[f]					
E. A. Whitaker	2.57 ±0.02	43.34 ±0.02					
Post touchdown OD[g]	2.500 ±0.017	43.347 ±0.008					
Lunar Orbiter III photograph	2.45	43.2					

[a]1σ dispersion ellipse on lunar surface where SMAAD = Semimajor axis, SMIAD = semiminor axis, and THETA = orientation angle of semimajor axis measured counterclockwise from lunar equator.

[b]GMT refers to June 2, 1966. All OD estimated unbraked impact times are based on an assumed lunar elevation of 1735.6 km.

[c]OD unbraked impact time uncertainty includes an *a priori* uncertainty of 1.0 km in lunar elevation.

[d]Obtained by extrapolating observed AMR mark time to lunar surface.

[e]OD unbraked impact point adjusted for effect of terminal attitude maneuver and terminal descent (computed in terminal guidance program).

[f]No uncertainty stated.

[g]Preliminary values obtained by processing post-landing tracking data (C. Cary, JPL).

lunar surface) and the impact time predicted by the current best postmaneuver orbit solution, based on a lunar elevation of 1735.6 km, differ by only 0.05 s.

3. Conclusions. Based on the results of the comparison between inflight and postflight results, two principal conclusions can be drawn.

First, the premaneuver OD requirements were met, even though errors existed in the premaneuver tracking data. Improvement can be obtained by providing redundant early tracking coverage.

Second, the postmaneuver OD requirements were met, even though nongravitational trajectory perturbations existed and one entire pass of tracking data was lost. It is significant that the true trajectory was reestablished (at least within OD requirements) by use of near-moon tracking data, only, during the AMR backup computations.

IV. Postflight Analysis of the DSS Transponder Tracking Data for *Surveyor I*

This section presents the best estimate of the *Surveyor I* flight path and other significant results obtained from the DSS tracking data. Analysis verified that both the premaneuver and postmaneuver inflight orbit solutions were within the *Surveyor* Project orbit determination accuracy requirements, even though anomalies existed in the premaneuver tracking data and postmaneuver trajectory. The 0.05-s time difference between orbit determination program (ODP) predicted and observed AMR mark time, and the close agreement between predicted and observed landing point are both excellent measures of the accuracy of the estimated flight path. Also, the inflight philosophy of estimating only a minimum parameter set (i.e., the six components of the spacecraft position and velocity vectors) for the orbital computations was validated. This is based on (1) the assumption that the trajectory anomalies are no

worse than those observed during this mission, and (2) that a good set of physical constants and tracking station location parameters are used.

The tracking data were divided into two logical blocks: (1) premaneuver data taken between transfer orbit injection and the first attitude maneuver prior to midcourse thrust and (2) postmaneuver data taken between the time of Canopus reacquisition, after midcourse thrust, and the last two-way doppler data point prior to the terminal maneuver. The single precision orbit determination program of JPL was the principal analysis tool.

A. Summary of Data Used In Postflight Orbit Determination

For the postflight orbital computations and analyses, only two-way doppler data were used. Angular data and three-way noncoherent doppler data were available but were not used, since neither of these two data types would significantly contribute to the estimate of the spacecraft's flight path. Table 4 lists the number of data points used both in real-time and in postflight analysis. A comparison shows that about the same amount of two-way doppler data points were used for the postflight computations as for the inflight computations.

The same data weighting philosophy as outlined for the inflight orbital computations in Section III was used for the postflight analysis. Therefore, the same numerical values were used for the two-way doppler data.

B. Premaneuver Orbit Based on Premaneuver Tracking, Only

Prior to starting the analysis of the premaneuver tracking data, all known or suspected bad data points were removed. An orbit solution, based on estimating the standard 6 parameters, only, using both DSS 51 and DSS 11 data, was obtained and mapped forward to the target. Examination of the residual plots indicated a poor fit to the data. The same type of computation was repeated, but this time only DSS 51 data were used to obtain the solution, and the DSS 11 data were weighted out. This means that the SPODP does not use data that has been weighted out to obtain the orbit solution. The program does compute and plot residuals for such data. Residual plots from this solution indicated that the DSS 11 data was biased ($\approx$ 0.05 Hz, which is roughly equivalent to 0.765 m/s) with respect to the DSS 51 data. The predicted unbraked impact points from these two solutions compared very favorably (i.e., $|\Delta \text{ lat}| \cong 0.06$ deg, $|\Delta \text{ lon}| \cong 0.06$ deg). Therefore, an attempt was made to remove the effect of the bias by expanding the estimated parameter set from 6 to 15 to include the three station location parameters for both stations. A 15 × 15 orbit solution was then obtained and mapped forward to target. Examination of the residual plots (Figs. 10, 11, 12) indicate that the data fit was very good. It should be

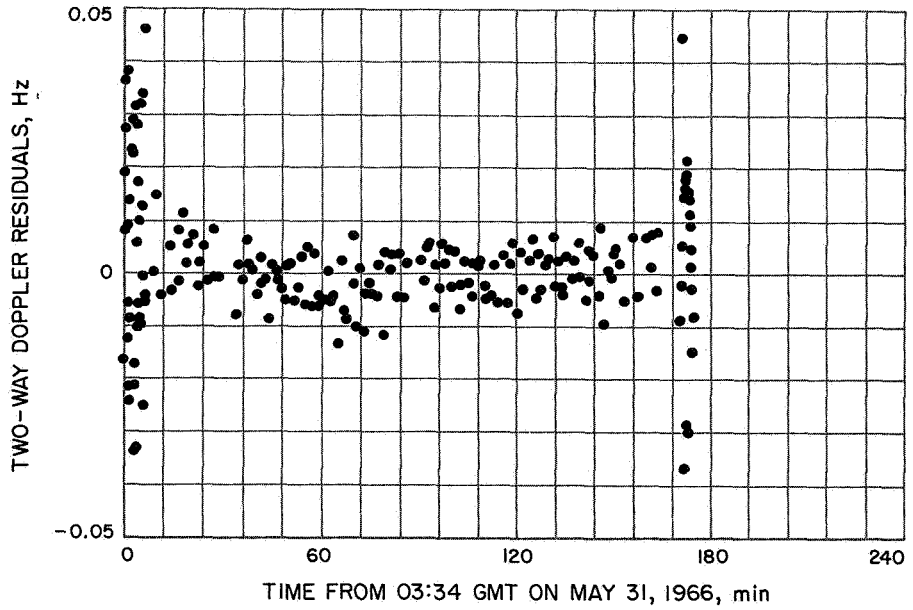

Fig. 10. DSS 11 premaneuver two-way doppler residuals

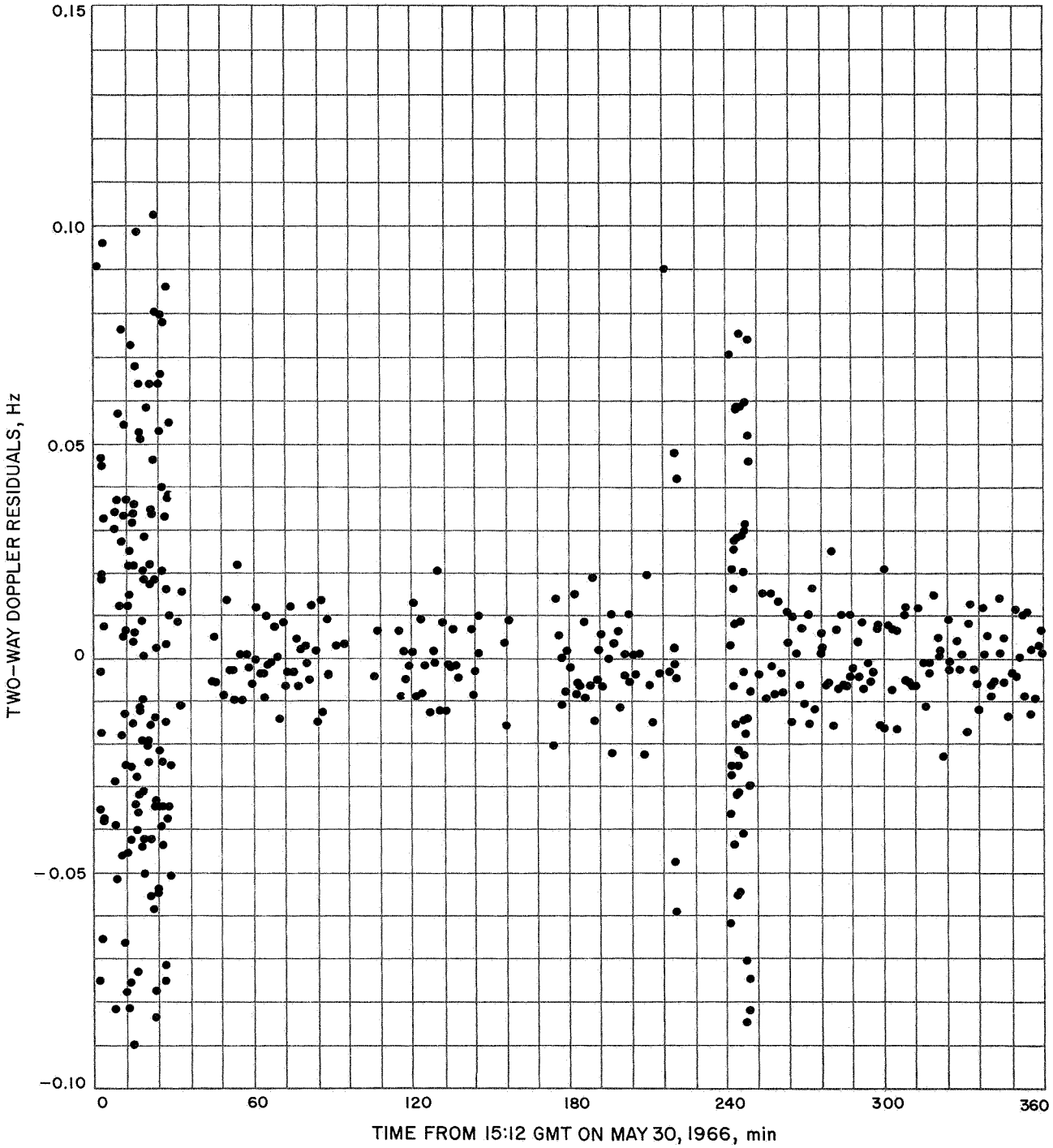

Fig. 11. DSS 51 premaneuver two-way doppler residuals

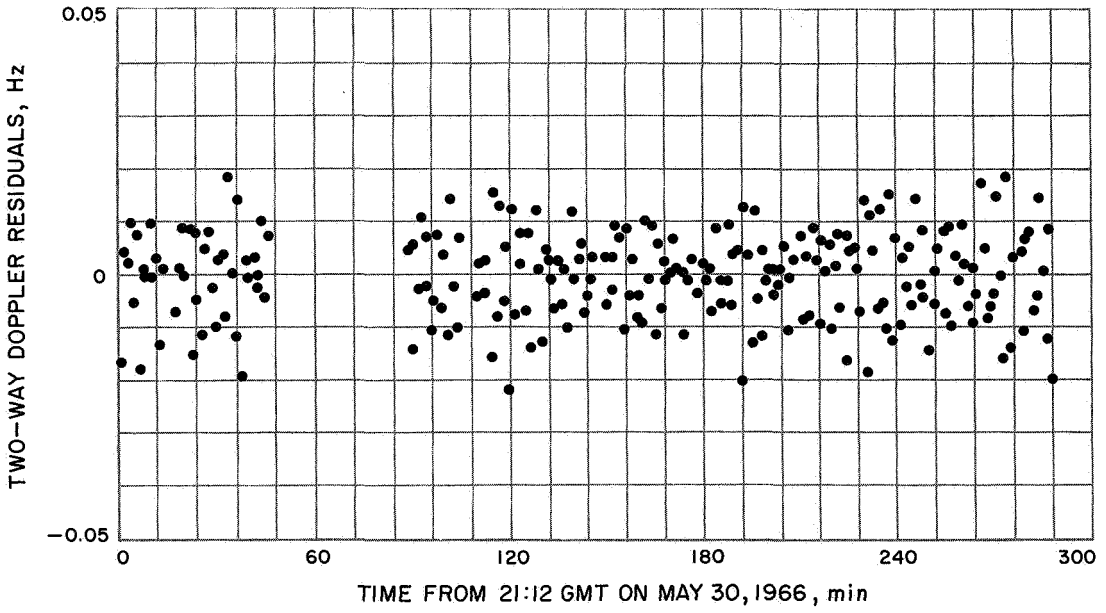

Fig. 12. DSS 51 premaneuver two-way doppler residuals

noted that the large peak-to-peak variations, seen in portions of Figs. 10 and 11, do not represent excessive data noise. These variations are due to the 1 sample/10-s sample rate and are as expected. All other residuals seen in the figures are based on a sample rate of 1 sample/60 s. The differences between the nominal station location parameters and the values obtained from this solution are negligible for DSS 51 – e.g., the change from the nominal longitude was 0.000003 deg, or ≅ 3 m. However, the change from the nominal longitude for DSS 11 was 0.0004 deg, or ≅ 40 m. This longitude change could represent a station timing error of approximately 0.1 s, which is unlikely, or it could result from an error in station longitude. The latter does not seem likely, since consistent estimates[6] of the station longitude difference between the Johannesburg Deep Space Station and the Echo Deep Space Station at Goldstone, located approximately 7 mi from DSS 11, were obtained from the *Ranger* missions, and the longitude difference between the Echo Deep Space Station and the Pioneer Deep Space Station at Goldstone has been well established by land survey. If the difference between DSS 12 and DSS 11 is subtracted[7] from the difference between DSS 51 and DSS 12, the longitude difference between DSS 51 and DSS 11 will be well established, and the longitude of DSS 11 can be uniquely determined with respect to the DSS 51 longitude. Based on this method, a nominal longitude difference of 215.46541 deg between DSS 51 and DSS 11 is obtained. A comparison between the nominal value and the value obtained from the 15 × 15 solution indicates an absolute delta longitude difference of 0.0008 deg (≅ 80 m), which does not appear reasonable.

Another contributing error could be in the ground station transmitter reference frequency; however, an error in transmitter frequency of approximately 40 Hz would be required to account for the 0.05-Hz bias. Since the transmitter frequency is continuously monitored at the ground station, an error of this magnitude does not seem possible. This apparent data bias is still being investigated. However, use of the biased data does not degrade the premaneuver orbit solution. This is evidenced by the negligible difference between the predicted unbraked impact points of the two 6 × 6 solutions.

Based on the above, the 15 × 15 solution is considered to be the best estimate of the spacecraft premaneuver orbit. The uncorrected impact point predicted by this solution (latitude = 3.25°S, longitude = 54.25°W) was 8.18 deg south and 10.42 deg west of the prelaunch aim point (latitude = 3.25°S, longitude = 43.83°W). This is roughly equivalent to 245.4 km and 312.6 km, respectively. Other numerical values from this solution are presented in Tables 5 and 6. The number of data points, together with the data noise statistics, are given

[6]These estimates were all within 0.00011 deg, or ≅ 11 m.

[7]By convention, the ODP performs all topocentric computations referenced to east longitude. Subtraction is required since DSS 11 is east of DSS 12, and DSS 51 is east of DSS 11.

in Table 7. A graphical comparison between the predicted unbraked impact (in the **B**-plane system) of this solution and the inflight solutions may be seen in Fig. 7.

C. Postmaneuver Orbit Based on Postmaneuver Tracking, Only

Prior to starting the analysis of the postmaneuver tracking data, all known or suspected bad data points were removed. As stated in Section III, DSS 11 did not provide any usable tracking data during its second post-midcourse view period because of ground station equipment malfunction. The objective of the analysis in this section was to obtain an orbit solution based on processing all postmaneuver tracking data in one block. This differed from the inflight computations, which required that the data be processed in two blocks to meet the AMR backup requirements. During the inflight computations, the following minor discrepancies were noted:

(1) There was a glitch in the DSS 42 doppler residuals that coincided with a gyro drift check period.

(2) In general, the postmaneuver data did not fit as well as expected – i.e., the long term waveform seen in the doppler residuals was not as expected.

(3) The predicted unbraked impact changed more than expected during the orbit computations made in the last 10 to 14 h of the flight; after the fourth post-midcourse orbit, the predicted unbraked impact time continuously increased as later tracking data was included in the fit. The changes became much smaller when only the near-encounter data were used in the orbit computations. This implied that there was some long-term trajectory perturbation that was not being taken into account.

The first item investigated was the apparent glitch in the DSS 42 data, which occurred during the period from 07:34:15 to 09:52:16 GMT on June 1, 1966. Starting at 07:34:15 GMT, the doppler residuals appeared to drift in a negative direction until 09:52:16, at which time a definite positive shift of 0.01 Hz ($\cong$ 0.153 m/s) was noted (see Fig. 8). The first time coincided with a command to the spacecraft to switch to *inertial mode*. In this mode, the attitude of the spacecraft is controlled by error signals from gyros located on the three spacecraft axes. The second time coincided with a command to the spacecraft to switch to *sun acquire mode*, which effectively switches control of the sun axis attitude from a gyro to the spacecraft sun sensor. Other gyro drift checks, of the same time duration, were made during the postmaneuver transit, but nothing was observed in the doppler residuals. At first it was thought that the shift could be caused by an erroneous transmitter frequency. However, examination of the tracking station

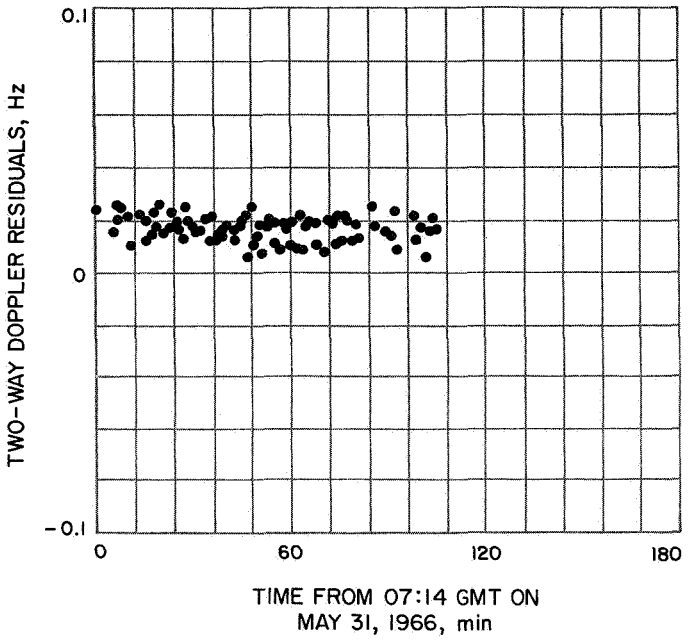

Fig. 13. DSS 11 postmaneuver two-way doppler residuals: Trajectory *not* corrected for perturbations

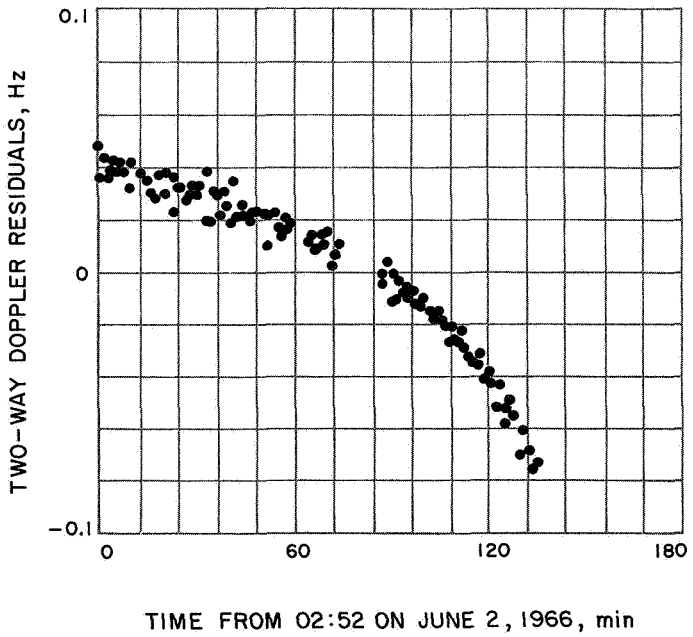

Fig. 14. DSS 11 postmaneuver two-way doppler residuals: Trajectory *not* corrected for perturbations

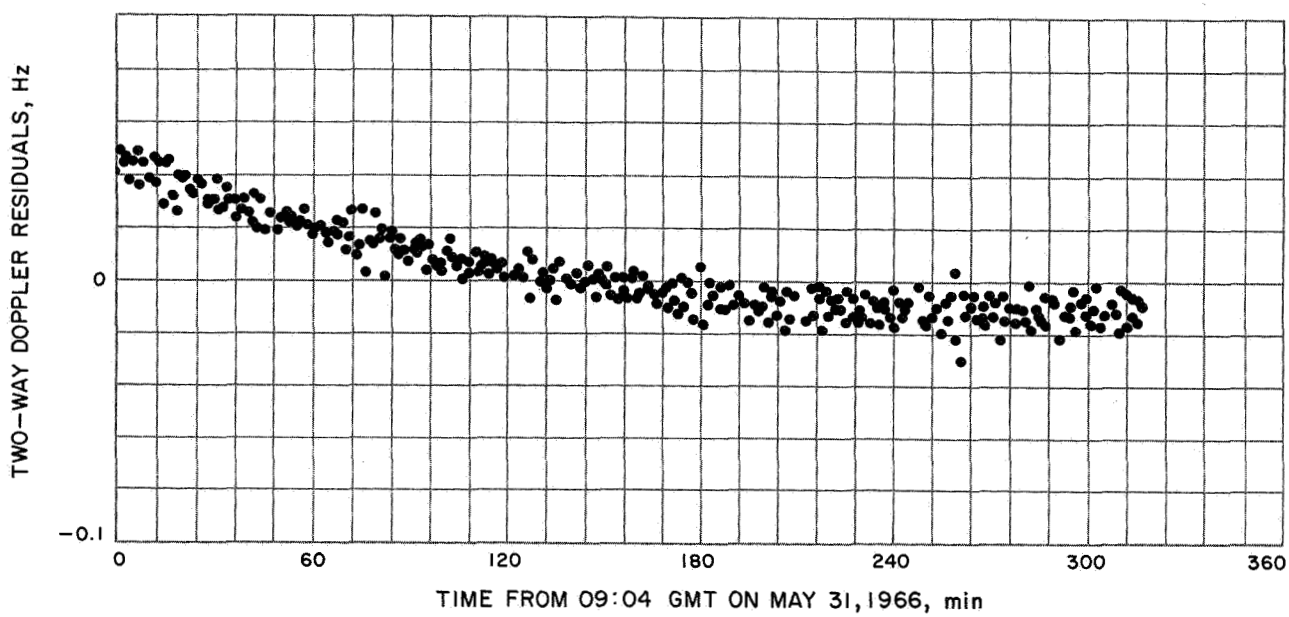

Fig. 15. DSS 42 postmaneuver two-way doppler residuals: Trajectory *not* corrected for perturbations

records verified that the reported frequency was correct, and no station malfunctions were noted during this period. The attitude control telemetry and analog records were then examined, but no anomalies were noted. Both the attitude and vernier fuel records were examined; again, no anomalies were discovered. A number of orbit computations were then made to determine if the shift represented an actual spacecraft velocity change and to determine if the use of these data would degrade the postmaneuver orbit solution. One solution was obtained with all postmaneuver data and another was obtained with only the data taken after the shift. These two solutions, plus a third solution in which the data was processed as though a velocity change had occurred, were in good agreement. Based on this agreement, it was decided to retain these data in the postmaneuver orbit computations.

The next item investigated was the poor fit of the postmaneuver data. A 6 × 6 orbit solution based on all postmaneuver data was obtained and mapped forward to target. Examination of the residual plots (Figs. 13 to 22) indicated a very poor fit. The predicted unbraked impact location from this solution was in very good agreement with the inflight results, but the impact time was approximately 0.5 s earlier than the observed time. Since the only obvious anomaly observed in the doppler residuals had been thoroughly investigated as indicated in the previous paragraph, the next step was to reverify that all data were consistent. A number of 6 × 6 orbit

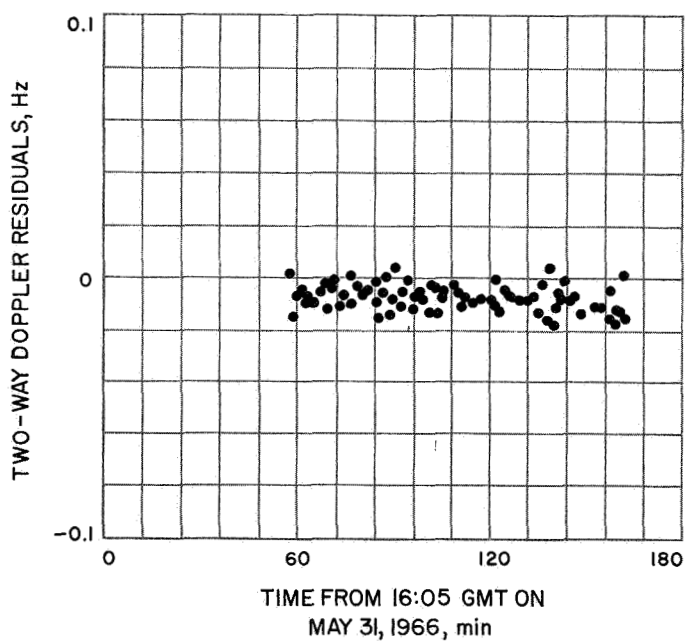

Fig. 16. DSS 42 postmaneuver two-way doppler residuals: Trajectory *not* corrected for perturbations

computations were made using various combinations of data from the three stations. A comparison of the resulting orbit solutions indicated that all data were consistent. An attempt was made to improve the fit by expanding the estimated parameter set to 15 to include the station location parameters of the three stations.

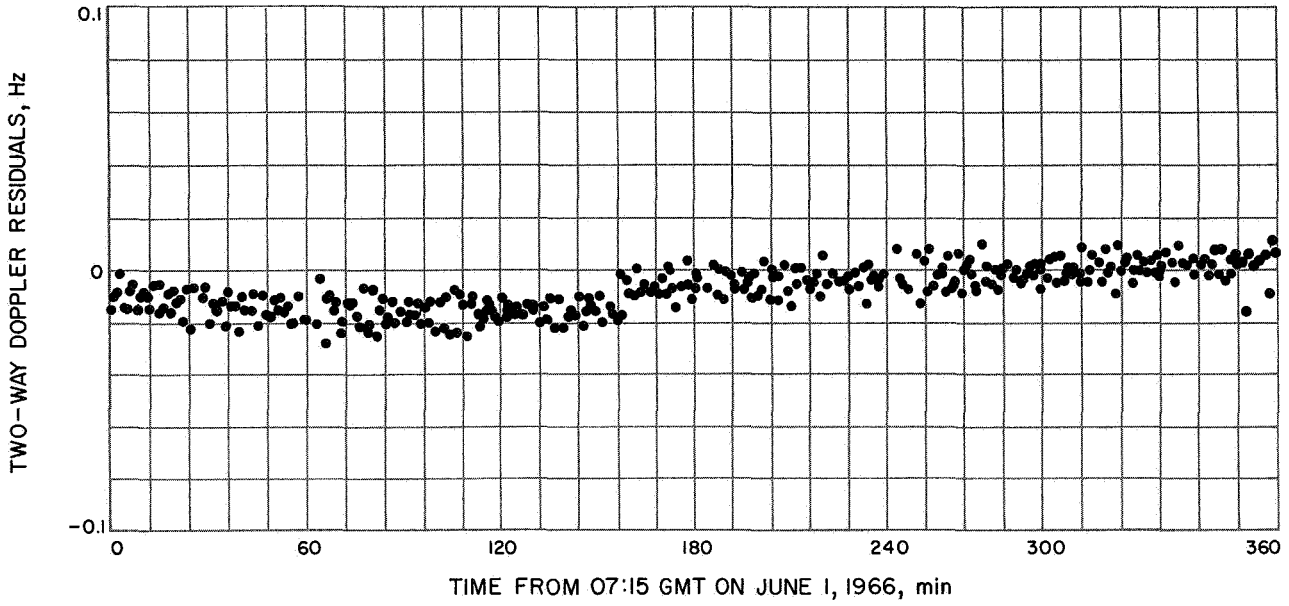

Fig. 17. DSS 42 postmaneuver two-way doppler residuals: Trajectory *not* corrected for perturbations

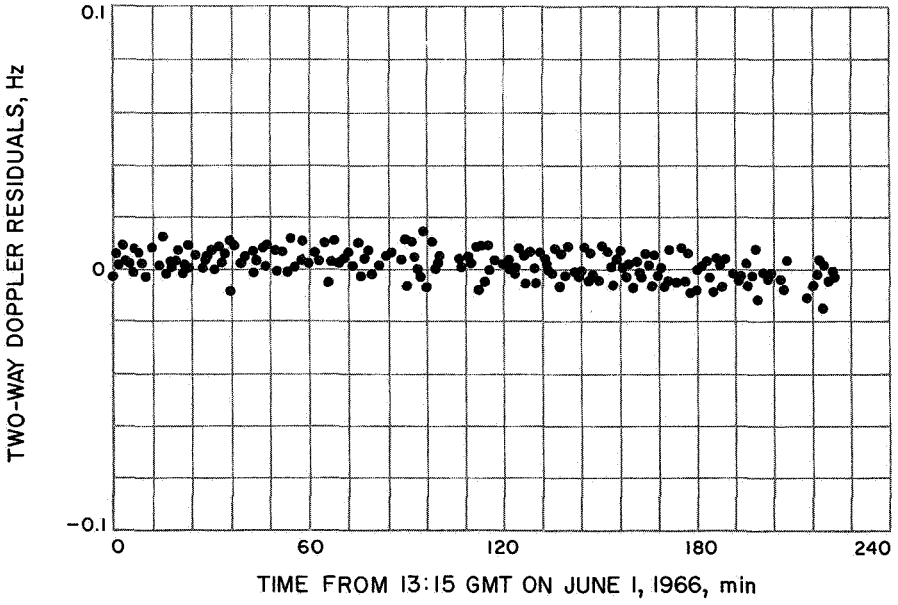

Fig. 18. DSS 42 postmaneuver two-way doppler residuals: Trajectory *not* corrected for perturbations

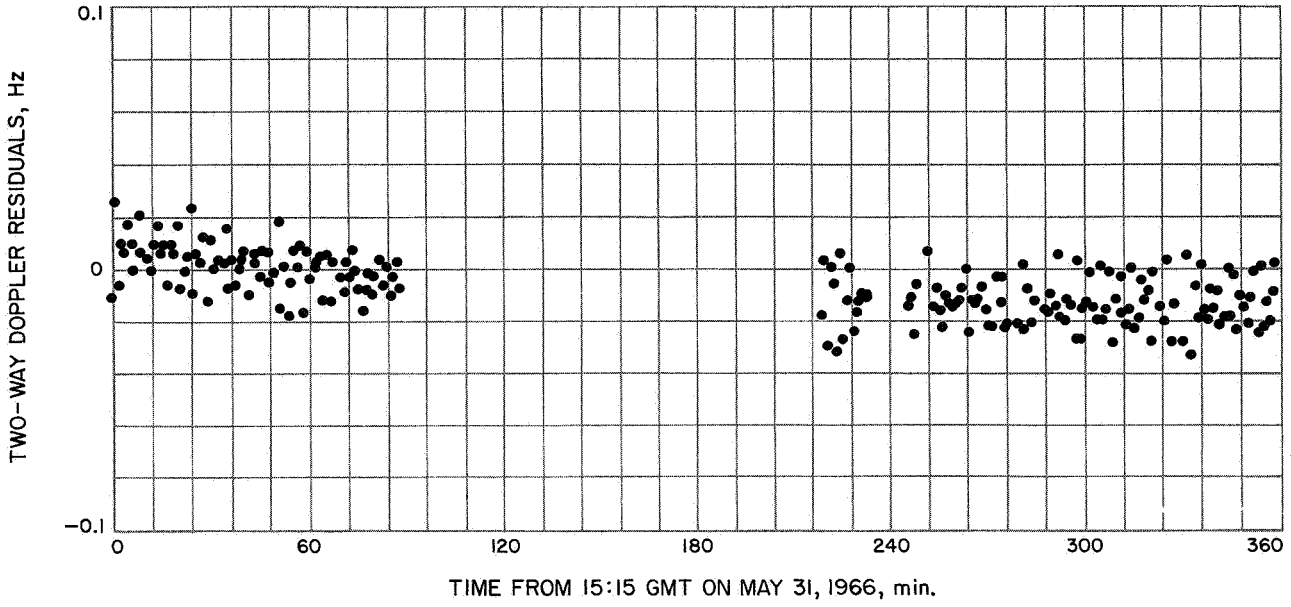

Fig. 19. DSS 51 postmaneuver two-way doppler residuals: Trajectory *not* corrected for perturbations

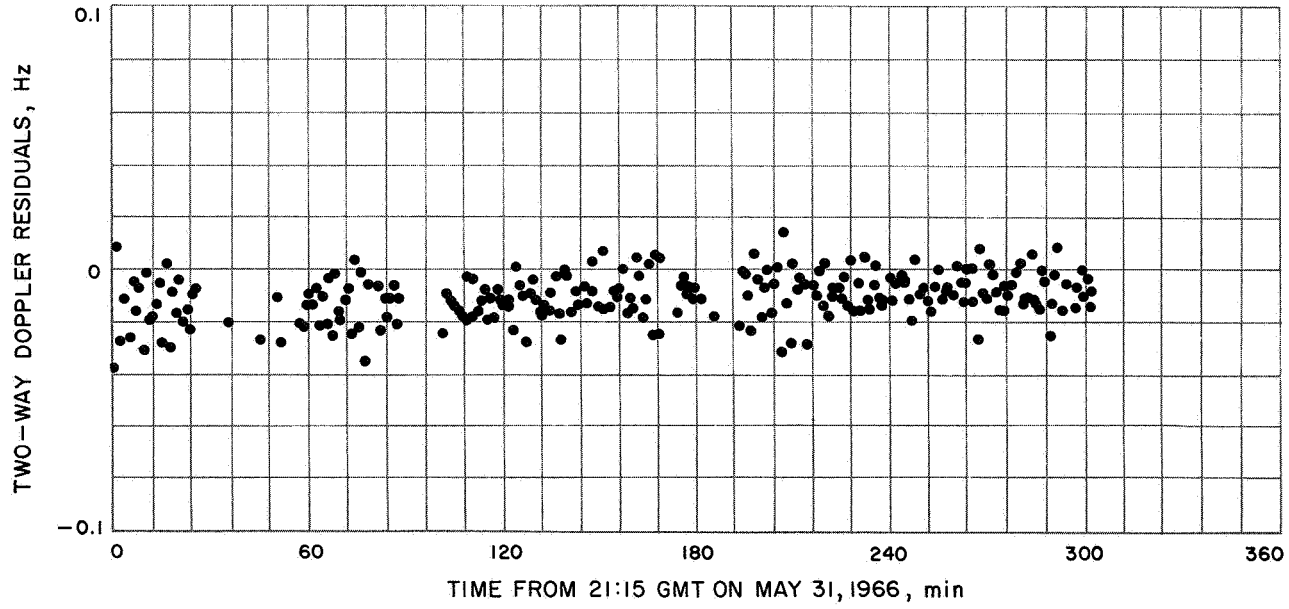

Fig. 20. DSS 51 postmaneuver two-way doppler residuals: Trajectory *not* corrected for perturbations

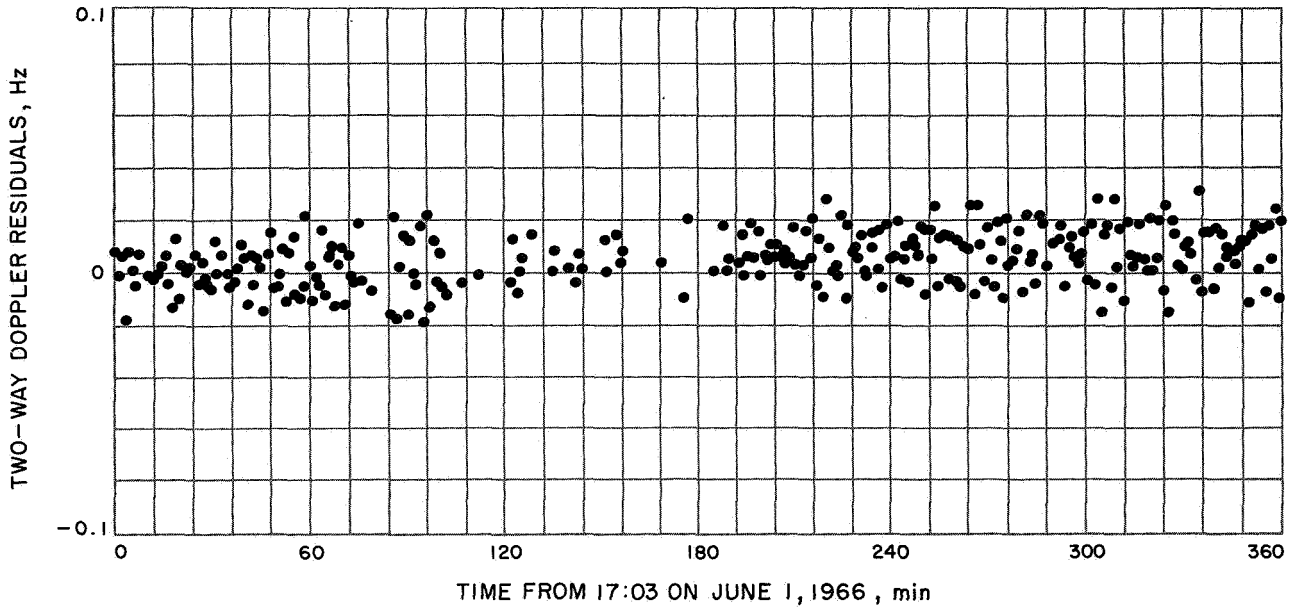

Fig. 21. DSS 51 postmaneuver two-way doppler residuals: Trajectory *not* corrected for perturbations

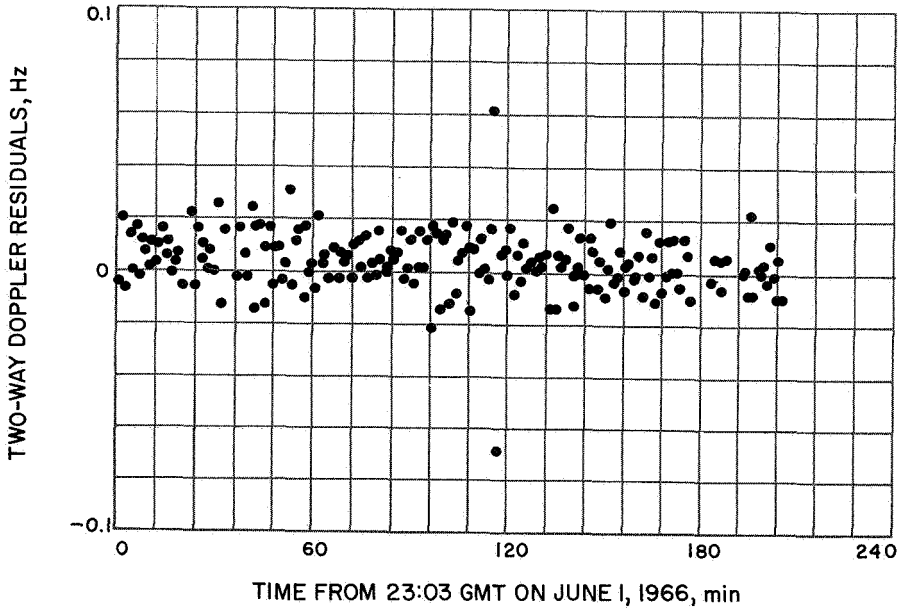

Fig. 22. DSS 51 postmaneuver two-way doppler residuals: Trajectory *not* corrected for perturbations

Examination of the residual plots from this 15 × 15 solution still did not indicate a good fit. In addition, the predicted target parameters did not agree with any previous results, and the estimated station longitudes deviated by as much as four standard deviations (4σ) from the nominal values. The estimated parameter set was expanded to 17 and now consisted of the standard six parameters, plus the nine-station location parameters, the earth's gravitational coefficient ($GM_{\oplus}$), and the moon's gravitational coefficient ($GM_{\mathbb{C}}$). The resulting 17 × 17 solution was no better than the 15 × 15 solution, at least in terms of data fit. The estimated station longitudes were within 1σ of nominal values, but the physical constants $GM_{\oplus}$ and $GM_{\mathbb{C}}$ differed from the nominal values by 5 to 6 σ.

A thorough examination of the inflight computations revealed that the data fit appeared reasonable until data from the last half of the second postmaneuver view period of DSS 51 was added to the orbit solution. Also, it was seen that a very good data fit was obtained during the AMR backup computations when only the near encounter data was used to obtain the orbit solution. Starting from the last good inflight data fit, data were added to the computations in 2-h blocks until the fit was degraded. Careful scrutiny of the doppler residuals in this region revealed a slight shift occurring in the residuals at 00:00 GMT on June 2, 1966. First, all pertinent tracking station records were examined, but no malfunctions or anomalies were noted that could explain the shift. This type of shift could occur if there were a bad point on the lunar ephemeris tape. That is, the spacing between data points on the ephemeris tape is 12 h (one point at 00:00 and the next at 12:00, etc). Intermediate points are obtained via interpolation. Thus, at 00:00 GMT, a new point from the ephemeris tape would be added to the interpolation routine, and if this point were bad, a definite shift in the residuals could occur. A number of trajectory runs were made to compare this ephemeris tape (EPHEM 1) with previous versions. The differences, if any, between the different ephemeris tapes were negligible. In addition, EPHEM 1 was checked for 25 days before and after 00:00 GMT on June 2, and the sixth differences were plotted. No blunder points or anomalies were observed in these plots. A check with SPAC personnel indicated that nothing unusual had occurred onboard the spacecraft at this time. Based on the foregoing, it was concluded that the degradation in the data fit was not caused by any single event occurring in the immediate vicinity of this time. Therefore, the degradation most likely had to be caused by some previous trajectory perturbation that became apparent only after the spacecraft was well within the moon's sphere of influence.

Trajectory perturbations caused by gas leaks in the attitude control systems were observed during the *Mariner IV* and *Pioneer VI* missions. Based on the postflight analysis of *Mariner IV* data by G. Null (JPL), an improved model for handling nongravitational (non-drag) trajectory perturbations was included in a new version of the SPODP. The equations for this model are as follows:

$$\Delta\ddot{\mathbf{r}} = \left[f_i \left(1 - \alpha_1 \tau - \alpha_2 \tau^2\right) + \frac{A_p}{m_p} \frac{(SC)}{r^2_{\odot,S/C}} \left(1 + G + \Delta G\right) \right] \mathbf{U}_{SP}$$

$$+ \left[f_2 \left(1 - \alpha_1 \tau - \alpha_2 \tau^2\right) + \frac{A_p}{m_p} \frac{(SC)}{r^2_{\odot,S/C}} \left(G_T + \Delta G_T\right) \right] \mathbf{T} \qquad (1)$$

$$+ \left[f_3 \left(1 - \alpha_1 \tau - \alpha_2 \tau^2\right) + \frac{A_p}{m_p} \frac{(SC)}{r^2_{\odot,S/C}} \left(G_N + \Delta G_N\right) \right] \mathbf{N}$$

= change of acceleration of probe due to solar radiation pressure and small forces such as gas leaks in attitude control system, noncoupled attitude control jets, etc.

where the solved-for parameters are:

f_1, f_2, f_3 = accelerations due to gas leaks

α_1, α_2 = coefficients of polynomial in τ

G, G_T, G_N = solar radiation coefficients in the radial, tangential, and normal directions

and where the constants, or not-solved-for parameters, are:

$\tau = T_C - T_0$ where T_C = current time, T_0 = initial epoch

A_p = nominal area of spacecraft projected onto plane normal to sun–probe line in m^2
$\cong 6.7\ m^2$ for *Surveyor I*

m_p = instantaneous mass of probe in kg
$\cong 997.273$ kg for *Surveyor I*

$r_{\odot,S/C}$ = distance from sun to probe in km for
$\cong 0.15 \times 10^9$ km for *Surveyor I*

SC = spacecraft solar radiation constant

$$= \frac{J(\mathrm{AU})^2}{c} \times \frac{1\ \mathrm{km}^2}{10^6\ \mathrm{m}^2}$$

$$= 1.031 \times 10^8\ \frac{\mathrm{km}^3\ \mathrm{kg}}{\mathrm{s}^2\ \mathrm{m}^2}$$

where

J = solar radiation constant

$= 1.383 \times 10^3\ \mathrm{W/m^2}$

$= 1.383 \times 10^3\ \mathrm{kg/s^2}$

AU = astronomical unit

$= 1.496 \times 10^8$ km

c = speed of light

$= 2.99725 \times 10^5$ km/s

$\mathbf{U}_{SP}$ = a unit vector directed out from the sun as in the case of a radiation pressure force (For *Surveyor I* this corresponds to the spacecraft $+Z$ direction, or roll axis.)

$\mathbf{T}$ = a unit vector in the direction of Canopus. (For *Surveyor I* this corresponds to the spacecraft $-X$ direction, or pitch axis.)

$\mathbf{N}$ = a unit vector in the direction required to make $\mathbf{T}$, $\mathbf{N}$, $\mathbf{U}$ a right-handed orthogonal system. (For *Surveyor I* this corresponds to the spacecraft $+Y$ direction, or yaw axis.)

ΔG, ΔG_T, ΔG_N = input values specified at up to 100 time-points with linear interpolation between points

The portion of the trajectory during which these accelerations are estimated is under option control. That is, during a given orbit computation, the acceleration can be estimated either for specific parts of the trajectory or for the entire trajectory.

A number of orbital computations were made using the revised SPODP in an attempt to improve the data fit and, thereby, provide a refined estimate of the post-maneuver orbit. All computations, unless otherwise indicated, used the nominal physical constants and station location parameters. The coefficients of the time polynomial (α_1, α_2) were not estimated for any case, and for most cases the solar radiation coefficients (G, G_T, G_N) were not estimated. In such computations, the above equation was reduced to simply

$$\Delta\ddot{\mathbf{r}} = f_1\,\mathbf{U}_{SP} + f_2\mathbf{T} + f_3\mathbf{N} \qquad (2)$$

A 9 × 9 orbit solution, using all postmaneuver tracking data, was obtained and mapped forward to target. This solution was based on estimating the standard six parameters plus the accelerations f_1, f_2, and f_3 for the entire postmaneuver trajectory. Examination of the doppler residual plots (Figs. 23–32) indicated that the fit had been significantly improved. Also, the predicted unbraked impact point agreed very well with the inflight results, and the predicted impact time agreed with the observed time to within 0.05 s. Several other 9 × 9 orbit solutions were obtained, based on estimating the acceleration over different parts of the postmaneuver trajectory. None of these solutions provided a better data fit or a better estimate of unbraked impact parameters. Next, an 18 × 18 orbit solution, using all postmaneuver data, was obtained and mapped to target. This solution was based on estimating the standard six parameters, the station location parameters for the three stations (nine parameters total), and the three accelerations for the entire trajectory. The residual plots did not indicate an improvement over the corresponding 9 × 9 solution plots. The location of the unbraked impact point agreed with the 9 × 9 solution to within 0.01 deg (in both parameters), and the predicted impact time agreed to within 0.08 s. Estimated station longitudes from this solution agreed with the nominal values to within 0.0001 deg ($\cong$ 10 m). This may be compared to the 166-m change seen in the 15 × 15 solution, which did

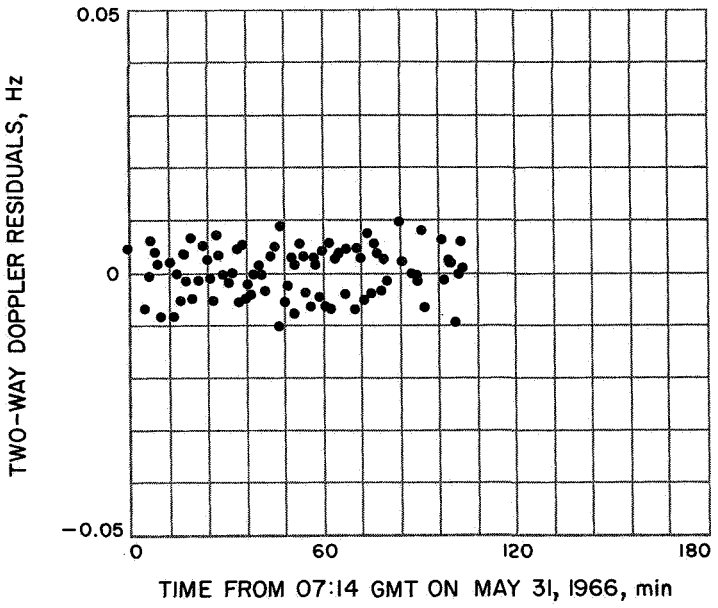

Fig. 23. DSS 11 postmaneuver two-way doppler residuals: Trajectory *corrected* for perturbations

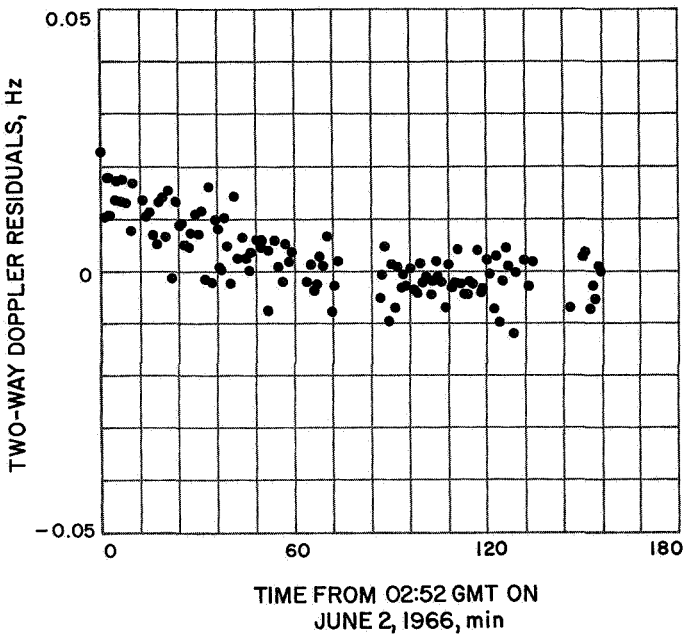

Fig. 24. DSS 11 postmaneuver two-way doppler residuals: Trajectory *corrected* for perturbations

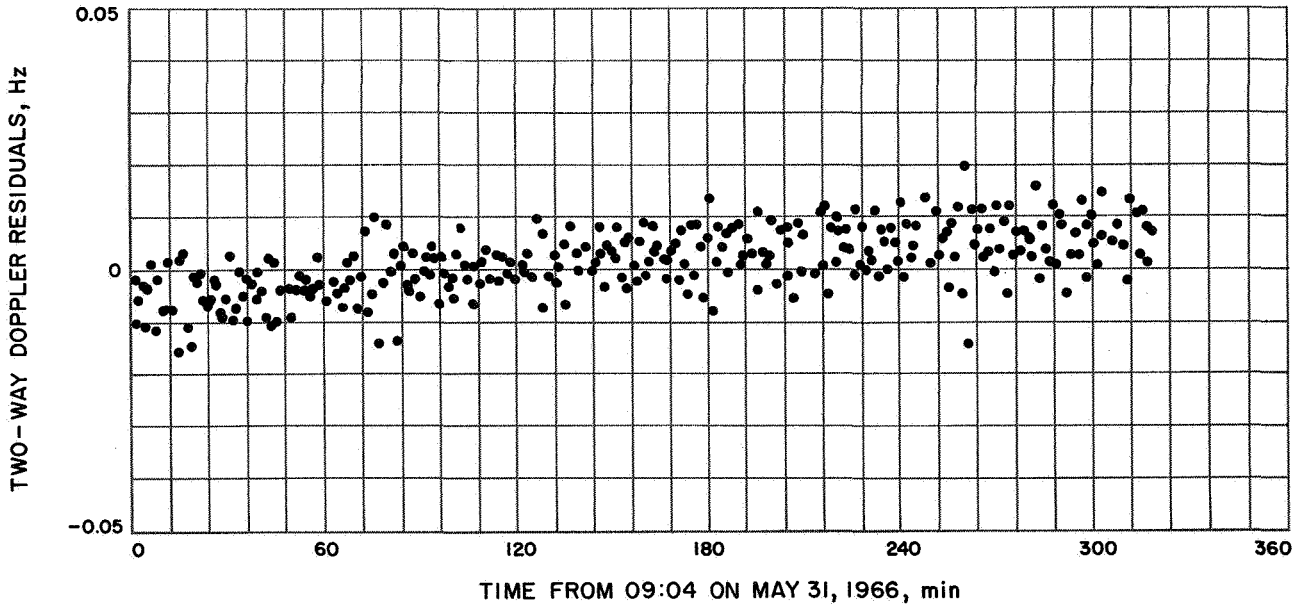

Fig. 25. DSS 42 postmaneuver two-way doppler residuals: Trajectory *corrected* for perturbations

not estimate the acceleration forces. Based on the foregoing, the 9 × 9 orbit solution using all postmaneuver data is considered to be the current best estimate of the *Surveyor I* postmaneuver orbit.

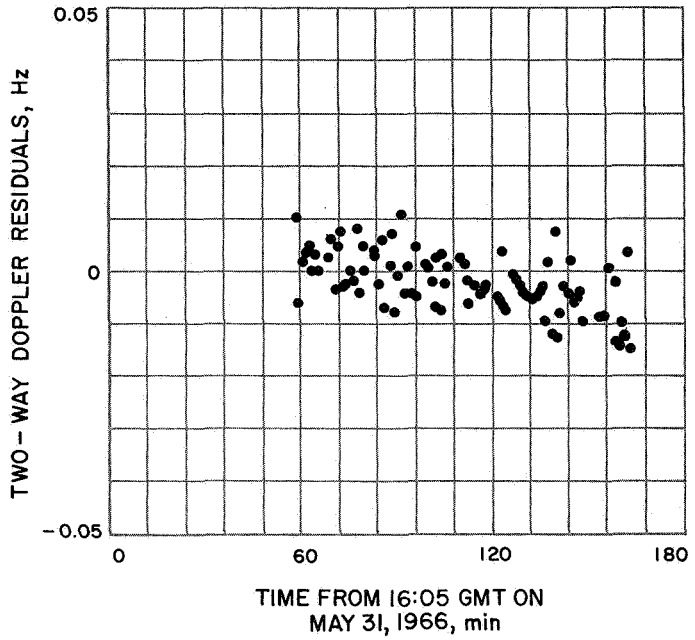

Fig. 26. DSS 42 postmaneuver two-way doppler residuals: Trajectory *corrected* for perturbations

The following are the acceleration changes estimated in the 9 × 9 solution

$$f_1 = 0.15 \times 10^{-9} \quad \pm 0.71 \times 10^{-10} \quad \text{km/s}^2$$

$$f_2 = 0.13 \times 10^{-9} \quad \pm 0.36 \times 10^{-9} \quad \text{km/s}^2$$

$$f_3 = 0.14 \times 10^{-9} \quad \pm 0.75 \times 10^{-9} \quad \text{km/s}^2$$

$$\Delta\ddot{\mathbf{r}} \cong 0.242 \times 10^{-9} \text{ km/s}^2$$

This acceleration change would result in a positional change of approximately 2.23 km at the target. The force resulting from this acceleration change would be approximately 24 dynes. In an attempt to correlate such an acceleration change with some physical phenomenon, the analog and telemetry records of the attitude jet firings, the attitude fuel system, and the vernier fuel system were examined for the postmaneuver trajectory. It was found that the gas leaks in both fuel systems were within specifications, and could account for a maximum of only 4 to 5 dynes. Attitude jet firings in roll, pitch, and yaw appeared to be *hard limit cycle*; the firings were equally spaced about the zero line for all three axes. The yaw control jets are designed to fire as a couple which should produce only angular velocity about the spacecraft *cg*. The pitch and roll attitude jets impart an incremental velocity parallel to the direction of thrust plus the desired angular velocity needed for attitude control. The limit cycle period for pitch jet firing is approximately 300 s; for roll jet firing it is approximately 600 s.

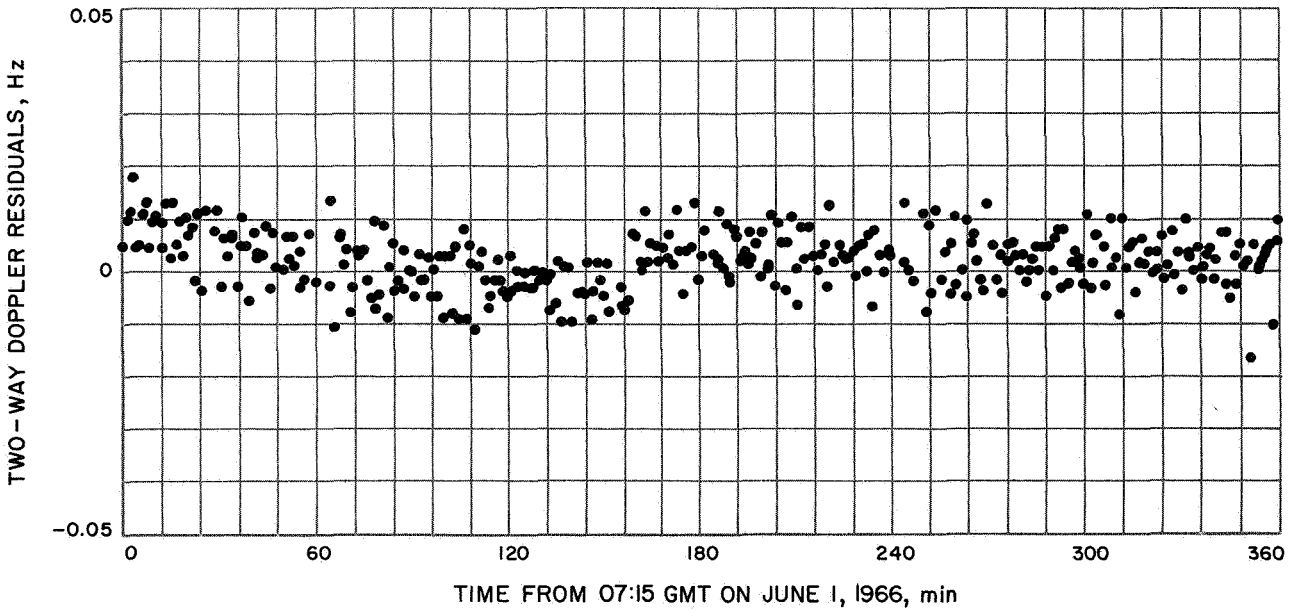

Fig. 27. DSS 42 postmaneuver two-way doppler residuals: Trajectory *corrected* for perturbations

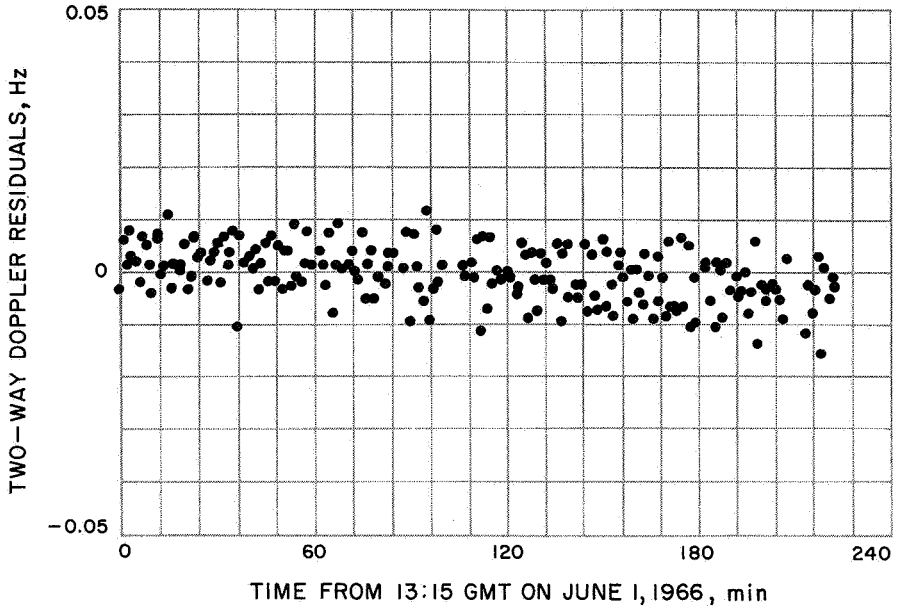

Fig. 28. DSS 42 postmaneuver two-way doppler residuals: Trajectory *corrected* for perturbations

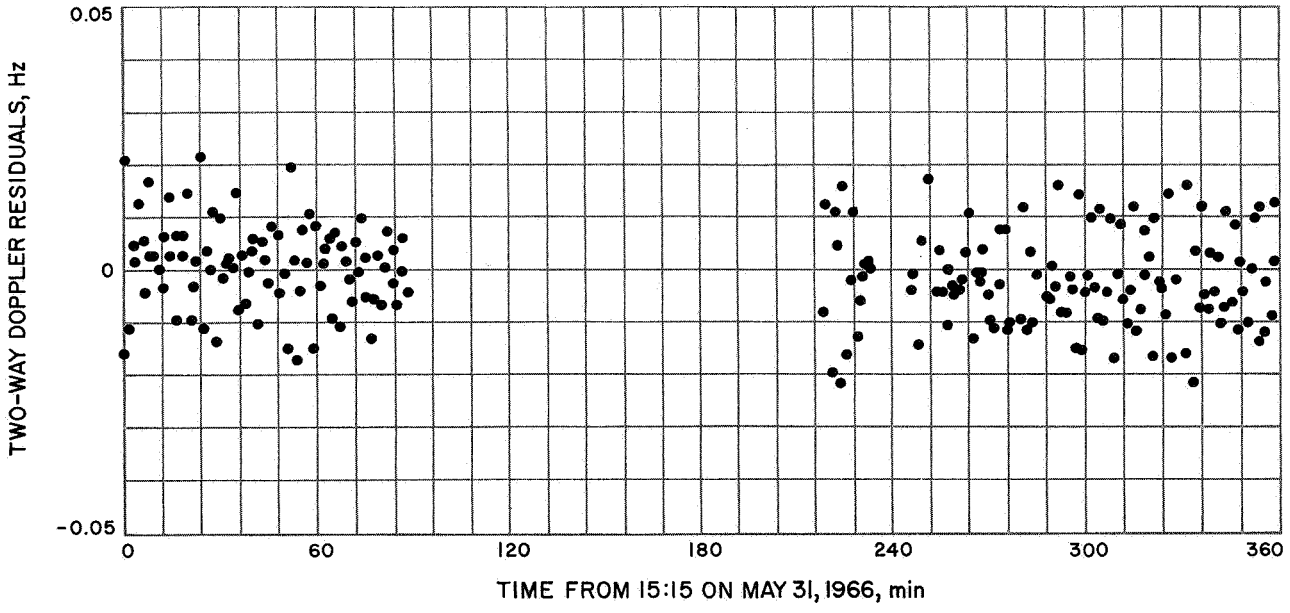

Fig. 29. DSS 51 postmaneuver two-way doppler residuals: Trajectory *corrected* for perturbations

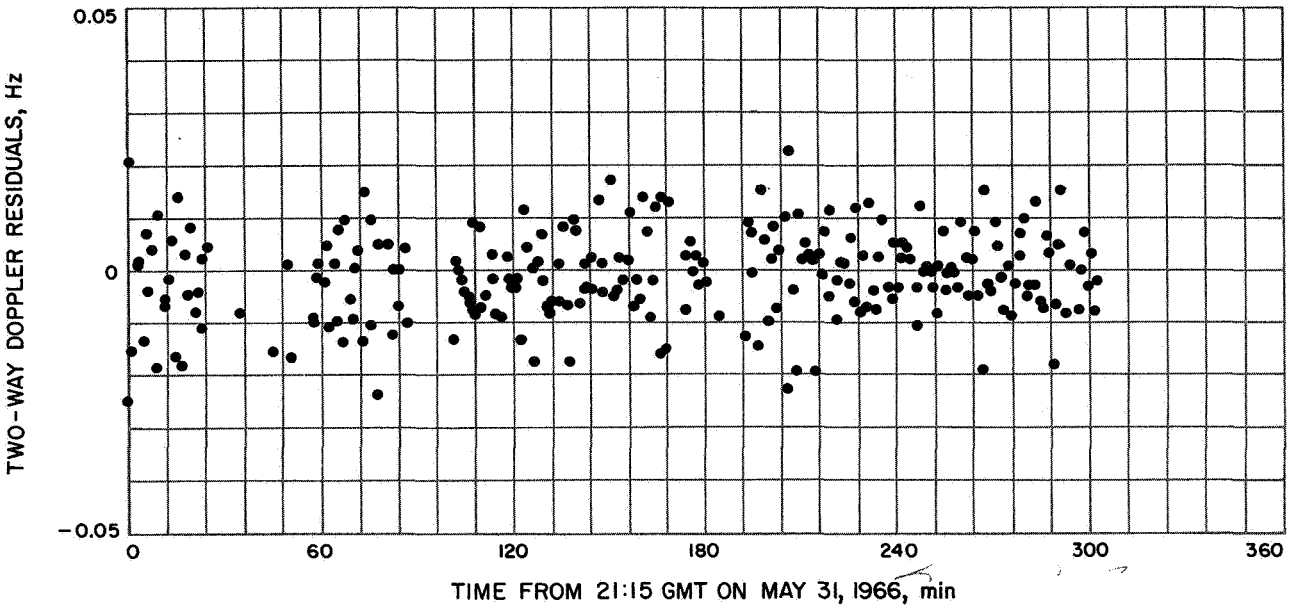

Fig. 30. DSS 51 postmaneuver two-way doppler residuals: Trajectory *corrected* for perturbations

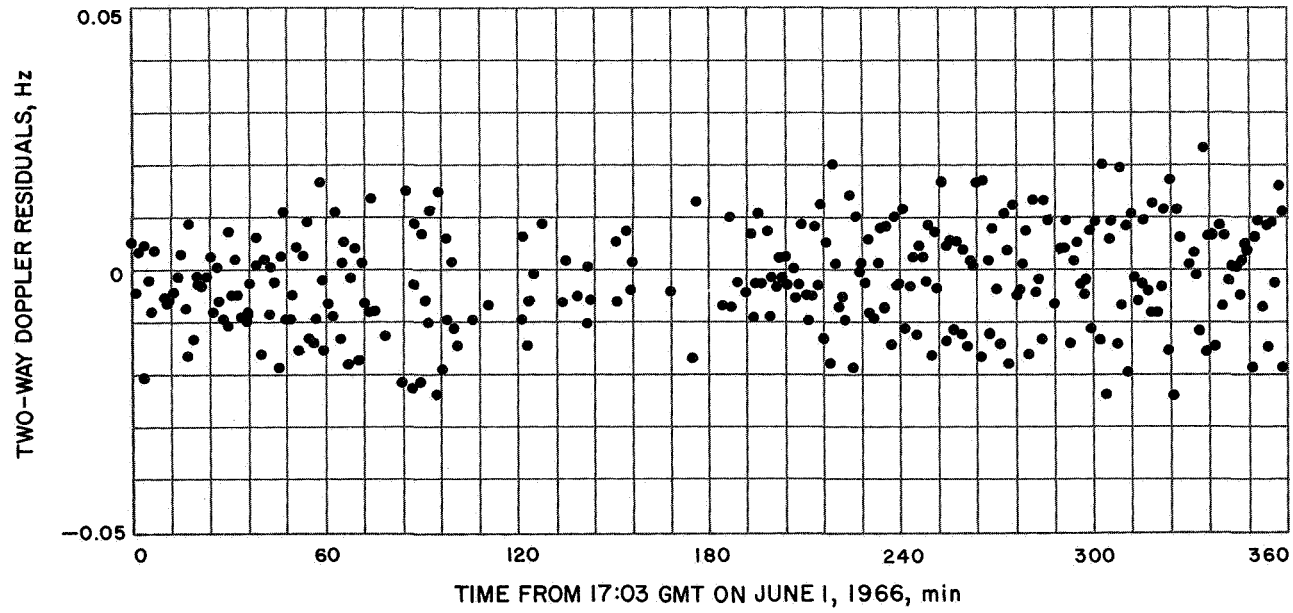

Fig. 31. DSS 51 postmaneuver two-way doppler residuals: Trajectory *corrected* for perturbations

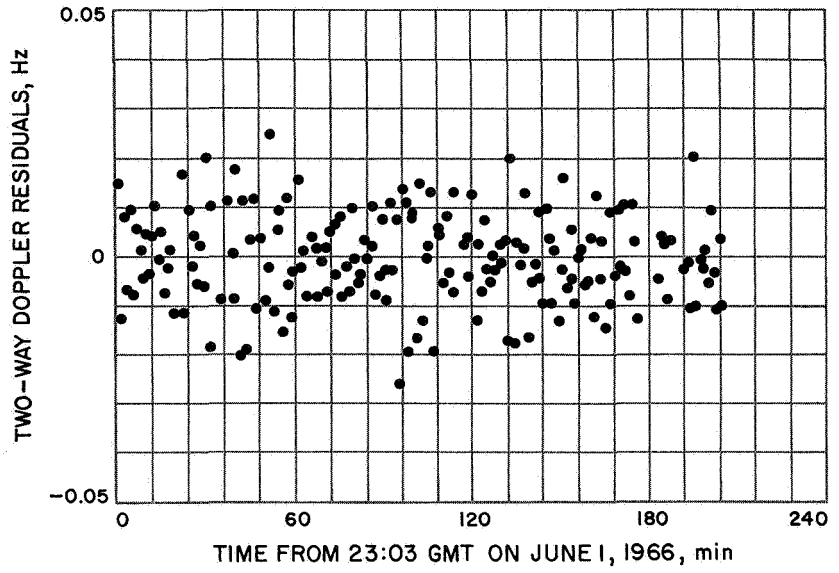

Fig. 32. DSS 51 postmaneuver two-way doppler residuals: Trajectory *corrected* for perturbations

Pitch jet firing will impart an incremental velocity of 0.0001 m/s to the spacecraft along the roll axis, and roll jet firing will impart an incremental velocity of 0.001 m/s along the pitch axis. The incremental velocity due to pitch jet firing will be in opposite directions along the roll axis for alternate firing (i.e., one firing on positive side of limit cycle, next firing on negative side of limit cycle, etc.) and will tend to cancel. A similar statement may be made for roll jet firing. However, the flight path (velocity vector) angle is constantly changing. Therefore, the incremental velocities will not be completely canceled out and a net spacecraft velocity change will be accumulated during the postmaneuver trajectory.

Part of the estimated acceleration changes (f_1, f_2, f_3) may be attributed to solar radiation pressure since Eq. (2) was used to obtain $\Delta\ddot{\mathbf{r}}$. From Eq. (1), it can be seen that the greatest solar pressure effect will be in the U_{SP} direction, which corresponds to the spacecraft +Z axis (away from the sun). An upper limit of the magnitude of the acceleration change due to solar radiation pressure (*SRP*) in this direction can be obtained, as follows:

$$SRP = \frac{A_p}{m_p} \frac{(SC)}{r^2_{\odot,S/C}} (1 + G + \Delta G)$$

$$= \frac{6.7}{997.273} \frac{1.031 \times 10^8}{(0.15 \times 10^9)^2} (1 + G + \Delta G)$$

$$\cong 0.308 \times 10^{-10} (1 + G + \Delta G)$$

$$\cong \begin{cases} 0.308 \times 10^{-10}, & G = \Delta G = 0 \text{ km/s}^2 \\ 0.616 \times 10^{-10}, & G = 1, \Delta G = 0 \end{cases}$$

The symbol G represents the percentage of reflected radiant energy, and a value of 1 indicates 100% reflection. Hence, if the upper bound value of 0.616×10^{-10} is used, solar radiation pressure could account for a maximum of approximately 41% of the estimated acceleration change in the U_{SP} direction.

Another 9 × 9 orbit solution was obtained and mapped forward to the target. In this computation, the last 5 h of tracking data were not used. The predicted unbraked impact time from this solution differed by only 0.144 s from the 9 × 9 solution which used all postmaneuver data. The difference in predicted impact time between corresponding inflight solutions was 2.241 s.

Based on the foregoing investigations and analyses, it is the author's conclusion that nongravitational (nondrag) perturbations did exist in the postmaneuver trajectory and that their effect can be removed by solving for an acceleration change, using the model in the SPODP. Further, the acceleration change estimated from the postmaneuver data cannot be attributed to any single cause, but most likely is caused by a combination of solar radiation pressure, uncanceled velocity increments from the normal operation of the attitude control system, possible attitude jet misalignment and, possibly, attitude

and vernier fuel leaks. It is interesting to note that even though these trajectory perturbations were not accounted for during inflight computations, the orbit determination requirements were met. Numerical values from the best estimate 9 × 9 postmaneuver orbit solution are presented in Tables 8 and 9. The amount of data used in this solution, together with associated noise statistics, is shown in Table 10.

D. Evaluation of Midcourse Maneuver Based on DSS Tracking Data

The *Surveyor I* midcourse maneuver can be evaluated by examining the velocity changes at midcourse epoch and by comparing the maneuver aim point with the target parameters from the best estimate post-midcourse orbit solution.

The *observed* velocity changes due to midcourse thrust (applied by igniting the vernier engines) are determined by differencing the velocity components of best estimate orbit solutions based on *postmaneuver* data, only, and *premaneuver* data, only. These solutions are independent — *a priori* information from premaneuver data is not used during the processing of postmaneuver data. The estimated maneuver execution errors, at midcourse epoch, are determined by differencing the observed velocity changes and the commanded maneuver velocity increments. The remaining major contribution to the total maneuver error is made by the orbit determination process. This error source includes SPODP computational and model errors, and errors in tracking data. These errors may be obtained by differencing, at midcourse epoch, the position and velocity components of the best estimate premaneuver orbit and the inflight orbit solution used for the maneuver computations. Numerical results of this part of the evaluation are presented in Table 13. In the table, it can be seen that the execution errors are very small; i.e., error in total velocity increment ($\simeq -0.11$ m/s) was roughly ½% of desired or commanded velocity increment (20.34726 m/s). Part of this error (see Section V) may be attributed to the burn duration which was 0.05 s less than commanded (commanded = 20.80 s, analog recorded = 20.75 s). This would result in a velocity increment of approximately −0.05 m/s, or about one half of the velocity execution error. OD errors are also relatively small. For this mission, these errors were primarily caused by a bias in the DSS 11 initial tracking data, some of which were included in the orbit solution used for the maneuver computations. The observed position changes, and the position execution errors result from the SPODP computational errors — i.e., they do not represent an actual spacecraft positional change. It should be noted that all are within the stated parameter uncertainty. Total maneuver errors for *Surveyor I* were well within specifications.

A more meaningful evaluation can be made by examining certain critical target parameters. Since the primary objective of the midcourse maneuver is to achieve lunar encounter at a selected landing site, the maneuver unbraked aim point is used as the basic reference for this evaluation. The aim point for *Surveyor I* was −2.33 deg latitude and 316.17 deg longitude. Based on the predicted unbraked impact point from the best estimate inflight orbit solution (LAPM XB), trajectory corrections were computed to achieve landing at the desired site. The total maneuver consisted of a roll–yaw attitude maneuver, to align the spacecraft to the proper thrust direction, and a midcourse thrust, to achieve the computed velocity correction. To evaluate the total maneuver error at the target, the maneuver aim point is compared with the predicted unbraked impact point from the current best estimate postmaneuver orbit solution. Orbit determination errors can be obtained by differencing the unbraked target parameters of the current best estimate premaneuver orbit solution and the inflight orbit solution used for maneuver computations. Execution errors, consisting of both attitude maneuver errors and engine system errors, are then determined by differencing the total and OD errors. Numerical results of these computations are presented in Table 14. In the table, it can be seen that landing was achieved within −0.072 deg latitude and 0.501 deg longitude of the desired aiming point. These differences in latitude and longitude are roughly equivalent to −2.190 and 15.030 km, respectively, on the lunar surface. OD position errors ($\Delta \mathbf{B} \cdot \mathbf{T}T$ = 13.887 km, $\Delta \mathbf{B} \cdot \mathbf{R}T$ = −5.692 km) are well within the 50 × 20 km, one standard deviation, guaranteed accuracy and are very close to the 15 × 5 km expected accuracy. It is interesting to note that during flight, the orbit solution used for maneuver computations was estimated to be in error by approximately 10 to 15 km, primarily in lunar longitude direction. The OD predicted unbraked impact time error (Δt impact) of −11.187 s is slightly greater than the 10-s guaranteed accuracy. In general, the accuracy of the *Surveyor I* midcourse maneuver was well within *Surveyor* Project specifications. It should be noted that these results cannot be used to evaluate the *Centaur* injection accuracy, since the inflight aim point was not the same as the prelaunch aim point (see Section V).

Table 13. *Surveyor I* midcourse maneuver evaluated at midcourse epoch[a]

Position and velocity element	Premaneuver position and velocity[b]		Postmaneuver position and velocity,[b] current best estimate	Change in position and velocity elements	Estimated change in position and velocity from maneuver, best postmaneuver minus best premaneuver	Commanded[c] maneuver position and velocity change	Total maneuver errors	
	Current best estimate	Inflight[c] estimate					Execution errors observed change minus commanded change	OD errors, best premaneuver minus inflight
x	−103399.91	−103396.55						
Δx[d]	+.21	+.21						
$x + \Delta x$	−103399.70 ±4.2 km	−103396.34 ±1.9	−103397.85 ±1.3	Δx	1.85[e] km	0.21[f]	1.64[e]	−3.36
y	−107007.16	−107010.83						
Δy	+.04	+.04						
$y + \Delta y$	−107007.12 ±5.4 km	−107010.79 ±1.9	−107007.03 ±2.6	Δy	0.09	0.05	0.04	3.67
z	−66322.976	−66322.757						
Δz	+.003	+.003						
$z + \Delta z$	−66322.973 ±7.9 km	−66322.754 ±1.2	−66324.784 ±2.3	Δz	1.810	0.003	1.807	0.219
Dx	−909.31486 ±0.100 m/s	−909.22818 ±0.057	−889.55294 ±0.041	ΔDx	19.76192 m/s	19.891847	−0.12993	−0.08668
Dy	−1542.1420 ±0.046 m/s	−1542.1712 ±0.014	−1537.7926 ±0.041	ΔDy	4.3494	4.2710491	0.07835	0.0292
Dz	−621.27892 ±0.110 m/s	−621.34739 ±0.058	−620.97894 ±0.021	ΔDz	0.29998	0.2891142	0.01087	−0.06847
V	1895.0047	1895.0094		ΔV	20.23711	20.34726	−0.11015	−0.0047

[a]Midcourse epoch = end of motor burn = May 31, 1966, 06:45:53.800 GMT.

[b]All position and velocity components are given in geocentric space-fixed cartesian coordinates.

[c]Based on inflight premaneuver orbit solution (LAPM XB) used for midcourse maneuver computations.

[d]Δ in first two columns indicates the positional change during midcourse thrusting from the relationship $\Delta X = \frac{1}{2}\, a_x t^2 = \frac{1}{2}\, \dot{V}_x t$, where t = engine burn time = 20.80 s and $\dot{V}_x = \dot{V}_x$ (best postmaneuver) minus $\dot{V}_x$ (best premaneuver). $\Delta x \rightarrow \Delta y \rightarrow \Delta z$.

[e]Position errors in these columns are the result of ODP computational errors; they *do not* reflect an actual spacecraft position change. It should be noted that all are within the stated parameter uncertainty.

[f]Δ's in this column are same as in (d) except $\dot{V}_x = \dot{V}_x$ (commanded).

Table 14. *Surveyor I* midcourse maneuver evaluated[a] at target unbraked impact point

Error source	ΔB•TT, km	ΔB•RT, km	Δ_T impact, s	Δ latitude (lunar)		Δ longitude (lunar)	
				deg	≈ km	deg	≈ km
OD errors[b]	13.887	−5.692	−11.187	0.102	3.060	0.301	9.030
Execution errors[c]	11.404	9.435	10.375	−0.174	−5.250	0.200	6.000
Total errors[d]	25.291	3.743	−0.812	−0.072	−2.190	0.501	15.030

[a]Latitude and longitude of aim and impact points:

Prelaunch aim point	3.25°S lat	43.83°W lon
Uncorrected impact point	11.43°S lat	54.25°W lon
Maneuver aim point	2.33°S lat	43.83°W lon
Best estimate impact point	2.40°S lat	43.33°W lon

[b]OD errors = current best premaneuver orbit estimate *minus* orbit used for maneuver computations.

[c]Execution errors = attitude maneuver errors plus engine system errors
= total errors minus OD errors.

[d]Total errors = current best postmaneuver orbit estimate *minus* maneuver aim point.

E. Evaluation of Station Locations and Physical Constants

1. Computations. To determine the best estimate of $GM_\oplus$, $GM_\leftmoon$ and station location parameters for the *Surveyor I* mission, the total parameters estimated were: the spacecraft position and velocity at an epoch; the gravitational masses of the earth and moon; the spacecraft accelerations f_1, f_2 and f_3; the solar radiation constant, G; and two components (geocentric radius and longitude) of station location for each of the three tracking stations. These solutions were computed by use of the two-way doppler data only, from DSS 51 for the pre-midcourse phase and from DSS 11, DSS 51 and DSS 42 for the post-midcourse phase. In an effort to obtain the best estimate of the solved-for parameters, the pre-midcourse data block was combined with the post-midcourse data block. The procedure of combining the two data blocks was the same as that outlined in Ref. 8. Essentially, the procedure is to fit only the pre-midcourse data and to accumulate the normal equations at the injection epoch, then to map the converged estimate to the midcourse epoch with a linear mapping of the inverted normal equation matrix (i.e., covariance matrix). The estimate is then incremented with the best estimate of the maneuver, and the mapped covariance is corrupted in the velocity component and used as *a priori* for the post-midcourse data fit. The ephemeris used in the reduction was one of the latest JPL ephemerides[8] (DE 19) with the updated mass ratios and Eckert's corrections.

[8]Tape No. 9325; RE = 6378.1495.

2. Results. The solved-for station locations are presented in Table 15 in an unnatural station coordinate system (geocentric radius, latitude, and longitude) and in a natural coordinate system[9] (r_s, λ, z) where r_s is the distance off the spin axis in the station meridian, λ is the station longitude, and z is along the earth spin axis. The natural coordinate system is illustrated in Fig. 33. The numerical results were computed with improved values[10] of DSS indices of refraction. The previous nominal index of refraction of 340 was used for all

[9]The coordinate transformation of the results was performed by Neil Mottinger of JPL.

[10]The new index of refraction was provided by A. S. Liu of JPL. The index for DSS 11 is 240; DSS 51, 240; DSS 42, 310.

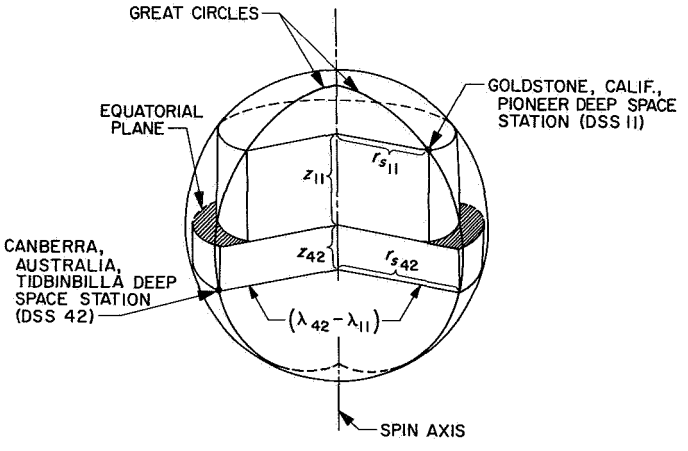

Fig. 33. Station coordinate system

Table 15. Station locations and statistics, *Surveyor I*

Station	Data source	Distance off spin axis, km	1σ standard deviation, m	Geocentric longitude, deg	1σ standard deviation, m	Geocentric radius, deg	Geocentric latitude, deg
DSS 11	*Surveyor I, post-midcourse, only*	5206.3200	50.8	243.15098[a]	59.4	6371.9975	35.208192
	Surveyor I, post-touchdown	276	2.9	085	23.8	6372.6446	16317
	Mariner II	357	3.9	058	8.8	.0044	08035
	Mariner IV, cruise	404	10.0	067	20.0	.0188	08144
	Mariner IV, post-encounter	378	37.0	072	40.0	.0161	08151
	Pioneer VI, Dec. 1965–June 1966	359	9.6	092	10.3	.0286	08030
	Goddard land survey, Aug. 1966	718	29.0	094	35.0	.0640	08230
DSS 42	*Surveyor I,* post-midcourse only	5205.3465	32.7	148.98166	41.1	6371.6834	−35.219372
	Surveyor I, post-touchdown	.3474	3.5	130	22.1	.6651	19123
	Mariner IV, cruise	.3478	10.0	136	20.0	.6882	19410
	Mariner IV, post-encounter	.3480	28.0	134	29.0	.6824	19333
	Pioneer VI, Dec. 1965–June 1966	.3384	5.0	151	8.1	.6932	19620
	Goddard land survey, Aug. 1966	.2740	52.0	000	61.0	.7030	20750
DSS 51	*Surveyor I,* inflight	5742.9380	38.2	27.68578	41.2	6375.5144	−25.739169
	Combined *Rangers,* LE3[b]	315	8.5	72	22.2	.5072	9169
	Ranger VI, LE3	203	19.7	72	69.3	.4972	9215
	Ranger VII, LE3	211	25.5	83	61.3	.4950	9157
	Ranger VIII, LE3	372	22.3	48	85.0	.5130	9159
	Ranger IX, LE3	626	56.6	80	49.5	.5322	8993
	Mariner IV, cruise	363	10.0	40	20.0	.5120	9148
	Mariner IV, post-encounter	365	40.0	57	38.0	.5143	9198
	Pioneer VI, Dec. 1965–June 1966	332	11.6	69	12.0	.5094	9176
	Goddard land survey, Aug. 1966	706	39.0	86	43.0	.5410	8990

[a]This number is questionable because DSS 11 data appeared to be biased.

[b]Lunar ephemeris 3 (DE 15).

stations by other missions. The new index of refraction significantly improved the data fit for the DSS 11 data. The improvement in the data fit for DSS 51 and DSS 42 was also observed.

The station locations obtained from *Surveyor I* inflight data compared favorably with other missions (Refs. 9 and 10). The station locations for DSS 11 and DSS 42 were computed with the post-midcourse maneuver data, only. Prior to midcourse maneuver, DSS 42 did not track the spacecraft and DSS 11 data appeared to be biased as mentioned in Section III. The r_s and λ obtained for DSS 51 are approximately 7 m from the combined *Ranger* estimates. The statistics obtained with the station location are higher than those from other missions because a larger effective data-weighting sigma was used for *Surveyor I* mission and, in addition, the amount of data used in these computations was also smaller than that used in other missions.

The solved-for $GM_\oplus$ and $GM_\leftmoon$ for the *Surveyor I* mission are given in Table 16. The numerical results are in excellent agreement with the combined *Ranger* estimates (Ref. 11). The *Surveyor I* $GM_\oplus$ and $GM_\leftmoon$ differ from the combined *Ranger* estimates by 0.05 km^3/s^2 and 0.018 km^3/s^2, respectively. Table 16 also shows the *Lunar Orbiter II* estimates (Ref. 11) for comparison. Table 17 gives the correlation matrix.

3. Conclusion. The $GM_\oplus$ and $GM_\leftmoon$ estimates were well within the 1σ limit of the combined *Ranger* values, and the station location parameters are in good agreement with the *Ranger, Mariner* and *Pioneer* missions. Efforts are being continued to improve the present

Table 16. Physical constants and statistics, *Surveyor I*

Data source	$GM_{\oplus}$, km^3/s^2	1σ standard deviation, km^3/s^2	$GM_{\leftmoon}$, km^3/s^2	1σ standard deviation, km^3/s^2
Surveyor I, inflight	398601.27	0.77	4902.6492	0.24
Lunar Orbiter II (doppler)	398600.88	2.14	4902.6605	0.29
Lunar Orbiter II (doppler and ranging)	398600.37	0.68	4902.7562	0.13
Combined *Rangers*	398601.22	0.37	4902.6309	0.074
Ranger VI	398600.69	1.13	4902.6576	0.185
Ranger VII	398601.34	1.55	4902.5371	0.167
Ranger VIII	398601.14	0.72	4902.6304	0.119
Ranger IX	398601.42	0.60	4902.7073	0.299

solution for *Surveyor I* mission. When an improved set of physical constants and station location parameters is obtained, the present solution will be updated.

V. Midcourse and Terminal Maneuver Analysis for *Surveyor I*

The purpose of this section is to present the inflight, and some limited postflight, results of the *Surveyor I* midcourse and terminal maneuver analysis. The midcourse correction and the terminal retromaneuver are accomplished with the propulsion system on board the spacecraft. The *Surveyor* spacecraft propulsion system consists of three liquid-propellant variable-thrust vernier engines and one solid-propellant fixed-impulse engine. The solid-propellant engine is used for the main retrograde phase of the mission. This retromaneuver decreases the velocity of the spacecraft with respect to the moon by approximately 8300 ft/s. The liquid-propulsion vernier engines are used for (1) the midcourse correction, (2) the attitude control during the main retrograde phase and (3) the final descent and landing after main retroengine burnout.

The midcourse correction is chosen to null the miss on the lunar surface and to optimize certain trajectory parameters, such as arrival time or main retroengine burnout velocity. Hence, a nominal terminal descent must be simulated during the midcourse selection.

A nominal terminal descent is described as follows. As the spacecraft approaches the moon, approximately 62 h after launch, it is in view of the Goldstone station. At this time, the attitude of the spacecraft is adjusted so that the thrust axis is nearly aligned with the spacecraft velocity vector. At a slant range of approximately 60 mi from the lunar surface, the spacecraft altitude marking radar generates a signal which, after a suitable time delay, initiates the ignition of the vernier engines used to control the spacecraft attitude during main retrorocket burning. One second after vernier ignition, the solid main retroengine is ignited. The retrorocket thrust decay is sensed by an acceleration switch that initiates a time delay of 12 s. At this time, the empty main retrorocket case is separated from the spacecraft by explosive bolts.

Shortly after separation, vernier engine thrust is reduced to a level corresponding to an axial acceleration of 0.9 lunar g. The radar on board the spacecraft, the radar altimeter and doppler velocity sensor (RADVS), acquires the lunar surface and provides measurements of range and velocity to the spacecraft flight control system, and the thrust axis is aligned with the spacecraft velocity vector. When the RADVS senses that the preprogrammed range velocity contour has been reached, the thrust is increased to an acceleration level such that spacecraft descends along this contour until a 10-ft/s velocity is reached. The dynamic characteristics of this descent trajectory (a *gravity turn* trajectory) are such that when the spacecraft reaches the 10-ft/s point, the thrust attitude will be nearly aligned to the vertical. The vehicle attitude is then inertially held and maximum acceleration is commanded until the speed is reduced to 5 ft/s. This speed is maintained down to an altitude of 13 ft when the engines are shut off and the vehicle free-falls to the lunar surface with a nominal landing speed of 13 ft/s (Fig. 34). The reader is directed to Refs. 13 through 18 for a more detailed description of the midcourse and terminal guidance problems.

Parameter	Standard deviation			
		x	y	
x	1.498, km	1	−0.473	−
y	1.681, km		1	−
z	2.808, km			
Dx	0.302×10^{-4}, km/s			
Dy	0.217×10^{-4}, km/s			
Dz	0.484×10^{-4}, km/s			
$GM_{\oplus}$	7.752, km^3/s^2			
G	0.0100			
$GM_{\leftmoon}$	2.371, km^3/s^2			
f_1	0.803×10^{-10}, km/s^2			
f_2	0.516×10^{-9}, km/s^2			
f_3	0.276×10^{-9}, km/s^2			
R (DSS 11)	6.223, km			
Lon (DSS 11)	5.934, deg			
R (DSS 42)	4.001, km			
Lon (DSS 42)	4.110, deg			
R (DSS 51)	4.251, km			
Lon (DSS 51)	4.123, deg			

Table 17. Correlation matrix on postmaneuver data with premaneuver data as *a priori* at maneuver epoch, *Surveyor I*

Parameter														
Dx	*Dy*	*Dz*	$GM_{\oplus}$	G	$GM_{\mathbb{C}}$	f_1	f_2	f_3	*R* (DSS 11)	Lon (DSS 11)	*R* (DSS 42)	Lon (DSS 42)	*R* (DSS 51)	Lon (DSS 51)
−0.412	0.514	0.202	−0.164	0.603	−0.465	0.360	0.142	0.173	−0.608	0.309	0.874	0.286	0.229	0.310
0.829	0.113	−0.323	−0.168	0.197	0.764	−0.273	−0.820	−0.103	0.309	−0.113	0.697	−0.723	0.609	−0.708
0.328	−0.601	0.288	0.330	−0.288	−0.606	−0.864	−0.745	−0.637	−0.267	−0.165	−0.778	0.478	−0.817	0.443
1	−0.454	−0.573	0.306	−0.183	0.456	−0.926	−0.853	−0.146	−0.489	0.114	0.956	0.290	0.647	0.304
	1	−0.457	−0.394	−0.930	−0.156	0.470	0.364	0.383	−0.194	−0.405	0.570	−0.440	0.622	−0.403
		1	−0.250	0.222	−0.312	0.518	0.802	−0.193	0.446	0.288	−0.693	0.235	−0.638	0.182
			1	0.509	0.947	−0.114	−0.224	−0.196	−0.252	−0.291	−0.589	0.535	0.406	0.295
				1	−0.700	−0.208	0.193	−0.429	0.232	0.252	0.760	−0.719	−0.541	−0.413
					1	−0.594	−0.246	−0.469	0.145	0.164	0.221	0.151	0.190	0.908
						1	0.730	0.319	0.291	−0.227	−0.247	−0.178	−0.159	−0.193
							1	−0.309	0.661	−0.320	−0.308	−0.189	−0.216	−0.251
								1	−0.390	−0.126	0.283	−0.442	−0.525	0.712
									1	−0.470	0.412	−0.333	0.493	−0.416
										1	−0.139	0.530	−0.869	0.535
											1	−0.573	0.883	−0.541
												1	−0.530	0.932
													1	−0.503
														1

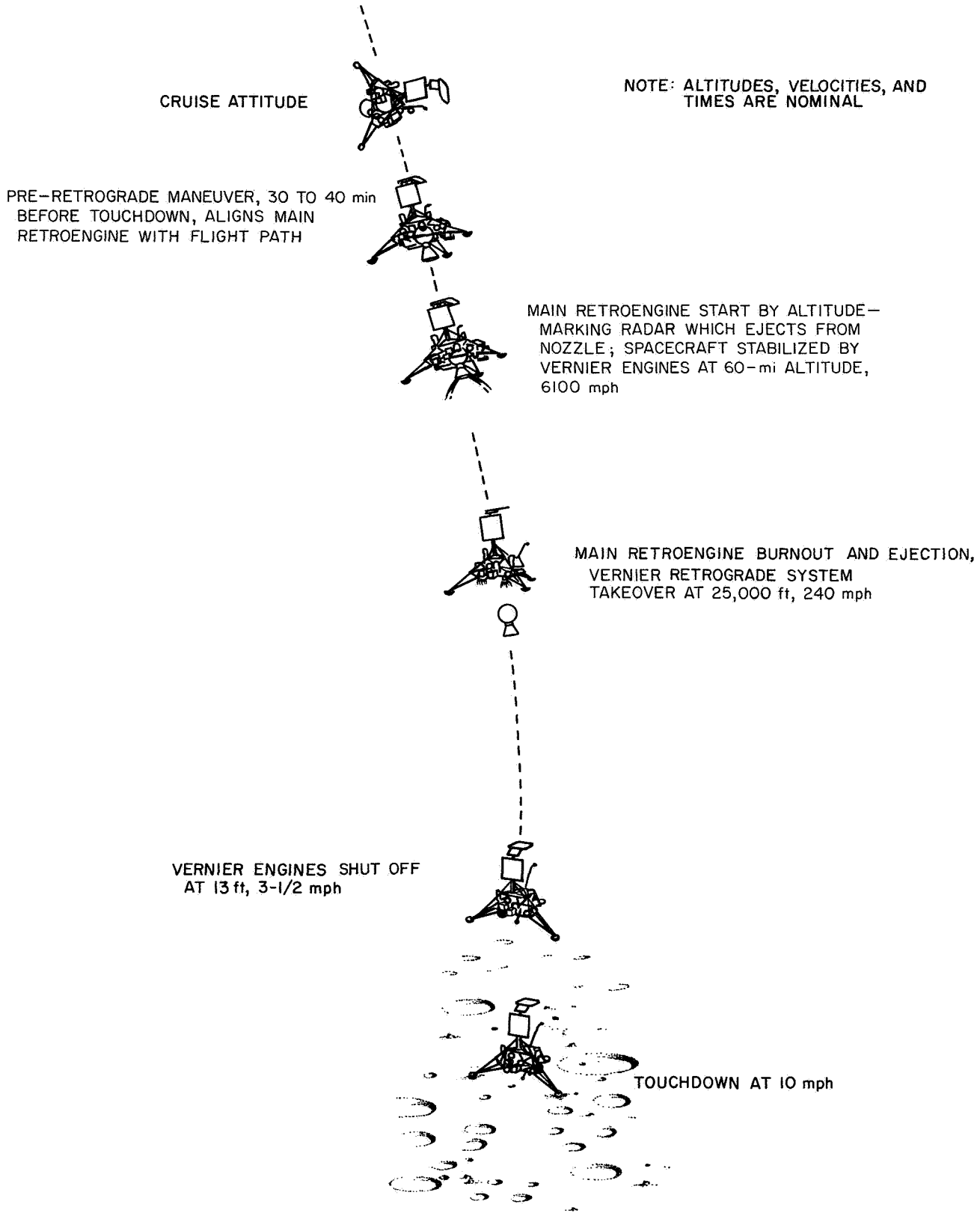

Fig. 34. Terminal descent nominal events

A. Midcourse Maneuver

The *Surveyor I* midcourse correction computed to enable the spacecraft to soft-land at the desired landing site, −2.33 deg latitude and 316.17 deg longitude, was 20.35 m/s. This correction was executed on ground command at approximately 06:45 GMT on May 31, 1966. The resulting soft-landing site is estimated from the *Lunar Orbiter* photograph to be at −2.45 deg lat and 316.8 deg lon, well within the 3σ dispersions predicted prior to the correction. Figure 35 shows the prelaunch targeted site, the inflight selected aim point, the actual soft-landing site, and the associated dispersions at the midcourse time.

The 99% dispersions are shown as an ellipse on the surface with a semimajor axis of 38.7 km and a semiminor axis of 28.7 km. To take advantage of the small uncertainties that resulted from the small required midcourse correction, the aim point was biased to the north approximately 0.92 deg by changing the aim point from the original targeted value of −3.25 and 316.17 deg, thereby minimizing the probability of landing in the craters Flamsteed or Flamsteed E. Estimates and dispersions related to the knowledge of the actual landing site are presented in Table 12.

The maximum midcourse correction capability, as a function of the unbraked impact speed, is shown in Fig. 36. The expected 3σ *Centaur* injection guidance dispersions and the effective lunar radius (impact radius) are also shown. The midcourse capability contours are in the conventional **R**, **S**, **T** coordinate system (Appendix B).

The maneuver execution time of 15.85 h after injection was chosen. This time allowed 4 h, 36 min of pre-midcourse and 3 h, 49 min of post-midcourse visibility from the Goldstone tracking facility.

The predicted results of the selected midcourse correction and other possible alternatives considered are given in Table 18. The required velocity component in the critical plane, i.e., correct miss only, was 3.74 m/s.

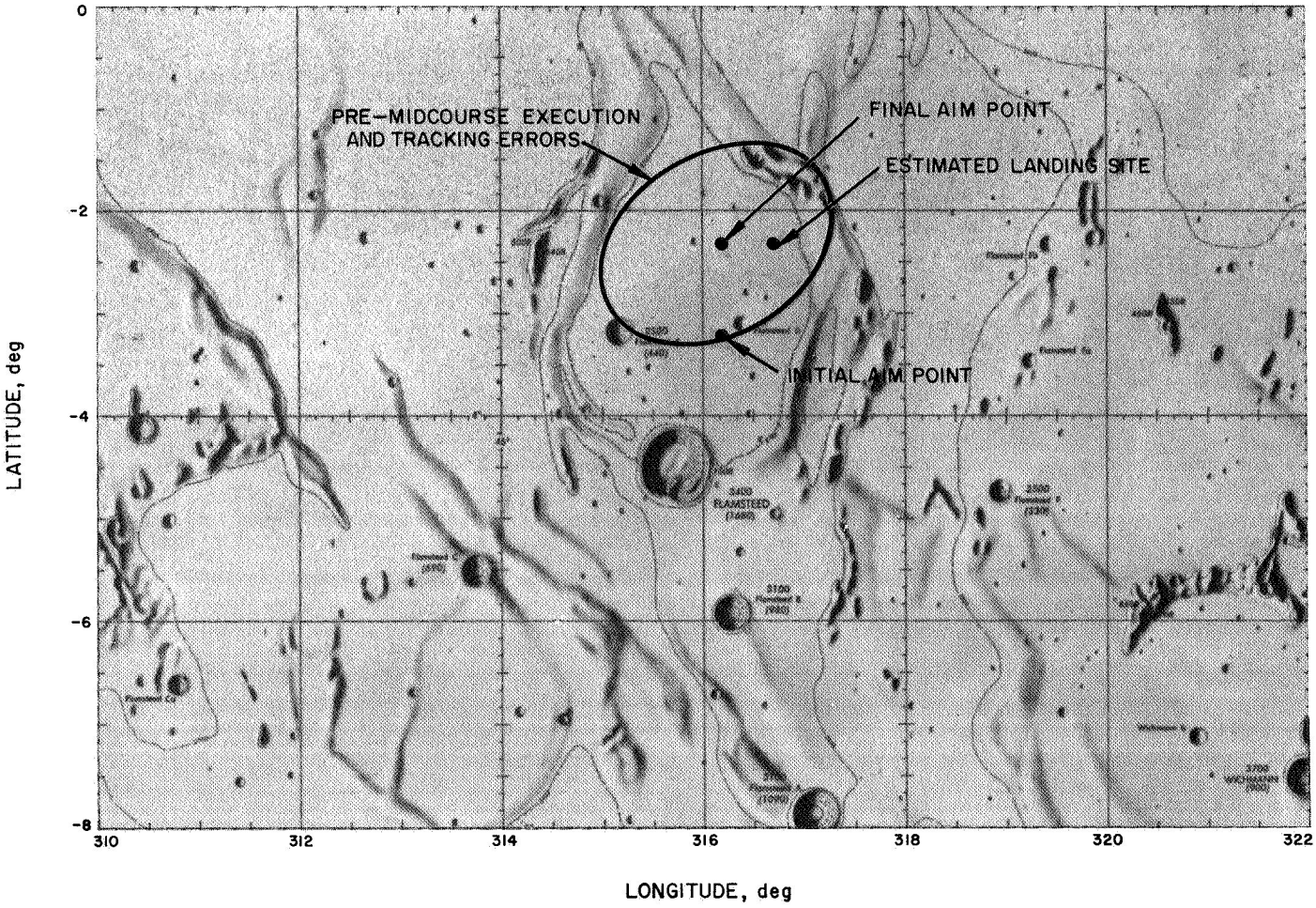

Fig. 35. *Surveyor I* landing locations

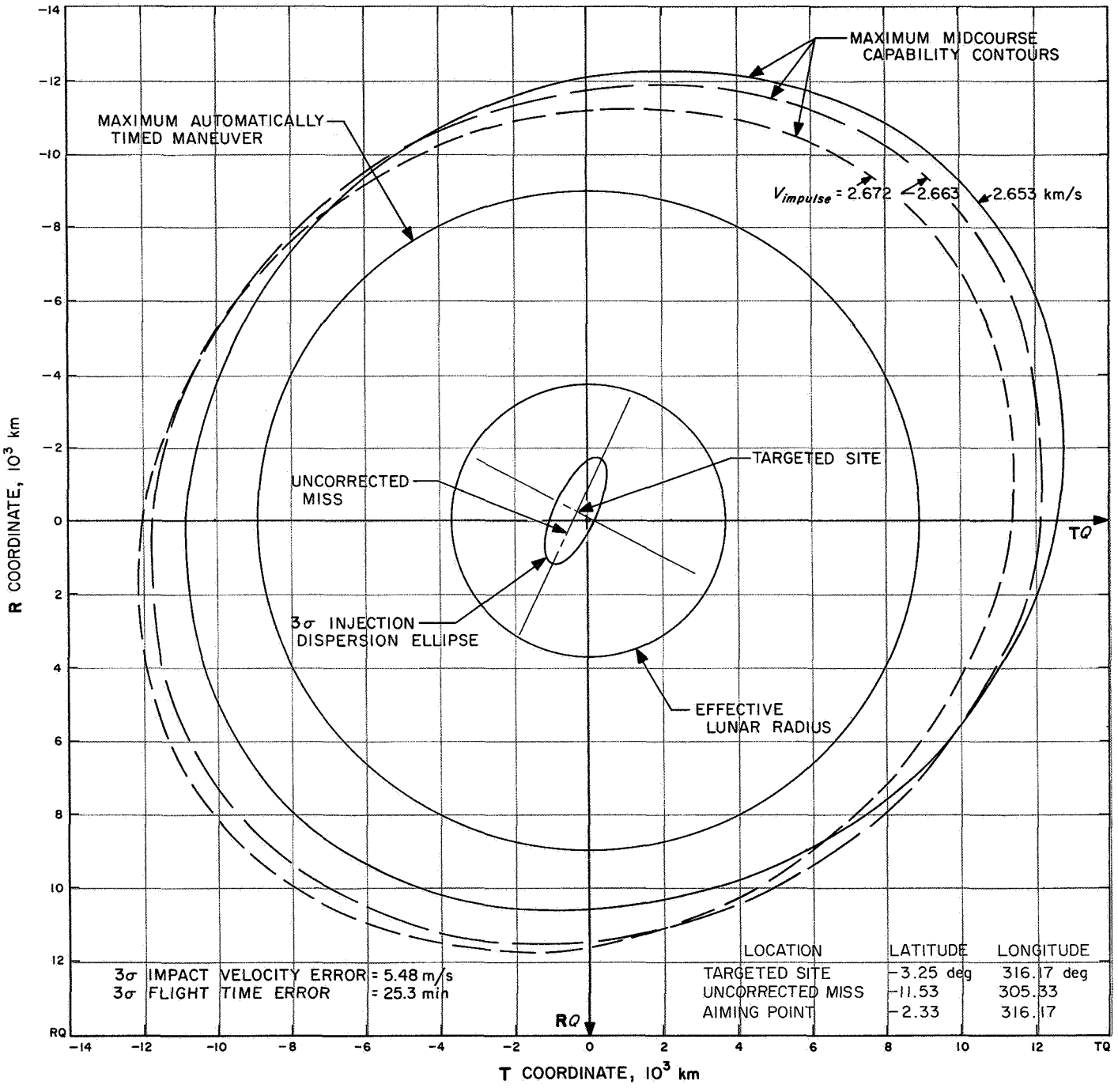

Fig. 36. Midcourse capability contours for May 30, 1966, launch

Table 18. Midcourse maneuver alternatives

Data type	Selected midcourse correction	Alternate considerations			
		No midcourse correction	Midcourse at $L + 40$ h	1-rotation maneuver, only	Sunline correction
Midcourse data					
Velocity magnitude, m/s	20.35		21.18	3.51	2.91
Critical plane, m/s	3.74		6.96	3.36	
Noncritical direction, m/s	20.00		20.00	1.00	
Propellant weight, lb	16.81		17.49	2.90	2.40
First rotation (roll), deg	−86.50		−77.57	0	0
Second rotation (yaw), deg	−57.99		−44.43	−35.56	0
Omnidirectional antenna	B–B		B–B	B–N	B
Engine burn time, s	20.80		21.65	3.58	2.97
Spacecraft mechanization errors (3σ), km (on the surface)					
SMAA	31.0	0	32.2	5.35	4.44
SMIA	30.6	0	31.8	5.12	4.25
Terminal data					
Latitude (aim point), deg	−2.33	−11.53	−2.33	−3.25	−9.86
Longitude, deg	316.17	305.53	316.17	316.17	317.29
Incidence angle, deg	6.02	10.14	6.02	5.75	1.62
Impact speed, km/s	2.655	2.666	2.656	2.665	2.665
Burnout velocity, ft/s	392.	514.	400.	500.8	506.9
Burnout altitude, ft	28,571		28,353	38,137	38,673
Fuel margin, lb	33.9	33.3	33.8	33.4	33.1
Descent propellant, lb	120.7		120.7	135.3	136.02
Descent time, s	170.5		170.4	184.2	184.9
First rotation (roll), deg	89.33	89.33	89.33	89.33	89.33
Second rotation (yaw), deg	59.92	59.92	59.92	59.92	59.92
Third rotation (roll), deg	94.09	94.09	94.09	94.09	94.09
Ignition delay, s	7.825		7.96	6.37	6.37
Landing site errors (3σ), km [(on the surface) orbit determination plus spacecraft mechanization]					
SMAA	38.7	23.2	34.2	23.8	23.6
SMIA	28.7	17.2	32.8	17.9	17.7

The noncritical direction component, $\dot{U}_3$, that resulted from a weighted selection of flight time, main retroengine burnout velocity, and vernier propulsion system fuel margin was 20 m/s. Figure 37 shows the possible flight times, burnout velocities, and fuel margins for the range of available noncritical component velocity corrections. The fuel margin and arrival times were acceptable over a wide spectrum. Flight control stability considerations, however, made a nominal main retroengine burnout below 450 ft/s highly desirable. The value of $\dot{U}_3$ = 20 m/s was chosen as a good compromise, which reduced the retroengine burnout velocity to 392 ft/s. If the maneuver strategy were to correct miss plus flight time, the required noncritical component would have been 4.3 m/s, to give a total of approximately 6.1 m/s.

Since the aim point was changed during the flight, the above required correction does not properly evaluate the performance of the *Centaur* guidance system. Use of the results of the last pre-midcourse orbit and corrections to the original aim point give a miss-only requirement of 3.55 m/s. Miss plus flight time was 5.89 m/s.

B. Terminal Maneuvers

Following the midcourse maneuver, only one significant problem remained to be solved prior to the terminal phase – to obtain a decision on the terminal attitude maneuvers. All other problems, such as burnout velocity, propellant margin, time of flight, etc., were essentially determined at midcourse. Subsequent post-midcourse orbits would only affect these parameters in a minor way.

Because of the apparent failure of antenna A to deploy, attitude maneuvers in the terminal phase were selected to optimize signal strength from antenna B.

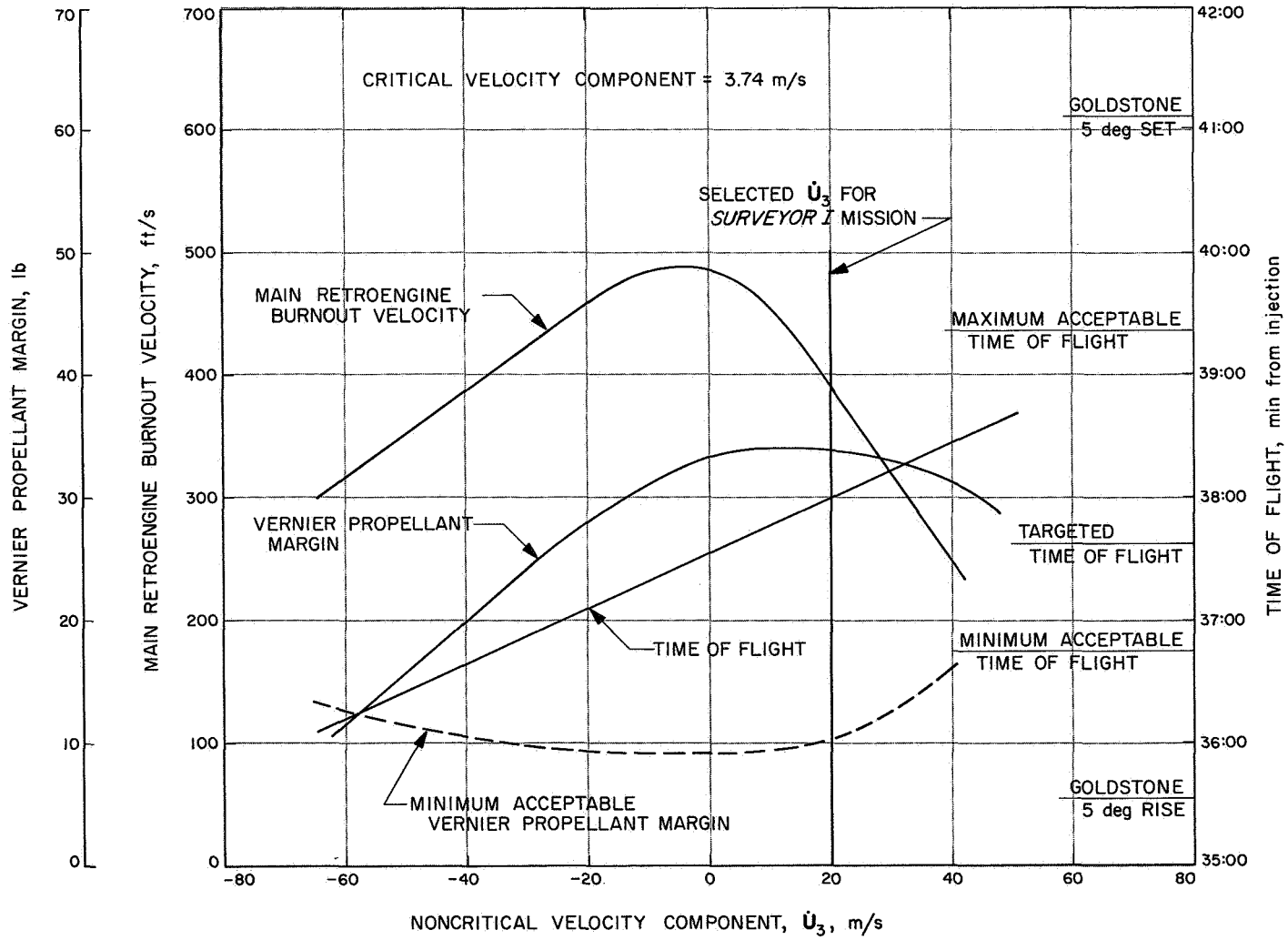

Fig. 37. Effect of noncritical velocity increment on terminal descent parameters

Study of this problem showed that there were two possible maneuver sequences that would maintain relatively high signal strength during, and following, the maneuvers. The first maneuver sequence was a roll–yaw–roll combination that gave a final spacecraft roll orientation such that the Deep Space Station was in the most favorable location. The second maneuver sequence was a roll–pitch combination. This maneuver sequence also resulted in an equally favorable final roll orientation.

However, the latter maneuver sequence was discarded because of several disadvantages that the first sequence did not have. First, the pitch maneuver channel had not been exercised at midcourse, as had the yaw channel. Second, the roll–pitch combination could not be computed directly with the MTGS programs, and thus there could be no compensation for a sensor group deflection of 0.34 deg and a known y gyro drift of approximately 0.75 deg/h. The net result of these two uncompensated error sources was an estimated 0.4-deg offset in the retrophase thrust vector. With this expected thrust offset, the flight path angle uncertainty (3σ) at the start of the vernier phase was 28 deg, as compared with an uncertainty of 20 deg when these errors are compensated. Table 19 contains the recommended and actual command times corresponding to certain important preignition events.

Table 19. Command times corresponding to preignition events

Event	Command time, GMT	
	Recommended	Sent
Initiation of first roll maneuver	5:36:44	5:36:46
Initiation of yaw maneuver	5:42:43	5:41:48
Initiation of final roll maneuver	5:49:43	5:45:18
Radar power on		6:09:56
Enable	6:12:54	6:12:57

Predicted values of the more important terminal parameters are given in Table 20. These predictions are based on the final post-midcourse computer run of the terminal guidance program completed approximately 2.5 h prior to main retroengine ignition. Figure 38 is a plot of required usable touchdown propellant margin as a function of burnout velocity to account for the 99% burnout dispersions. The requirement for the *Surveyor I* mission, based on the predicted burnout velocity, was about 10.5 lb; actually, there was 33.9 lb of propellant available.

Table 20. Predicted values of terminal parameters

Terminal parameters	Values
Ignition time delay	7.826 s
Ignition altitude	246,636 ft
Ignition velocity	8,565.3 ft/s
Main retro burnout altitude	28,571 ft
Main retro burnout velocity	392 ft/s
Flight path angle	6.02 deg
Nominal propellant consumption (vernier phase)	78.2 lb
Propellant margin (touchdown)	33.9 lb
Usable touchdown propellant margin required for 99% burnout dispersions	10.5 lb
Landing site	−2.411 deg lat 316.655 deg lon

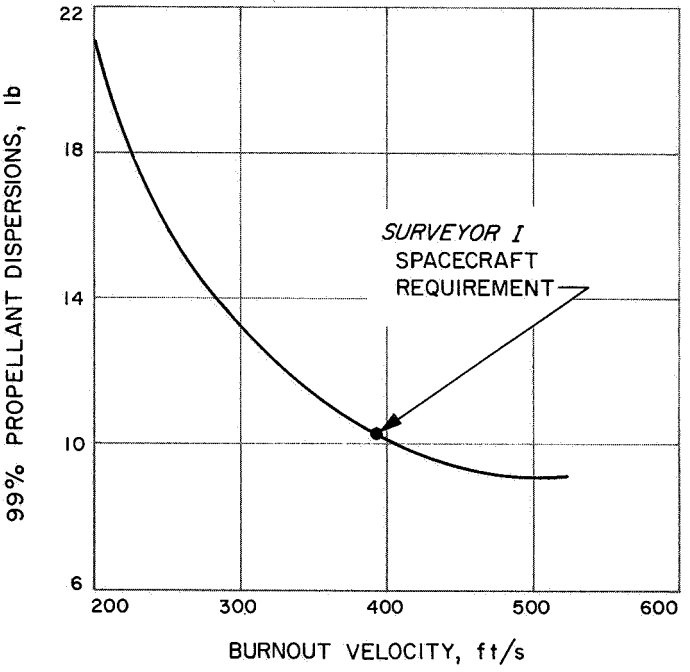

Fig. 38. 99% vernier propellant dispersions vs burnout velocity

C. Comparison of Actual and Commanded Maneuvers

1. Midcourse maneuver. An analysis of the midcourse velocity correction has been performed utilizing two independent sources of data: orbit determination and combined data from spacecraft telemetry and preflight measurements. The orbit determination results given in Table 13 indicate a ΔV correction of 20.237 m/s, whereas

the telemetry and preflight results yield 20.365 m/s. These estimates are not only in good agreement with each other but, also, with the desired correction, 20.347 m/s. With respect to the desired correction, the orbit determination result indicates a velocity magnitude error of 0.081 m/s and a maximum pointing error of 0.221 deg. The telemetry-and-preflight result indicates a velocity magnitude error of 0.018 m/s and a pointing error of 0.313 deg. Tables 21 and 22 detail the spacecraft error sources used to obtain the telemetry and preflight results.

Table 21. Midcourse angular error

Parameter	3σ requirement	Performance value	Comments
Initial position errors			
Sensor group roll axis to sun–spacecraft line	0.2 deg	0.005 deg	
Pitch/yaw limit cycle	0.3 deg	0.014 deg −0.232 deg	
Sensor group roll–pitch plane to Canopus–spacecraft line	0.2 deg	0.031 deg	
Roll limit cycle	0.3 deg	0.15 deg	
Rotational magnitude errors			
Gyro torquer scale factor 45-deg rotation 180-deg rotation	0.05%	0.08%	From precession rate determination. Desired rate is 0.5000 deg/s. The actual rate was 0.5004 deg/s.
Precision current accuracy (0.13) 45-deg rotation 180-deg rotation	0.13%		
Timing source accuracy 45-deg rotation 180-deg rotation	0.2 s	0.015 deg (roll) 0.1 deg (yaw)	These values correspond to a timing error of 0.03 s for the roll maneuver and 0.20 s for the yaw maneuver.
Precession current circuit drift 45-deg rotation 180-deg rotation	0.1%		
Rotational axis error			
Gyro alignment to inertial reference unit (IRU) *A*, *B*, and *C* axis	0.1 deg		
IRU roll and pitch axis to sensor group roll and pitch axis	0.1 deg		
Final position errors			
Vernier engine thrust vector to nozzle centerline	0.33 deg	0.280 deg	With respect to spacecraft coordinates, the vector representation is $\mathbf{I}_A = -0.00462\,\mathbf{I}_X - 0.00160\,\mathbf{I}_Y - \mathbf{I}_Z$
Installation alignment and bracket bending compensation	0.1 deg		
Spacecraft roll axis to sensor group roll axis	0.1 deg		
Attitude control steady-state error	0.1 deg	0.005 deg	Based on a moment disturbance value of 74 in.-lb.
Reference axis drift gyro non-g drift	1 deg/h	0.121 deg	Calculated value of pointing error due to a drift
Midcourse maneuver duration	15 min	4 min, 36 s	From time and events log
Total attitude error	0.7 deg	0.313 deg	

Note: The performance values cannot be added algebraically to obtain the total error because the problem is three-dimensional.

Table 22. Midcourse magnitude error

Parameter	Requirement, 3σ or limit	Magnitude, ft/s	Performance value[a], ft/s
Errors[b] proportional to maneuver magnitude			
Accelerometer accuracy	1.1%	0.732	
Reference signal	0.5%	0.334	
Flight control electronics null	0.15%	0.098	
Thrust bias variation	0.09%	0.061	
Control channel gain variation	0.07%	0.045	
Accelerometer misalignment	0.06%	0.406	
Total proportional errors (rss)	1.22%	0.816	0.615[c]
***Errors independent of* maneuver magnitude**			
Shutdown impulse dispersion	±0.63 lb-s	0.016	
Hysteresis limit cycle	3 mA	0.035	
Ignition transient	—	0.30	
Timing granularity	—	0.16	−0.11
Total *independent errors* (rss)	—	0.335	—
Total magnitude errors (rss)	—	0.865	−0.725

[a]The difference between the actual of ΔV and the desired value is −0.266 ft/s.

[b]Much of the error was anticipated and was included in the calculation of the desired burn time.

[c]This value is more meaningful than the −0.725 ft/s given as performance value.

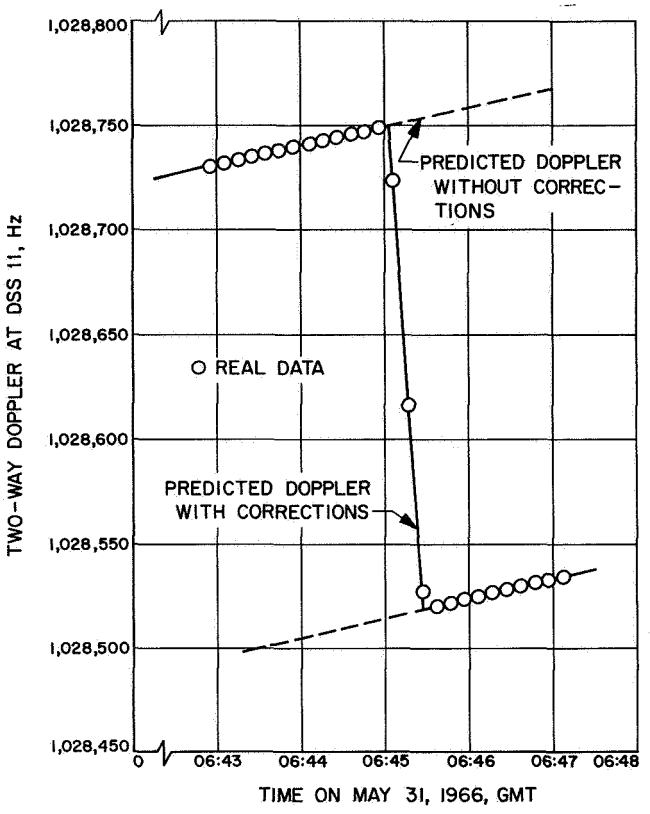

Fig. 39. *Surveyor I* doppler during midcourse correction

Figure 39 presents the spacecraft doppler data taken during the midcourse correction. The comparison of these data with the predicted doppler is an important indication of the performance of the midcourse correction. The data indicate good agreement between the predicted and measured results.

2. Terminal phase. Table 23 lists predicted and actual times for various terminal descent events, together with the estimated accuracy in the measurements. These predictions were made approximately 2.5 h prior to main retroengine ignition. Both analog and digital telemetry

Table 23. Predicted and actual terminal descent event times

Event	Event times, GMT		Maximum error, s
	Predicted	Best estimate	
Radar mark	06:14:37.97	06:14:38.45	0.04
Vernier engine ignition	06:14:46	06:14:46:27	0.04
Retroengine ignition	06:14:47	06:14:47.37	0.04
Actual 3.5 *g* point	06:15:26	06:15:26.42	0.1
3.5 *g* switch	—	06:15:26.70	0.015
Retroengine eject	06:15:33	06:15:40.85	0.015
Start RADVS[a]	06:15:40	06:15:41.85	0.015
Segment acquisition	06:16:15	06:16:04.65	0.01
1000-ft mark	06:17:12	06:17:09.25	0.05
10-ft/s mark	06:17:30	06:17:27.43	0.025
13-ft mark	06:17:35	06:17:32.93	0.025
Touchdown	06:17:37	06:17:34.26	0.05

[a]Vernier phase start.

data are used in determining event times. Event times such as vernier ignition, retroengine ignition, retroengine eject, 13-ft mark, etc., are time-tagged by commutated digital words switching from an *off* to an *on* state. However, since these digital words are commutated as little as once per commutator cycle, they could be received only once per second, resulting in an equivalent error. By using such analog data as accelerometer output, which is commutated at a different point in time, such events as retroengine ignition may be pinpointed more accurately. Where event times are correlated by the spacecraft internal timer, an additional improvement may be obtained in event timing. To demonstrate where this method is most effective, consider the sequential events 3.5 *g* switch, retroengine eject, and start RADVS. These first two events are separated by an internal 12.00-s delay and the latter two by 2.15 s. Thus, the telemetry data available to establish these time points are: three digital words, three increased analog thrust commands at the 3.5 *g switch* point, and three decreasing analog thrust commands at the *start RADVS* point, assuming a radar-reliable-operate condition. With nine telemetered quantities distributed over one commutated cycle, an accurate determination of times may be made. The obvious problem with this method is that it is dependent on the spacecraft's timer functioning within its specified tolerances. Since there are no indications that the counter was not functioning as designed, this method was used where appropriate in constructing Table 23. To determine the *actual* 3.5 *g* point as compared to the 3.5 *g* switch point, it was necessary to plot and calibrate the retro accelerometer data (see Fig. 40). The accelerometer data is, at most, accurate to 10% due to hysteresis given no calibration data; however, given the highly accurate calibration point during the vernier minimum acceleration phase (0.9 lunar *g*) and actual test data indicating good sensor linearity with decreasing acceleration levels, acceleration levels during retropropulsion tailoff depicted in Fig. 40 may be considered accurate to about 0.2 earth *g* with a resulting accuracy in *actual* 3.5 *g* of 0.1 s.

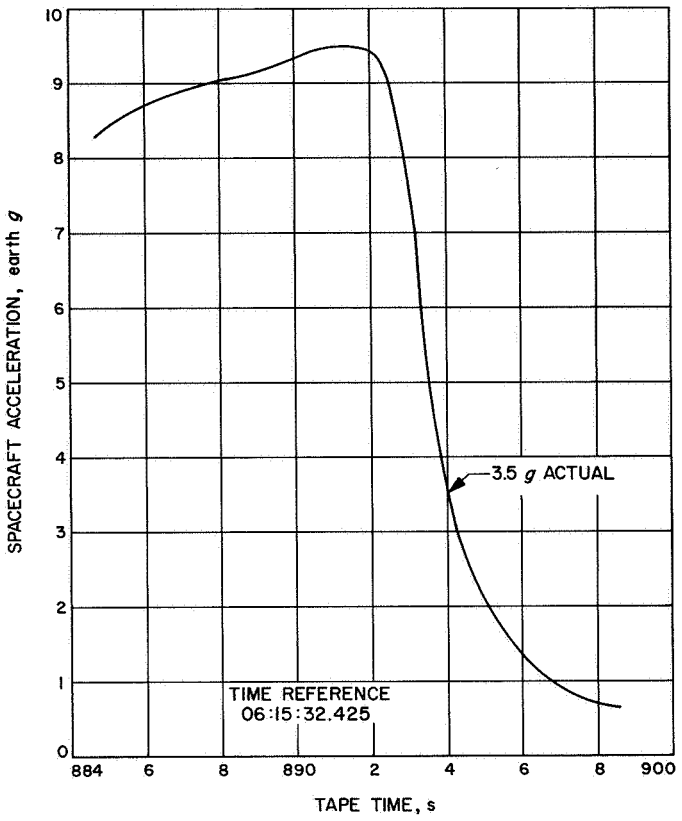

Fig. 40. Spacecraft acceleration vs time

3. Retrograde phase trajectory. The spacecraft retrophase trajectory performance beginning with *vernier ignition* and ending with *start RADVS* can most easily be measured by comparing the predicted conditions at the end of the retrophase with the actual conditions. For missions like *Surveyor I* where practically all telemetry data are available, the comparison can be made by simply analyzing the telemetered velocity components along the spacecraft *X*, *Y*, and *Z* axes. By taking out known biases in the telemetry data, the following comparison can be made:

	Velocity components, ft/s		
	X	*Y*	*Z*
Predicted	30	−6	392
Actual	71	−4	428

By simple vector addition, these differences in burnout velocities can be transformed into equivalent errors of retrograde phase differential velocity (ΔV) where ΔV is the velocity change due (1) to retroengine and vernier thrust acceleration from *vernier ignition* to *start RADVS* and (2) to thrust vector alignment errors. Figure 41 depicts the vector geometry.

V_{BO} is the velocity at main retroengine burnout (RADVS start), and gt is the velocity gained due to gravity during the retroengine burn. The third term in the vector equation, V_0, is the spacecraft velocity at vernier ignition. Its magnitude and direction are computed from the postmaneuver injection conditions, as

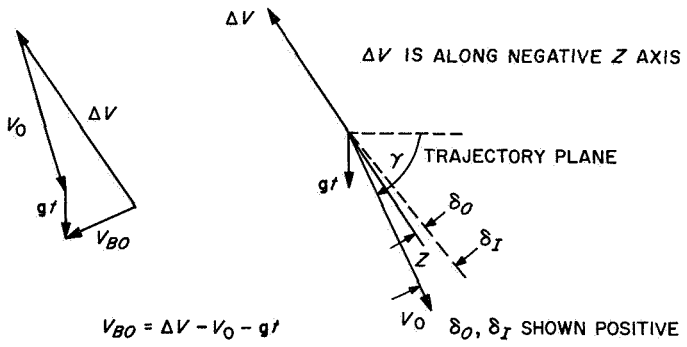

Fig. 41. Retrograde phase vector geometry

calculated by orbit determination and the nominal ignition altitude. Errors associated with this vector are small, since the 3σ uncertainty in impact velocity is < 0.3 m/s, and the 3σ contribution in V_0 uncertainty due to ignition altitude dispersions is < 0.3 m/s. The error contribution from the gt term is also small since the approximation of a constant direction gt vector is in error by only 0.22 deg as a result of lateral spacecraft translation during the retrophase.

It may be said then that the major source of error in computing retrophase ΔV is from uncertainties in the telemetered burnout velocities. While premission 3σ estimates of telemetered velocities are on the order of 10%, postmission calibration of these data would indicate uncertainties of $< 2\%$. This estimate is substantiated by use of one-way doppler tracking data that agrees within 10 ft/s when computing ΔV.

Because telemetry data indicate a stable attitude condition, attitude thrusting errors computed from the burnout velocity are assumed to be constant throughout the retrophase. Based on this assumption, the in-plane attitude error (δ_I) is computed to be 0.26 deg and the out-of-plane error (δ_O) is 0.08 deg. The total retrophase ΔV is computed to be 8415 ft/s, as compared with a predicted value of 8451 ft/s. This decrease in $|\Delta V|$ indicates a loss in retrophase performance of approximately 0.43%.

Spacecraft range radar telemetry data indicate an altitude at burnout of 29,300 ft, as compared with a predicted value of 28,600 ft.

Figure 42 presents one-way doppler received during the retrograde phase of the *Surveyor I* mission.

4. Terminal phase tracking. Due to operational considerations, two-way doppler tracking is dropped before

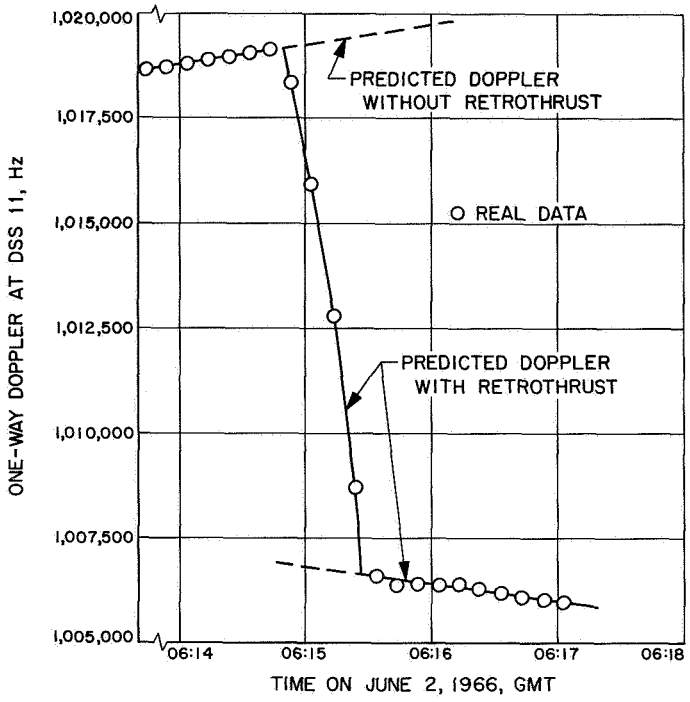

Fig. 42. *Surveyor I* doppler (one-way) during retrograde phase

initiation of the powered phase of the terminal descent. While a source of very precise velocity data is thus lost, it has been found that one-way lock with the spacecraft transmitter frequency, when compared with a stable ground source, can also produce accurate data. Figure 43 is a plot of doppler data obtained in this manner that has been converted into equivalent radial velocity change. Both raw data based on doppler counts over 2-s intervals and corrected data for transmitter frequency shifts are plotted. Since the correction factor amounts to $< 1\%$ of the total change in velocity and control or calibration points before retroignition and after touchdown indicate drift rate consistency of $> 10\%$, it is estimated that the total change in radial velocity can be computed to within 0.1%, or 5 to 6 ft/s. These data, however, cannot be used directly to compute main retrophase performance unless the geometry associated with the thrusting direction and tracking station–spacecraft vector is known. Through use of the maneuver analysis terminal guidance program, a nominal value for the thrust vector to tracking station included-angle can be computed. When this value was corrected for apparent misalignment of the thrust vector as obtained from burnout velocity data, the total retrophase ΔV, as computed from one-way doppler, was found to agree within 10 ft/s of the value computed from ignition and burnout velocities obtained from telemetry data and orbit determination.

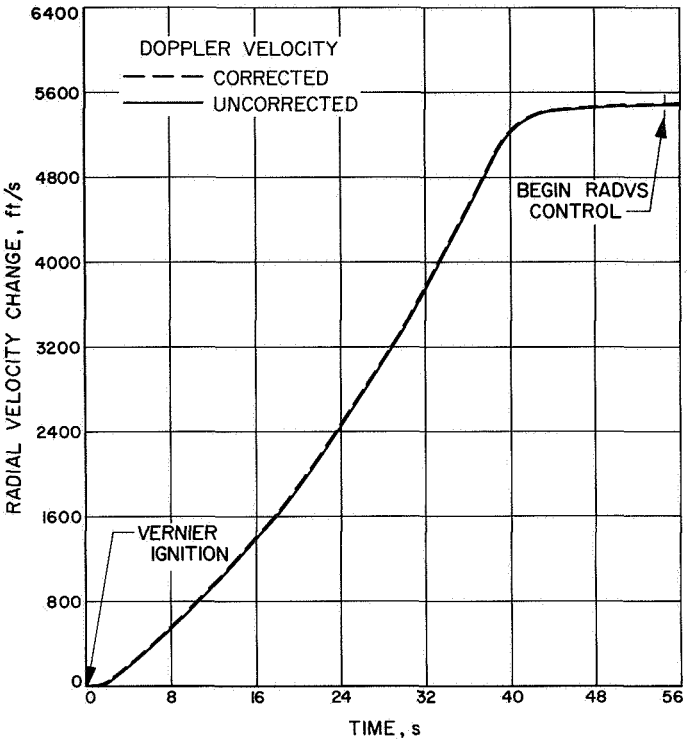

Fig. 43. Spacecraft radial velocity change relative to earth, retrograde phase

Figure 44 presents converted doppler data, both corrected and uncorrected, for the vernier phase. As will be noted from the plot, transmitter drift is a substantial part of the total frequency change, with a resultant degradation of overall accuracy. However, performance evaluation of the vernier phase does not require the same high accuracy as the retrograde phase. All significant events from first segment acquisition to touchdown are evident on the curve.

VI. Trajectory Analysis for *Surveyor I*

Two seconds after the *Surveyor I* 14:41:00.990 GMT liftoff from Cape Kennedy on May 30, 1966, the *Atlas/Centaur* (*AC*-10) launch vehicle began a 13-s programmed roll that oriented the vehicle from a pad-aligned azimuth of 105 deg to a launch azimuth of 102.285 deg. At 15 s, a programmed pitch maneuver was initiated. The nominal and actual time for the *Atlas/Centaur* boost phase events are summarized in Table 24. All mark times were nominal except mark 8 (*Centaur* main engine cutoff), which occurred 6 s late. It was subsequently determined that this value is within the 3σ tolerance. The launch phase ascent trajectory profile is

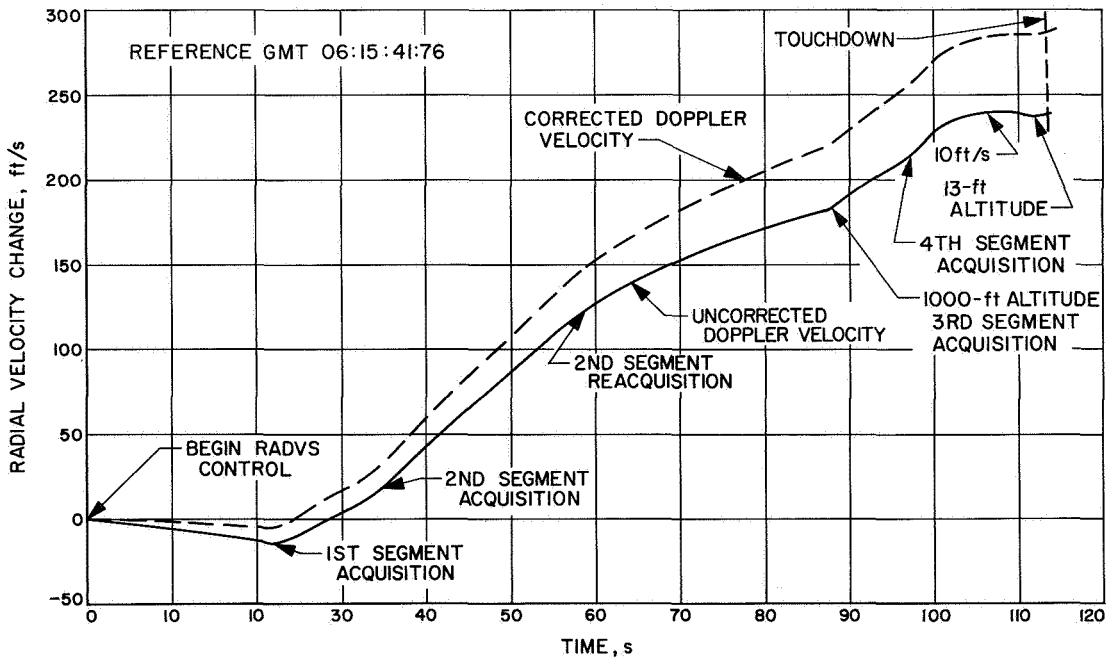

Fig. 44. Spacecraft radial velocity change relative to earth, vernier engine phase

illustrated in Fig. 45. The total mission profile is shown in Fig. 46.

Separation of *Surveyor I* from the *Centaur* occurred at 14:53:37.2 GMT on May 30, 1966 at a geocentric latitude and longitude of 17.6 and 312.1 deg, respectively. The spacecraft was in the sunlight at separation and entered neither the earth's nor the moon's shadow during the transit trajectory.

The predicted view periods for the three committed tracking stations are shown in Table 25. This summary is a compilation of the pre- and post-midcourse trajectories. The rise and set criteria are included under the *event* column. This table shows that the Tidbinbilla Deep Space Station at Canberra, Australia, did not see the spacecraft until about 15 h after launch. Some trajectories yield a small view period for this station during the first Johannesburg pass.

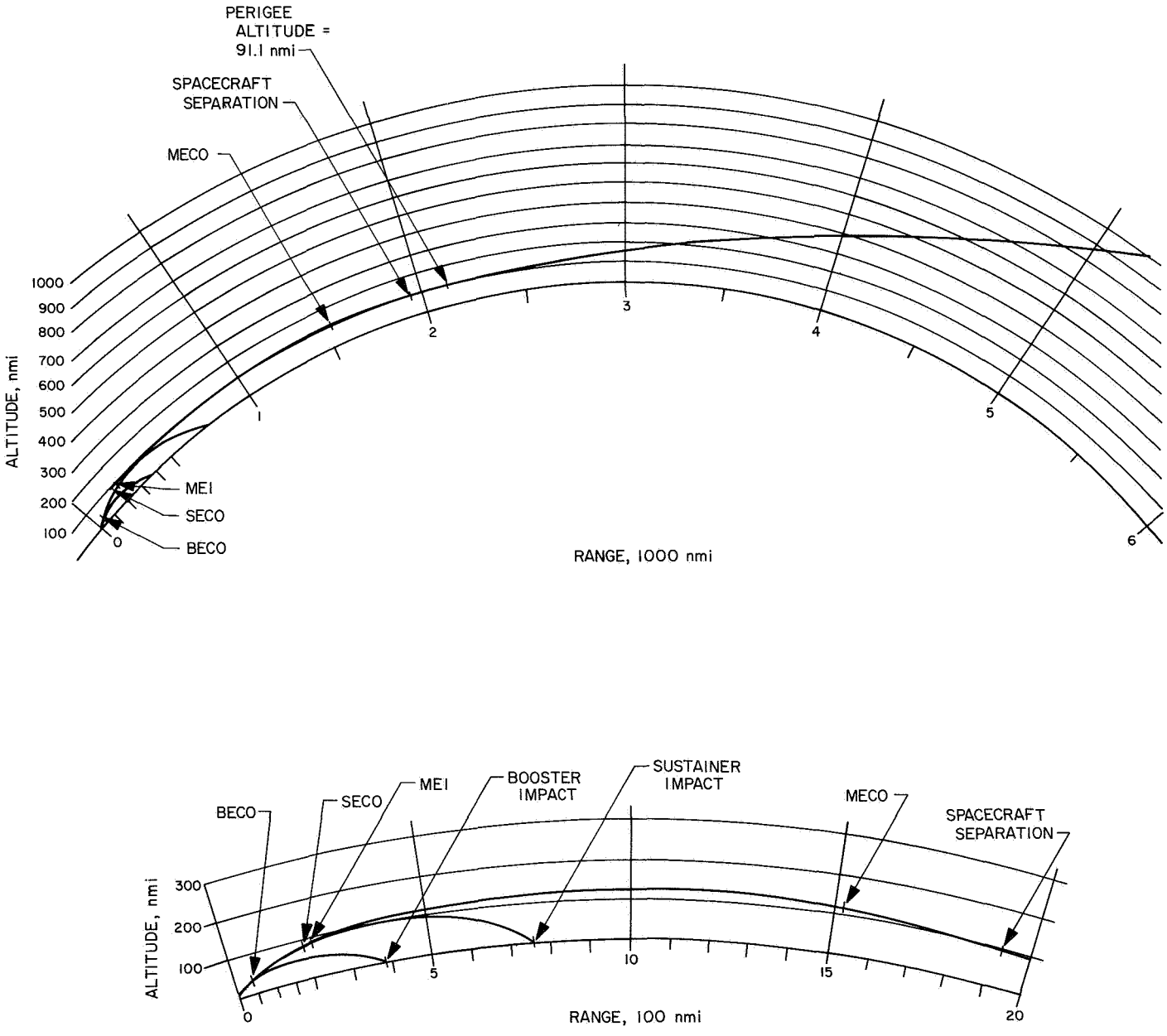

Fig. 45. Launch phase trajectory profile

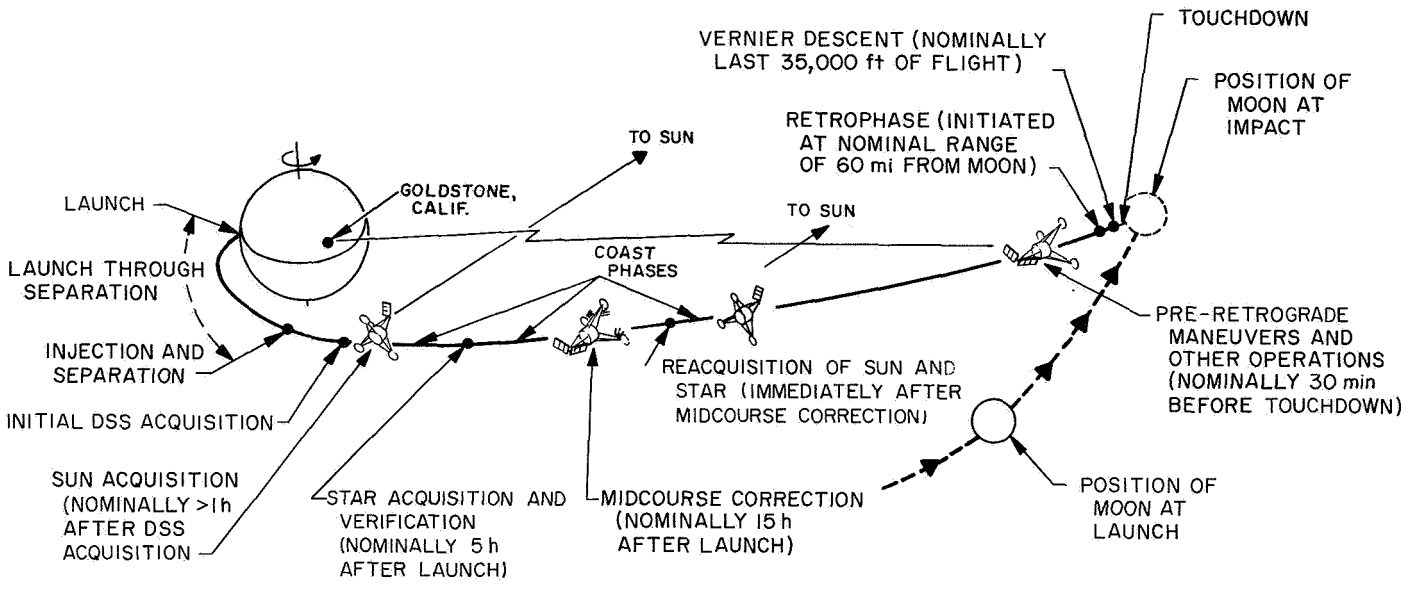

Fig. 46. Mission profile

Table 24. Mark events

Mark No.	Event	Nominal time, s	Actual time, s
	2-in. motion (liftoff, 14:41:00.99 GMT)	0.0	0.0
1	Booster engine cutoff (guidance discrete, staging acceleration 5.7g)	142.5	142.2
2	Jettison booster package	145.6	145.6
3	Jettison insulation panels	176.5	176.2
4	Jettison nose fairing	203.5	203.0
5	Sustainer engine cutoff (by propellant depletion)	239.7	239.3
6	Atlas/Centaur separation	241.7	241.8
7	Start Centaur main engines (SECO + 11.5 s)	251.2	251.9
8	Centaur main engine cutoff (guidance discrete)	683.3	689.3
9	Surveyor landing gear extend command	715.2	715.5
10	Surveyor omnidirectional antenna extend command	725.7	725.7
11	Surveyor high-power transmitter on	746.2	745.4
12	Centaur/Surveyor electrical disconnect	751.7	752.3
13	Separate spacecraft	757.2	757.1
14	Admit guidance	762.2	759.5
15	Start H_2O_2 engines (V), 180-deg turnaround mode	802.2	NA
16	Stop H_2O_2 engines, 180-deg turnaround mode	822.2	NA
17	Start retrothrust (Centaur tank blowdown)	997.2	996.0
18	Stop retrothrust	1247.2	1247.7
19	Energize power changeover switch	1247.2	1258.5

Table 25. Predicted view period summary

Station	Event	Time of event	
		Date 1966	GMT
DSS 51	5-deg el rise	5/30	15:04:30
DSS 11	5-deg el rise	5/31	02:08:40
DSS 51	90-deg HA set	5/31	02:16:36
DSS 42	5-deg el rise	5/31	05:59:23
DSS 11	5-deg el set	5/31	10:33:47
DSS 51	270-deg HA rise	5/31	15:00:04
DSS 42	5-deg el set	5/31	19:25:16
DSS 11	5-deg el rise	6/1	02:23:28
DSS 51	90-deg HA set	6/1	02:58:45
DSS 42	5-deg el rise	6/1	06:29:44
DSS 11	5-deg el set	6/1	11:08:04
DSS 51	270-deg HA rise	6/1	15:14:32
DSS 42	5-deg el set	6/1	19:36:12
DSS 11	5-deg el rise	6/2	02:25:13
DSS 51	90-deg HA set	6/2	03:09:12
DSS 42	5-deg el rise[a]	6/2	06:38:55
DSS 11	5-deg el set[a]	6/2	11:25:08

[a]View periods of moon's center.

Table 26. Pre-and post-midcourse injection and terminal conditions for *Surveyor I*

Coordinate system	Pre-midcourse injection conditions, May 30, 1966, 14:53:37.385 GMT					
Inertial cartesian	X = 2813.6136 km	Y = 5574.0461 km	Z = 1979.7524 km	DX = −8.3688738 km/s	DY = 5.5320036 km/s	DZ = −4.4497759 km/s
Inertial spherical	RAD = 6550.2540 km	DEC = 17.592224 deg	RA = 63.216706 deg	VI = 10.974589 km/s	PTI = −1.2120495 deg	AZI = 114.75517 deg
Earth-fixed spherical	RAD = 6550.2540 km	LAT = 17.592224 deg	LON = 312.14293 deg	VE = 10.562934 km/s	PTE = −1.2592931 deg	AZE = 115.78965 deg
Orbital elements	C3 = −1.2639824 km^2/s^2	ECC = 0.97923824	INC = 30.044723 deg	TA = −2.4498112 deg	LAN = 276.45793 deg	APF = 145.31695 deg
Coordinate system	**Pre-midcourse encounter conditions, June 2, 1966, 05:28:59.985 GMT**					
Selenocentric	RAD = 1738.09 km	LAT = −11.419473 deg	LON = 305.85900 deg	VP = 2.6649810 km/s	PTP = −79.992989 deg	AZP = 266.77994 deg
Miss parameter earth equator	BTQ = −585.25804 km	BRQ = 305.93221 km	B = 660.39495 km			
Miss parameter moon equator	BTT = −656.92308 km	BRT = 67.634913 km	B = 660.39565 km			
Coordinate system	**Post-midcourse injection conditions, May 31, 1966, 06:45:53.800 GMT**					
Inertial cartesian	X = −103401.67 km	Y = −107006.61 km	Z = −66323.279 km	DX = −0.88951855 km/s	DY = −1.5378124 km/s	DZ = −0.62099156 km/s
Inertial spherical	RAD = 1629.1439 km	DEC = −24.023111 deg	RA = 225.98155 deg	VI = 1.8819512 km/s	PTI = 76.179004 deg	AZI = 72.573537 deg
Earth-fixed spherical	RAD = 1629.1439 km	LAT = −24.023111 deg	LON = 236.18758 deg	VE = 10.581803 km/s	PTE = 9.9447604 deg	AZE = 270.74016 deg
Orbital elements	C3 = −1.3516429 km^2/s^2	ECC = 0.97691524	INC = 29.371361 deg	TA = 159.89571 deg	LAN = 278.34842 deg	APF = 144.00209 deg
Coordinate system	**Post-midcourse encounter conditions, June 2, 1966, 06:15:14.632 GMT**					
Selenocentric	RAD = 1735.6000 km	LAT = −2.3555486 deg	LON = 316.64097 deg	VP = 2.6553638 km/s	PTP = −83.868529 deg	AZP = 343.30690 deg
Miss parameter earth equator	BTQ = −253.86534 km	BRQ = −327.05272 km	B = 414.01824 km			
Miss parameter moon equator	BTT = −114.52272 km	BRT = −397.86410 km	B = 414.01824 km			

Definitions of computer printout terms

X, Y, Z } cartesian components of spacecraft radius vector

DX, DY, DZ } cartesian components of spacecraft velocity vector

RAD spacecraft radius distance

DEC spacecraft declination angle

RA spacecraft right ascension angle

VI, VE spacecraft velocity

PTI, PTE pitch angle of the spacecraft velocity vector with respect to the local horizontal

AZI, AZE azimuth angle of the spacecraft velocity vector measured east of true north

C_3 twice the total energy

ECC eccentricity

INC inclination of the orbit plane to the equatorial plane

TA true anomaly

LAN longitude of ascending node

APF argument of the ascending node

VP selenocentric spacecraft velocity

PTP selenocentric pitch angle

AZP selenocentric azimuth angle

BTQ projection of the impact parameter B upon the vector T (T parallel to the earth equatorial plane)

BRQ projection of the impact parameter B upon the vector R (T parallel to the earth equatorial plane)

BTT projection of the impact parameter B upon the vector T (T parallel to the true lunar equator)

BRT projection of the impact parameter B upon the vector T (T parallel to the true lunar equator)

B magnitude of the impact parameter

The midcourse maneuver was performed on May 31 at 06:45; the Pioneer Deep Space Station at Goldstone had viewed *Surveyor* for about 4½ h, pre-midcourse, and for about 3¾ h, postmidcourse. Pre- and postlanding, Goldstone visibility was approximately 4 and 5 h, respectively. Predicted touchdown time was June 2, 1966 at 06:17:36.8 GMT.

In Table 26 pre- and post-midcourse injection and terminal conditions have been tabulated. These results, obtained several days after the mission, are considered final. The slight difference between the Table 26 data and the final OD data is from the computer input–output conversion errors.

The proximity of the uncorrected and the original aim point is shown in Fig. 47. The uncorrected, unbraked impact point is located on the western edge of Oceanus Procellarum, west of the crater Hansteen. The coordinates

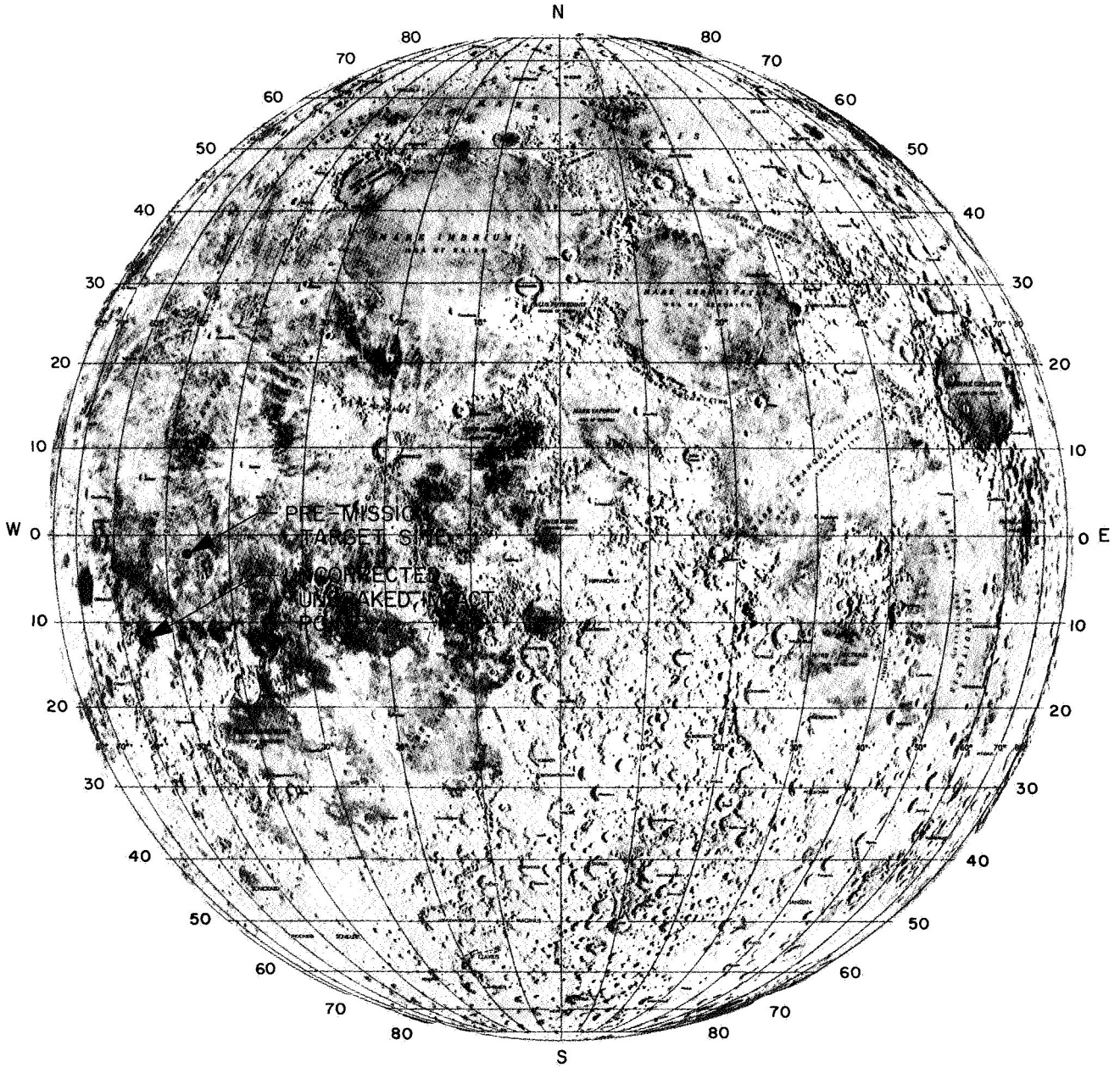

Fig. 47. *Surveyor I* target and uncorrected impact points

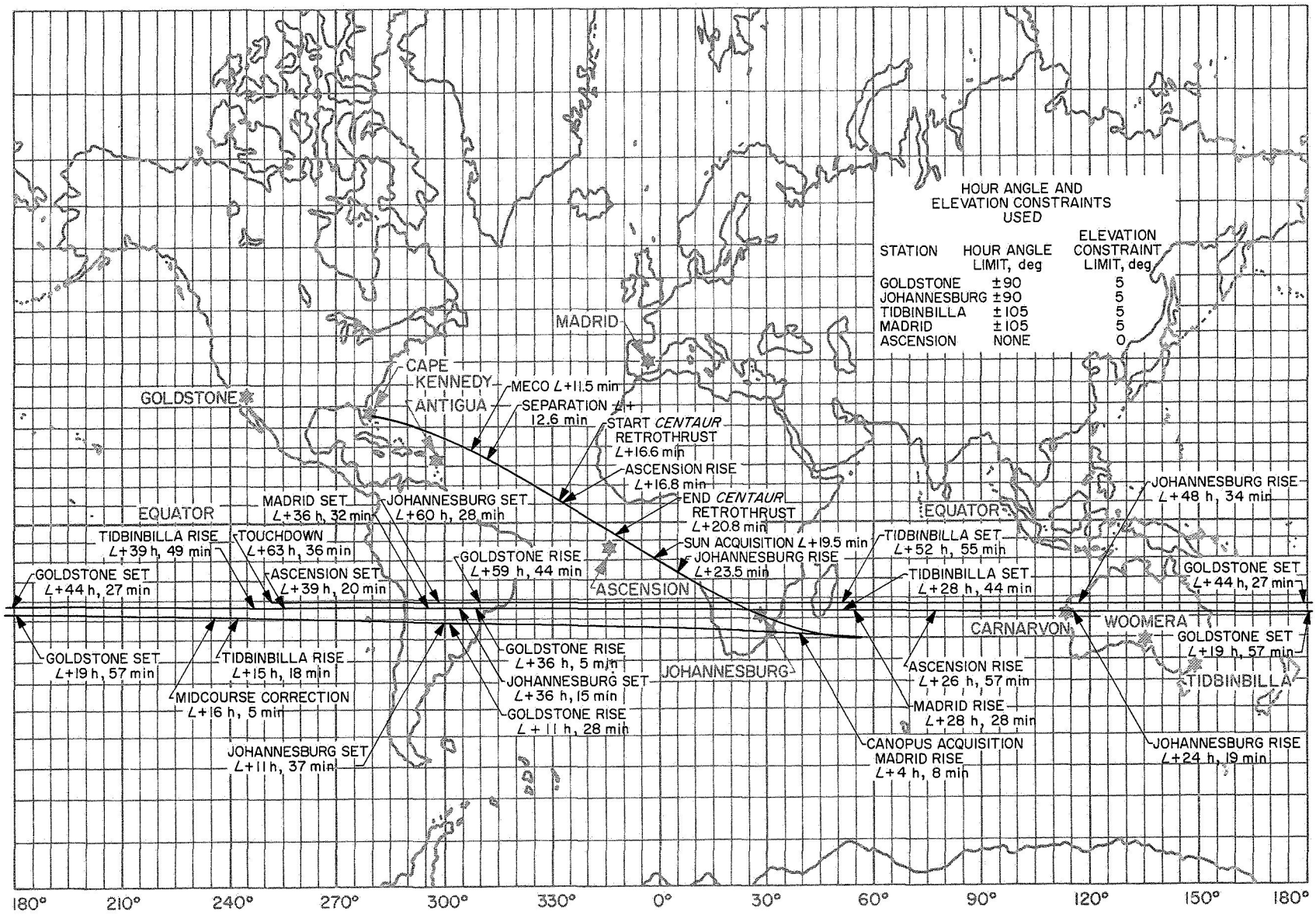

Fig. 48. *Surveyor I* earth track

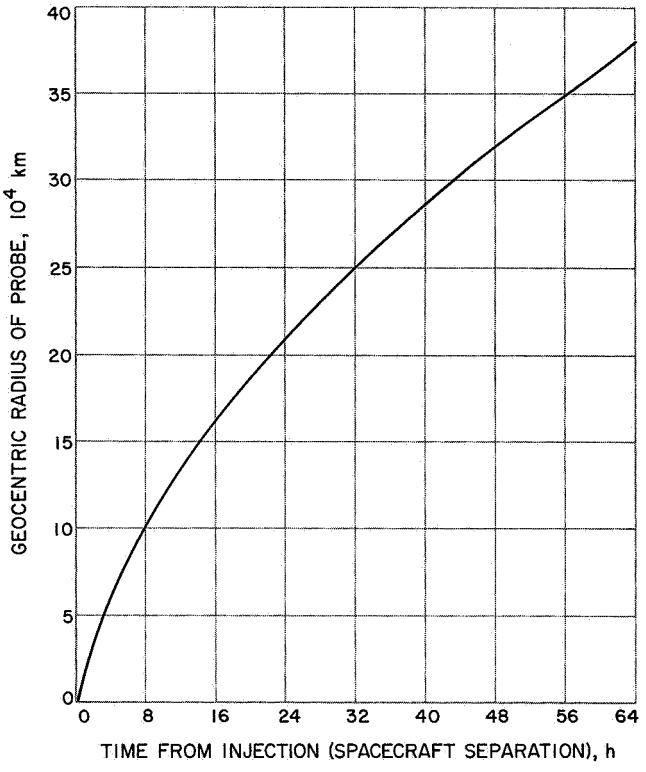

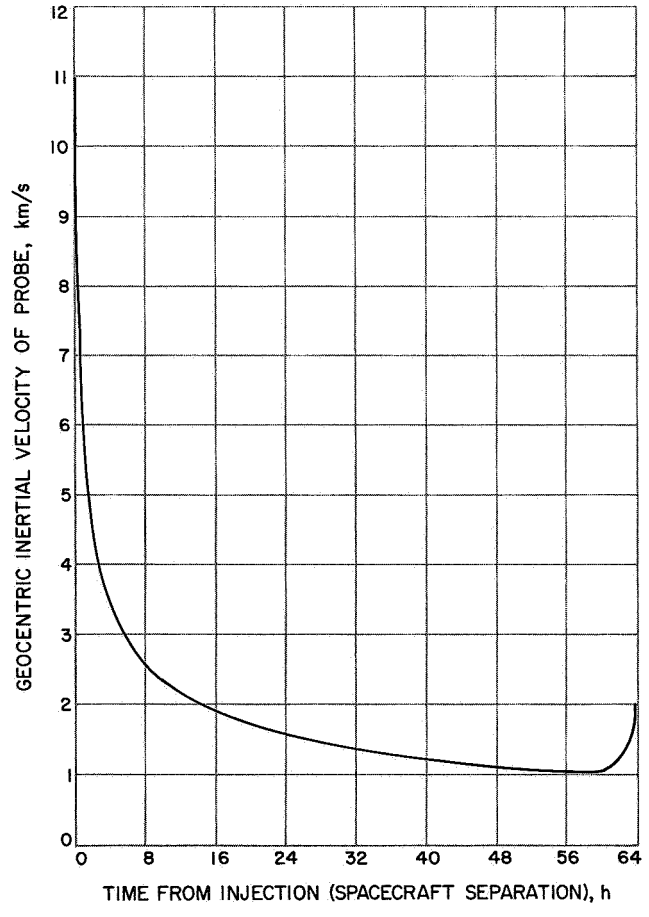

Fig. 50. Probe geocentric inertial velocity vs time

are approximately −11.425 deg latitude and 305.853 deg longitude.

The aim point is approximately 400 km to the northeast just north of the crater Flamsteed (i.e., −3.25 deg latitude and 316.17 deg longitude).

Figure 48 gives the earth track traced by *Surveyor I* and shows its position at such specific events as sun and Canopus acquisition, midcourse maneuver, touchdown. Rise and set times for the Deep Space Stations are also shown. Figures 49 and 50 are plots of the probe's geocentric radius and velocity as functions of time from injection, or the spacecraft's separation from *Centaur*. Figure 51 shows the earth–probe–moon, sun–probe–moon, and earth–probe–sun angles vs time from injection. Figure 52 shows the cone and clock angles as

Fig. 49. Probe geocentric radius vs time

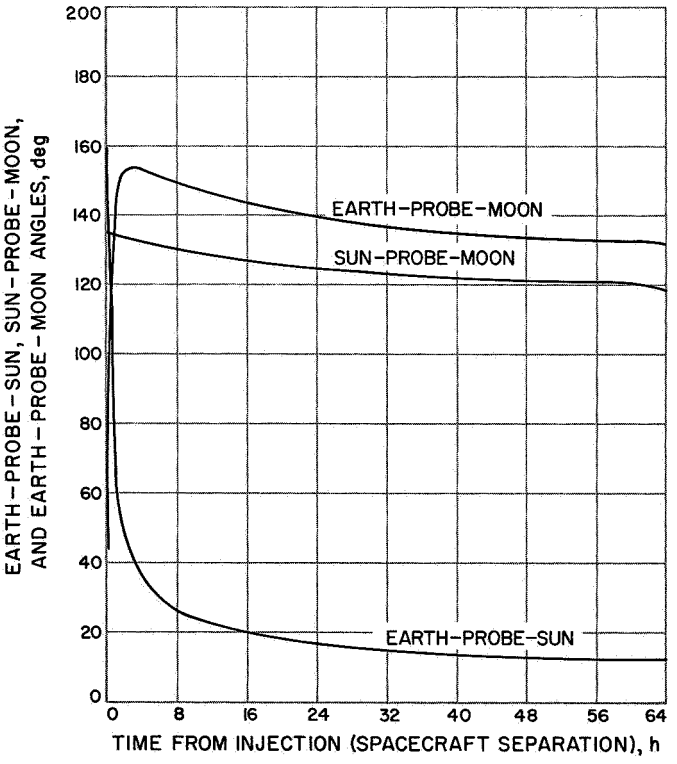

Fig. 51. Earth–probe–sun, sun–probe–moon, and earth–probe–moon angles vs time from injection (spacecraft separation)

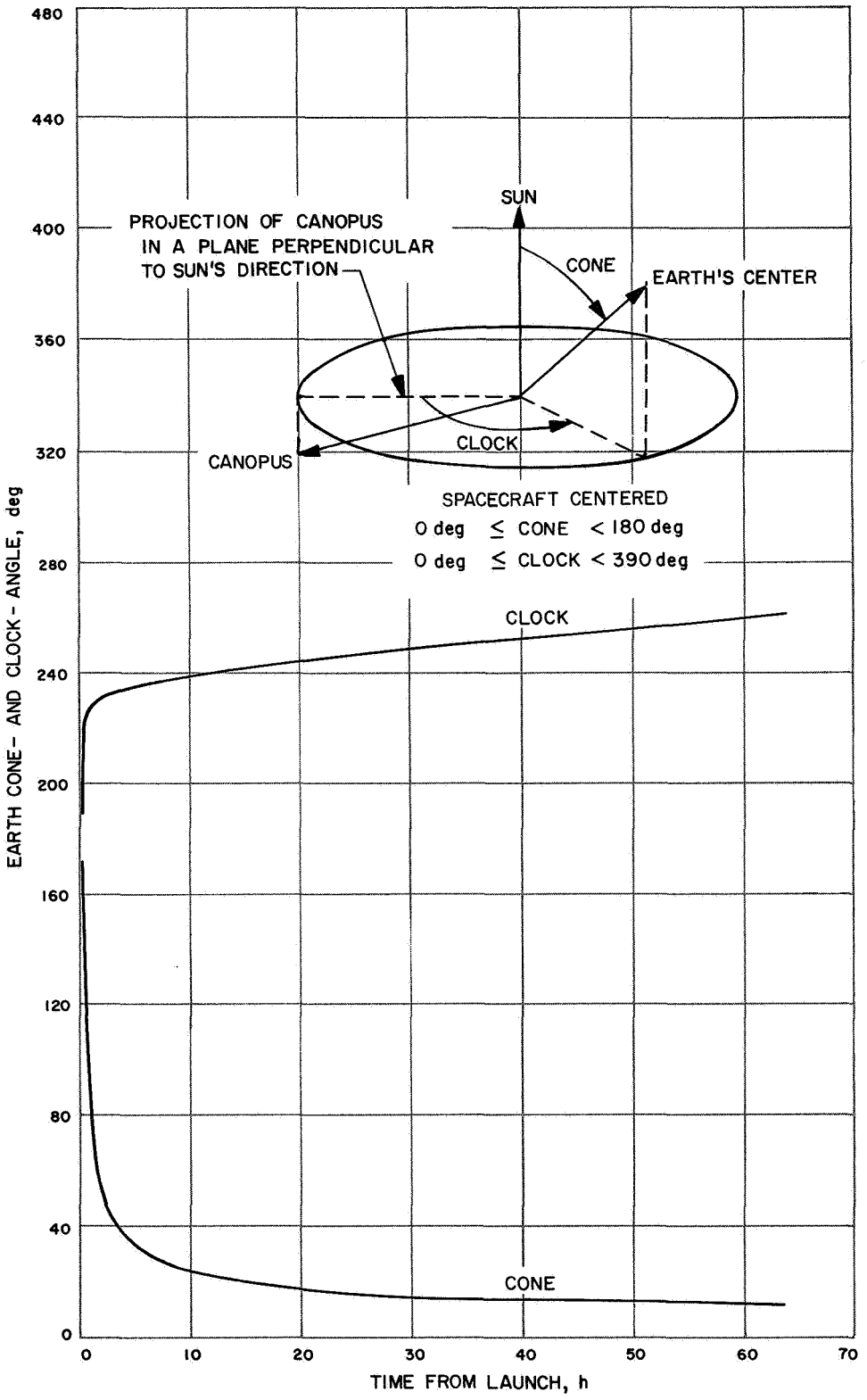

Fig. 52. Earth cone and clock angles vs time from launch

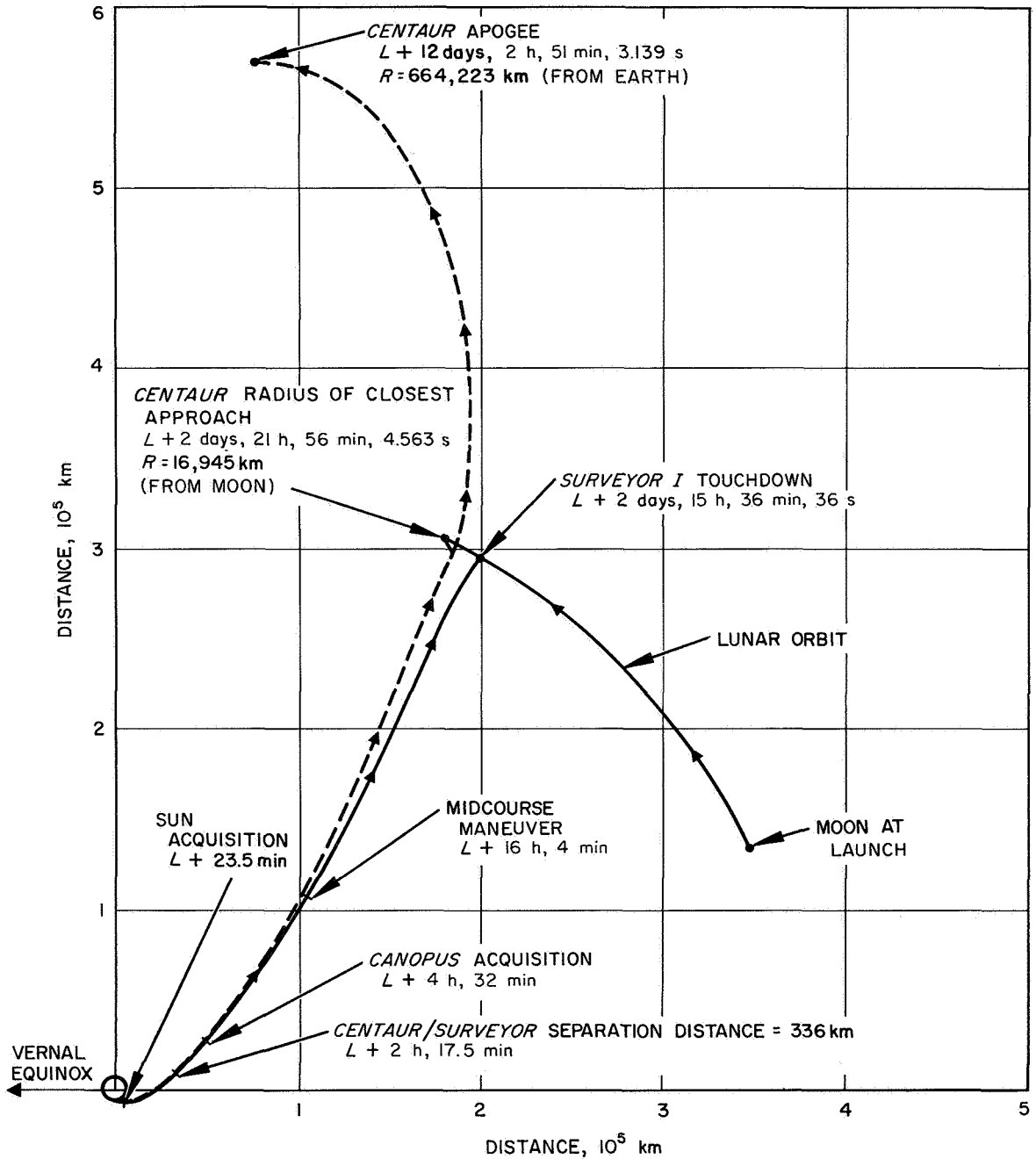

Fig. 53. *Surveyor I* and *Centaur* trajectories in earth's equatorial plane

functions of time. The coordinate system is defined on the figure. In the cruise mode, the spacecraft $-Z$ axis is aligned to the sun and the $-X$ axis to the projection of Canopus.

Figure 53 illustrates the *Centaur* and *Surveyor* trajectories. The projection of each trajectory is plotted on the earth's equatorial plane. The best estimate of the *Centaur* injection conditions was obtained from AFETR. These conditions were computed inflight based on post-retromaneuver data. A mission design constraint stated that the *Centaur–Surveyor* separation distance was required to be 336 km by at least 5 h after injection to eliminate possible *Centaur* interference during Canopus acquisition. The required separation distance was reached 2 h and 17.5 min after launch. The *Centaur* passed above and behind the moon about 6 h and 20 min after *Surveyor I* touchdown.

During lunar encounter, the *Centaur* experienced a 5-deg orbit-plane change and an increase in *vis viva* energy of about 0.5 km^2/s^2. First apogee occurred June 11, 1966 at 17:32:04.139 at a distance of 644,223 km from earth. Perigee occurred June 23, 1966 at 21:15:30.923; the radius at closest approach to the earth was 32,722 km.

VII. Analysis of Air Force Eastern Test Range Tracking Data for *Surveyor I*

A. Initial Flight Phase Requirements

During the *Surveyor I* mission, the AFETR was responsible for providing classical orbit elements for the spacecraft transfer orbit and the *Centaur* postretro orbit and also for providing initial acquisition information to the DSS tracking stations. These calculations were performed on a CDC 3600 computer located at AFETR with use of *Centaur* vehicle tracking data obtained from the downrange AFETR tracking stations. Results of these calculations were transmitted to the JPL Space Flight Operations Facility (SFOF) in Pasadena. The acquisition information was relayed to the DSN stations, where the initial orbital elements are nominally used as starter values for the initial JPL orbital calculation.

In addition to the above requirements, AFETR transmitted the C-band pulse radar data obtained during the transfer orbit and the *Centaur* post-retromaneuver orbit to the SFOF. The transfer orbit data was used during flight operations to provide a backup to the AFETR computations. The *Centaur* post-retromaneuver data were important for verifying the *Centaur* retroengine firing and the *Centaur* post-retromaneuver orbit. The retromaneuver was performed (1) to ensure that the *Centaur* did not impact the lunar surface and (2) to provide a separation between the *Centaur* and the spacecraft so that the Canopus sensor on board the spacecraft would not lock up on the *Centaur* instead of Canopus.

During the period between the main engine cutoff and the start of retrothrust on *Surveyor I* mission, only one low-density data point (1 point/6 s) was obtained. This data point was from the Antigua 91.18 station. Usable low-density data were obtained from the Ascension 12.18 radar from 30 s before the completion of the retromaneuver to 16:56:48 GMT. After this time, the Ascension radar intermittently lost lock on the *Centaur*. The Pretoria station obtained usable low-density data from 4 min, 35 s after the retromaneuver to 15:23:00 GMT; thereafter, the radar only intermittently locked on the *Centaur*. The Ascension and Pretoria coverage and the associated spacecraft events are shown in Fig. 54. This figure also illustrates the elevation angles of the data obtained from the stations.

B. Analysis of the Transfer Orbit Data

Since JPL received only one usable low-density data point between main engine cutoff and retrothrust, no attempt was made to determine the transfer orbit at real time nor was one made postflight.

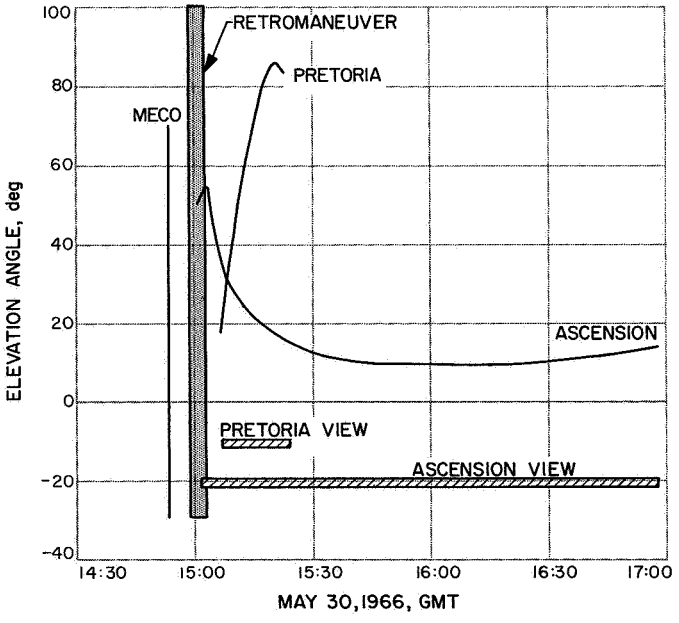

Fig. 54. AFETR station coverage and elevation angle

Table 27. Summary of data for post-retromaneuver orbit

Station	Data type	Data acquisition time, GMT		Data points received	Data points used	Data points rejected	Comment
		Start	End				
Ascension	Range	15:01:18	17:04:54	910	877	33	12.18 radar had intermittent lock on *Centaur* after 16:56:47 GMT.
	Azimuth			910	887	23	
	Elevation			908	883	25	
Pretoria	Range	15:04:30	20:02:33	139	125	14	13.16 radar had intermittent lock on *Centaur* after 15:23:00 GMT.
	Azimuth			139	127	12	
	Elevation			139	125	14	

C. Analysis of the Post-retromaneuver *Centaur* Data

Centaur post-retromaneuver tracking data were received from both the Ascension and Pretoria tracking stations. The amounts of data, by data type, available from these stations is summarized in Table 27. Three postflight orbit solutions, based on the post-retromaneuver data, were obtained at JPL: (1) a solution using only Ascension data, (2) a solution using only Pretoria data, and (3) a combined solution using both Ascension and Pretoria data. These solutions indicated that the *Centaur* would miss the moon by approximately 21,000 km. The numerical values for the parameters from the three solutions are given in Table 28. Two AFETR realtime post-retromaneuver solutions are also presented in the table, as are the differences between the comparable JPL and AFETR solutions. Amounts of data, together with associated noise statistics, used in the JPL computations are given in Table 29.

The residual plots, or the observed minus computed values (O − C) from the initial postflight orbit computation with data from both Pretoria and Ascension, indicated that the data were inconsistent. A check with AFETR personnel revealed that the time tag on the Ascension data was in error by −50 ms. Another combined orbit solution was obtained after the time correction to Ascension data. Examination of the residual plots indicated that the data fit had improved slightly, but inconsistencies still existed. Residuals > 600 m could be seen in the Ascension range data, and > 100 m in the Pretoria range data. In an attempt to determine the cause of these large residuals, the station location parameters of the Ascension radar were solved. This location solution changed the geocentric radius by 6 km from the survey radius. Examination of the residual plots indicated no improvement in the range data fit, and only a slight improvement in elevation data fit. Therefore, this solution was discarded.

From examining the single-station solutions, the Pretoria solution indicates a fairly good orbit fit with O − C range residuals less than 30 m. However, the O − C azimuth residuals showed that Pretoria radar has noisy azimuth data, particularly the span after 15:18:54 GMT. By passing the converged conditions of the Ascension solution through the Pretoria data, the elevation and azimuth residuals showed a trend change and a sudden jump in the azimuth residual at approximately 15:17 GMT. This change indicates that there are some problems with the Pretoria angle data. The Ascension solution indicates an inconsistency between the range, elevation, and azimuth data. Some O − C range residuals were in excess of 300 m, and these residuals have long-period sinusoidal effects. By passing the converged conditions from the Pretoria solution through the Ascension data, the O − C residuals showed that the inconsistency is caused by the Ascension range data. The single-station solutions show that there are discrepancies in the tracking data from both stations. It was these discrepancies that caused the poor fits to the solutions.

D. Conclusions

No AFETR transfer orbit data were obtained to check the initial orbit estimates based on DSIF data. However, the Ascension and Pretoria data were useful for verifying the retrofiring and for determining the *Centaur* post-retromaneuver orbit.

Table 28. Post-retromaneuver orbit parameter solutions

Parameter	JPL postflight orbit solutions			AFETR realtime post-retromaneuver orbit solutions		Differences between JPL and AFETR solutions	
	Data from Ascension and Pretoria	Data from Pretoria, only	Data from Ascension, only	Orbit 1: Data from Ascension, only	Orbit 2: Data from Ascension and Pretoria	Data from Ascension, only	Data from Ascension and Pretoria
Epoch, May 30, 1966	14:52:27.500 GMT	14:52:27.500 GMT	14:52:27.500 GMT	15:03:56.9 GMT	15:22:59.9	—	—
Radius, km	6588.2492	6587.7314	6593.9651	—	—	—	—
Latitude, deg	20.267938	20.254827	20.237263	—	—	—	—
Longitude, deg	306.01748	305.99662	306.05822	—	—	—	—
Velocity, km/s	10.508606	10.509051	10.503371	—	—	—	—
Elevation angle, deg	−4.6363887	−4.6396305	−4.6562714	—	—	—	—
Azimuth, deg	113.64807	113.62309	113.68757	—	—	—	—
Semimajor axis, km	231528.47	231778.96	231174.11	230657.3	226655.8	516.8	4872.7
Eccentricity	0.97171917	0.97175219	0.97165273	0.9716148	0.971116	0.0000379	0.000603
Inclination, deg	30.067297	30.041599	30.074162	30.04640	30.07320	0.02776	0.0059
Lon of node, deg	276.43258	276.42740	276.38212	276.4254	276.4593	0.0433	0.0267
Argument of perigee	145.30922	145.30683	145.43868	145.35265	145.33082	0.08603	0.02160
C_3, km^2/s^2	−1.7216080	−1.7197474	−1.7242471	−1.72	−1.75	0	0.03
B, km	20931.117	20909.696	21171.993	21032.103	20860.546	139.890	70.571
B • **T**T, km	16913.770	16883.678	16825.137	17071.845	16965.417	246.708	51.647
B • **R**T, km	−12330.538	−12335.187	−12851.771	−12284.196	−12138.246	567.575	192.292

Table 29. Post-retromaneuver orbit data statistics

Station	Data type	Number of points	Two-station solution		Single-station solution	
			Standard deviation	Mean	Standard deviation	Mean
Pretoria	Range, km	125	0.0523	0.0580	0.0107	0.000419
	Azimuth, deg	127	0.129	0.00268	0.0926	0.00292
	Elevation, deg	125	0.0243	−0.0240	0.0229	0.00921
Ascension	Range, km	877	0.235	0.0116	0.164	0.00235
	Azimuth, deg	887	0.0142	−0.00674	0.0346	−0.0237
	Elevation, deg	883	0.0255	0.0200	0.0452	0.0683

VIII. *Surveyor II* Mission Summary

For *Surveyor II*, the landing site selected prior to launch for targeting of the launch vehicle ascent trajectory was near the center of the *Apollo* zone of interest at 0.0-deg latitude, 359.33-deg longitude (0.67 deg west longitude). The following factors influenced the selection of this site: predicted terrain smoothness, desire to land within the *Apollo* zone, off-vertical approach angle of near 25 deg, and good postlanding lighting. An unbraked impact speed was selected so that the Goldstone arrival visibility constraints would be satisfied for all launch days in the launch period.

The *Surveyor II* spacecraft was launched from AFETR launch site 36A at Cape Kennedy, Florida, on Tuesday, September 20, 1966, using an *Atlas/Centaur* (*AC*-7) boost vehicle. The launch was held until the close of the launch window when difficulties were experienced with the *Atlas* boiloff and liquid oxygen topping valve. Liftoff occurred at 12:31:59.824 GMT. Two seconds after liftoff, the launch vehicle began a 13-s programmed roll that oriented the vehicle from a pad aligned azimuth of 105 deg to a launch azimuth of 114.361 deg. At 15 s, a programmed pitch maneuver was initiated. The actual times for the *Atlas/Centaur* boost phase events were nominal.

Separation of *Surveyor* from *Centaur* occurred at 12:44:32.4 GMT on September 20, 1966, at a geocentric latitude and longitude of 12.9 and 309.8 deg, respectively. The spacecraft was in the sunlight at separation and never entered the earth's shadow during the transit trajectory.

For approximately the first 16½ h of flight, a nominal mission was achieved, including Canopus star acquisition. When the three vernier engines were commanded on for midcourse velocity correction, which lasted 9.8 s, vernier engine 3 failed to provide thrust, causing the spacecraft to tumble at a rate of about 1.22 rev/s.

The nitrogen gas jet system, which is normally enabled during and after the midcourse velocity correction, operated for several minutes to stabilize the spacecraft. Although the spin rate was reduced to 0.97 rev/s, the gas jet system was inhibited after about 60% of the gas had been expended and it became evident that the remaining gas supply was insufficient to stop the spinning.

During the remaining life of the spacecraft, a total of 39 attempts were made to overcome the vernier engine problem by firing the engines for short periods, ranging from 0.2 to 2.5 s and, finally, for 21.5 s. Vernier engine 3 did not respond to any of these attempts. However, thrust was delivered by the other two vernier engines in each firing, and the spacecraft finally reached a spin rate of 2.3 deg/s.

About 28½ h after the attempted midcourse correction, when very little battery power remained, a final sequence was commanded that fired the main retromotor and vernier engines 1 and 2. The spacecraft signal was lost about 30 s after main retroengine ignition, which brought the *Surveyor II* mission to an end.

Reference 19 presents a more detailed description of the *Surveyor II* mission.

A. Trajectory Characteristics

Figures 55, 56 and 57 show the trajectory path on the stereographic projection of DSS 51, DSS 11, and DSS 42, respectively. In Table 30 pre-midcourse injection and terminal conditions have been tabulated.

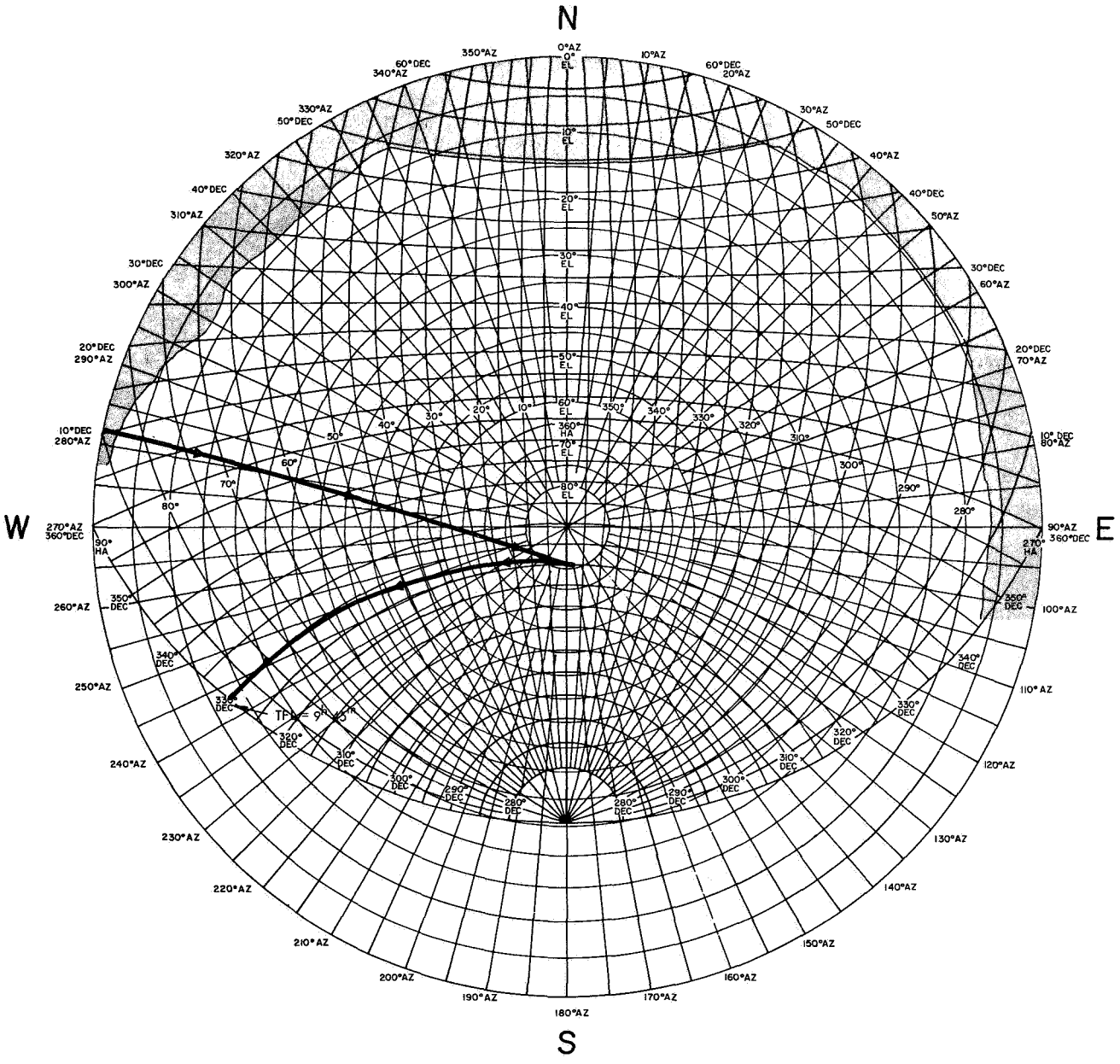

Fig. 55. Stereographic projection, DSS 51, Johannesburg Deep Space Station, *Surveyor II*

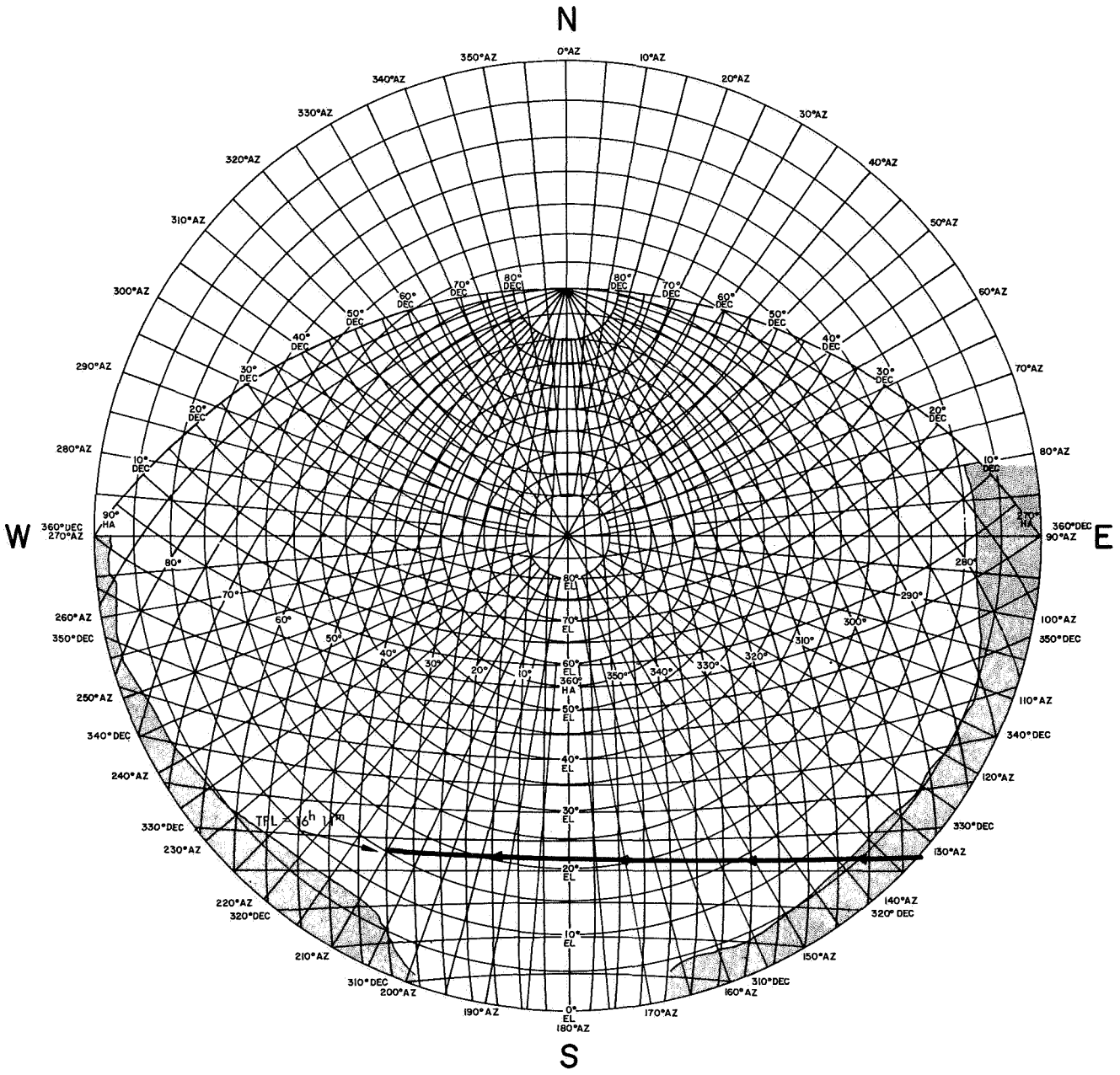

Fig. 56. Stereographic projection, DSS 11, Pioneer Deep Space Station, *Surveyor II*

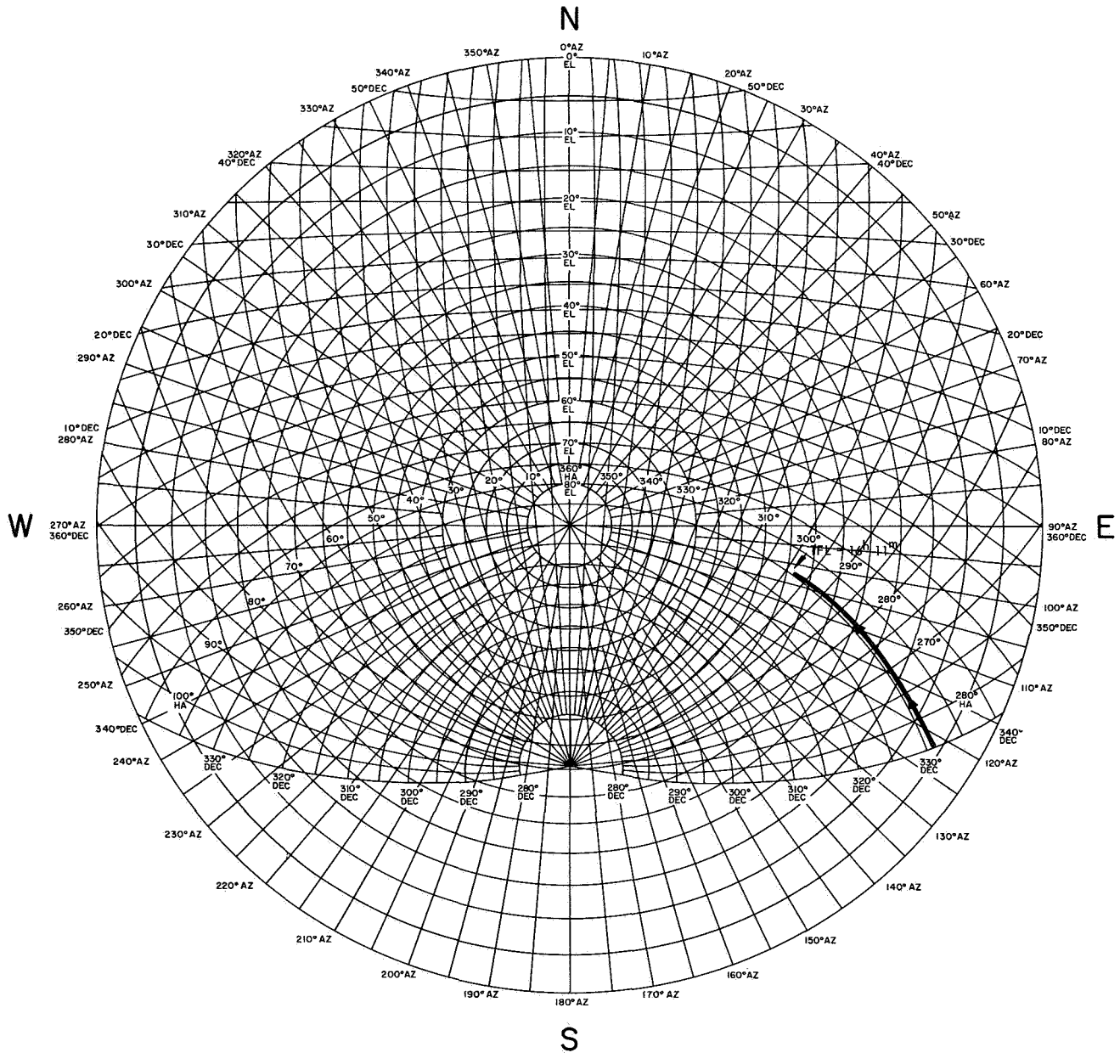

Fig. 57. Stereographic projection, DSS 42, Tidbinbilla Deep Space Station, *Surveyor II*

Table 30. Pre-midcourse injection and terminal conditions for *Surveyor II*

Coordinate system	Pre-midcourse injection conditions on September 20, 1966, 12:43:13.670 GMT					
Inertial cartesian	X = −4360.9041 km	Y = 4616.8513 km	Z = 1896.4001 km	DX = −8.7282187 km/s	DY = −4.5253066 km/s	DZ = −4.7559824 km/s
Inertial spherical	RAD = 6627.9056 km	DEC = 16.626021 deg	RA = 133.36699 deg	VI = 10.921519 km/s	PTI = 6.4654237 deg	AZI = 119.42063 deg
Earth-fixed spherical	RAD = 6627.9056 km	LAT = 16.626021 deg	LON = 303.60264 deg	VE = 10.523257 km/s	PTE = 6.7112166 deg	AZE = 120.66787 deg
Orbital elements	C3 = −1.0001392 km^2/s^2	ECC = 0.98358240	INC = 33.423575 deg	TA = 13.039233 deg	LAN = 340.26840 deg	APF = 135.66564 deg
Coordinate system	**Pre-midcourse encounter conditions on September 23, 1966, 03:19:54.426 GMT**					
Selenocentric	RAD = 1738.5 km	LAT = −0.051930781 deg	LON = 354.70985 deg	VP = 2.6614642 km/s	PTP = −69.779146 deg	AZP = 90.222833 deg
Miss parameter earth equator	BTQ = 1321.7977 km	BRQ = 1793.8803 km	B = 1333.9151 km			
Miss parameter moon equator	BTT = 1333.9064 km	BRT = 5.1242575 km	B = 1333.9162 km			

Definitions of computer printout terms

X, Y, Z } cartesian components of spacecraft radius vector

DX, DY, DZ } cartesian components of spacecraft velocity vector

RAD spacecraft radius distance

DEC spacecraft declination angle

RA spacecraft right ascension angle

VI, VE spacecraft velocity

PTI, PTE pitch angle of the spacecraft velocity vector with respect to the local horizontal

AZI, AZE azimuth angle of the spacecraft velocity vector measured east of true north

C_3 twice the total energy

ECC eccentricity

INC inclination of the orbit plane to the equatorial plane

TA true anomaly

LAN longitude of ascending node

APF argument of the ascending node

VP selenocentric spacecraft velocity

PTP selenocentric pitch angle

AZP selenocentric azimuth angle

BTQ projection of the impact parameter B upon the vector T (T parallel to the earth equatorial plane)

BRQ projection of the impact parameter B upon the vector R (T parallel to the earth equatorial plane)

BTT projection of the impact parameter B upon the vector T (T parallel to the true lunar equator)

BRT projection of the impact parameter B upon the vector T (T parallel to the true lunar equator)

B magnitude of the impact parameter

The proximity of the uncorrected and the original aiming point is shown in Fig. 58. The uncorrected, unbraked impact point is located on the western edge of Sinus Medii, just northeast of the crater Mosting. The selenographic coordinates of this point are approximately −0.0837 deg latitude and 354.658 deg longitude. The targeted aiming point was 0.0 deg latitude and 359.33 deg longitude. The two points are approximately 142 km (88 mi) apart on the surface of the moon. Also shown on Fig. 58 is the approximate final impact site of the spacecraft.

B. Midcourse Correction Characteristics

A midcourse correction 9.587 m/s was computed with the intent of softlanding *Surveyor II* at a desired site, +0.55-deg latitude and +359.17-deg longitude, on the lunar surface. This correction was executed upon ground command at 05:00 GMT on September 21, 1966.

The 99% dispersions are shown as an ellipse on the surface with a semimajor axis of 53.9 km (1.77 deg), a semiminor axis of 17.17 km (0.56 deg) and an orientation

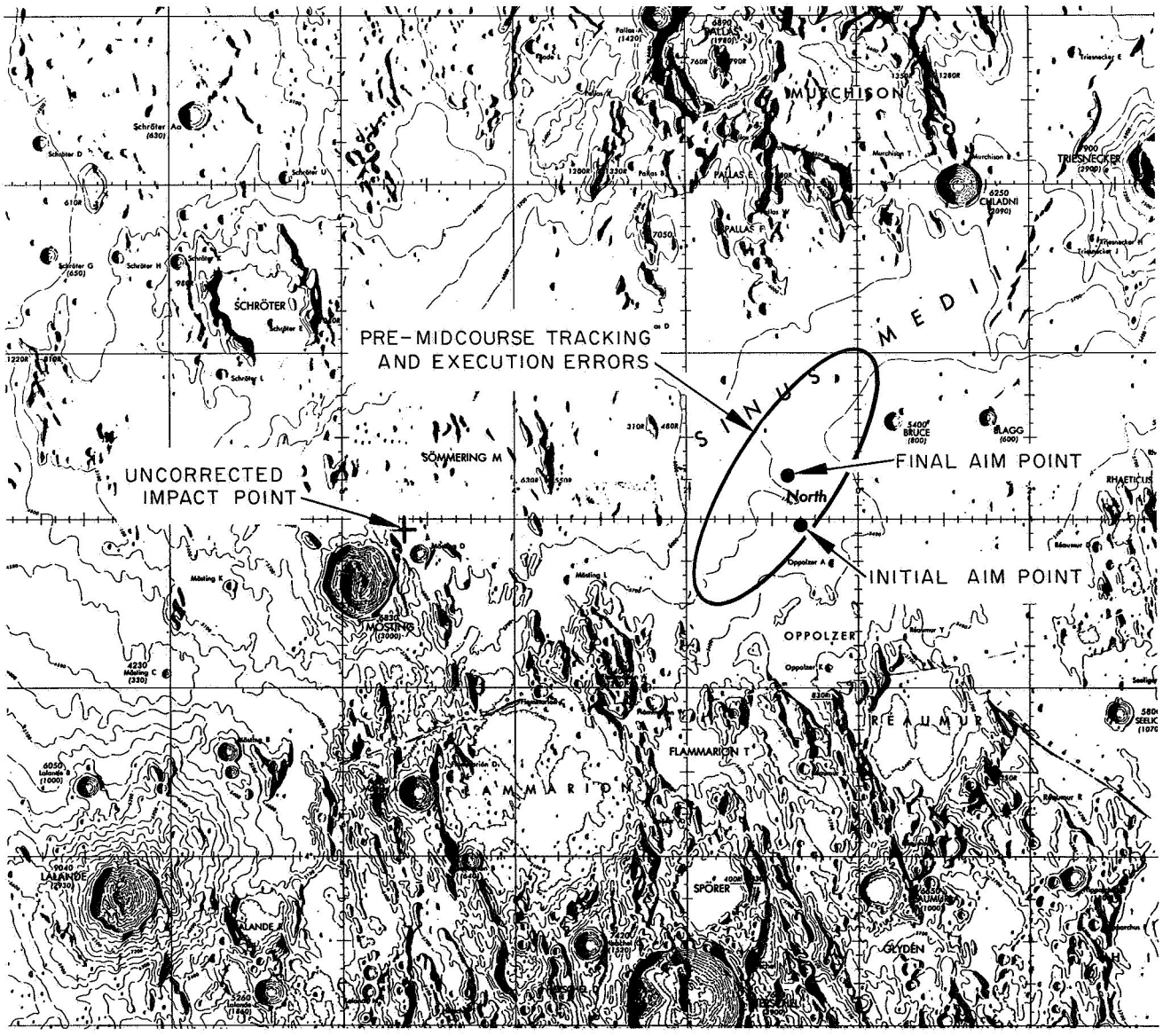

Fig. 58. *Surveyor II* impact locations

angle of −57.1 deg (see Fig. 58). To maximize the probability of softlanding, the aim point was biased from the original target value of 0.0 deg latitude and 359.33 deg longitude. The biasing was based on a detailed examination of *Lunar Orbiter* photographs.

The maximum midcourse correction capability, as a function of the unbraked impact speed, is shown in Fig. 59. The expected 3σ *Centaur* injection guidance dispersions and the effective lunar radius are also shown.

The maneuver execution time of 16.2795 h after injection was chosen. This time allowed 6 h, 17 min of premidcourse and 1 h, 11 min of postmidcourse visibility from the Goldstone tracking facility. Nominally, the midcourse time was 14.5295 hours after injection, but was delayed 1 h, 45 min because of operational difficulties.

The predicted results of the selected midcourse correction and other alternatives considered are given in Table 31. The required velocity component in the critical plane, to correct miss only, was 1.185 m/s. The

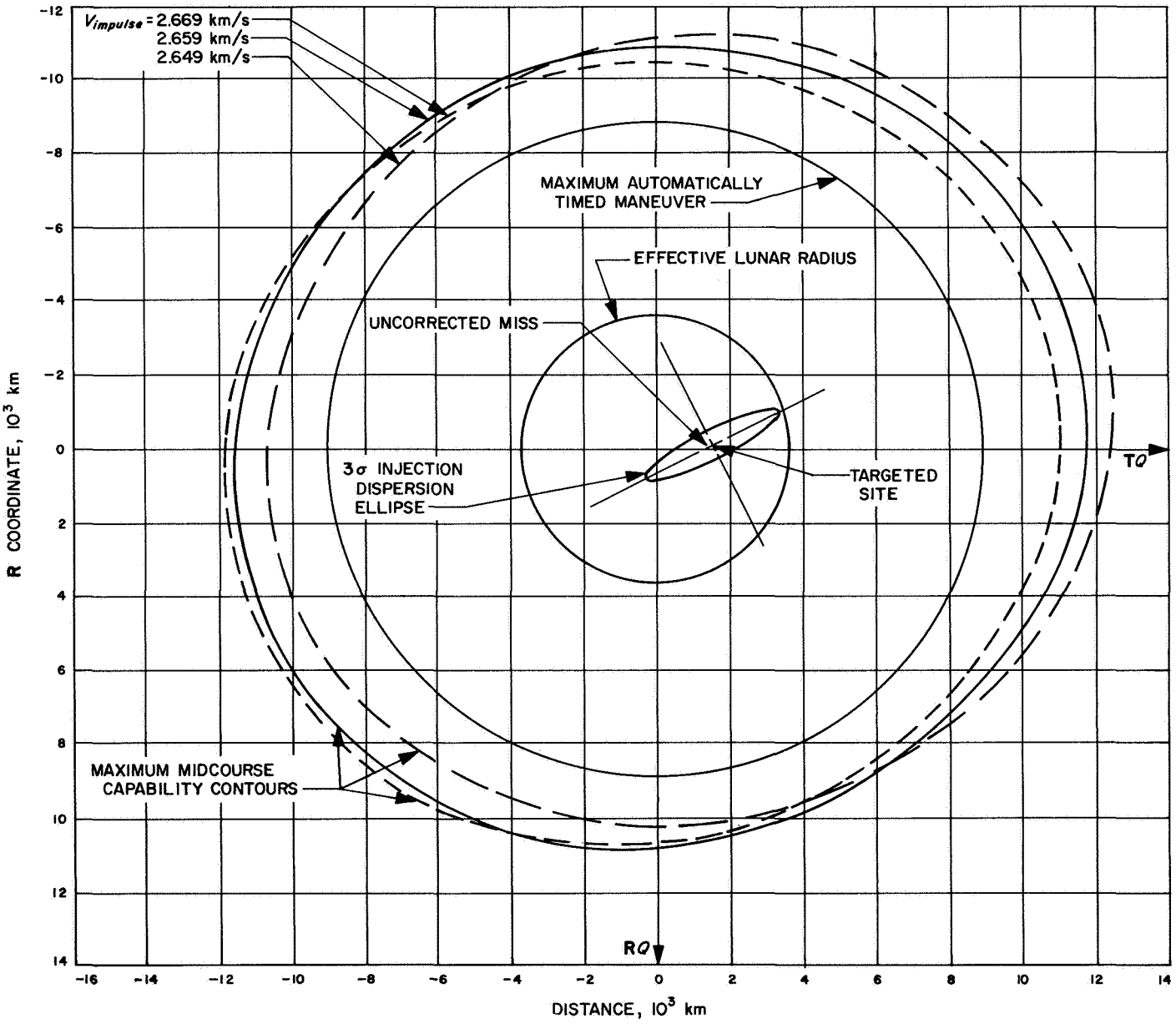

Fig. 59. Midcourse capability contours for *Surveyor II*

Table 31. Midcourse maneuver alternatives, *Surveyor II*

Element	Final midcourse correction, $L + 16.5$ h	Alternate considerations					
		No midcourse correction	$L + 14.5$-h correction			$L + 38.8$-h correction	
			Plan 1	Plan 2	Plan 3	Plan 1	Plan 2
Critical plane, m/s	1.18		0.51	0.51	0.51	1.0	2.24
Noncritical direction, m/s	9.50		2.0	15.0	−33.4	1.7	17.0
Total correction, m/s	9.59		2.1	15.0	33.4	2.0	17.2
Propellant, lb	7.96		1.6	12.0	26.4	1.6	14.26
Impact speed, km/s	2.658	2.663	2.662	2.654	2.681	2.662	2.656
Burnout velocity, ft/s	450	515	505	400	400	505	408
Fuel margin, lb	30.5	31	31	31	33.4	31	30
Arrival time 9/23, GMT	3:42	3:20	3:25	3:57	3:42	3:22	3:38
Visibility from DSS							
Prelanding	4 h, 41 min	4 h, 19 min	4 h, 24 min	4 h, 56 min	4 h, 41 min	4 h, 21 min	4 h, 37 min
Postlanding	3 h, 25 min	3 h, 47 min	3 h, 42 min	3 h, 10 min	3 h, 25 min	3 h, 45 min	3 h, 29 min
Landing errors							
SMAA (3σ), km	53.9	20	20	33.5	63	5.5	16.3
SMIA, km	17.7	5	5	27	55	3.7	15.6
Theta, deg	−57	−56	−56	−55	−60	−46	−52

noncritical direction component that resulted from a weighted selection of flight time, main retroengine burnout velocity, and vernier propulsion system fuel margin was 9.5 m/s. Figure 60 shows the possible flight times, burnout velocities, and fuel margins for the range of available noncritical component velocity corrections. Since all three were acceptable over a wide range of values, a nominal burnout velocity of 450 ft/s was chosen because of favorable landing site errors and backup midcourse correction capability in the event the first midcourse correction became nonstandard.

If the maneuver strategy were to correct miss plus flight time, the required noncritical component would have been 4.325 m/s, giving a total of approximately 4.48 m/s.

Since the aim point was changed during the flight, the above required correction does not properly evaluate the performance of the *Centaur* guidance system. Using the results of the last pre-midcourse orbit and correcting to the original aim point gives a miss, only, requirement of 1.015 m/s. Miss plus flight time was 4.44 m/s.

IX. *Surveyor II* Inflight Orbit Determination Analysis

A. Deep Space Stations Supporting *Surveyor II*

The ground stations that provided tracking data during the *Surveyor II* mission were the Johannesburg Deep Space Station, the Tidbinbilla Deep Space Station, the Pioneer Deep Space Station, and the Ascension Island Deep Space Station. Figure 61 summarizes the tracking station view periods and their data coverage for the period from launch to lunar touchdown. The locations of the tracking stations are given in Table 1.

B. Summary of Data Used in Orbit Determination

Table 32 summarizes the tracking data used for both the inflight and postflight orbital calculations and analyses. This table provides a general picture of the performance of the data recording and handling systems. The JPL tracking data processor (TDP) and orbit data generator (ODG) programs, used to edit all incoming tracking data, prepared a data file for input to the SPODP. The total number of data points received in near real time were first read into the TDP, which checked each

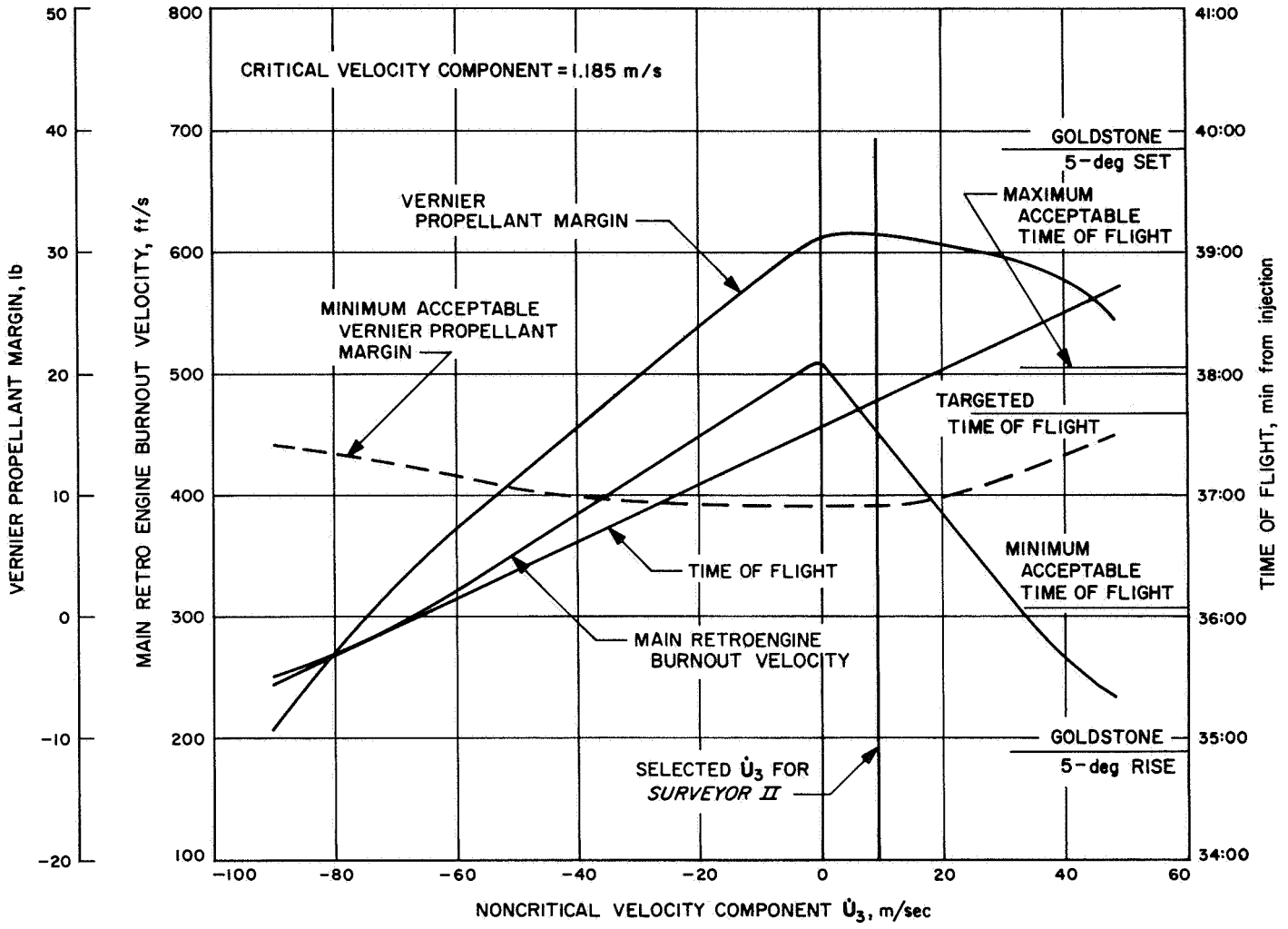

Fig. 60. Effect of noncritical velocity component on terminal descent parameters, *Surveyor II*

Table 32. Summary of premaneuver data used in orbit determination, *Surveyor II*

Station	Data Type	Points Received	Points used in real time		Bad format		Bad data condition code		Blunder points		Rejection limits on blunder points	Points used in postflight analysis, obtained from station tapes[a]
			Number	% of recd	Number	% of recd	Number	% of recd	Number	% of recd		
DSS 11	CC3	314	86	27.4	7	2.2	37	11.8	0	0.0	0.06 Hz	276
DSS 51	CC3	650	529	81.4	9	1.4	83	12.8	2	0.3	0.15 Hz	529
	HA	650	540	83.1	9	1.4	61	9.4	21	3.2	0.20 deg	0
	Dec	650	540	83.1	9	1.4	61	9.4	24	3.7	0.20 deg	0
DSS 72	CC3	857	303	35.4	261	30.5	249	29.1	17	2.0	0.06 Hz	309
	Az	857	225	26.3	261	30.5	38	4.4	29	3.4	0.20 deg	0
	El	857	222	25.9	261	30.5	38	4.4	14	1.6	0.20 deg	0

[a]Data points are obtained from station tapes to avoid transmission errors.

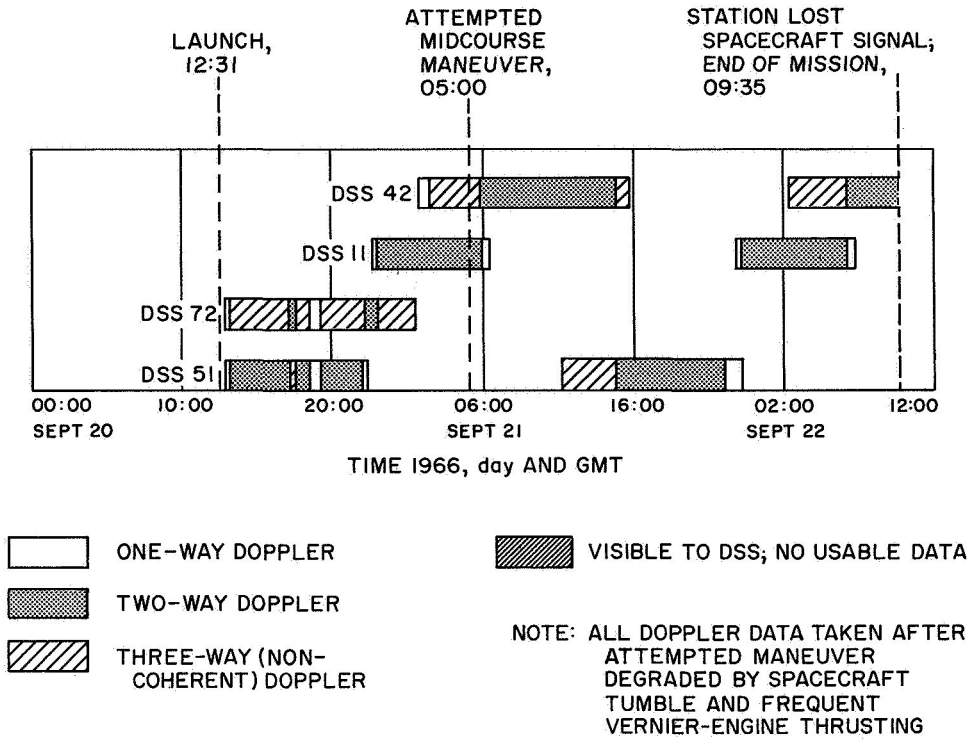

Fig. 61. Tracking station view periods and doppler data coverage, *Surveyor II*

data sample for acceptable format – i.e., it checked to determine if the sample were 1 of 30 acceptable message formats, if each item in the sample were in the proper field, and if there were any items that contained a missing or illegal character. The data points that failed this test are shown in the table. It should be noted that during flight operations, no attempt was made to reconstruct data points which were rejected for bad format.

The next item the TDP checked was the data condition code. A data point is given a bad-data condition code when automatic detectors at the station sense that the data would be unusable. These detectors have manual overrides that are used (1) whenever an equipment malfunction is suspected and (2) during periods when the transmitter is being returned prior to transferring transmitting assignment to another station. The number of data points that had a bad-data condition code are recorded in the table. A coarse in-range value check was made to determine if each data type were within an acceptable limit – i.e., within 360 deg for angles and 10^4 cycles for doppler. All data that passed these checks or were not rejected on a user option were time-sorted and written on both disk and magnetic tape for access by the ODG. The ODG read the data file and if it included angular data, the values were corrected to remove systematic antenna pointing errors – mechanical deflection as the antenna tracks from horizon to horizon. Next, the doppler data were checked for monotonicity, valid tracking mode, valid sample rate, and converted from cycles to cycles/second by differencing adjacent samples and dividing by the sample time. Pertinent transmitter and receiver frequencies were entered on the file with each doppler sample; these frequencies were read in by the user or, in some cases, were included in the data sample. The data were then written on both disk and magnetic tape for access by the SPODP.

The blunder points are the data points rejected by the TDP and ODG either during the validity checks or when the rejection limits are applied during the orbit computation. These limits are based on experience gained in previous missions and on the philosophy that, if they could create difficulties in converging to an orbit, it is better to reject questionable points immediately than to attempt to salvage every point. This is particularly true when very few data points are available during the early phase of the mission.

C. Premaneuver Orbit Estimates Based on DSS Tracking Data

Initial estimate of the spacecraft orbit was obtained by the realtime computing facility at Cape Kennedy.

This estimate was based on Antigua acquired data in the pre-retromaneuver from *Centaur* C-band tracking data. A backup computation, with the Antigua pre-retromaneuver data, was made at the Space Flight Operations Facility at JPL. This solution, when mapped to the moon, indicated that lunar encounter would be achieved without a midcourse correction.

The first estimate of the spacecraft orbit (PROR X) based on DSS data, only, was completed at L + 1 h, 37 min. For this solution, approximately 33 min of DSS 51 tracking data and 40 min of DSS 72 data were available. Since DSS 72 was a new tracking station and its tracking data capabilities had not been completely validated, a decision was made to eliminate these data from the orbital computations until a comparison could be made with the DSS 51 tracking data. When the PROR X orbit solution was mapped forward to the target, it verified that the spacecraft was on a lunar encounter trajectory. Further, it indicated that the correction required to achieve encounter at the prelaunch aiming point was well within the nominal midcourse correction capability. These results were verified by the second orbit computation (ICEV) completed at L + 2 h, 42 min.

During the third orbit computation period from L + 3 h, 30 min to L + 4 h, 10 min, a comparison was made between the DSS 51 and DSS 72 tracking data. On the prime computer, the orbit computation (PREL XA) was made using only DSS 51 angular and two-way doppler (CC3) data in the least-squares fit and weighting out the DSS 72 angular and three-way doppler (C3) data. On the backup computer, the orbit computation (PREL YB) was made by use of both DSS 51 and DSS 72 data in the fit. Examination of the offline ODP output from these two computations indicated that the data noise quality of the DSS 72 tracking data was good. A comparison between the estimated target parameters of these two solutions showed a discrepancy of approximately 100 km on the lunar surface. At the time, very little confidence was placed in the DSS 72 data since a time error, on the order of seconds, had been discovered in this station's tracking data during *Surveyor I* mission (DSS 72 tracked *Surveyor I* on a training basis only). To resolve this discrepancy, and to obtain meaningful data for use in the data consistency computations, a request was made to allow DSS 72 to assume command of the spacecraft and obtain two-way doppler data. Since the communications lines to DSS 72 were excessively noisy, it was requested that the station transmit data at a 10-s sample rate to recover a maximum amount of data in real time.

During the data consistency (DACO) computation period from L + 5 h, 55 min to L + 8 h, 40 min, nine orbital solutions were obtained by use of various combinations of available tracking data. It should be noted that it is necessary to have independent blocks of tracking data to obtain meaningful results from these computations. Angular tracking data from more than one station is not sufficient, since all angular data from the DSS stations are biased due to mechanical deflection as the antenna moves from horizon to horizon. In fact, it was discovered during these computations that an excessive bias in some of the early DSS 51 angular data was responsible for most of the discrepancy between the two PREL orbit solutions. Three-way doppler data is not completely independent, since the transmitter and receiver are at two different locations that do not have a common time or frequency reference. Time blocks of two-way doppler data from more than one station are independent, at least in terms of biases at one station affecting the data obtained at another station. The most representative solutions obtained during this time block were based on: (1) DSS 51 and DSS 72 two-way doppler, plus Antigua range data (DACO YC); (2) DSS 51 two-way doppler only (DACO YD); (3) DSS 51 angular data (excluding the first 7 min) and two-way doppler (DACO YE); and (4) DSS 51 and DSS 72 two-way doppler only (DACO XE). Results of these solutions revealed that the angular data from both DSN stations were biased, and the Antigua range data appeared to have a small bias with respect to the DSS data. In general, all four solutions appeared to be consistent with a maximum difference of 23 km in a lunar latitude direction.

At the beginning of the last pre-midcourse (LAPM) orbit computation time block, the following amounts of two-way doppler data were available:

DSS 51: 8 h, 46 min

DSS 72: 1 h, 22 min

DSS 11: 41 min

As a final data consistency check, the orbit solution on the prime computer (LAPM XA) contained only DSS 72 and DSS 11 two-way doppler, and the solution on the backup computer contained only DSS 51 and DSS 11 two-way doppler. Both of these solutions appeared consistent, and the data file was updated to include an additional 1 h, 7 min of DSS 11 two-way doppler for the final pre-midcourse orbit computation (LAPM YB). This solution, when mapped to the moon, indicated that uncorrected unbraked lunar impact would occur at 0.08° S lat and 5.34° W lon.

Table 33. Estimated premaneuver position and velocity at injection epoch[a], *Surveyor II*

Orbit ID	Geocentric space-fixed position			Geocentric space-fixed velocity			Uncertainties, 1σ					
							Position			Velocity		
	x, km	y, km	z, km	Dx, km/s	Dy, km/s	Dz, km/s	σ_x, km	σ_y, km	σ_z, km	σ_{Dx}, m/s	σ_{Dy}, m/s	σ_{Dz}, m/s
AFETR pre-retromaneuver check orbit	−4355.5596	4620.1069	1899.2695	−8.7305178	−4.5251269	−4.7529019	0.1540	0.4095	0.3482	3.6898	8.9923	7.4430
PROR X	−4356.7910	4618.8569	1894.0651	−8.7319587	−4.5218411	−4.7561241	2.5320	2.7561	4.5432	2.2368	2.0875	1.6348
ICEV X	−4357.9767	4617.2504	1896.6363	−8.7314696	−4.5226921	−4.7554199	1.6351	0.9690	1.6323	1.8257	1.6356	1.3397
PREL XA	−4358.0818	4617.2397	1896.6243	−8.7314684	−4.5228384	−4.7553650	1.4190	0.4771	0.7265	1.5152	1.4746	1.1627
DACO YC	−4361.1735	4616.4561	1896.9676	−8.7285414	−4.5265947	−4.7540331	0.0350	0.1789	0.2953	0.3319	0.4880	0.9757
DACO YD	−4360.7574	4616.9390	1896.2933	−8.7283456	−4.5252316	−4.7559435	1.5095	1.2111	1.5595	0.3511	3.3911	3.9813
DACO YE	−4360.5679	4617.0434	1896.1718	−8.7284830	−4.5250215	−4.7560528	0.4600	0.3323	0.4225	0.2559	0.8691	1.0008
DACO XE	−4360.6974	4616.9919	1896.2237	−8.7283529	−4.5251057	−4.756092	1.4822	1.1693	1.4992	0.3645	3.3	3.9
DACO 1.5	−4360.8654	4616.8526	1896.4064	−8.7283302	−4.5254825	−4.7556511	0.8217	0.7174	0.9382	0.1439	2.0910	2.6060
LAPM XA	−4359.5703	4614.8999	1896.2705	−8.7301177	−4.5265199	−4.7556863	30.3548	24.4160	9.4683	32.6745	24.4229	29.1071
LAPM YA	−4361.0942	4616.6822	1896.6227	−8.7282276	−4.5258066	−4.7553555	0.8692	0.7768	1.0218	0.0987	2.2738	2.8577
LAPM YB	−4360.9967	4616.7897	1896.4763	−8.7281984	−4.5255173	−4.7557481	0.6960	0.6218	0.8161	0.0924	1.8223	2.2947
Postflight 6 × 6 solution	−4360.8679	4616.9010	1896.3301	−8.7281925	−4.5251846	−4.7561653	0.3102	0.2710	0.3522	0.0849	0.7899	0.9949
Best pre-maneuver estimate	−4360.9042	4616.8514	1896.4001	−8.7282190	−4.5253067	−4.7559824	0.3127	0.2756	0.3588	0.0897	0.8036	1.0181

[a]Injection epoch = September 20, 1966, at 12:43:13.670 GMT.

Table 34. Estimated premaneuver unbraked target parameters and statistics, *Surveyor II*

Orbit ID	Time computed, GMT		Target parameters and statistics										Selenocentric conditions at unbraked impact			Solution type	Data used
	Start	Stop	B, km	B • TT, km	B • RT, km	TL, h	SMAA, km	SMIA, km	THETA, deg	σ_T IMPACT, s	PHI 99, deg	SVFIX R, km/s	Latitude, deg (Positive N)	Longitude, deg (East)	GMT		
	Day 263 (Sept. 20, 1966)																
AFETR pre-retromaneuver check orbit	13:14	13:38	1134.48	1131.39	−83.60	62.71	1592.28	339.53	21.316	2485.359	46.020	8.324	1.744	350.336	03:19:53.434[a]	6 × 6[b]	Antigua (AFETR) Pre-retromaneuver data
PROR X	13:44	14:15	1492.03	1482.78	−165.97	62.68	287.04	82.55	84.328	69.814	5.387	0.638	3.369	358.065	03:19:07.178	6 × 6	DSS 51 angles and CC3
ICEV X	14:45	15:14	1457.96	1457.95	−4.46	62.70	94.84	68.59	95.246	19.732	1.669	0.611	0.138	357.448	03:19:51.141	6 × 6	DSS 51 angles and CC3
PREL XA	16:16	16:45	1453.56	1453.55	−6.07	62.70	59.89	35.04	0.291	6.456	1.013	0.609	0.170	357.350	03:19:51.390	6 × 6	DSS 51 angles and CC3
DACO YC	20:11	20:30	1333.82	1333.77	12.20	62.70	8.49	4.73	139.253	1.805	0.103	0.008	−0.192	354.711	03:19:59.228	6 × 6	DSS 51 CC3, DSS 72 CC3, and Antigua range
DACO YD	20:37	21:00	1338.52	1338.52	−3.95	62.70	60.19	4.22	54.699	14.292	1.212	0.039	0.130	354.816	03:19:53.626	6 × 6	DSS 51 CC3, only
DACO YE	21:07	21:29	1344.72	1344.67	−11.54	62.70	21.37	3.63	54.720	3.904	0.398	0.010	0.283	354.952	03:19:52.365	6 × 6	DSS 51 angles and CC3
DACO XE	20:51	21:22	1339.77	1339.75	−6.60	62.70	56.91	5.62	52.363	14.026	1.173	0.610	0.183	354.838	03:19:52.954	6 × 6	DSS 51 CC3 and DSS 72 CC3
DACO 1.5	23:20	24:09	1335.93	1335.93	−0.66	62.70	30.47	2.36	56.780	8.390	0.634	0.610	0.064	354.754	03:19:54.628	6 × 6	DSS 51 CC3 and DSS 72 CC3
	Day 264 (Sept. 21, 1966)																
LAPM XA	00:09	00:32	1338.84	1338.56	27.36	62.70	353.90	203.04	94.730	96.058	6.669	0.697	−0.497	354.813	03:19:52.676	6 × 6	DSS 72 CC3 and DSS 11 CC3
LAPM YA	00:36	01:07	1330.16	1330.11	10.83	62.70	31.55	2.46	57.440	9.194	0.667	0.027	−0.166	354.631	03:19:56.464	6 × 6	DSS 51 CC3 and DSS 11 CC3
LAPM YB[c]	01:13	01:47	1331.49	1331.47	6.75	62.70	25.07	2.23	57.486	7.214	0.529	0.021	−0.084	354.661	03:19:55.424	6 × 6	DSS 51 CC3, DSS 72 CC3, and DSS 11 CC3
Postflight 6 × 6 solution	Postflight		1333.95	1333.95	3.12	62.70	11.20	2.18	56.925	3.023	0.232	0.609	−0.012	354.711	03:19:53.907	6 × 6	DSS 51 CC3, DSS 72 CC3, and DSS 11 CC3
Best premaneuver estimate	Postflight		1333.85	1333.84	5.17	62.70	11.31	2.35	57.500	3.045	0.233	0.609	−0.053	354.708	03:19:54.223	9 × 9[d]	DSS 51 CC3, DSS 72 CC3, and DSS 11 CC3
Prelaunch aim point													0.000	359.330			

[a]Predicted unbraked impact occurs on September 23 at indicated GMT.

[b]6 × 6 refers to geocentric space-fixed cartesian position and velocity vectors, estimated at initial epoch.

[c]Orbit solution used for final midcourse maneuver computations.

[d]9 × 9 refers to position and velocity vectors, estimated at initial epoch plus the three-station location parameters for DSS 72.

NOTE: All tabulated uncertainties are one standard deviation (1σ).

Table 35. Premaneuver tracking data statistics, *Surveyor II*

Orbit ID	Station	Data type	Begin data, time		End data, time		Number of points	Standard deviation	Root mean square	Mean error	Data sample rate, s
			Date 1966	GMT	Date 1966	GMT					
AFETR pre-retromaneuver check orbit	AFETR 91	Az, deg	9/20	12:43:30	9/20	12:44:30	10	0.0063 deg	0.0063 deg	0.0000 deg	6
		El, deg	9/20	12:43:30	9/20	12:44:30	10	0.0184 deg	0.0184 deg	0.0000 deg	6
		R, km	9/20	12:43:30	9/20	12:44:30	8	0.0013 km	0.0013 km	0.0000 km	6
PROR X	DSS 51	CC3, Hz	9/20	13:06:22	9/20	13:39:22	180	0.0606 Hz	0.0606 Hz	0.0000 Hz	10
		HA, deg	9/20	13:06:27	9/20	13:39:27	179	0.0221 deg	0.0221 deg	−0.0002 deg	10
		Dec, deg	9/20	13:06:27	9/20	13:39:27	179	0.0105 deg	0.0105 deg	0.0003 deg	10
ICEV X	DSS 51	CC3, Hz	9/20	13:06:22	9/20	14:31:32	244	0.0542 Hz	0.0542 Hz	0.0005 Hz	10 and 60
		HA, deg	9/20	13:06:27	9/20	14:32:02	246	0.0197 deg	0.0197 deg	0.0005 deg	10 and 60
		Dec, deg	9/20	13:06:27	9/20	14:32:02	246	0.0110 deg	0.0115 deg	0.0030 deg	10 and 60
PREL XA	DSS 51	CC3, Hz	9/20	13:06:22	9/20	13:42:42	200	0.0597 Hz	0.0597 Hz	0.0002 Hz	10
		HA, deg	9/20	13:06:27	9/20	13:42:47	199	0.0218 deg	0.0219 deg	0.0010 deg	10
		Dec, deg	9/20	13:06:27	9/20	13:42:47	199	0.0110 deg	0.0111 deg	0.0010 deg	10
		CC3, Hz	9/20	13:44:32	9/20	15:41:32	104	0.0109 Hz	0.0109 Hz	0.0002 Hz	60
		HA, deg	9/20	13:44:02	9/20	15:42:02	112	0.0064 deg	0.0064 deg	−0.0005 deg	60
		Dec, deg	9/20	13:44:02	9/20	15:42:02	111	0.0060 deg	0.0134 deg	0.0120 deg	60
DACO YC	DSS 72	CC3, Hz	9/20	17:05:32	9/20	17:44:47	89	0.2040 Hz	0.2130 Hz	−0.0620 Hz	10
	DSS 51	CC3, Hz	9/20	13:06:22	9/20	18:25:32	386	0.0438 Hz	0.0454 Hz	−0.0110 Hz	10 and 60
	AFETR 91	R, km	9/20	12:43:24	9/20	12:47:24	30	0.1030 km	0.1140 km	−0.0480 km	6
DACO YD	DSS 51	CC3, Hz	9/20	13:06:22	9/20	20:22:32	446	0.0408 Hz	0.0408 Hz	−0.0002 Hz	10 and 60
DACO YE	DSS 51	CC3, Hz	9/20	13:06:22	9/20	20:40:32	464	0.0401 Hz	0.0401 Hz	−0.0003 Hz	10 and 60
		HA, deg	9/20	13:13:07	9/20	20:45:02	540	0.0154 deg	0.0205 deg	0.0130 deg	10 and 60
		Dec, deg	9/20	13:13:07	9/20	20:45:02	540	0.0101 deg	0.0115 deg	0.0050 deg	10 and 60
DACO XE	DSS 51	CC3, Hz	9/20	13:06:22	9/20	13:42:42	200	0.0594 Hz	0.0594 Hz	−0.0002 Hz	10
		CC3, Hz	9/20	13:44:32	9/20	19:53:22	221	0.0121 Hz	0.0122 Hz	0.0004 Hz	60
	DSS 72	CC3, Hz	9/20	17:07:32	9/20	17:07:32	85	0.0437 Hz	0.0439 Hz	−0.0040 Hz	10
DACO 1.5	DSS 72	CC3, Hz	9/20	17:07:32	9/20	22:58:27	300	0.0414 Hz	0.0415 Hz	−0.0021 Hz	10
	DSS 51	CC3, Hz	9/20	13:06:22	9/20	13:42:42	200	0.0594 Hz	0.0594 Hz	−0.0006 Hz	10
		CC3, Hz	9/20	13:44:32	9/20	21:54:32	314	0.0085 Hz	0.0086 Hz	0.0003 Hz	60
LAPM XA	DSS 72	CC3, Hz	9/20	17:07:32	9/20	22:58:17	305	0.0409 Hz	0.0409 Hz	0.0004 Hz	10
	DSS 11	CC3, Hz	9/20	23:08:32	9/20	23:49:32	30	0.0042 Hz	0.0042 Hz	0.0004 Hz	60
LAPM YA	DSS 51	CC3, Hz	9/20	13:06:22	9/20	21:54:32	529	0.0373 Hz	0.0373 Hz	0.0000 Hz	10 and 60
	DSS 11	CC3, Hz	9/20	23:08:32	9/21	00:23:32	59	0.0042 Hz	0.0064 Hz	0.0048 Hz	60
LAPM YB	DSS 72	CC3, Hz	9/20	17:05:32	9/20	22:58:27	303	0.0464 Hz	0.0474 Hz	−0.0095 Hz	10
	DSS 11	CC3, Hz	9/20	23:08:32	9/21	00:56:32	86	0.0045 Hz	0.0112 Hz	0.0100 Hz	60
	DSS 51	CC3, Hz	9/20	13:06:22	9/20	21:54:32	529	0.0374 Hz	0.0374 Hz	−0.0003 Hz	10 and 60
Pre-midcourse cleanup XC	DSS 72	CC3, Hz	9/20	17:07:32	9/20	22:58:12	309	0.0406 Hz	0.0406 Hz	0.0004 Hz	10
	DSS 11	CC3, Hz	9/20	23:08:32	9/21	04:39:32	261	0.0062 Hz	0.0068 Hz	0.0020 Hz	60
		CC3, Hz	9/21	04:40:57	9/21	04:43:37	15	0.0212 Hz	0.0229 Hz	−0.0080 Hz	10
	DSS 51	CC3, Hz	9/20	13:06:22	9/20	13:42:42	202	0.0594 Hz	0.0594 Hz	0.0013 Hz	10
		CC3, Hz	9/20	13:44:32	9/20	21:54:32	327	0.0094 Hz	0.0094 Hz	−0.0009 Hz	60

The numerical results of the representative realtime premaneuver orbit computations are presented in Tables 33 and 34. Amounts and types of tracking data used in these computations, together with associated noise statistics, are shown in Table 35.

D. Postmaneuver Orbit Estimates

In an orbit determination sense, all post-midcourse data were degraded by spacecraft tumble – the variance in the doppler data reflects the spacecraft antenna motion about the *cg*. The tumble rate was not constant; it increased slightly each time the verniers were fired. In addition, the trajectory was perturbed with each vernier engine firing. These two factors precluded any precise orbital computations. As a result, only a limited number of orbit solutions were obtained. For these computations, only data taken during the 12-h cruise period were used. The numerical results of these computations are presented in Tables 36 and 37. The amounts of tracking data used, plus the associated noise statistics, are given in Table 38.

It can be seen that the estimated spacecraft position and velocity at initial epoch from Table 36 and the estimated unbraked impact point from Table 37 vary considerably between solutions. This is primarily because *a priori* information from the pre-midcourse tracking data could not be used for the post-midcourse computations. Hence, the estimated parameters will vary until sufficient data have been accumulated to define the orbit. Of major interest is the final orbit solutions based on use of all of the cruise data (2.5B POM). The difference in predicted impact point between this solution and the pre-midcourse solution was approximately 3 deg in latitude and 8 deg in longitude. Thus, it appears that the attempted midcourse plus four additional vernier engine firings did not appreciably change the pre-midcourse trajectory. Instead, the vernier engine firings appeared rather to cause the spacecraft to spin or tumble at an increasing rate.

During the 12-h cruise period, a small block of data was taken at a sample rate of 1 sample/s to look at the tumble rate. A residual plot (observed data minus computed value) of these data is shown in Fig. 62. In the figure, the period appears to be approximately 16 s. However, since the period of the tumble based on received-signal strength measurements was reported to be approximately 1.06 s, the residual plot can be interpreted as displaying a heterodyne type effect. That is, the 1 cycle/16 s seen in the residual plot represents either the sum or difference between a rate of 1 cycle/s and the true rate. If it were the sum, this would mean that 17 cycles would be accumulated in 16 s. Therefore, the period would be 17/16 or 1.06 s, as reported from the signal strength measurements.

E. Observations and Conclusions

Because of the spacecraft midcourse malfunction, this discussion will be restricted to the pre-midcourse phase.

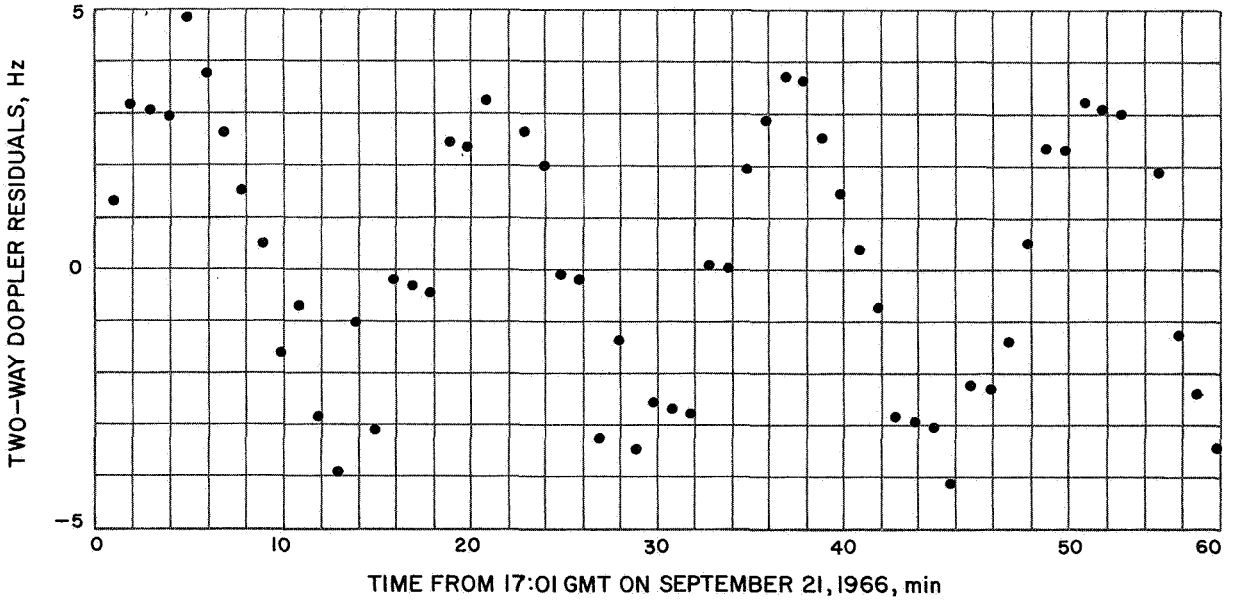

Fig. 62. DSS 51 postmaneuver doppler residuals showing effect of spacecraft tumble

Table 36. *Surveyor II* postmaneuver position and velocity at initial epoch

Orbit ID	Geocentric space-fixed position			Geocentric space-fixed velocity			Uncertainties, 1σ					
							Position			Velocity		
	x, km	y, km	z, km	Dx, km/s	Dy, km/s	Dz, km/s	σ_{x_f} km	σ_{y_f} km	σ_{z_f} km	σ_{Dx_f} m/s	σ_{Dy_f} m/s	σ_{Dz_f} m/s
1 POM	32690.823	−159392.63	−91890.867	0.67759293	−1.4801336	−0.76234823	45.6912	62.1947	44.1543	2.1048	2.0559	2.9836
1.5 POM	32699.679	−159399.22	−91881.627	0.67809120	−1.4796081	−0.76307510	37.8787	30.7436	40.3354	0.9740	1.1685	1.9161
2 POM	32701.480	−159401.00	−91880.472	0.67811222	−1.4795259	−0.76320909	33.2501	30.2406	38.3865	0.9710	1.0956	1.7814
2.5 POM	32675.257	−159474.29	−91729.642	0.68109305	−1.4773393	−0.76576358	3.0108	1.0432	1.2359	0.4689	0.3294	0.4333
2.5A POM	32600.594	−159420.43	−91747.926	0.68163066	−1.4794731	−0.76189066	32.0813	35.6668	72.8754	1.6261	1.0401	1.3568
2.5B POM	25606.641	−143772.36	−83560.632	0.70216298	−1.5875112	−0.83033967	3.0223	1.0463	1.2375	0.3753	0.2929	0.4104

Table 37. *Surveyor II* postmaneuver orbital computations

Orbit ID	Target parameters and statistics										Selenocentric conditions at unbraked impact			Solution type	Data used
	B, km	B•TT, km	B•RT, km	TL, h	SMAA, km	SMIA, km	THETA, deg	σ_T IMPACT, s	PHI 99, deg	SVFIX R, km/s	Latitude, deg	Longitude, deg	GMT		
1 POM	1377.09	1289.65	−482.88	43.52	576.10	175.27	68.139	63.885	9.083	0.795	9.689	354.164	03:16:41.002	6 × 6	DSS 42
1.5 POM	1264.72	1220.99	−352.88	43.53	327.97	106.19	84.255	50.380	4.989	0.666	7.085	352.565	03:17:52.493	6 × 6	DSS 42 and DSS 51
2 POM	1274.21	1224.37	−329.70	43.53	306.46	105.23	83.536	49.847	4.691	0.665	6.621	352.469	03:17:03.138	6 × 6	DSS 42 and DSS 51
2.5 POM	886.41	884.33	60.67	43.59	98.08	26.09	56.562	127.291	1.746	0.620	−1.167	345.134	03:19:56.828	6 × 6	DSS 42 and DSS 51
2.5A POM	1046.04	854.47	−603.40	43.60	254.17	138.68	56.985	90.983	5.450	0.765	12.257	344.885	03:20:29.489	6 × 6	DSS 42 and DSS 51
2.5B POM	945.02	929.35	171.37	46.44	91.50	21.78	61.181	24.215	1.558	0.615	−3.399	346.102	03:19:42.302	6 × 6	DSS 42 and DSS 51

Table 38. Summary of DSS tracking data used in *Surveyor II* post-midcourse orbit computations

Orbit ID	Station	Data type	Begin data		End data		Number of points	Standard deviation	Root mean square	Mean error
			Date 1966	GMT	Date 1966	GMT				
1 POM	DSS 42	CC3	9/21	08:11:32	9/21	13:53:32	326	0.514 Hz	0.514 Hz	0.0000 Hz
		HA	9/21	08:11:02	9/21	13:54:02	336	0.013 deg	0.013 deg	−0.0041 deg
		Dec	9/21	08:11:02	9/21	13:54:02	336	0.013 deg	0.013 deg	−0.0003 deg
1.5 POM	DSS 42	CC3	9/21	08:11:32	9/21	14:53:32	374	0.520 Hz	0.520 Hz	0.0012 Hz
		HA	9/21	08:11:02	9/21	14:53:02	389	0.013 deg	0.013 deg	−0.0021 deg
		Dec	9/21	08:11:02	9/21	14:53:02	389	0.014 deg	0.015 deg	−0.0027 deg
	DSS 51	CC3	9/21	15:03:32	9/21	16:12:32	41	0.212 Hz	0.214 Hz	−0.0252 Hz
2 POM	DSS 42	CC3	9/21	08:11:32	9/21	14:53:32	374	0.520 Hz	0.520 Hz	0.0011 Hz
		HA	9/21	08:11:02	9/21	14:53:02	389	0.013 deg	0.013 deg	−0.0016 deg
		Dec	9/21	08:11:02	9/21	14:53:02	389	0.015 deg	0.015 deg	−0.0027 deg
	DSS 51	CC3	9/21	15:03:32	9/21	18:05:32	95	0.219 Hz	0.219 Hz	−0.0119 Hz
2.5 POM	DSS 42	CC3	9/21	08:11:32	9/21	14:53:32	374	0.519 Hz	0.519 Hz	−0.0077 Hz
	DSS 51	CC3	9/21	15:03:32	9/21	18:51:32	117	0.214 Hz	0.214 Hz	0.0726 Hz
2.5A POM	DSS 42	CC3	9/21	07:51:10	9/21	14:53:32	455	2.160 Hz	2.160 Hz	0.0057 Hz
	DSS 51	CC3	9/21	15:03:32	9/21	21:36:02	975	1.270 Hz	1.270 Hz	−0.0054 Hz
2.5B POM	DSS 42	CC3	9/21	08:11:32	9/21	14:53:32	374	0.520 Hz	0.520 Hz	−0.0134 Hz
	DSS 51	CC3	9/21	15:03:32	9/21	18:51:32	117	0.227 Hz	0.261 Hz	0.1280 Hz

The two-way doppler data taken during the pre-midcourse phase were of excellent quality, and practically all data were usable for the orbit computations. In addition to the bias that remains after the angular data are corrected for systematic antenna pointing errors, an anomaly was noted in the DSS 51 early angular data. This was evidenced by a larger variance in both the hour angle and declination angle residuals, and by a slightly greater bias in the HA data. These data, when included in the orbit computation, caused a difference in the predicted impact point (in B-plane coordinates) of approximately 36 km in $\mathbf{B}\cdot\mathbf{T}T$ and -10 km in $\mathbf{B}\cdot\mathbf{R}T$. It should be noted that this did not affect the final pre-midcourse orbit computations, since the angular data are not used after the first 7 to 10 h of the mission. However, these data caused some confusion during the early inflight orbit computations.

The most meaningful comparison between inflight and postflight orbit determination results can be made by examining the critical unbraked target parameters in Table 34. The difference between the best postflight premaneuver orbit estimate and the orbit solution used for the midcourse maneuver computations (Δ = best inflight) was 0.031 deg in latitude and 0.047 deg in longitude at unbraked impact. These differences are roughly equivalent to 0.9 km and 1.4 km on the lunar surface. This represents a significant improvement over the results obtained during the *Surveyor I* mission in which the largest difference was approximately 14 km. The major contributor to the *Surveyor I* error was some biased early DSS 11 data that were included in the final pre-midcourse orbit computation. However, part of the improvement noted during this mission is because the planned maneuver time was delayed for approximately 2 h, which allowed more DSS 11 data to be accumulated before starting the final orbit computation. In addition, a small amount of data were available from a third tracking station (DSS 72). This improvement should demonstrate the benefits to be obtained by multi-station premaneuver tracking coverage, and implies that the nominal maneuver policy should be to schedule the maneuver as close as possible to DSS 11 horizon set.

X. Postflight Analysis of the DSS Transponder Tracking Data for *Surveyor II*

The analysis made to obtain the best estimate of the *Surveyor II* premaneuver flight path verified that the premaneuver predicted unbraked target parameters from the inflight orbit solutions were well within the *Surveyor* Project orbit determination accuracy requirements. As previously stated, all post-midcourse tracking data were degraded by spacecraft tumbling and corrupted by periodic vernier engine firings. Therefore, no postflight analysis was performed on these data.

A. Data Used in Analysis

For the postflight computations and analyses, only two-way doppler data were used. Both angular data and three-way noncoherent doppler data were available; however, they were not used because neither of these two data types would contribute to the estimate of the spacecraft's flight path. The data available for the postflight computations are summarized in Table 32.

The same data weighting philosophy as outlined for *Surveyor I* was used for the postflight analysis of *Surveyor II*. Therefore, the same numerical weight values were used for the two-way doppler data.

B. Premaneuver Orbit Based on All Usable Premaneuver Two-Way Doppler Data

Prior to starting the analysis of the premaneuver tracking data, all known, or suspected, bad data points were removed, and the data file was updated to include all two-way doppler data up to the pre-midcourse spacecraft attitude maneuvers. An orbit solution was obtained based on estimation of only the standard six parameters with data from DSS 51, DSS 72, and DSS 11. Examination of the residual plots indicated a slight skew in the DSS 72 doppler residuals. Since only a survey location was available for this station, it was decided to estimate the station location parameters to determine if the skew could be removed. The residual plots from this 9 × 9 solution indicated that the DSS 72 data fit had been improved. Although very little confidence can be placed in the estimated station location parameters because of the small amount of data, it was noted that the change from the survey location was comparatively small – the geocentric radius changed by 48 m, the latitude by 10 m, and the longitude by -49 m (the longitude was moved to the west). A change of this magnitude from the survey location is possible since similar changes were noted when the station parameters from DSS 51 and DSS 42 were estimated by use of the *Ranger* Block III and *Mariner IV* data. The difference in predicted, unbraked impact point between the 9 × 9 solution and the 6 × 6 solution was approximately -0.05 deg in lunar latitude, and -0.003 deg in lunar longitude. This is roughly equivalent to 1.5 and 0.09 km on the lunar surface.

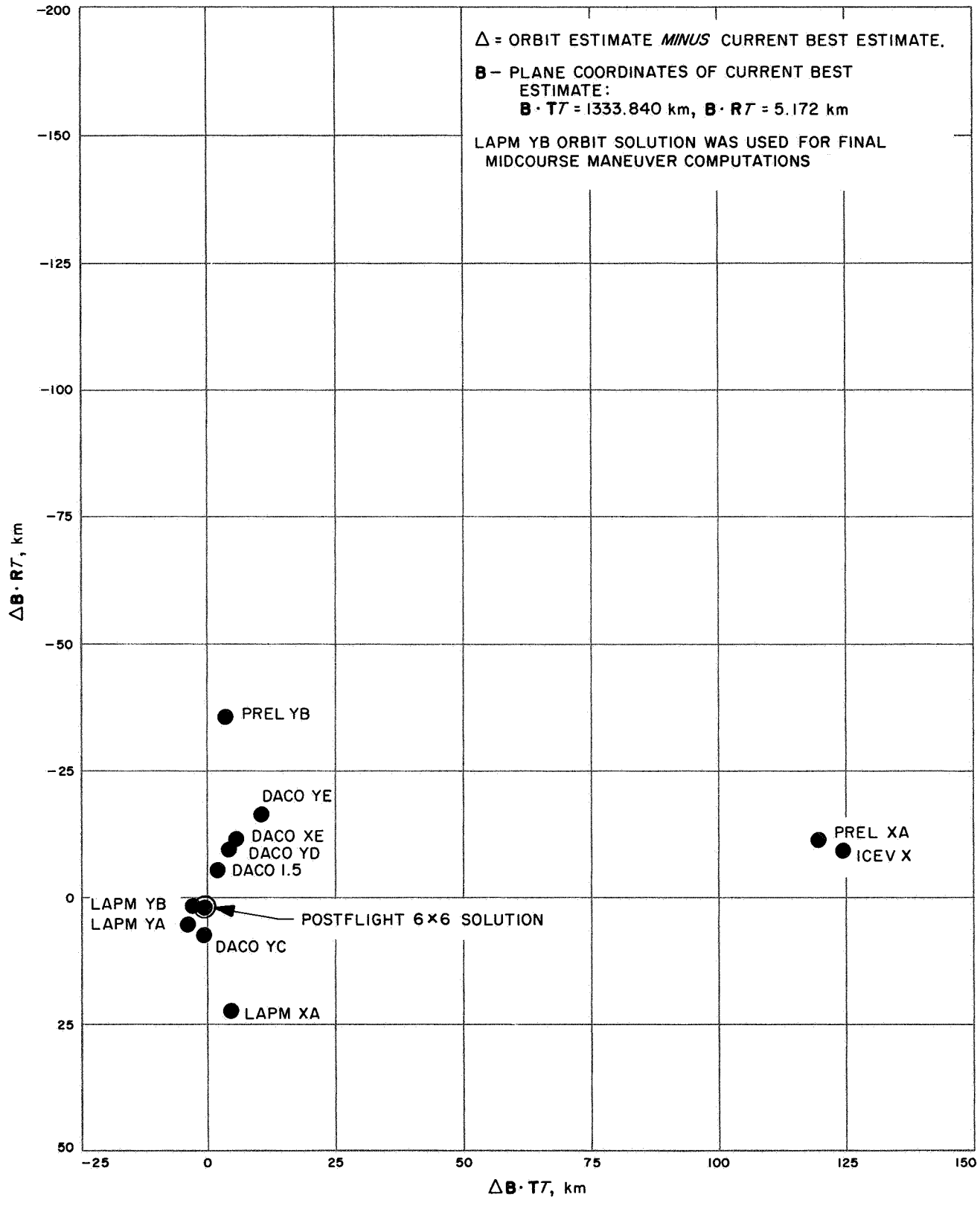

Fig. 63. B-plane differences in predicted unbraked impact point between realtime solutions and current best pre-midcourse estimate, *Surveyor II*

Based on the improved fit to the DSS 72 data obtained by estimating the station parameters, the 9 × 9 solution is considered to be the best estimate of the spacecraft premaneuver orbit. Numerical values from these two solutions are presented in Tables 33 and 34. The number of data points, together with the data noise statistics, are given in Table 35. A graphical comparison between the predicted unbraked impact point (in **B**-plane coordinates) between the 9 × 9 solution and the inflight solutions may be seen in Fig. 63. Plots of the doppler residuals from the 9 × 9 solution may be seen in Figs. 64 through 68.

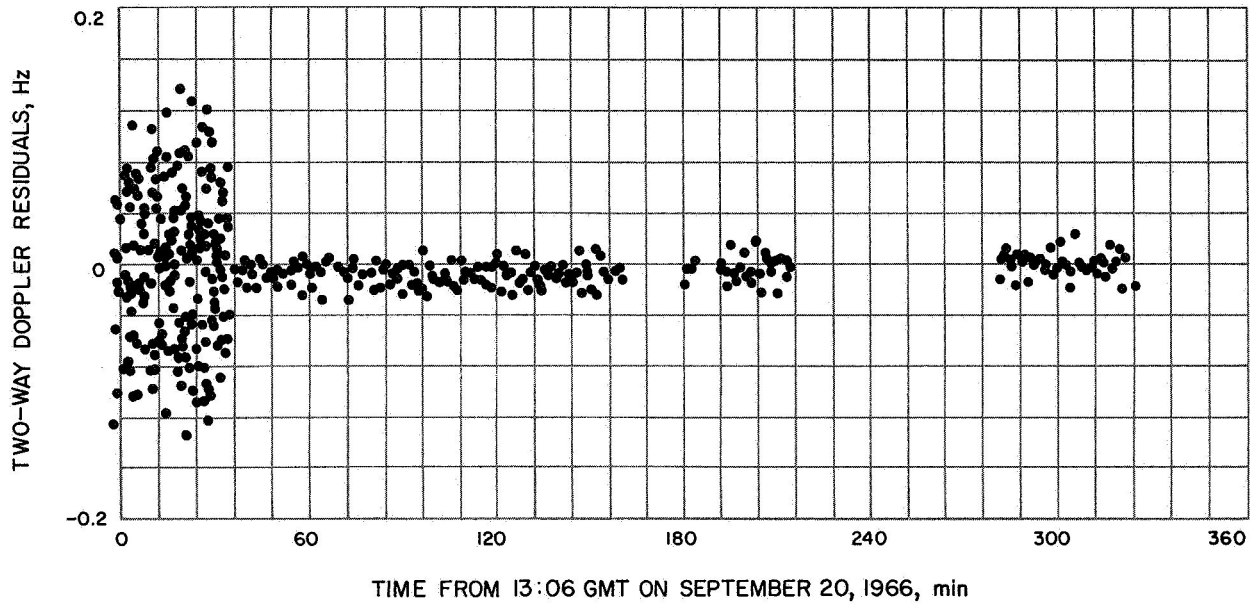

Fig. 64. DSS 51 premaneuver two-way doppler residuals, *Surveyor II*

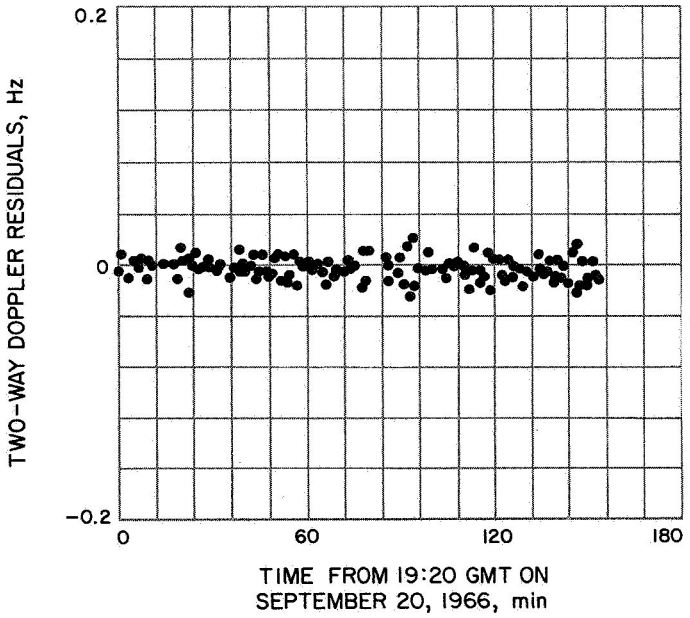

Fig. 65. DSS 51 premaneuver two-way doppler residuals, *Surveyor II*

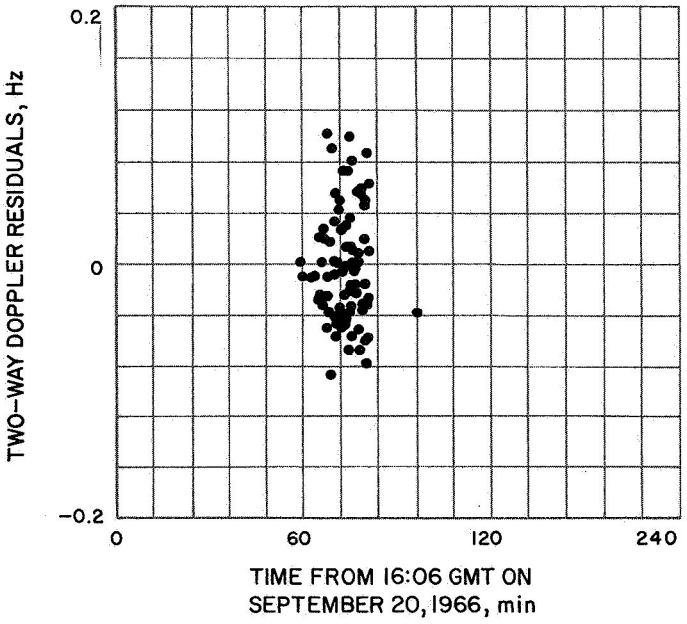

Fig. 66. DSS 72 premaneuver two-way doppler residuals, *Surveyor II*

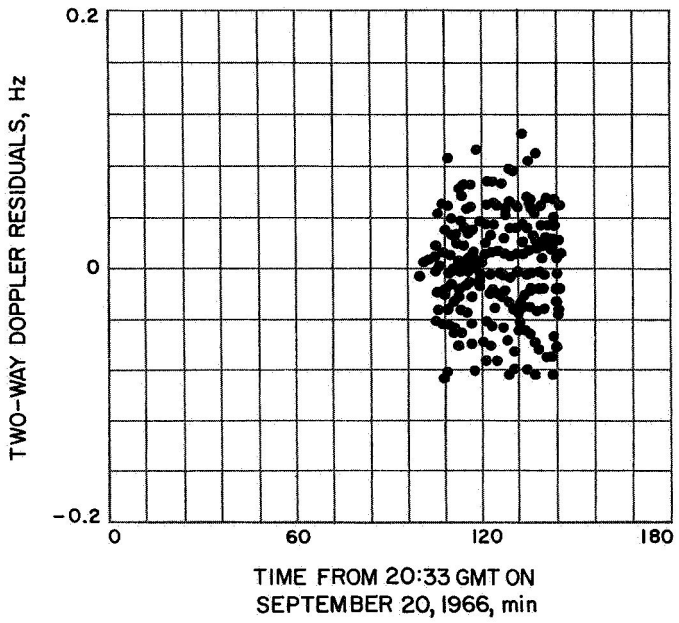

Fig. 67. DSS 72 premaneuver two-way doppler residuals, *Surveyor II*

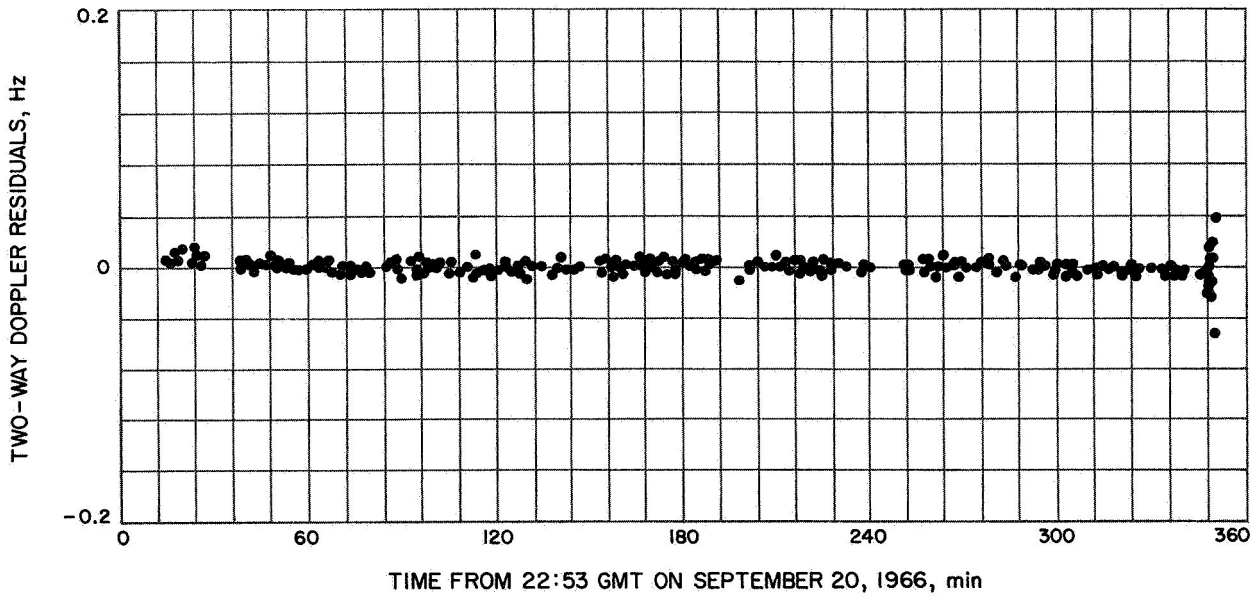

Fig. 68. DSS 11 premaneuver two-way doppler residuals, *Surveyor II*

XI. Analysis of Air Force Eastern Test Range Tracking Data for *Surveyor II*

The Air Force Eastern Test Range provided the classical orbit elements for the spacecraft transfer orbit and the *Centaur* postretro orbit and, also, for the initial acquisition information to the DSN tracking stations. The calculations, made with *Centaur* C-band tracking data obtained from the downrange AFETR tracking stations, were transmitted to the SFOF at JPL. The acquisition information was relayed to the DSS stations, and the initial orbital elements were used as starter values for the initial JPL orbital calculation.

In addition to the above requirements, AFETR transmitted the C-band pulse radar data obtained during the transfer orbit and the *Centaur* post-retromaneuver orbit to the SFOF. The transfer orbit data were used during

flight operations to provide a check and a backup to the AFETR computation. The *Centaur* post-retromaneuver data were important for verifying the *Centaur* retro-engine firing and the *Centaur* post-retromaneuver orbit. The retromaneuver was performed (1) to ensure that the *Centaur* did not impact the lunar surface and (2) to provide a separation between the *Centaur* and the spacecraft so that the Canopus seeker on board the spacecraft did not lock up on the *Centaur* instead of Canopus.

The *Centaur* C-band pre-retromaneuver data were obtained from Antigua and Trinidad radar stations. However, all the Trinidad data were obtained before the main engine cutoff (MECO), and they were not used in the orbit computations. The Antigua data were obtained from before MECO to approximately the start of retromaneuver. The elevation angles for these data were ranged from 2 to 22 deg. The *Centaur* post-retromaneuver data were obtained from Ascension and Pretoria radar stations. The Pretoria tracking data indicated that its radar had difficulties in locking on to the *Centaur*. The elevation angles for the Ascension and Pretoria data were ranged from 38 to 72 deg and from 20 to 81 deg, respectively. The AFETR data coverage and the associated spacecraft event is shown in Fig. 69.

A. Analysis of the Transfer Orbit Data

The *Centaur* transfer orbit was computed by use of angular and range data from Antigua at the span between MECO and the separation of the spacecraft from the *Centaur*. The AFETR converged conditions at injection epoch in geocentric cartesian coordinates are given in Table 39 (top). Since the AFETR and JPL transfer orbits each have a different epoch, the JPL converged conditions were mapped to the AFETR epoch to enable comparison of the converged conditions. The comparison showed that the conditions are in good agreement with exception of velocity in the y direction (Dy). The Dy

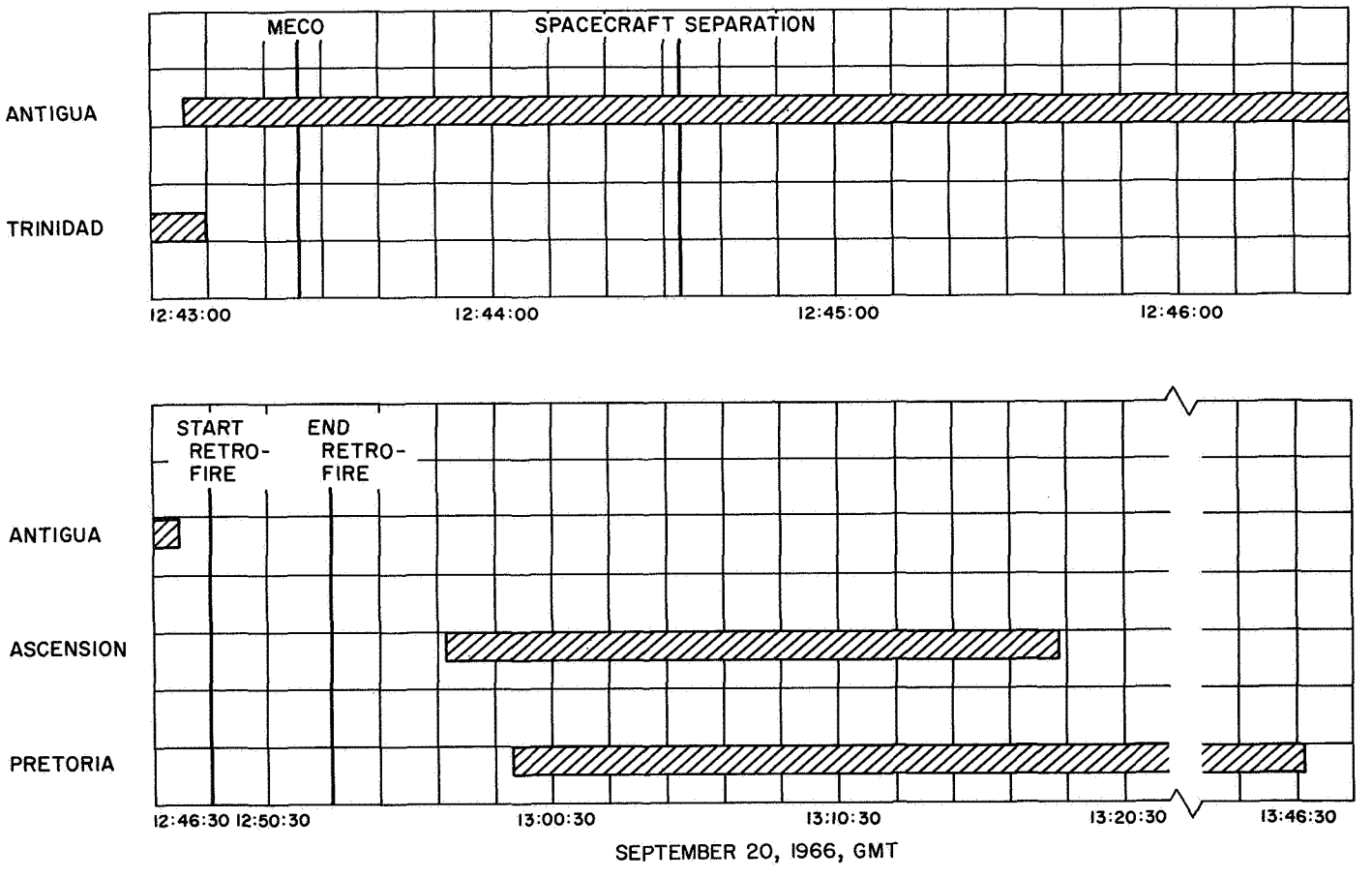

Fig. 69. AFETR data coverage on *Surveyor II*

Table 39. Converged conditions at injection epoch in space-fixed cartesian coordinates, *Surveyor II*

a. Epoch: September 20, 1966 at 12:43:44.7 GMT

Element	AFETR transfer orbit by JPL	AFETR transfer orbit	Difference between orbits by JPL and AFETR
x, km	−4623.5519	−4627.0752	−3.5233
y, km	4476.6927	4473.8791	2.8136
z, km	1750.5699	1748.2758	2.2941
Dx, km/s	−8.5413224	−8.5438704	0.0025480
Dy, km/s	−4.7168291	−4.7037681	−0.0130610
Dz, km/s	−4.8300580	−4.8258955	−0.0041625

b. Epoch: September 20, 1966 at 12:43:13.670 GMT

Element	AFETR transfer orbit by JPL	Best DSIF orbit	Difference between AFETR transfer and DSIF orbit
x, km	−4355.5597	−4360.9042	+5.3445
y, km	4620.1069	4616.8514	+3.2555
z, km	1899.2697	1896.4001	+2.8696
Dx, km/s	−8.7305161	−8.7282190	−0.0022971
Dy, km/s	−4.5251290	−4.5253067	0.0001777
Dz, km/s	−4.7529068	−4.7559824	0.0030756

showed a difference of 13 m/s. A comparison on the converged conditions was also made between the JPL transfer orbit and the best DSS orbit (Table 39). The two sets of conditions are in good agreement.

The orbital parameters obtained from the best premaneuver orbit, based on DSS data only, and from the JPL transfer orbit, based on Antigua data only, showed very good consistency between the two sets of numbers. The values of the parameters for these solutions are shown in Table 40, as are the differences between these two sets of parameters.

The orbital parameter that showed a significant difference between the JPL transfer orbit and the AFETR transfer orbit solutions is the semimajor axis. The difference between the two semimajor axes is 4642.3 km. The values of the parameters for the AFETR transfer orbit are given in Table 40 along with the differences in the parameter value between the JPL and AFETR transfer orbit. The B-plane miss also showed a significant difference between the JPL and AFETR transfer orbit. The B-plane miss for the JPL solution is 1133 km; for the AFETR solution it is 4849 km.

The differences that existed between the JPL and AFETR transfer orbit solutions quite likely relate to the burn data (data obtained before MECO) that AFETR

Table 40. *Surveyor II* transfer orbit parameter solutions, September 20, 1966

Parameter	Best DSIF orbit 12:43:13.670 GMT	AFETR transfer orbit by JPL 12:43:13.670 GMT	AFETR transfer orbit 12:43:30.0 GMT	Difference between transfer orbit by JPL and DSIF orbit	Difference between transfer orbits by JPL and AFETR
Radius, km	6627.9055	6627.4814	6650.0	−0.4241	—
Latitude, deg	16.626021	16.653008	15.859	+0.026987	—
Longitude, deg	303.60264	303.54741	305.001	−0.05523	—
Velocity, km/s	10.523257	10.523595	10.504	+0.000338	—
Elevation, deg	6.7112166	6.6631594	7.533	−0.0480572	—
Azimuth, deg	120.66787	120.63482	121.072	−0.03305	—
Semimajor axis, km	398546.27	399167.16	403809.5	+620.89	−4642.3
Eccentricity	0.98358241	0.98360598	0.9837955	+0.00002357	−0.0001895
Inclination, deg	33.423575	33.408964	33.40954	−0.014611	−0.00058
Longitude of node, deg	340.26840	340.27930	340.3491	+0.01090	−0.0698
Argument of perigee, deg	135.66564	135.69079	135.61014	+0.02515	+0.08065
C3, km^2/s^2	−1.0001380	−0.99858234	−0.98	+0.0015557	−0.02
Encounter					
B, km	1333.8490	1133.3926	4849.0525	−200.4564	−3715.6599
B•RT, km	5.1720951	−83.149355	−1203.0983	−88.3214501	+1119.9489
B•TT, km	1333.8397	1130.3389	4697.4317	−203.5008	−3567.0928
Latitude, deg	0.052885300	1.7351301	11.617893	+1.7880154	−9.882763
Longitude, deg	354.70848	350.31350	92.109330	−4.39498	−101.79583

used in its orbit computation. The JPL transfer orbit computations utilized approximately 60 s of Antigua data (1 point/6 s) between MECO and separation, whereas, the AFETR transfer orbit was based on 40 s of Antigua data (5 points/s), of which 1.4 s of data were obtained before MECO. It should be pointed out at this time that the inclusion of burn data in the computation of the AFETR transfer orbit was not a discrepancy on AFETR's part. AFETR was responsible for computing a quick-look orbit to provide initial acquisition information to the DSS tracking stations. AFETR has fulfilled this obligation. Since AFETR transfer orbit was computed before the confirmation of MECO by the telemetry system, it is not possible to determine when the burn data end. The amount and types of tracking data, together with the associated data noise statistics used in the transfer orbit computations are given in Table 41. The observed minus computed residuals for the transfer orbit are shown in Fig. 70.

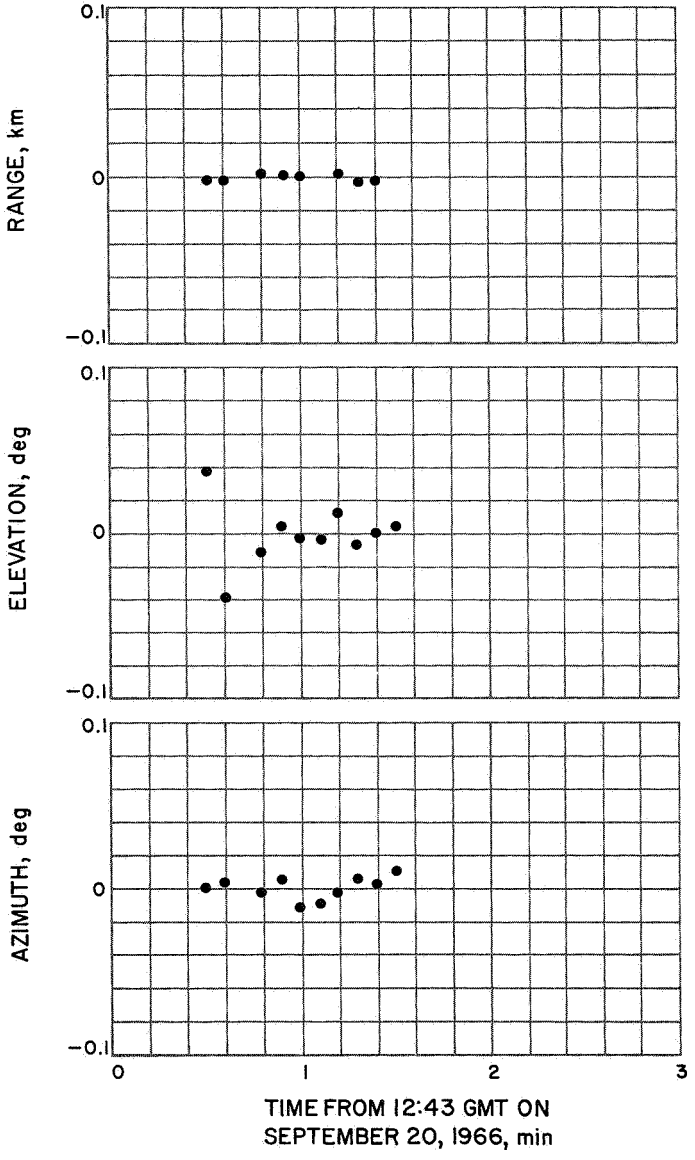

Fig. 70. Antigua residuals: Transfer orbit solution, *Surveyor II*

B. Analysis of Post-Retromaneuver Orbit Data

Three JPL post-retromaneuver orbit solutions were computed during postflight analysis: (1) a solution from Ascension and Pretoria data, (2) a solution from the Ascension data, only, and (3) a solution using the Pretoria data, only. The amount and types of tracking data, along with the associated data statistics, used in the post-retromaneuver orbit computations are given in Table 41. The three JPL postretro orbit solutions showed a **B**-plane miss of 14871 km for the combined data, 13517 km for Ascension data, and 14600 km for solution with Pretoria data. The orbital parameters for the three solutions are given in Table 42. These three JPL solutions are quite different from the AFETR solutions that had a **B**-plane miss of 8105 km. The AFETR post-retromaneuver orbit was computed using 13 points of Pretoria data. The orbital parameters for the AFETR solution are given in Table 42. The differences between the JPL and AFETR solutions based on Pretoria data can be explained with the help of Fig. 71, which shows the O − C residual for the Pretoria station with the converged condition from Ascension solution passed through the Pretoria data. The AFETR computed its post-retromaneuver orbit using 13 points of Pretoria data obtained before 13:01:18 GMT, whereas, JPL used all the Pretoria data obtained after 13:01:18 GMT for its orbit computation. It appears that the bad early range data are the cause of the difference between the two solutions, since the early angle data are of good quality (as shown in Fig. 71).

The best JPL post-retromaneuver orbit is the solution using only the Ascension data. The Ascension data are of excellent quality, and a very good orbit fit was obtained from these data, as shown in Fig. 72. However, the postretro orbit computed using Pretoria data only showed an inconsistency between radar parameters (range R, el, az) as shown in Fig. 73. This figure showed the O − C residuals for the Pretoria radar parameter. A slight skew was observed in the elevation angle residuals. The figure also indicates that the Pretoria radar has noisy angle data and has difficulties in locking on

Table 41. Summary of AFETR tracking used in *Surveyor II Centaur* orbit computations

Orbit ID	AFETR station	Data type	Begin data		End data		Number of points	Standard deviation	Root mean square	Mean error
			Date 1966	GMT	Date 1966	GMT				
AFETR transfer orbit	91	Az	9/20	12:43:30	9/20	12:44:30	10	0.0064	0.00636	0.0000
		El	9/20	12:43:30	9/20	12:44:30	10	0.0184	0.0184	0.0000
		R	9/20	12:43:30	9/20	12:44:30	8	0.0014	0.00137	0.0000
AFETR post-retromaneuver orbit A	76	Az	9/20	13:17:54	9/20	13:46:42	38	0.2080	0.215	−0.0532
		El	9/20	13:17:54	9/20	13:46:42	37	0.0559	0.0574	0.0129
		R	9/20	13:17:54	9/20	13:46:42	33	0.0269	0.0269	0.0003
	79	Az	9/20	13:16:36	9/20	13:18:12	15	0.0080	0.0141	0.0116
		El	9/20	13:16:36	9/20	13:18:12	15	0.0101	0.0113	−0.0052
		R	9/20	13:16:36	9/20	13:18:12	15	0.0038	0.00391	−0.0007
AFETR post-retromaneuver orbit B	76	Az	9/20	13:17:54	9/20	13:46:42	38	0.214	0.215	0.0260
		El	9/20	13:17:54	9/20	13:46:42	37	0.0528	0.0529	0.0026
		R	9/20	13:17:54	9/20	13:46:42	34	0.106	0.106	0.0000
AFETR post-retromoneuver orbit C	79	Az	9/20	13:17:54	9/20	13:18:12	15	0.0079	0.0079	0.0000
		El	9/20	13:17:54	9/20	13:18:12	15	0.0100	0.0100	0.0000
		R	9/20	13:18:12	9/20	13:18:12	15	0.0038	0.0038	0.0000

Station 91 is located at Antigua, station 76 at Pretoria, and station 79 at Ascension.

Table 42. *Surveyor II* post-retromaneuver orbit parameter solutions for epoch, September 20, 1966 at 13:01:18 GMT

Parameter	Ascension and Pretoria data	JPL orbit with Ascension data	JPL orbit with Pretoria data	AFETR orbit with Pretoria data	JPL and AFETR orbit with Pretoria data
Radius, km	11026.956	11030.061	11028.280	11032	−4
Latitude, deg	−18.641189	−18.627901	−18.607261	−18.626	−0.019
Longitude, deg	356.62162	356.60894	356.65348	356.672	−0.019
Velocity, km/s	7.9162791	7.9160532	7.9158323	7.923	−0.007
Elevation, deg	42.363012	42.304837	42.355927	42.346	0.010
Azimuth, deg	121.75462	121.79491	121.81728	121.840	−0.023
Semimajor axis, km	271386.90	275782.95	271329.17	306054.9	−34725.7
Eccentricity	0.97589463	0.97623146	0.97588246	0.9785863	−0.0027
Inclination, deg	33.395660	33.419678	33.423428	33.45231	−0.029
Longitude of node, deg	340.14031	340.18483	340.27472	340.2969	−0.0222
Argument of perigee, deg	135.66616	135.74055	135.57623	135.73180	−0.1556
C3, km^2/s^2	−1.4687565	−1.4453442	−1.4690690	−1.30	−0.17
B, km	14871.130	13517.028	14600.281	8105.8635	6494.417
B•TT, km	13634.010	12336.910	13514.409	7456.1152	6058.294
B•RT, km	−5938.3733	−5523.6489	−5525.3007	−3179.8379	−2345.463

to the *Centaur* C-band beacon. When the converged condition of the Ascension solution was passed through the Pretoria data, the O − C range residuals indicated that there is a problem in the range data as shown in Fig. 74. The range residuals showed a parabolic effect. Because of the difficulties with the Pretoria radar, the confidence in the post-retromaneuver orbit solutions that utilized the Pretoria data in its orbit computations was limited. With the converged condition of the Pretoria solution passed through the Ascension data (Fig. 75), no indication of discrepancy was shown in the Ascension data. Figures 76 and 77 show the Pretoria and Ascension O − C residuals, respectively, on the two-station solution.

C. Conclusion

The Antigua tracking data were very useful during flight operation for validating the initial orbit estimates based on DSIF data. In addition, combined DSIF and AFETR (Antigua) solutions were obtained. The solutions indicate that the Antigua data were consistent with the DSIF data.

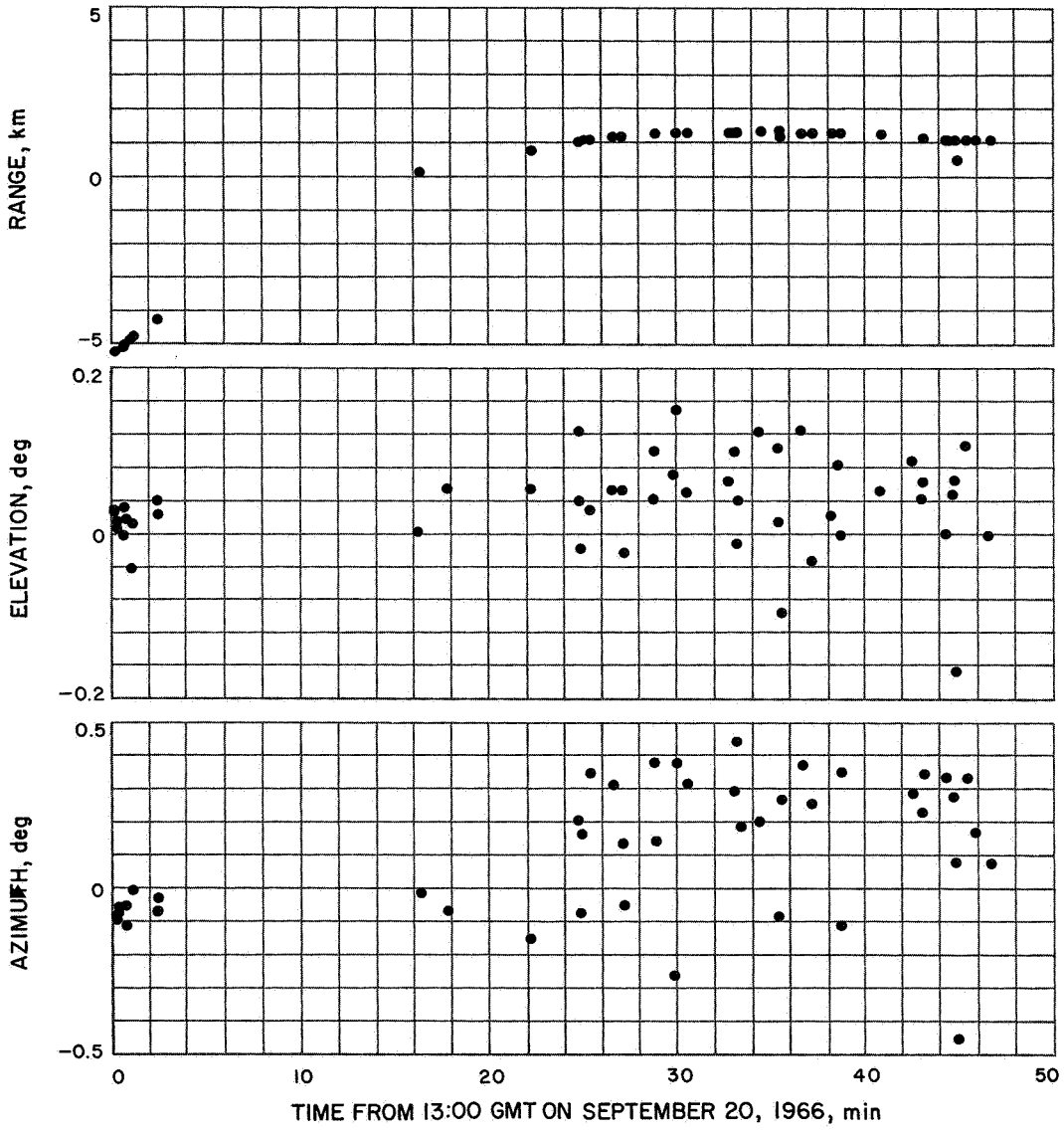

Fig. 71. Pretoria residuals: Solution from Ascension data only, *Surveyor II*

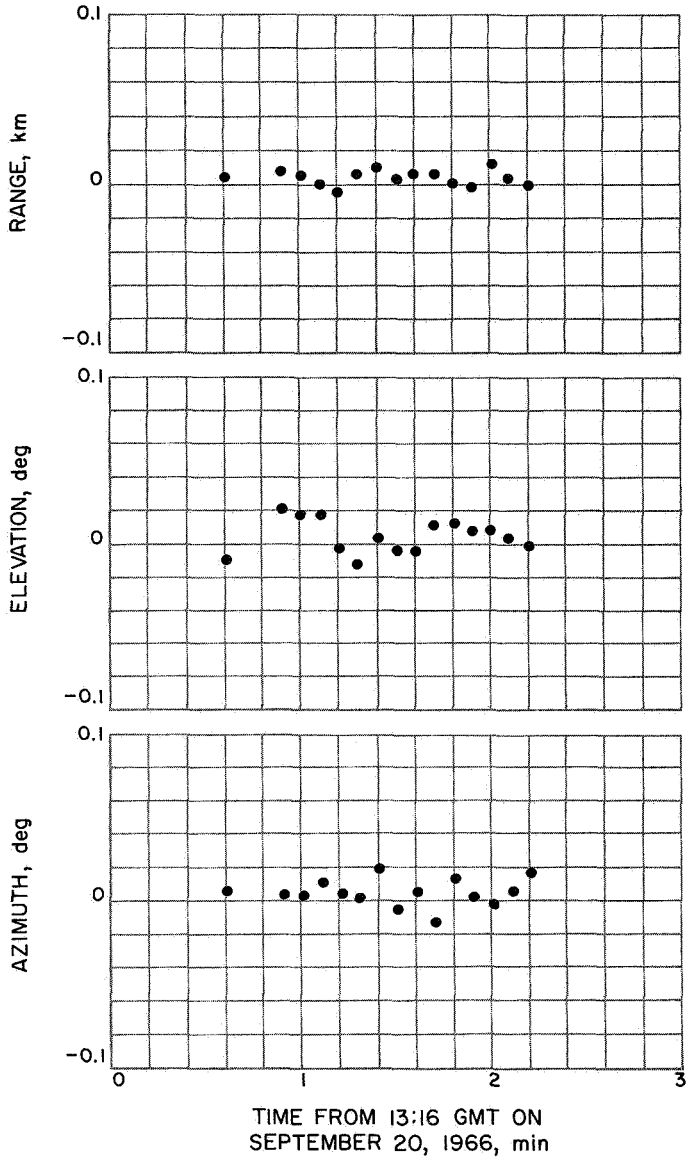

Fig. 72. Ascension residuals: Solution using Ascension data only, *Surveyor II*

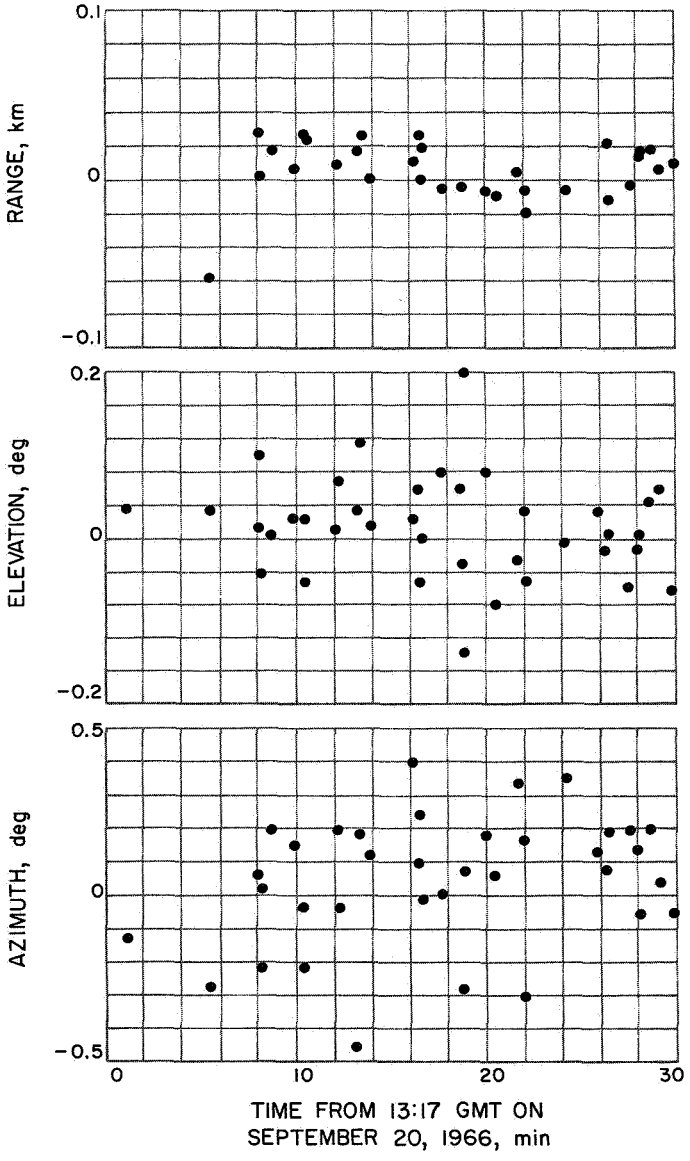

Fig. 73. Pretoria residuals: Solution using Pretoria data only, *Surveyor II*

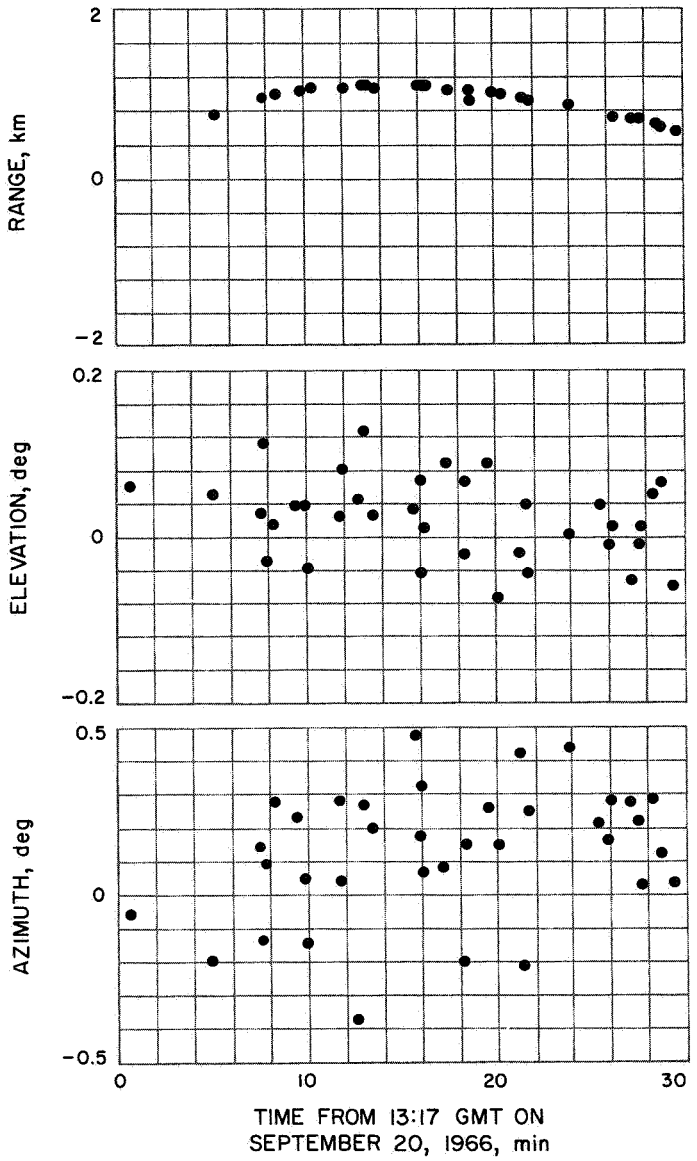

Fig. 74. Pretoria residuals: Solution using Ascension data only, *Surveyor II*

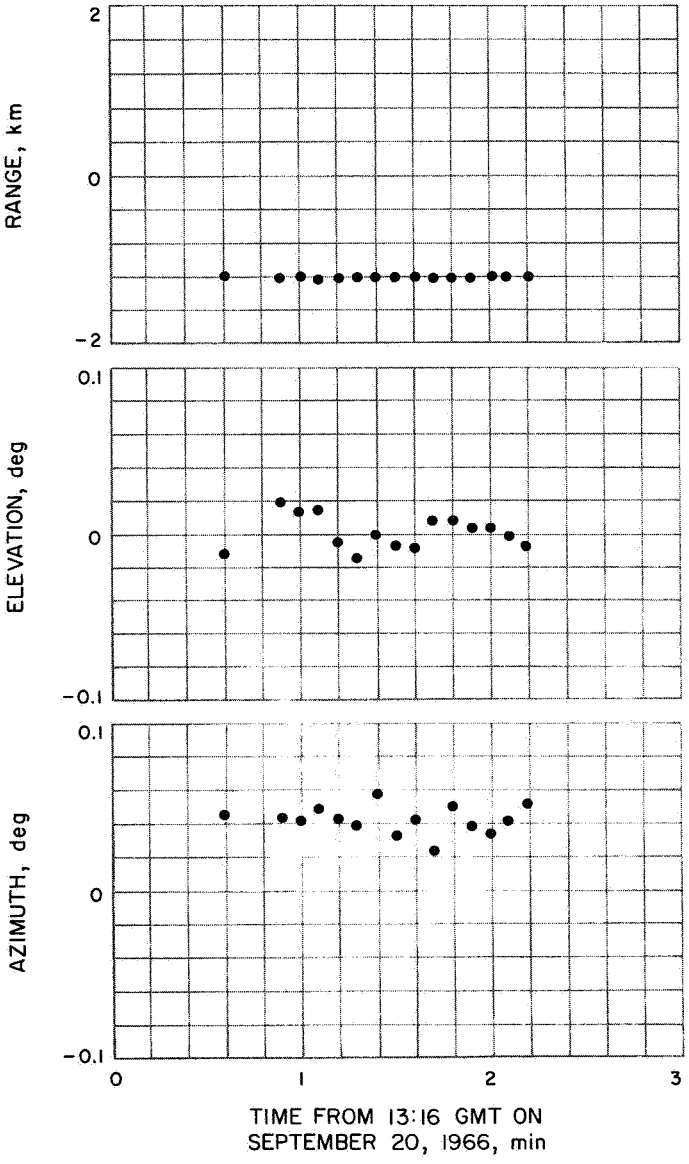

Fig. 75. Ascension residuals: Solution using Pretoria data only, *Surveyor II*

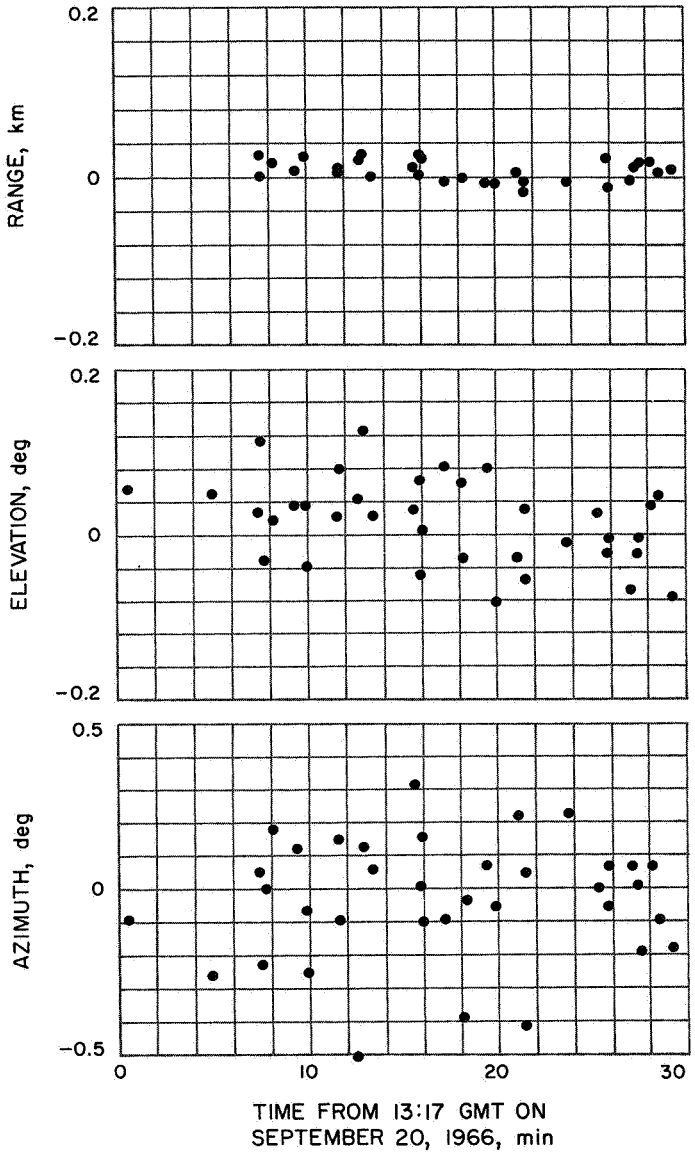

Fig. 76. Pretoria residuals: Solution from Ascension and Pretoria data, *Surveyor II*

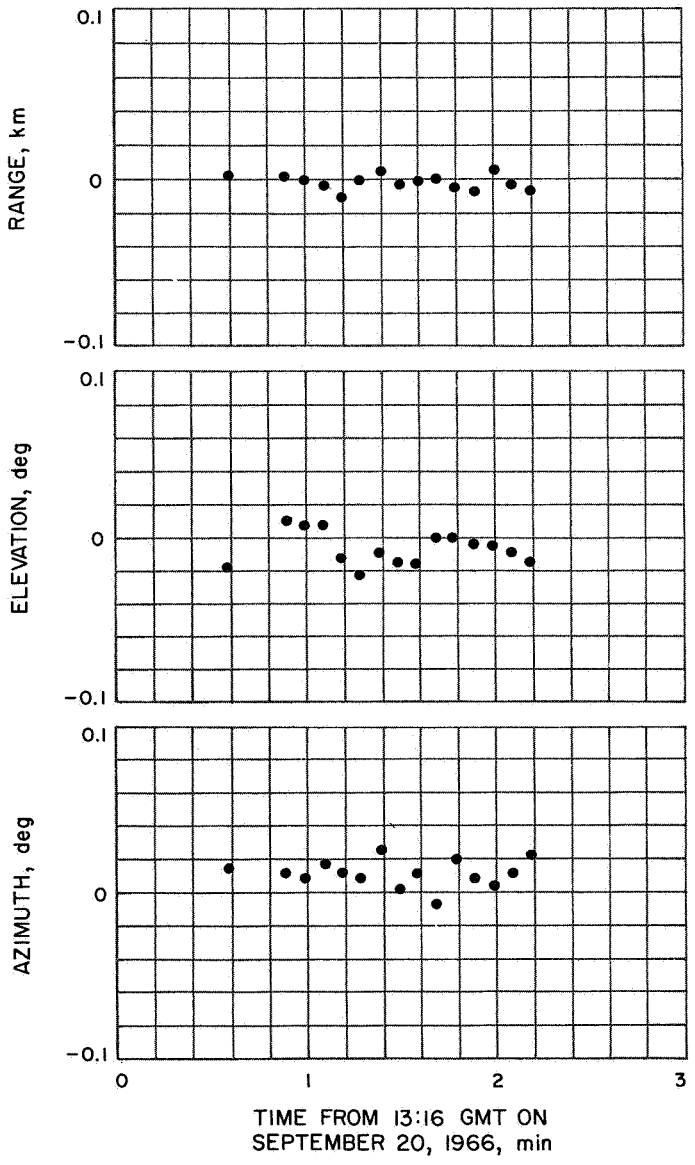

Fig. 77. Ascension residuals: Solution using Ascension and Pretoria data, *Surveyor II*

Appendix A
Definition of Doppler Data Types

Three types of doppler data were obtained by the DSN tracking stations – one-way, two-way, and three-way doppler. The following sketches and definitions distinguish the methods.

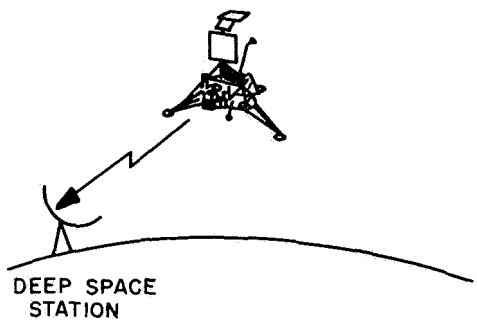

ONE-WAY DOPPLER

The spacecraft transmits to the ground station. The ground station operates in receive mode, only.

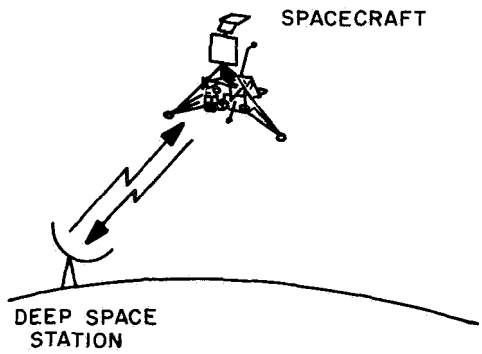

TWO-WAY DOPPLER

The ground station transmits to the spacecraft; the spacecraft retransmits signal to the same ground station. The ground station operates in both transmit and receive modes.

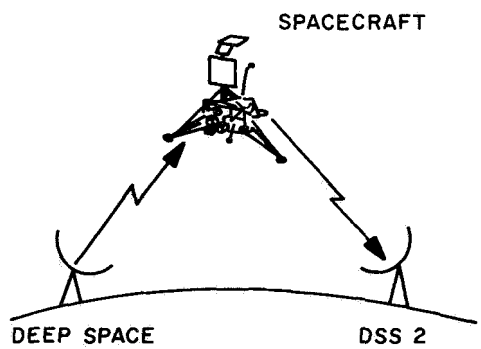

THREE-WAY DOPPLER
(NONCOHERENT)

The first ground station transmits a signal to the spacecraft; the spacecraft retransmits the signal to the second ground station. Station 1 does *not* transmit a reference frequency to station 2.

Appendix B

Definition of the Miss Parameter B

The miss parameter **B** is used at JPL to measure miss distances for lunar and interplanetary trajectories; it is described by W. Kizner in Ref. B-1. The parameter has the desirable feature of being very nearly a linear function of changes in injection conditions.

The osculating conic at closest approach to the target body is used in defining **B**, which is the vector from the target's center of mass, perpendicular to the incoming asymptote. Let $\mathbf{S}_I$ be a unit vector in the direction of the incoming asmyptote. The orientation of **B** in the plane normal to $\mathbf{S}_I$ is described in terms of two unit vectors, **R** and **T**, normal to $\mathbf{S}_I$. Unit vector **T** is taken parallel to a fixed *reference plane*, and **R** completes a right-handed orthogonal system. Figure B-1 illustrates the system.

For *Surveyor*, two reference planes have been used: the plane of the earth's equator **T***Q* or the plane of the moon's equator **T***T*.

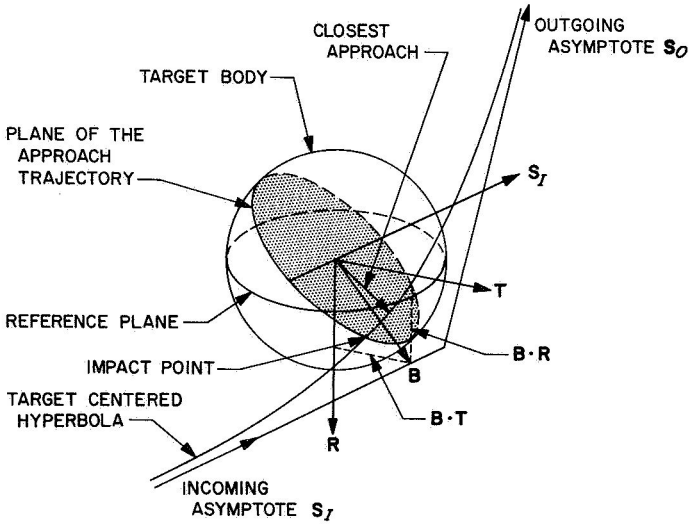

Fig. B-1. Definition of B·T, B·R system

Glossary

AFETR	Air Force Eastern Test Range
AMR	altitude marking radar
az	azimuth
CS	computer support
C3	three-way doppler (noncoherent)
CC3	two-way doppler
DACO	data consistency orbit
dec	declination
DPES	direct-ascent powered-flight simulator
DSN	Deep Space Network
DSS	Deep Space Station
E	encounter
el	elevation
FPAC	flight path analysis and command
$GM_{\oplus}$	gravitational mass of the earth
$GM_{\mathbb{C}}$	gravitational mass of the moon
HPPS	Hughes post processor
IRU	inertial reference unit
L	launch
lat	latitude
lon	longitude
MA	maneuver analysis (group)
MC	midcourse
MECO	*Centaur* main engine cutoff
MTGS	midcourse and terminal guidance program
OD	orbit determination
ODG	orbit data generator
ODP	orbit determination program
SMAA	semimajor axis of dispersion ellipse
SMIA	semiminor axis of dispersion ellipse
SPAC	spacecraft performance analysis and command
SSAC	space science analysis and command
SPODP	single-precision orbit determination program
SPACE	single-precision Cowell trajectory program
TDA	tracking data analysis (group)
TDP	tracking data processor
TFL	time from launch
TG	trajectory group
TQ	plane of earth's equator
TRJX	JPL trajectory program
TT	plane of moon's equator

References

1. *Surveyor I Mission Report, Part I. Mission Description and Performance,* Technical Report 32-1023, pp. 111–114. Jet Propulsion Laboratory, Pasadena, Calif., Aug. 31, 1966.

2. Warner, M. R., and Nead, M. W., *SPODP — Single Precision Orbit Determination Program,* Technical Memorandum 33-204. Jet Propulsion Laboratory, Pasadena, Calif., Feb. 15, 1965.

3. White, R. J., et al., *SPACE — Single Precision Cowell Trajectory Program,* Technical Memorandum 33-198. Jet Propulsion Laboratory, Pasadena, Calif., Jan. 15, 1965.

4. Wollenhaupt, W. R., et al., *Ranger VII Flight Path and Its Determination From Tracking Data,* Technical Report 32-694. Jet Propulsion Laboratory, Pasadena, Calif., Dec. 15, 1964.

5. Clarke, V. C., Jr., *Constants and Related Data for Use in Trajectory Calculations,* Technical Report 32-604. Jet Propulsion Laboratory, Pasadena, Calif., Mar. 6, 1964.

6. *Surveyor I. A Preliminary Report,* NASA SP-126. NASA Scientific and Technical Information Facility, College Park, Maryland, June 1966.

7. Whitaker, E., "*Surveyor I* Location," *Science,* Vol. 153, No. 3743, pp. 1550–1551, Sept. 23, 1966.

8. Sjogren, W. L., et al., *The Ranger VI Flight Path and Its Determination from Tracking Data,* Technical Report 32-605. Jet Propulsion Laboratory, Pasadena, Calif., Dec. 15, 1964.

9. Mottinger, N. A., and Trask, D. W., "Status of DSS Location Solution for Deep Space Probe Missions: I. Initial Comparisons," *The Deep Space Network,* Space Programs Summary 37-48, Vol. II. Jet Propulsion Laboratory, Pasadena, Calif., Nov. 30, 1967.

10. Vegos, C. J., and Trask, D. W., "Tracking Station Locations as Determined by Radio Tracking Data: Comparison of Results Obtained From Combined Ranger Block III Missions and From Baker-Nunn Optical Data," *The Deep Space Network,* Space Programs Summary 37-43, Vol. III. Jet Propulsion Laboratory, Pasadena, Calif., Jan. 31, 1967.

11. Mottinger, N. A., and Sjogren, W. L., "Consistency of *Lunar Orbiter II Ranger* and Doppler Data," *The Deep Space Network,* Space Programs Summary 37-46, Vol. III. Jet Propulsion Laboratory, Pasadena, Calif., July 31, 1967.

12. Vegos, C. J., and Trask, D. W., "*Ranger* Combined Analysis, Part II: Determination of the Masses of the Earth and Moon From Radio Tracking Data," *The Deep Space Network,* Space Programs Summary 37-44, Vol. III. Jet Propulsion Laboratory, Pasadena, Calif., Mar. 31, 1967.

References (contd)

13. Meredith, C. M., and Cheng, R. K., "Midcourse Guidance Equations for the *Surveyor* Spacecraft," AIAA paper 64-654. Presented at American Institute of Aeronautics and Astronautics, and Institute of Navigation, Astrodynamics Guidance and Control Conference, Los Angeles, Calif., Aug. 24–26, 1964.

14. Cheng, R. K., and Conrad, D. A., "Design Considerations for the *Surveyor* Terminal Descent System," AIAA paper 64-644. Presented at American Institute of Aeronautics and Astronautics, and Institute of Navigation, Astrodynamics Guidance and Control Conference, Los Angeles, Calif., Aug. 24–26, 1964.

15. Ribarich, J. J., and Meredith, C. M., "Analysis of *Surveyor* Midcourse Guidance as a Problem in the Theory of Maxima and Minima," *J. Spacecraft Rockets,* Vol. 3, No. 7, p. 997, July 1966.

16. Cheng, R. K., Meredith, C. M., and Conrad, D. A., "Design Considerations for *Surveyor* Guidance," *J. Spacecraft Rockets*, Vol. 3, No. 11, p. 1159, Nov. 1966.

17. Ribarich, J. J., "*Surveyor* Guidance Program," *Non-Hardware Aspects of Space Navigation: Institute of Navigation, National Space Navigation Meeting, Los Angeles, Calif., March 14–15, 1967, Proceedings.* Institute of Navigation, Washington, D. C., 1967, pp. 75–83.

18. Ribarich, J. J., "*Surveyor* Spacecraft Landing Accuracy," *Proceedings of the AIAA Guidance, Control and Flight Dynamics Conference, Huntsville, Ala., Aug. 14–16, 1967.*

19. *Surveyor II Mission Report: Mission Description and Performance,* Technical Report 32-1086, Jet Propulsion Laboratory, Pasadena, Calif., Apr. 1, 1967.

B-1. Kizner, W. A., *A Method of Describing Miss Distances for Lunar and Interplanetary Trajectories,* External Publication 674, Jet Propulsion Laboratory, Pasadena, Calif., Aug. 1, 1959.